DEFORMATION MECHANISMS IN HONEYCOMBS

Thesis submitted in accordance with the requirements of the University of Liverpool for the degree of Doctor in Philosophy by Iain George Masters.

Department of Materials Science & Engineering

August 1994.

ABSTRACT

This thesis describes the experimental techniques used and the results obtained from an investigation into the properties of novel auxetic honeycombs , comprising re-entrant shaped cells, and conventional honeycombs containing hexagonal cells.

Existing work on the properties of honeycomb materials is reviewed with particular reference to in-plane elastic deformation and modelling of the re-entrant cell structure.

The popular flexure model has already been used to accurately predict the in-plane behaviour of conventional honeycombs which deform by flexing of the cell walls. However, two additional mechanisms by which honeycombs may deform in-plane can be identified, namely stretching and hinging of the cell walls. Mathematical models are developed here to describe these latter types of deformation. The models relate the material properties of the cell walls to the geometry of the cell and writing each model in terms of a force constant enables the three deformation mechanisms to be combined into a general model.

Tensile and compressive tests on aluminium and card honeycombs have been used to validate the flexure and hinging models respectively, for both hexagonal and re-entrant cell shapes.

In-plane indentation behaviour was investigated using both flat and semi-circular indenters. The re-entrant celled honeycombs were observed to have a higher resistance to indentation than their hexagonal cell counterparts due to densification of the material below the indenter as a result of the effective Poisson's ratio being negative.

Conventional hexagonal cell honeycombs deform anticlastically when bent out of plane due to the effective Poisson's ratio of the honeycomb being positive. When the Poisson's ratio is negative, as for the re-entrant cell shape, the out of plane curvature becomes synclastic enabling domed shapes to be produced naturally. For the card honeycombs the extremely low forces required to operate the hinges combine with the synclastic curvature to produce highly flexible cores with which it is possible to generate very tight curvatures without damage to the cell structure. This has obvious advantages over conventional honeycomb in the fabrication of doubly curved surfaces e.g. radomes, boat hulls.

Finally the general model is shown to be a useful first order calculation for predicting the properties of molecular, cellular structures without having to resort to time consuming and expensive computer techniques for molecular modelling and finite element analysis.

ACKNOWLEDGEMENTS

This thesis is based on the results of research carried out by the author between January 1991 and December 1993 at the University of Liverpool. I would like to acknowledge the support of:-

Professor P.Goodhew in making available the facilities in the Department of Materials Science and Engineering and the technical staff for their assistance.

Dr. K.E.Evans for his supervision and guidance throughout the project, and also the members of the Polymer and Composites Research Group, particularly Dr. B.D.Caddock, for many helpful suggestions.

The Science and Engineering Research Council for their financial support of the project.

Ciba-Geigy Bonded Structures and CMB Cartons Ltd., for their generous supply of materials.

Finally I would like to thank my parents for their continued encouragement and support.

CONTENTS

1) DEVELOPMENT & MANUFACTURE OF HONEYCOMB CORE MATERIALS

1.1 Development of honeycomb core materials

Sandwich structures, incorporating a lightweight core separating two strong stiff skins, occur naturally in, for example, the human skull or a bird's wing (Gibson *et al.* 1988a). The principle of a sandwich panel is the same as that of an "I" beam, i.e. the amount of material in the region of the neutral axis is reduced to a minimum. When a panel is bent the high strength skin material carries the maximum stress at the surface where the strain is highest, while near the neutral axis where the stresses and strains are small a relatively low yield, low weight core material is all that is required (Rao, 1978). The core material must, however, be stiff enough in shear to prevent the skins from sliding over each other and stiff enough in compression to keep the skins the correct distance apart (Johnson *et al.* 1986).

The first man-made sandwich panels were constructed from natural cellular materials such as cork and balsa wood. Balsa wood cut perpendicular to the grain and sandwiched between plywood skins was used in the construction of the de Havilland DH91 Albatross airliner in 1937 (Middleton, 1990) and again to great effect in the DH98 Mosquito fighter/bomber, the world's fastest combat aircraft of it's day (Hardy, 1977). Balsa is still used in the modern aircraft industry for example in the cargo floors of the Boeing 747 and in applications where complex curvatures are required (Colucci, 1990) since it has been found to be more durable and cheaper than synthetic equivalents. It's disadvantage however, is that as a natural material it cannot be grown or produced to a specified density and it's strength and stiffness are affected by the absorption of moisture (Wood, 1989). In serious cases rotting can occur.

The Second World War created the need for easily produced core materials with controllable and uniform properties which would remain unaffected by moisture. Experiments were carried out with foamed resin cores but it was found that lighter and more structurally efficient sandwich panels could be produced using a honeycomb structure as the core. This lead to the development, in 1943, of Dufaylite™ (a phenol-formaldehyde resin impregnated, all-wood, kraft paper honeycomb) by Dufay Ltd. in collaboration with the Royal Aircraft Establishment (May, 1957., Gordon, 1978.). This material was successfully used in radomes and many other military applications.

The modern equivalents of these early paper materials are manufactured from aluminium, stainless steel and GRP. The non-metallic Nomex™ core, manufactured by Du Pont and licensees, is produced from paper-like sheets of synthetic aromatic polyamide fibres and fibrids (fibre/film hybrids with a high surface area) coated with a phenolic resin (Wood, 1989).

1.2 Manufacture of commercial honeycombs

The most common methods of producing commercial honeycomb are shown schematically in Figs.1.1 & 1.2.

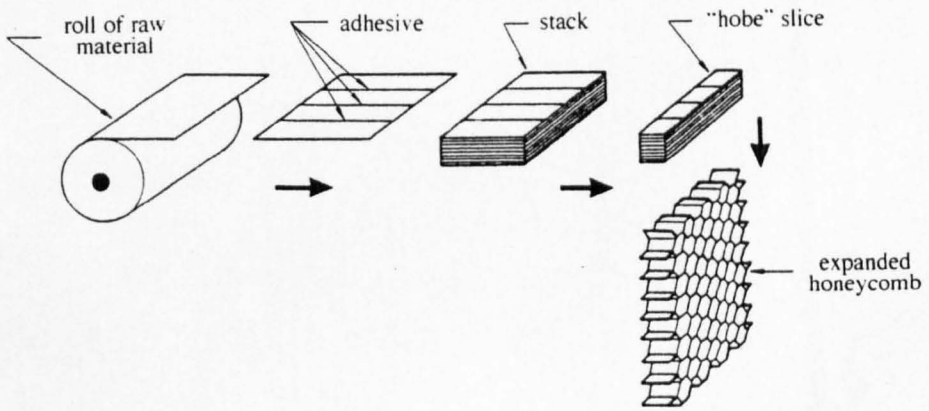

Fig.1.1 *Expansion process for manufacturing honeycomb.*

Aluminium foil honeycombs are produced by the expansion route (May, 1947). Parallel lines of adhesive are accurately printed on to the upper surface of sheets of material which are then stacked together, each sheet off-set from it's nearest neighbours by half a glue-line spacing. Heat and pressure are applied to the stack to cure the adhesive. Slices, sometimes called "hobe (honeycomb before expanding) slices", of the required thickness are then cut from the stack and expanded to produce conventional hexagonal cell material. (N.B. in the expanded core the direction of the adhesive bonds is called the 'ribbon direction').

A similar process is used to produce honeycombs from Nomex™ paper, but in this case the whole stack is dipped in resin after expansion. The density is controlled by the number of dipping operations, and after curing, the expanded stack is cut into slices of the required thickness.

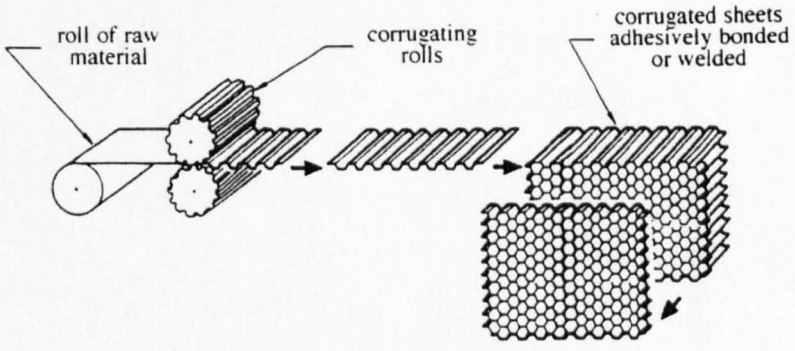

Fig.1.2 *Corrugation process for manufacture of honeycomb.*

Stainless steel and titanium honeycombs, for use in jet engine and other high temperature applications, are produced from heavier gauge material which must first be corrugated between profiled rollers. Individual sheets are then spot welded together by either resistance or laser welding (Fig.1.2).

Many types of core material are now available and the selection of an appropriate core is determined by the final application of the component being fabricated

(Parker, 1990). The operational environment is particularly important since, for example, aluminium honeycombs may be susceptible to certain corrosive media whereas resin based cores can be affected by high temperatures. A sample of the wide variety of applications for which honeycomb cores are now used is shown in Table.1.1

Core material	Application
Cardboard	Packaging Interior doors & partitions
Nomex	Helicopter rotor blades Aircraft luggage racks Boat hulls, bulkheads & decks
GRP	Missile & spacecraft components
Aluminium	Aircraft floors, tailplanes etc. Helicopter platforms
Stainless steel/Nickel based superalloys	Jet engine abradeable seals
Titanium	Jet engine compressor blades

Table 1.1. *Applications of honeycomb core materials.*

1.3 Properties of honeycomb cores

It is obvious from examination of a 2-D honeycomb structure that deformation in a plane perpendicular to the axes of the cells can arise from bending, hingeing or stretching of the cell walls.

Commercially available honeycombs are considered to deform elastically by flexing of the cell walls. This behaviour has been quite accurately described by a flexure model based on the assumption that the cell walls bend like beams (Gibson *et al.* 1982).

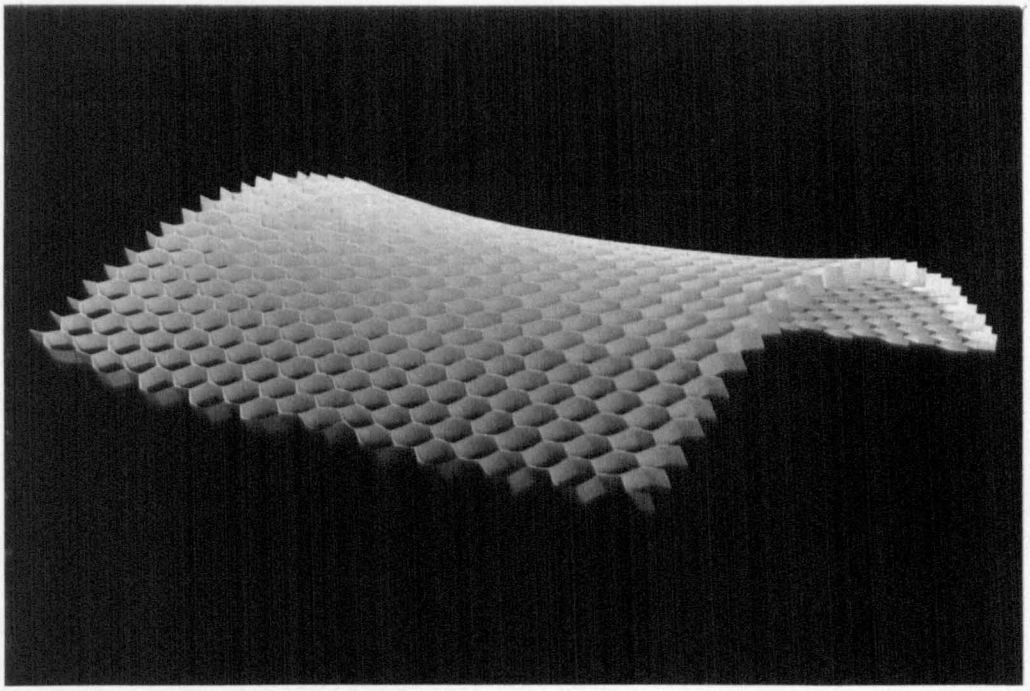

Fig.1.3 *A hexagonal cell, cardboard honeycomb demonstrating characteristic anticlastic curvature.*

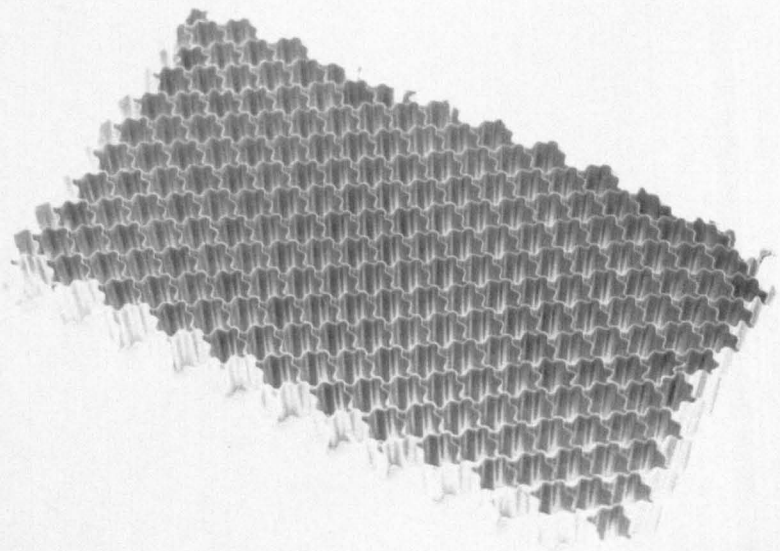

Fig.1.4 *Double-flex™ - a flexible aluminium core produced by Hexcel Corp.*

Experiments with card honeycombs (Caddock *et al.* 1991, Masters *et al.* 1993) have shown that hinging can be the dominant mechanism, ie. deformation occurs by a change in the cell angle alone. The final mechanism is stretching, in which the cell angles are considered fixed and deformation occurs by axial extension of transversely stiff cell walls. Gillis (1984) and Wei (1991) have both combined hinging and stretching mechanisms to describe molecular behaviour. Gibson *et al.* (1988b) considered both flexing and stretching for a honeycomb under in-plane biaxial stress. In this thesis the stretching and hinging models are developed separately in chapter 3 for elastic deformations only.

In general macro-honeycomb, of the type used in sandwich structures, will deform by either flexing or hinging since out-of-plane stiffness precludes stretching. The particular mechanism which operates is determined by the properties of the cell wall material and the cell geometry. Stretching only becomes significant on a molecular scale. However, it is feasible to imagine that all three mechanisms could operate concurrently and that a general elastic deformation model can be obtained by combining the appropriate equations.

1.4 Limitations of the hexagonal cell shape

As can be seen from Figs. 1.1 & 1.2 hexagonal celled honeycomb is very simple to produce, but it has the disadvantage, that when a sheet of core is bent out-of-plane, it produces the anticlastic or saddle shaped curvature shown in Fig.1.3. This is because the effective in-plane Poisson's ratio of the honeycomb structure, in common with that of nearly all known materials, is positive.

The first attempt to overcome this problem was made by Dufay Ltd. during the 1950's (May, 1957). A flexible paper core was produced for use in radomes etc. by making the length of the glued joints in the honeycomb only half the core thickness enabling the top of the joint to open when the core was bent to shape. Three methods are used commercially today. Firstly changing the cell angle; eg. by

over expanding the core to give square or rectangular cells enables cylinders to be generated. Secondly incorporating corrugations in the cell wall makes the core more flexible eg. Double-flex™ Fig.1.4 allowing compound curves to be formed. It should be noted however, that even this type of core will naturally assume an anticlastic curvature when bent out of plane. Compound curvatures can only be achieved by forcing the core to the required shape, a process made easier by the corrugations in the cell walls.

The third method is to machine a block of conventional, hexagonal cell honeycomb to the required contours but this is obviously expensive both in material and machining time.

Synclastic curvatures will only occur naturally if the core structure has a negative Poisson's ratio. This is achieved by making the cells re-entrant in shape as shown in Fig.1.5. The synclastic curvature is an obvious benefit and although the theoretical behaviour of such structures have been examined (Almgren, 1985., Evans, 1990., Warren, 1990), very little experimental work has been carried out on re-entrant celled honeycombs.

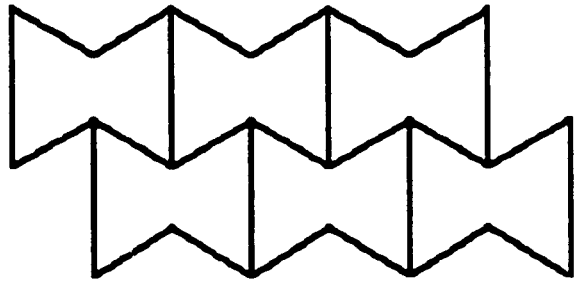

Fig.1.5. *A network made up from re-entrant cells.*

1.5 Aim and scope of this research

The primary purpose of the research presented in this thesis was to investigate the properties of the re-entrant celled honeycomb using both mathematical modelling

and practical experimentation and comparing them with those of the more conventional hexagonal celled honeycomb.

Existing work studying the properties of 2-D honeycombs is reviewed in the following chapter. Extending this work, models for the deformation mechanisms of stretching and hinging are developed and combined with the existing flexure model to produce a general deformation model in chapter 3. The behaviour of the separate models is investigated in chapter 4 by varying the cell geometry. Chapter 5 describes the experimental techniques used for determining the properties of both re-entrant and hexagonal celled honeycombs and the results of these tests are presented in chapter 6. These results are analysed in chapter 7 and a more general discussion on the benefits and applications of the re-entrant structure is contained in chapter 8. Finally conclusions from the research and some ideas for future work are listed in chapter 9.

References

ALMGREN,R.F.,
Journal of Elasticity,
Vol.15, Pages 427-429, 1985.

CADDOCK,B.D., EVANS,K.E. & MASTERS,I.G.,
"Proceedings of the 8th International Conference on Composite Materials",
SAMPE Publications, Covina (1991)

COLUCCI,F.,
Aerospace Composites and Materials,
Vol.2 No.1 Mar - Apr 1990. Pages 44-47. Shephard Press Ltd.

EVANS,K.E.,
Chemistry and Industry,
Pages 654-657, 1990.

GIBSON,L.J. & ASHBY,M.F.,
"Cellular Solids: Structure and Properties".
a) Chapter 9, Page 241.
b) Chapter 4, Pages 97-98.
Pergamon Press, Oxford (1988).

GIBSON,L.J., ASHBY,M.F., SCHAJER,G.S. & ROBERTSON,C.I.
Proceedings of the Royal Society, London,
Vol.A382, Page 25. 1982.

GILLIS,P.P.,
Carbon,
Vol. 22, Pages 387-391. 1984.

GORDON,J.E.,
"Structures".
Chapter 13, Pages 295-296.
Penguin, London (1991).

HARDY,M.J.,
"The de Havilland Mosquito",
Chapter 1, Page 17.
David & Charles, London (1977)

JOHNSON,A.F. & SIMS,G.D.
Composites,
Vol.17 No.4. Pages 321-328. 1986.

MASTERS,I.G. & EVANS,K.E.,
"Proceedings of the 2nd Canadian Conference on Composite Materials",
CACSMA, Montreal, 1993.

MAY,G.,
U.K. Patent 591,772
August 1947.

MAY,G.
"Paper, plastics and weight saving construction in aircraft".
International Conference of Dufaylite Licensees and users, London. 15-16 May, 1957. Pages 7-8.
Dufaylite Developments Ltd..

MIDDLETON,D.H. (Editor),
"Composite materials in Aircraft Structures".
Chapter 1, Page 1-3.
Longman, U.K. (1990).

PARKER,I.
Aerospace Composites and Materials,
Vol.2 No.5 Nov - Dec 1990. Pages 32-35.
Shephard Press Ltd.

RAO,H.M.
Popular Plastics,
May 1978. Pages 27-31.

WARREN,T.L.,
Journal of Applied Physics,
Vol.67, No.12. Pages 7591-7594, 1990.

WEI,G.,
Journal of chemical physics
Vol.96, Pages 3226-3233, 1992.

WOOD,R. (Editor),
Advanced Composites Engineering,
March 1989. Pages 13-16.
The Design Council and The British Plastics Federation, London.

2) LITERATURE REVIEW

2.1 Introduction

The hexagonal cell structure is commonly found throughout nature from the bee's honeycomb to the structure of balsa wood (Easterling *et al.*, 1982) and cork (Gibson *et al.*,1981). When honeycombs began to be manufactured artificially the hexagonal cell proved to be the cheapest and easiest cell shape to produce as described in chapter 1. The elastic behaviour of a sheet of honeycomb under an applied load is similar to that of a solid material. Using simple mechanics the elastic properties of the honeycomb structure can be related to the properties of the cell wall material and the cell geometry.

2.2 Relationship between the elastic constants

For an anisotropic 3-D solid the compliance matrix is made up of 21 elastic constants (Gibson, 1981). Honeycombs are anisotropic because of the 2-D arrangement of the cells: in the plane of the honeycomb the moduli are determined by the flexing, hingeing and stretching of the cell walls: normal to this plane they are determined by their axial extension or compression. A honeycomb however, has orthotropic symmetry meaning that the structure has three perpendicular mirror planes. This symmetry reduces the number of moduli and if the axes of loading are aligned with the normals to these planes the compliance matrix simplifies to a set of nine independent compliances (Eqn. 2.1)

$$\mathbf{S} = \begin{bmatrix} \frac{1}{E_1} & \frac{-\nu_{21}}{E_2} & \frac{-\nu_{31}}{E_3} & & & \\ \frac{-\nu_{12}}{E_1} & \frac{1}{E_2} & \frac{-\nu_{32}}{E_3} & & & \\ \frac{-\nu_{13}}{E_1} & \frac{-\nu_{23}}{E_2} & \frac{1}{E_3} & & & \\ & & & \frac{1}{G_{23}} & & \\ & & & & \frac{1}{G_{31}} & \\ & & & & & \frac{1}{G_{12}} \end{bmatrix} \qquad (2.1)$$

where E_i=Young's modulus in direction i.

G_{ij}=Shear modulus in plane ij

ν_{ij}=Poisson's ratio in plane ij due to load applied in direction i.

2.3 Out of plane shear modulus

Early work on the properties of honeycomb cores concentrated on the out of plane shear and compression properties since in their primary use as sandwich panel cores a high shear strength is essential to produce a stiff rigid beam (Allen, 1969).

Kelsey *et al.* (1958) used unit load and unit displacement methods to derive expressions for the through thickness shear modulus of a hexagonal celled honeycomb core. Comparison of the two methods determined a set of upper and lower limits which defined the shear modulus. They established that the shear modulus was a function of direction in which the shear forces were applied across the cells and achieved good agreement between the theory and experimental results obtained using commercially available hexagonal cell honeycomb.

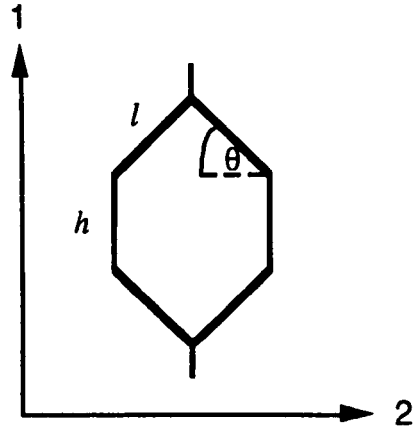

Fig.2.1 *The hexagonal cell of depth b showing the nomenclature used to describe its geometry.*

The shear modulus expressions derived by these workers are quite complicated and cumbersome but a simplified expression has been developed by Gibson *et al.* (1988a) using a strain energy method. Again upper and lower bounds are defined in the two orthogonal directions.

Using the nomenclature shown in Fig.2.1 the upper limits are

$$\frac{G_{13}}{G_s} \leq \frac{(h/l + 2\sin^2\theta)}{2(h/l + \sin\theta)\cos\theta} \times \frac{t}{l} \qquad (2.2)$$

and

$$\frac{G_{23}}{G_s} \leq \frac{\cos\theta}{(h/l + \sin\theta)} \times \frac{t}{l} \qquad (2.3)$$

Where G_s = Shear modulus of cell wall material

G_{13} = Shear modulus of cellular structure in direction 1

G_{23} = Shear modulus of cellular structure in direction 2

Comparison of equations (2.2) and (2.3) with the results of Kelsey *et al.* (1958) for aluminium and steel honeycombs show good agreement (Gibson, 1988a). (Using $-\theta$ in these equations gives results for a re-entrant cell structure).

It has been observed experimentally (Reichard,1972) that the shear modulus in direction 2 is approximately 40% lower than that in direction 1, the ribbon direction. At first this does not appear to agree with the theory of Gibson since when equations (2.2) and (2.3) are evaluated for regular hexagonal cells i.e. $h=l$ and $\theta=30^\circ$, we obtain the result

$$\frac{G_{13}}{G_s} = \frac{G_{23}}{G_s} = 0.577\left(\frac{t}{l}\right) \qquad (2.4)$$

If however the double wall thicknesses in direction 1 are allowed for then equation (2.2) becomes

$$\frac{G_{13}}{G_s} \leq \frac{(h/l + \sin^2\theta)}{(h/l + \sin\theta)\cos\theta} \times \frac{t}{l} \qquad (2.5)$$

Substituting $h/l=1$ and $\theta=30^{o}$ into this equation gives

$$\frac{G_{13}}{G_s} = 0.962\left(\frac{t}{l}\right) \qquad (2.6)$$

or $G_{23} \approx 0.6G_{13}$ as stated by Reichard.

If expressions (2.3) and (2.5) are equated it is possible to obtain the conditions required for uniform modulus in both the 1 and 2 directions. For an hexagonal array with $h/l = 1$ then $\theta=24^{o}$. This is greater than the angle of 15^{o} suggested by Kelsey *et al.* (1958) to obtain isotropy in the plane.

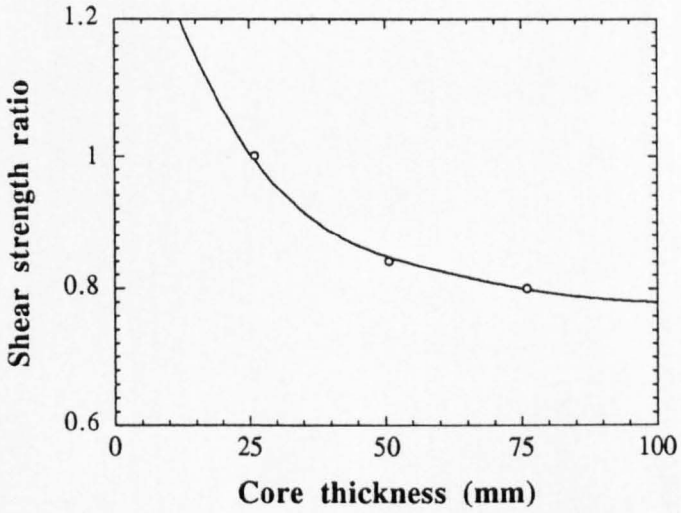

Fig.2.2 *Graph of shear strength ratio vs. core thickness for paper honeycomb used in the American construction industry (Reichard, 1972).*

Equations (2.3) and (2.5) imply that the shear modulus is independent of the thickness b of the core material. It should be noted however, that work carried out in the U.S.A. (Reichard, 1972), on paper honeycombs used in the construction industry, has shown that the shear strength is dependent on the core thickness, particularly when b is small (Fig.2.2).

Chang *et al.* (1961) studied the effect of the cell geometry on the shear modulus of sandwich panel cores. They made six basic assumptions to enable them to describe the behaviour of the honeycomb.

(1) The cell walls of the core behave elastically

(2) No buckling of the cell wall occurs

(3) The geometrical shape of the cell remains the same in each plane parallel to the sandwich faces, although displaced.

(4) The bond between the two cell walls is perfect.

(5) The direction of the applied load shear force is the same as the direction of the shear displacement.

(6) The thickness t of the cell wall is much smaller than the characteristic dimensions l. The bond length h is also much larger than t. The thickness of the core b should also be larger than t.

By considering the deflection of a plane parallel to the basal plane of the cell, through an angle ϕ, the expression derived for the relative shear modulus for a load applied in the ribbon direction (direction 1) is

$$\frac{G_{13}l}{Gt} = \frac{h/l + \sin^2\theta}{\cos\theta(h/l + \sin\theta)} \qquad (2.7)$$

and direction 2 is

$$\frac{G_{23}l}{Gt} = \frac{\cos\theta}{h/l + \sin\theta} \qquad (2.8)$$

These are identical solutions to the upper limits derived by Gibson when allowing for the double wall thickness in direction 1 (Eqns 2.3 and 2.5).

2.4 Core density

Chang *et al.* (1961) went on to describe how the core density is dependent on the cell geometry. In their calculations they have allowed for both the double wall thickness in the 1 direction and also the mass and thickness of the adhesive used to bond the foil sheets together.

Their expression for the relative core density is

$$\frac{\rho_{core}}{\rho_s} \times \frac{l}{t} = \frac{1 + \frac{h}{l}\left(1 + \frac{1}{2} \times \frac{\rho_{bond}}{\rho_s} \times \frac{t_{bond}}{t}\right)}{\cos\theta\left(\frac{h}{l} + \sin\theta\right)} \tag{2.9}$$

where ρ_{bond}=density of adhesive

t_{bond}=bond thickness

ρ_s=density of cell wall material

If we assume that the bond thickness is negligible then this expression is simplified to

$$\frac{\rho_{core}}{\rho_s} = \frac{t}{l} \times \frac{(1 + h/l)}{\cos\theta\left(h/l + \sin\theta\right)} \tag{2.10}$$

The equivalent expression derived by Gibson *et al.* (1988b) is

$$\frac{\rho_{core}}{\rho_s} = \frac{(2 + h/l) \times t/l}{2\cos\theta\left(h/l + \sin\theta\right)} \tag{2.11}$$

which reduces to Eqn. 2.10 when the double wall thickness is taken into consideration.

2.5 Out-of-plane Young's modulus

When a honeycomb is loaded in a direction parallel to the axis of the cells (i.e. direction 3 perpendicular to the page in Fig.2.1) the cell walls are extended or compressed elastically and no bending occurs. This makes the moduli much larger than those calculated for the in-plane loading.

As shown by Gibson *et al.* (1988a) the modulus E_3 of a honeycomb is just the modulus E_s of the cell wall material scaled by the area of the load bearing section i.e.

$$\frac{E_3}{E_s} = \left[\frac{h/l + 2}{2(h/l + \sin\theta)\cos\theta}\right]\frac{t}{l} = \frac{\rho_{core}}{\rho_s} \approx \frac{t}{l} \tag{2.12}$$

for cells of uniform wall thickness. Similarly if we have double wall thicknesses in direction 1 then

$$\frac{E_3}{E_s} = \left[\frac{h/l + 1}{(h/l + \sin\theta)\cos\theta}\right]\frac{t}{l} = \frac{\rho_{core}}{\rho_s} \qquad (2.13)$$

If the cell walls are considered to behave as plates constrained along two edges lying parallel to the direction of a compressive load, then the load at which elastic buckling occurs is given by

$$P_{elastic} = \frac{K E_s}{(1 - \nu_s^2)} \times \frac{t^3}{l} \qquad (2.14)$$

Gibson *et al.* (1988c) suggest that the constant K=4 for a honeycomb structure. Hence the stress at which elastic buckling occurs is

$$\frac{(\sigma_{elastic})_3}{E_s} \approx \frac{2}{(1 - \nu_s^2)} \times \frac{(l/h + 2)}{(h/l + \sin\theta)\cos\theta} \times \left(\frac{t}{l}\right)^3 \qquad (2.15)$$

Plastic collapse and failure of the honeycomb occurs when the stress in the plane perpendicular to the cell walls exceeds the yield stress σ_{ys} of the cell wall material (Gibson *et al.*, 1988d). This defines an upper limit of the plastic collapse strength of

$$\frac{[\sigma_{pl}]_3}{\sigma_{ys}} = \frac{(h/l + 2)}{2\cos\theta(h/l + \sin\theta)} \times \frac{t}{l} = \frac{\rho_{core}}{\rho_s} \qquad (2.16)$$

for honeycombs of uniform wall thickness. Wierzibicki's analysis gives an estimate of plastic buckling stress as

$$\frac{[\sigma_{pl}]_3}{\sigma_{ys}} \approx \frac{\Pi}{4} \times \frac{(h/l + 2)}{\cos\theta(h/l + \sin\theta)} \times \left(\frac{t}{l}\right)^2 \qquad (2.17)$$

2.6 Relationship between the elastic properties for a 2-D network

In the case of a 2-D cellular network like a honeycomb the stiffness in direction 3 is large and the resistance to shearing through the thickness is also great so that it can be assumed that

$$\frac{1}{E_3} = \frac{1}{G_{13}} = \frac{1}{G_{23}} = 0 \qquad (2.18)$$

When a load is applied in the 1 or 2 directions forces and displacements perpendicular to the plane i.e. in direction 3 are negligible so the honeycomb can be considered to be under plane stress conditions. Hence

$$-\frac{\nu_{13}}{E_1} = -\frac{\nu_{23}}{E_2} = -\frac{\nu_{31}}{E_3} = -\frac{\nu_{32}}{E_3} = 0 \tag{2.19}$$

which reduces the number of independent constants to four. The compliance matrix thus becomes

$$\mathbf{S} = \begin{bmatrix} \frac{1}{E_1} & \frac{-\nu_{21}}{E_2} & & & \\ \frac{-\nu_{12}}{E_1} & \frac{1}{E_2} & & & \\ & & - & & \\ & & & - & \\ & & & & - \\ & & & & \frac{1}{G_{12}} \end{bmatrix} \tag{2.20}$$

A core comprising regular hexagonal cells (Fig. 2.1) is isotropic in the plane (Lempriere 1968, Gibson *et al.* 1988e) which further simplifies the matrix so the relationship

$$G = \frac{E}{2(1+\nu)} \tag{2.21}$$

is obeyed. However, in nearly all commercially available honeycombs these ideal conditions are rarely achieved because of the double wall thickness in the 1 or ribbon direction, and the considerable variation in the cell angles. As a result the in-plane shear modulus G_{12} remains independent of E_1, E_2, ν_{12} and ν_{21}.

2.7 In-plane Young's modulus

The first work to look at the in-plane properties of honeycombs (Abd El-Sayed *et al.*, 1979) was based on the assumption that the double-thickness walls (h in Fig.2.1) remain straight when a load is applied and that the single-thickness cell walls l deform by flexure. Using a free energy method, the displacements of the centre points of the single-thickness cell walls can be determined and the Young's modulus calculated. Considering elastic deformation alone the expressions for the Young's moduli in orthogonal directions are

$$E_1 = \frac{2E_s t^3(h/l + \sin\theta)}{l\cos\theta(2l^2\cos^2\theta + 2t^2\sin^2\theta + th\cos\theta)} \tag{2.22}$$

and

$$E_2 = \frac{E_s t^3}{(h + l\sin\theta)(l^2 + t^2)\cos\theta} \tag{2.23}$$

Gibson *et al.* (1982, 1988f) also calculated the moduli by assuming flexure of the cell walls but only considered the case of all cell walls being of uniform thickness t. Each cell wall is imagined to behave like a beam guided and loaded at one end and using simple mechanics the relative displacement of one end of the beam to the other can be calculated. From these deflections the strains induced in the cell and hence the moduli of the network can be calculated for uniaxial loading. This gives the somewhat simpler expressions

$$E_1 = \frac{E_s(h/l + \sin\theta)t^3}{l^3\cos^3\theta} \tag{2.24}$$

$$E_2 = \frac{E_s t^3\cos\theta}{l^3(h/l + \sin\theta)\sin^2\theta} \tag{2.25}$$

Gibson (1981) extended the original flexure model to include stretching and shear deflections of the cell walls, but these refinements where found to provide negligible improvement due to the non regularity of the cells in commercial honeycombs. Equations 2.24 and 2.25 have been shown to give good agreement with experimental results for both metal and rubber honeycombs (Gibson *et al.*,

1982., Gibson *et al.*, 1988f).

2.8 In-plane Shear modulus

The in-plane shear modulus G_{12} is derived by noting that because of symmetry there is no relative movement of the points A, B and C in Fig.2.3 (Gibson *et al.* 1982)

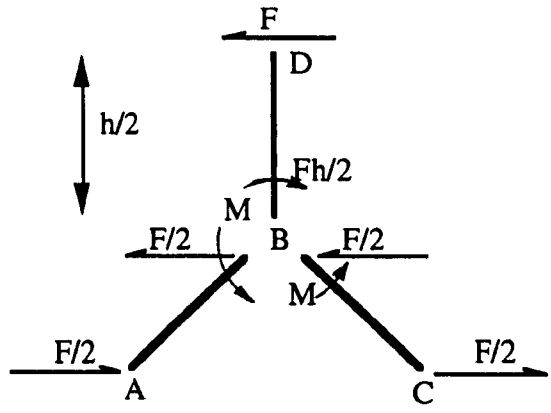

Fig.2.3 *Forces acting on the unit cell of an hexagonal cell honeycomb due to in-plane shear in direction 2.*

All the shear deflection is entirely due to the bending of the beam BD and its rotation about the point B. Assuming BD behaves as a cantilever the deflection, due to shear, of the mid-point of the cell wall length h can be calculated.

The angular rotation is obtained by treating the cell wall l as an encastré beam when the supports move. The expression obtained for shear modulus is

$$\frac{G_{12}}{E_s} = \left(\frac{t}{l}\right)^3 \frac{h/l + \sin\theta}{(h/l)^2(1 + 2h/l)\cos\theta} \qquad (2.26)$$

For commercial honeycombs it can be assumed that the double thickness walls in the ribbon direction do not flex (Klintworth *et al.*, 1987) so equation (2.26) is modified to

$$\frac{G_{12}}{E_s} = \frac{t^3(h/l + \sin\theta)}{h^2 l \cos\theta} \qquad (2.27)$$

2.9 In-plane Poisson's ratio

The Poisson's ratio ν is simply the ratio of the lateral or transverse strain ε_T and longitudinal strain ε_L developed in a body when it is subjected to a uniaxial stress (Hearn, 1982) i.e.

$$\nu = - \frac{(\varepsilon_T)}{(\varepsilon_L)} \tag{2.28}$$

For nearly all known materials ε_T is of opposite sign to ε_L so, for convenience the mathematical definition of Poisson's ratio includes a negative sign to make the ratio a positive value. Obviously a material which deforms such that ε_T and ε_L are of the same sign will produce a Poisson's ratio of negative value.

The Poisson's ratio is a specific characteristic of a material and as such is one of the elastic constants. Poisson himself tried to relate ν to the material microstructure (Rothenburg *et al.*, 1991) by considering a material made up of randomly packed smooth spheres interacting by forces acting along the line connecting the centres of the spheres. For this system he showed that $\nu = 0.25$. Strain energy methods show that for an isotropic solid $-1 \leq \nu \leq 0.5$.

During the early use of synthetic, cellular core materials it became apparent that the effective Poisson's ratio of a honeycomb structure could be much larger than those encountered in conventional materials, depending upon the shape and orientation of the cells. Poisson's ratios for commercially available honeycombs have been evaluated using a strain energy method (Hoffman, 1957) by assuming the walls of the cell to be 'S' shaped elements which, under small elastic deformations deformed by bending alone. A similar approach was used by Abd El-Sayed (1979) and again by Gibson *et al.* (1982) and both derived the following expression for the ratios ν_{12} and ν_{21} which is identical to the solution obtained by Hoffman.

$$\nu_{12} = \frac{1}{\nu_{21}} = \frac{\sin\theta\left(h/l + \sin\theta\right)}{\cos^2\theta} \tag{2.29}$$

Hoffman and Gibson showed that for certain geometries the Poisson's ratio can greatly exceed 1. As the Poisson's ratios in the plane are the same for either tensile or compressive loading the bending of a slab of core material is analogous to the bending of a plate. Hoffman also shows that the effect of large variations in the effective Poisson ratio of the core was negligible upon the stiffness of a sandwich panel.

2.10 In-plane indentation

Klintworth *et al.* 1988 studied the behaviour of conventional hexagonal cell honeycombs under in-plane or transverse loads. The bulk of the work was concerned with the elastic and plastic buckling of the honeycombs under large deformations for which several modes were identified. However they confirmed that honeycombs under in-plane loads initially deform in a linear elastic manner described by the flexure model (eqns. 2.24, 2.25, 2.29 & 2.27). The limit of the elastic behaviour occurs when the cell structure looses its elastic stability or the yield strength of the solid is exceeded.

The same authors went on to study the in-plane indentation of honeycombs by a flat indenter (Klintworth *et al.*,1989). Again the prime area of interest was the elastic yield of the honeycomb. Under normal loading in both the 1 and 2 directions the honeycombs deformed in a linear elastic manner up to a yield point after which further deformation occurred by progressive collapse of bands of cells. The elastic stiffness was higher in direction 1 than direction 2 and the authors observed that the indentation hardness of Aeroweb specimens was 30% to 60% greater than the uniaxial strength as a result of the lateral expansion of the crushing bands and the constraint provided by the neighbouring cells.

Lakes *et al.*, 1993 investigated the indentation of conventional and re-entrant cell copper foams by a 3.3mm diameter flat ended indenter. Re-entrant foams were observed to yield at stresses higher than those for conventional foams of the same

density despite being more compliant.

Little work seems to have been carried out concerning the indentation of cellular networks by spherical or hemispherical indenters. The initial elastic response of honeycombs loaded in-plane can possibly be related to the Hertz equation (Tabor, 1951) originally derived to describe the penetration of an isotropic elastic surface by an elastic ball.

$$a = \left[\frac{3}{4} W g r \left(\frac{1-\nu_B^2}{E_B} + \frac{1-\nu_M^2}{E_M}\right)\right]^3 \qquad (2.30)$$

where a = diameter of indentation

W = applied load

g = acceleration due to gravity

r = radius of ball

ν_B= Poisson's ratio of ball

E_B= Modulus of ball

ν_m= Poisson's ratio of material

E_m= Modulus of material

If the ball is considered to be infinitely stiff and we assume that a thin section of honeycomb deforming under a semi-circular indenter behaves in the same way as a surface under a ball then the equation 2.30 can be rewritten in terms of the load and depth of indentation d.

$$W = \frac{\left[8hr - 4d^2\right]^{1/6}}{\left[\frac{3}{4} g r \left(\frac{1-\nu_M^2}{E_M}\right)\right]} \qquad (2.31)$$

2.11 Out-of-plane of curvature of honeycomb plates

Hoffman (1957) observed that identical values of the Poisson's ratios ν_{12} and ν_{21} were obtained from both tensile and compressive tests on honeycombs. Hoffman

therefore believed it was acceptable to define the effective Poisson's ratio for a honeycomb in bending to be the same as that for axial loading, thus permitting an analogy between a slab of core material and a plate in bending.

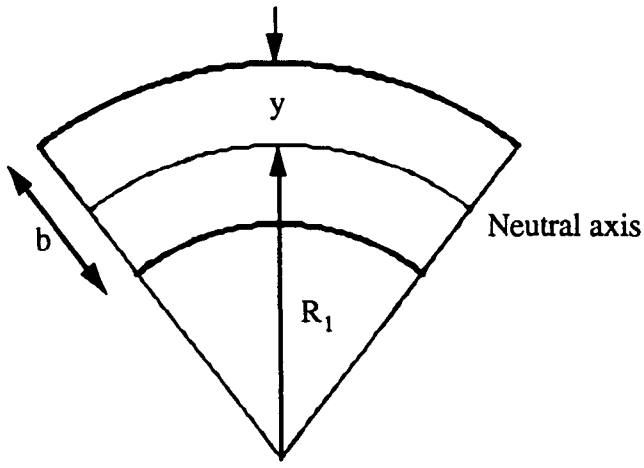

Fig.2.4 *Section of a beam subjected to pure bending*

When the beam shown in Fig.2.4 is bent the strain (ε) generated at a distance y from the neutral axis is given by

$$\varepsilon_1 = \frac{y}{R_1} = \frac{\sigma}{E} \tag{2.32}$$

where σ = stress at a distance y from the neutral axis

R_1 = radius of curvature

E = Young's modulus

This implies that

$$\frac{1}{R_1} = \frac{\varepsilon_1}{y} \tag{2.33}$$

The strain ε_1 induces a secondary strain ($-\nu\varepsilon_1$) at right angles to the beam which induces a curvature R_2 also at right angles to the beam such that

$$\frac{1}{R_2} = -\frac{\nu\varepsilon_1}{y} \tag{2.34}$$

If the radius of curvature in the plate is large, then conventional beam bending

theory is applicable. i.e. when a beam or plate is bent the radius of curvature R is related to the applied moment M by the expression (Hearn, 1981)

$$\frac{M}{EI} = \frac{1}{R} \tag{2.35}$$

where E = Young's modulus

I = Second moment of area

By considering an anisotropic plate subjected to moments M_1 and M_2 acting along adjacent edges it can be shown (Timoshenko, 1970., Evans, 1991a) that

$$M_1 = \frac{E_1 h^3}{12(1 - \nu_{12}\nu_{21})}\left(\frac{1}{R_1} + \frac{\nu_{21}}{R_2}\right) \tag{2.36}$$

$$M_2 = \frac{E_2 h^3}{12(1 - \nu_{12}\nu_{21})}\left(\frac{1}{R_2} + \frac{\nu_{12}}{R_1}\right) \tag{2.37}$$

If $M_2 = 0$ then M_1 generates a primary curvature R_1 and a secondary curvature $R_2 = - R_1/\nu_{12}$ and if $M_1 = 0$ then M_2 generates a primary curvature R_2 and a secondary curvature $R_1 = - R_2/\nu_{21}$. Thus it is possible to measure the Poisson's ratio of a core material by measuring the two radii of curvature of a sample (Caddock *et al.*, 1991).

Abd El-Sayed (1979) also investigated the out-of-plane bending of conventional honeycombs. He related the degree of bending to the torsional stiffness of the cell walls, since the walls of length l twist when the core is bent out-of-plane. Using a strain energy method for a regular hexagonal cell it is possible to relate the radii of curvature to the applied bending moment as follows,

$$\frac{1}{R_1} = \frac{M_2}{4\sqrt{3}G_s J} + \frac{M_1}{4G_s J} \tag{2.38}$$

and

$$\frac{1}{R_2} = \frac{M_2}{4\sqrt{3}G_s J} - \frac{M_1}{4G_s J} \tag{2.39}$$

where G_S=shear modulus of cell wall material

J=torsion constant

From these equations it can be inferred that for any values of M_1 and M_2

$$\frac{R_2}{R_1} = -1 \tag{2.40}$$

This agrees with the solution obtained from plate bending theory for a regular hexagon.

2.12 Re-entrant cellular honeycombs

Recent interest in materials with a negative Poisson's ratio, sometimes termed auxetic materials (Evans, 1991b), has returned attention to the re-entrant cell shape which has appeared several times in the patent literature during the last 30 years. Significantly, it has only appeared outside the patent literature in the last 5 years.

The first mention of a re-entrant celled honeycomb occurs in U.K.Patent 850,197 (and the equivalent U.S.Patent 3,018,205) filed by V.J.Barut and published in 1960. The re-entrant cell was perceived as the solution to three problems which had been identified with the conventional hexagonal cell honeycomb:-

a) Hexagonal cell honeycomb reduces in width with respect to the original block when expanded.
b) Expansion is not uniform, being more pronounced at the ends than at the centre.
c) The expanded core has a concave profile along its longitudinal edges.

Barut suggested using textile machinery to "box pleat" the material prior to bonding together in a stack. The increase in both length and width when a block of material, cut from the stack, is expanded is noted but this cell shape appears to have been suggested purely as an alternative route for producing irregular hexagonal cell honeycomb avoiding the problems mentioned in (a - c) above.

May (1965) suggested improvements on Barut's patents by scoring and folding slabs of the pleated material at 90° to the line of the pleats in U.K.Patent 992,117. This allowed automatic registration of the pleats in adjacent layers during the glueing process. No alternative methods for box pleating or potential uses of the re-entrant cell honeycomb were suggested.

In 1969 the United States Atomic Energy Commission obtained U.K.Patent 1,115,097 for a cellular core material which was sufficiently compliant to produce "complex geometrical shapes such as complete spheres or hollow toroids" from a flat sheet without crumpling or rupture of the honeycomb cell walls or glue lines. This again is done using a re-entrant cell structure generated by gluing together sheets of box pleated material. Reducing the width of the glue line in relation to the width of the pleat greatly enhances the flexibility.

The re-entrant structure appeared again in U.K.Patent 1,214,291, filed by Messrs. Molyneux and Smith in 1970, for the sole purpose of generating a synclastic curvature when bent out-of-plane thereby achieving greater structural efficiency in panels of compound curvature with reduced manufacturing costs.

The final mention in the patent literature of the re-entrant cell shape is in the U.K.Patent GB 2,195,953A (Saitoh *et al.*, 1988) which is nothing more than a series of modifications to Barut's patent 850,197, for the specific case of processing stainless steel. Several different cell shapes are achieved by altering the width of the glue lines and the positions of the fold lines. The re-entrant structure again is only used as a precursor to the production of irregular hexagonal cells and no mention is made of the enhanced flexibility resulting from this geometry.

Despite the number of patents published, two of which make specific reference to the synclastic curvature and great flexibility of the re-entrant structure, it appears that no such honeycombs have been produced on a commercial or even

development scale. The only experimental data available for a re-entrant structure is that of Gibson *et al.* (1988g), who measured the in-plane Poisson's ratios of a 2-D rubber network with the geometry h/l =2, θ=-30^0, and Lakes *et al.* (1993) who has investigated the properties of re-entrant cell 3-D foams.

2.13 Modelling of the re-entrant honeycomb

The re-entrant structure shown in Fig.2.5 has been identified by several workers (Almgren, 1985., Gibson *et al.* 1988g, Evans, 1990., Warren, 1990.) as producing a negative Poisson ratio.

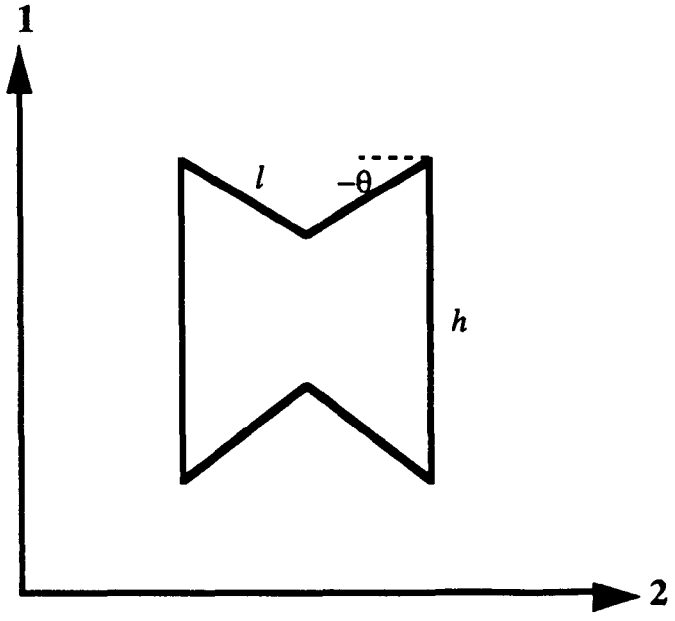

Fig.2.5 *Re-entrant cell structure with cell walls length h and l, cell angle* θ

Almgren used a 2-D array of rigid rods joined by elastic hinges, like that shown in Fig.1.5, from which a 3-D model with a negative Poisson's ratio is developed. He describes the latter as isotropic in its macroscopic elastic properties, but orthotropic would perhaps be a more accurate description. Almgren showed that the 2-D model is not isotropic in the plane although the properties in the 1 and 2 directions are equal i.e. $\nu_{12}=\nu_{21}=-1$ when h/l =2 and θ=-30^0. Evans (1991)

describes this condition as square symmetric since measuring Poisson's ratio along directions away from the principal axes yields values differing from -1. It should be noted that the same symmetry can be achieved with other combinations of h/l and θ.

To describe the deformation of 3-D foam structures Warren *et al.* (1987) and Warren (1990) used a combination of stretching and hingeing to develop a 3-D model for the Poisson's ratio of both hexagonal and re-entrant cell structures. Wei (1991) has generalised their models to describe the Poisson's ratios of polymer molecules. In these types of structures the orientations of the cells are random unlike the periodic honeycomb structures and consequently the results differ from those found in the more conventional 2-D models.

Milton (1992) has investigated producing composite structures which possess a negative Poisson's ratio. These basically consist of a deformable matrix containing an elastic network. The networks are made up of extensible but rigid beams. Several structures are suggested for the networks but nearly all consist of a hexagonal structure to ensure uniform dilation when an external load is applied since the rods can only deform by stretching. Again the hexagonal structure generates true isotropy. Deformation of these networks is only considered in a 2-D plane.

2.14 Graphite structure and molecular modelling

A natural example of a material possessing a hexagonal cell structure on a molecular scale is graphite. In the basal plane the atoms are arranged in a hexagonal structure with each atom connected by strong covalent bonds to three neighbours (Barrett *et al.*, 1980). The atom spacing within each layer is 0.14nm. The layers are bound together by weak Van der Waals forces and the separation is 0.33nm (Wyatt *et al.*, 1974) as shown in Fig.2.6.

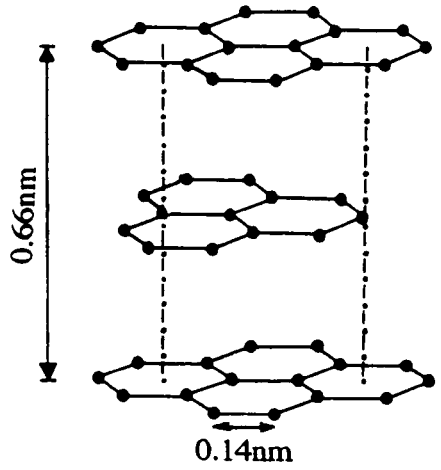

Fig.2.6 *The crystal structure of graphite*

The mechanical properties of graphite reflect the anisotropy of the structure with strength and stiffness being high in the direction parallel to the hexagonal planes but low in a perpendicular direction. Gillis (1984) quotes the measured elastic stiffness constants as:-

E_2 (parallel to hexagonal plane) = 1060 GPa

E_3 (perpendicular to hexagonal plane) = 36.5 GPa

Numerous workers have attempted to determine the elastic properties of graphite single crystals (Reynolds, 1968., Blackman, 1970) but it is not possible to measure all the elastic constants directly by experiment. The remainder must be computed from the stiffness and compliance matrices.

A theoretical model has been proposed (Gillis, 1984) which accurately reproduces three of the four independent elastic constants (including the shear modulus) using a stretching force constant and a bending force constant. A more detailed description of the force constants is given in Chapter 3 but briefly the stretching force constant relates the axial extension of an atomic bond to the force acting along its axis. The bending force constant is better described as a hinging

constant as it relates the change in cell angle to the force applied perpendicular to the cell wall which causes the angle change.

This model predicts that for a uniaxial load applied in direction 1 (Fig.2.1), parallel to the plane of hexagonal cells, the moduli are

$$S_{11} = \frac{1}{E_2} = \left(\frac{b\sqrt{3}}{24}\right)\left(\frac{18}{K_s} + \frac{6}{K_h}\right) \tag{2.41}$$

$$S_{22} = \frac{1}{E_1} = \left(\frac{b\sqrt{3}}{24}\right)\left(\frac{18}{K_s} + \frac{6}{K_h}\right) \tag{2.42}$$

$$S_{66} = \frac{1}{G_{21}} = b\sqrt{3}\left(\frac{1}{K_s} + \frac{1}{K_h}\right) \tag{2.43}$$

using the nomenclature defined in Fig.2.1. K_s and K_h are the stretching and hinging constants respectively.

Gillis (1984) observed that in the graphite structure three times as much deformation is caused by bond stretching as by changes in the bond angles since valence angle deformation is greatly stiffened by the network structure. This is an interesting observation since, as will be shown in chapter 3, a regular hexagon deforming by stretching due to an in-plane, uniaxial load has a negative Poisson's ratio. Gillis did not evaluate the in-plane Poisson's ratio and it is not recorded if direct measurement has yielded a negative value for this particular elastic constant in graphite.

Other workers (Nkansah *et al.*, 1994) using finite element analysis to model the deformation of closed cell molecular structures, of the type shown in Fig.2.7, have only compared their results to the flexure model and do not appear to have considered stretching or hinging as possible mechanisms. Baughman (1993), using similar techniques to Nkansah *et al.*, has designed a hypothetical carbon phase incorporating a bond which acts like a hinge. The molecules have been shown to have a negative Poisson's ratio and also a negative volumetric thermal expansion coefficient.

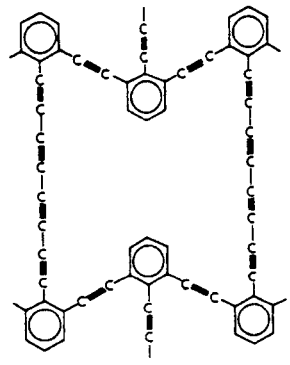

Fig.2.7 *Closed cell molecular structure of the type modelled by Nkansah, et al. 1994.*

References

ABD EL-SAYED,F.K., JONES.R.J. & BURGESS,I.W.,
Composites,
Pages 209-214, October 1979.

ALLEN,H.G.,
"Analysis and design of structural sandwich panels",
Chapter 1, Pages 1-2.
Pergamon Press Ltd., London (1969).

ALMGREN, R.F.,
Journal of Elasticity.
Vol.15, Pages 427-429, 1985.

BARRETT,C. & MASSALSKI,T.B.
"Structure of metals",
Pergamon Press, London (1980).

BARUT,V.J.,
U.K.Patent 850,197
October 1960.

BARUT,V.J.,
U.S.Patent 3,018,205
January 1962.

BAUGHMAN,R.H. & GALVAO,D.S.
Nature,
Vol. 365, Pages 735-737. (1993)

BLACKMAN,L.C.F. (Editor)
"Modern aspects of graphite technology",
Academic Press, London (1970).

CADDOCK,B.D., EVANS,K.E. & MASTERS,I.G.,
"Proceedings of the 8th International Conference on Composite Materials",
SAMPE Publications, Covina (1991).

CHANG,C.C., & EBCIOGLU,I.K.
Journal of Basic Engineering.
Pages 513-518, December 1961.

EASTERLING,K.E., HARRYSSON,R.,GIBSON,L.J. & ASHBY,M.F.
Proceedings of the Royal Society, London,
Vol. A383, Pages 31-41, 1982.

EVANS, K.E.,
Chemistry & Industry.,
Pages 654-657, 1990.

EVANS,K.E.[a]
Composite Structures
Vol.17, Pages 95-111, 1991.

EVANS,K.E.[b],
Endeavour,
Vol.15 No.4, Pages 170-174, 1991.

EVANS, K.E. & NKANSAH.M.A.,
Nature
Vol. 353, Page 124, 1991.

GIBSON, L.J.
"Elastic and plastic behaviour of cellular materials"
Ph.D Thesis (Cambridge)1981

GIBSON, L.J. & ASHBY, M.F.
"Cellular Solids : Structure & Properties",
a) Chapter 4, Pages 106-109.
b) Chapter 4, Page 76.
c) Chapter 4, Pages 109-111.
d) Chapter 4, Pages 111-112.
e) Appendix, Pages 345-349.
f) Chapter 4, Pages 77-81.
g) Chapter 4, Page 82.
Pergamon Press, London, (1988).

GIBSON,L.J., ASHBY, M.F., SCHAJER,G.S. & ROBERTSON,C.I.
Proceedings of the Royal Society, London,
Vol.A382, Page 25. 1982.

GIBSON,L.J., EASTERLING,K.E. & ASHBY,M.F.
Proceedings of the Royal Society, London,
Vol. A377, Pages 99-117, 1981.

GILLIS,P.P.,
Carbon,
Vol.22, Pages 387-391. 1984.

HEARN, E.J.
"Mechanics of Materials", Vol.1,
Chapter 4, Page 61,
Pergamon Press, London, (1981).

HOFFMAN, G.A.,
Report P-946,
Rand Corporation (1957).

KLINTWORTH,J.W. & STRONGE,W.J.,
International Journal of Mechanical Science,
Vol.30 No.3/4, Pages 273-292, 1988.

KLINTWORTH,J.W. & STRONGE,W.J.,
International Journal of Mechanical Science,
Vol.31 No.5, Pages 359-378, 1989.

KELSEY,S., GELATELY,R.A. & CLARK,B.W.
Aircraft Engineering
Pages 294-302,1958.

LAKES,R.S. & ELMS,K.,
Journal of Composite Materials,
Vol.27 No.12, Pages 1193-1202, 1993.

LEMPRIERE, B.M.,
AAIA Journal,
Vol.6 No.11, Pages 2226-7, 1968.

MAY,G.,
U.K.Patent 992,117
May 1965.

MILTON,G.W.,
Journal of Mechanics and Physics of Solids,
Vol. 90 No.5, Pages 1105-1137, 1992.

MOLYNEUX,W.G. & SMITH,G.E.,
U.K.Patent 1,214,291
December 1970.

NKANSAH,M., EVANS,K.E. & HUTCHINSON,I.J.
Modelling Simulation in Materials Science and Engineering,
Vol.2,. Pages 337-352. 1994

REICHARD,T.W.
National Bureau of Standards, Washington D.C.
Building Science Series No.43, April 1972.

REYNOLDS,W.N.
"Physical properties of graphite",
Elsevier Publishing Co., London (1968).

ROTHENBERG, L., BERLIN,A.A. & BATHURST,R.J.
Nature,
Vol. 354, Page 470, 1991.

SAITOH,Y. & TATSUMI,T.
U.K.Patent 2,195,953A
April 1988.

TABOR,D.,
"Hardness of metals",
Chapter 4, Page 44,
Clarendon Press. (1951).

TIMOSHENKO,S.P. & GOODIER,J.N.
"Theory of Elasticity" (3rd Ed.),
Chapter 9, Pages 288-90.
McGraw-Hill, (1970).

U.S.A.E.C.,
U.K.Patent 1,151,097
May 1969

WARREN,T.L.
Journal of Applied Physics,
Vol.67 No.12. Pages 7591-7594, 1990.

WARREN,W.E. & KRAYNIK,A.M.
Mechanics of materials
Vol. 6,Pages 27-37, 1987.

WEI,G.
Journal of chemical physics
Vol. 96, Pages 3226-3233, 1992.

WYATT,O.H. & DEW-HUGHES,D.
"Metals ceramics and polymers",
Cambridge University Press, London. (1974).

3) MODELS FOR THE DEFORMATION OF HONEYCOMBS

3.1 Introduction

As previously mentioned there are three principal mechanisms by which a 2-D honeycomb structure can deform, namely flexing and stretching of the cell walls or hinging of the cell wall junctions. Stretching and hinging have tended to be disregarded in relation to honeycomb core materials since the popular 'Flexure' model developed by Gibson *et al.* (1982, 1988a) has given good agreement with experimental data. However, this model has been shown (Evans *et al.* 1991) to consistently over estimate the the values of Poisson's ratio ν for theoretical molecular networks when compared with a molecular mechanics approach. This phenomenon has been attributed to the fact that stretching (and rotation) of the molecular chains, which tend to increase longitudinal deformation at the expense of transverse, are not accounted for by the flexure model.

Several workers have considered both stretching and hinging mechanisms for modelling deformations on a molecular scale. The model derived by Gillis (1984) for the hexagonal structure of graphite, combines these two mechanisms, and is particularly suitable for application to periodic network structures such as honeycombs. Gibson *et al.* (1988b) considered flexing and stretching of the cell walls for a honeycomb under biaxial stress, whilst Jones *et al.* (1991) have combined bending and stretching to describe the elasticity of rigid, disordered, 3D molecular networks.

In this chapter the stretching and hinging elements of the Gillis model are separated out and expanded to allow for other cell geometries. To aid comparison of the three models it is useful to write them in terms of force constants K_i. This also facilitates combining the three mechanisms to produce a general equation which describes the deformation of a 2-D honeycomb by any one, or combination of the three mechanisms i.e. flexure, stretching and hinging.

Graphs of the elastic constants vs. cell angle for each model have been generated for the specific case $h/l = 2$ which enables plots to be made for the full range of cell angles from -90^{o} to $+90^{o}$. The effects of varying the h/l and t/l ratios are considered in chapter 4.

The relative importance of the three mechanisms of deformation are then considered in relation to both conventional and auxetic phenomena. The importance of these considerations is highlighted with regard to the important technological problem of producing doubly curved honeycomb cores for sandwich panels and to the problem of deformation in auxetic molecular structures.

3.2 Force Constants

The elastic constants of a honeycomb can be derived by considering the displacement of a single cell, from which the honeycomb is produced by translational repetition, under appropriate loading conditions. In order to provide a general form of the model, use is made of force constants for the behaviour of the cell walls.

The force constants relate the displacement of the cell wall of a honeycomb to the applied force which causes it. For all three deformation models the force constant is defined by the general relationship

$$F = K_i \delta \qquad (3.1)$$

where F = Force applied

K_i = Force constant appropriate to the mode of deformation

δ = Displacement

The force constant contains details of the mechanical properties of the network structure itself. For example, in a molecular network K_i can be related directly to the atomic force constants. The conventional case of a macroscopic honeycomb of cell wall lengths l and h, thickness t and depth b (see Fig.2.1) is considered here and it is assumed that the elastic constants of the material forming the cell

walls are known; E_s being the Young's modulus and G_s being the shear modulus. Explicit relationships between K_i and the properties of the cell wall can therefore be derived for each of the deformation mechanisms of flexure, stretching and hinging.

3.2.1 Flexure force constant K_f

A cell wall of length l deforming by flexing can be likened to a cantilever beam loaded and guided at one end and fixed at the other (Gibson *et al.* 1982). The deflection of the guided end due to flexing is given by Roark *et al.* (1976) as

$$\delta = \frac{Ml^2}{12E_sI} \tag{3.2}$$

where M = Applied moment = Fl

I = Second moment of area of cell wall = $bt^3/12$

Therefore

$$\delta = \frac{Fl^3}{E_s bt^3} \tag{3.3}$$

Comparing this with equation (3.1) gives

$$K_f = \frac{E_s bt^3}{l^3} \tag{3.4}$$

3.2.2 Stretching force constant K_s

The extension of a cell wall, length l, due to the axial force F acting along it, is

$$\delta = \frac{Fl}{bt\,E_s} \tag{3.5}$$

Comparing this with equation (3.1) gives

$$K_s = \frac{bt\,E_s}{l} \tag{3.6}$$

3.2.3 Hinging force constant K_h

Finally, for a cell deforming by hinging, we assume that the cell wall is rigid along its length and deflection occurs at the junction with other cell walls by a

change of angle $\Delta\theta$. Hence

$$\delta = l \sin\Delta\theta \approx l\,\Delta\theta \tag{3.7}$$

if $\Delta\theta$ is small. Substituting into the general formula (equation 3.1) gives

$$F=K_h l\,\Delta\theta \tag{3.8}$$

The actual mechanism by which hinging occurs can be envisaged as one of two processes; global shear or local bending.

In global shear the relationship of K_h to material parameters is obtained by assuming that hinging occurs by shearing of the material at the cell wall junction (Fig.3.1).

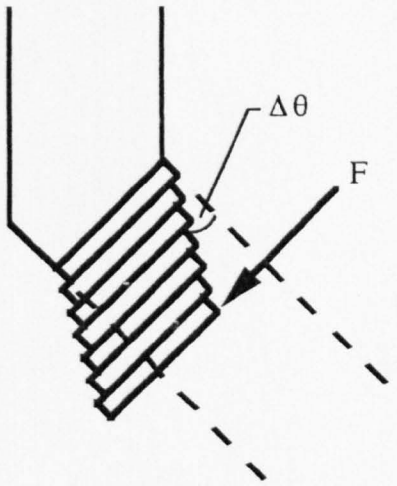

Fig.3.1 *Schematic diagram of hinging by shearing of the cell wall.*

Using the standard definition of shear modulus we can say

$$G_S = \frac{F}{bt\,\Delta\theta} \tag{3.9}$$

where G_S is the shear modulus of the cell wall material and F is the force applied perpendicular to the beam. Again comparing with equation (3.8) gives

$$K_h = \frac{G_S bt}{l} \tag{3.10}$$

The shear mechanism is important when considering small celled foams and molecular networks but is unrealistic for the macro networks, like the honeycombs considered in this thesis, where hinging is obviously a local effect. To model the latter type of behaviour we can imagine the hinge to be a short curved beam, of axial length q, in the vicinity of the cell node (Fig.3.2)

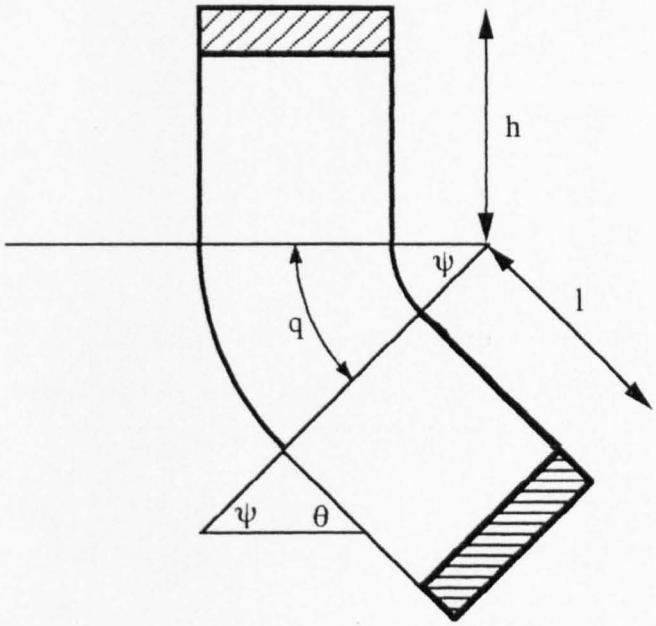

Fig.3.2 *Schematic diagram of hingeing achieved by local bending of the cell wall*

Assuming that a curved beam behaves in accordance with simple bending theory (Roark *et al.* 1965) then the change in angle ψ to ψ' due to an applied moment M is given by

$$\psi-\psi'=\Delta\psi=\int_0^q \frac{M}{E_sI}dq \tag{3.11}$$

i.e.
$$\Delta\psi=\frac{Mq}{E_sI} \tag{3.12}$$

But as can be seen from Fig.3.2, $\psi=90-\theta$ and $\psi'=90-\theta-\Delta\theta$. Hence we can say

$$\Delta\theta=\frac{Mq}{E_sI} \tag{3.13}$$

where θ is the cell angle.

If $q<<l$ then the moment acting on the hinge is approximately

$$M \approx \frac{Fl}{2} \tag{3.14}$$

Hence

$$\Delta\theta = \frac{Fl\,q}{2E_s I} \tag{3.15}$$

Comparing this with equation (3.8) and substituting for I we obtain

$$K_h = \frac{E_s b t^3}{6l^2 q} \tag{3.16}$$

Note that when q tends to l we do not achieve the global shear expression (Eqn.3.10) due to the different boundary conditions.

3.3 Flexure Model

Using the geometric configuration and co-ordinate system of Fig.3.3, Gibson and Ashby assumed that deformation occurred by flexing of the cell walls when an external load was applied.

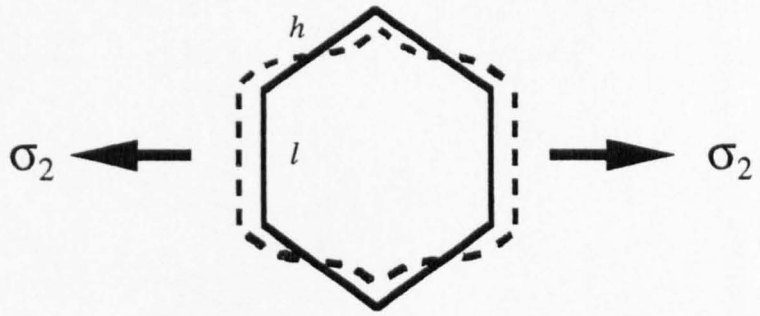

Fig.3.3 *Hexagonal cell deforming by flexure when a tensile load is applied in direction 2*

Treating the cell walls as beams and using simple mechanics they were able to derive the following equations for the elastic properties of honeycombs.

$$E_1 = \frac{E_s t^3(h/l + \sin\theta)}{l^3\cos^3\theta} \tag{3.17}$$

$$E_2 = \frac{E_s t^3\cos\theta}{l^3(h/l + \sin\theta)\sin^2\theta} \tag{3.18}$$

$$\nu_{12} = \frac{\sin\theta(h/l + \sin\theta)}{\cos^2\theta} \tag{3.19}$$

$$\nu_{21} = \frac{\cos^2\theta}{(h/l + \sin\theta)\sin\theta} \tag{3.20}$$

$$G_{12} = \left(\frac{t}{l}\right)^3 \frac{E_s(h/l + \sin\theta)}{(h/l)^2(1+ 2h/l)\cos\theta} \tag{3.21}$$

Where E_1, E_2, ν_{12}, ν_{21} and G_{12} are the elastic constants for the honeycomb; E_s etc. are the elastic constants for the material constituting the honeycomb.

An auxetic honeycomb is produced by the simple expedient of making θ negative (see Fig.2.5).

This model has been shown to be very successful for modelling a great variety of conventional honeycombs and reticulated foams (Gibson *et al.* 1988). To enable direct comparisons to be made with the other models presented here it is convenient to rewrite the moduli equations as

$$E_1 = \frac{K_f(h/l + \sin\theta)}{b\cos^3\theta} \tag{3.22}$$

$$E_2 = \frac{K_f\cos\theta}{b(h/l + \sin\theta)\sin^2\theta} \tag{3.23}$$

$$G_{12} = \frac{K_f(h/l + \sin\theta)}{b(h/l)^2(1+ 2h/l)\cos\theta} \tag{3.24}$$

where K_f is the flexural force constant (q.v. Section 3.2.1), combining the details

of the deformation of the cell wall itself within a single constant. Graphs for the flexure model when h/l =2 are shown in Fig.3.4.

N.B. Gibson *et al.* (1982) has shown that the Young's moduli and Poisson's ratio expressions for the flexure model comply with the reciprocal relation $E_1\nu_{21}=E_2\nu_{12}$ derived from linear elasticity theory.

(a)

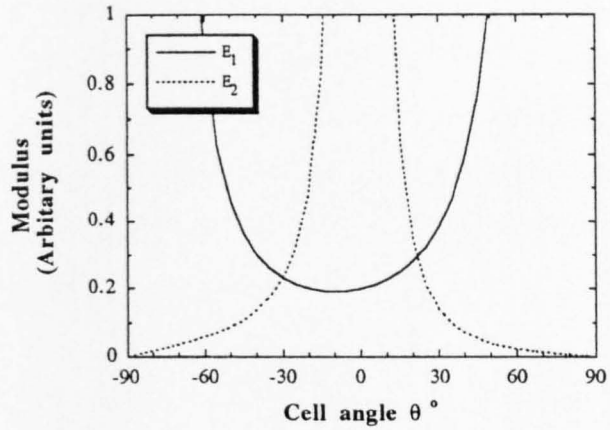

(b)

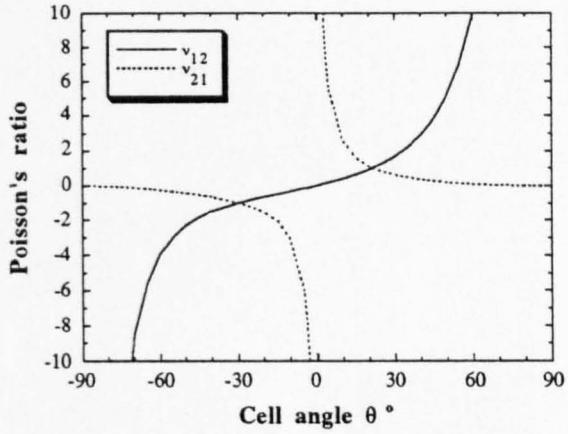

(c)

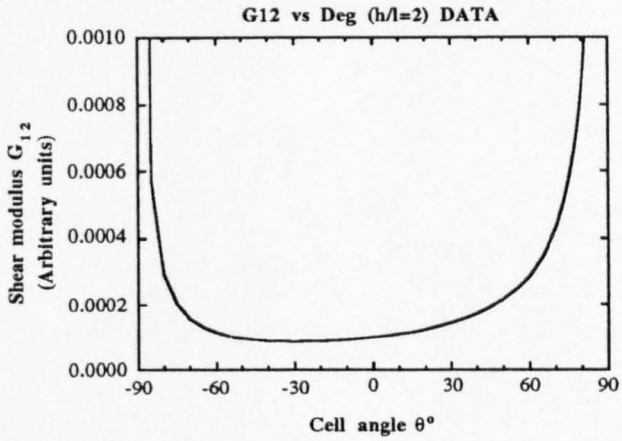

Fig.3.4 *Theoretical plots for the flexure model when h/l=2*
(a) Modulus vs. cell angle derived from equations (3.22) and (3.23)
(b) Poisson's ratio vs. cell angle derived from equations (3.19) and (3.20)
(c) Shear modulus vs. cell angle derived from equations (3.24)

3.4 Stretching

This model assumes that the cell walls, like the shock absorber model used by Rothenberg *et al.* (1991), are only able to deform by stretching along their axes with no change in angle. A model was constructed from perspex tubes, rods and springs to demonstrate this type of behaviour and is shown in Fig.3.5. The top right hand corner shows the displacement occurring in both directions 1 and 2 when the model is pulled in direction 1

Consider a hexagonal cell (Fig.3.6) subjected to a tensile load σ_2 in the 2 direction.

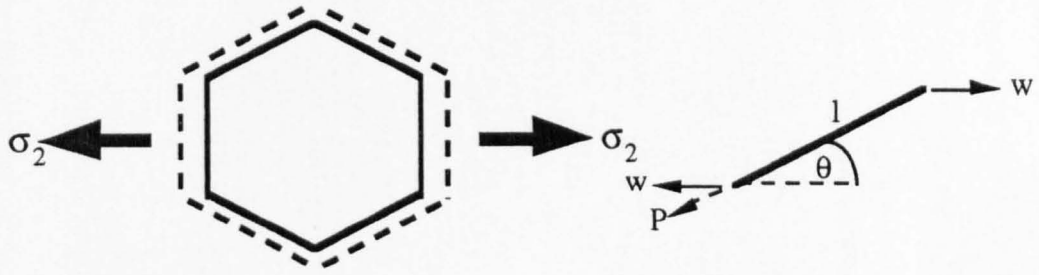

Fig.3.6 *Hexagonal cell deforming by stretching of the cell walls due to tensile load applied in direction 2.*

The load acting on the unit cell due to the applied stress σ_2 is $w=b\,(l\sin\theta + h)\sigma_2$ and the component P of w acting along the cell wall of length l is

$$P=b\,\sigma_2(l\sin\theta+h)\cos\theta \tag{3.25}$$

But $P=K_S\delta$ where K_S is the force constant for stretching, therefore

$$\delta_1=\frac{b\,\sigma_2\cos\theta(l\sin\theta+h)}{K_s} \tag{3.26}$$

The strain ε_2 in the 2 direction caused by the extension δ_1 is

$$\varepsilon_2=\frac{b\,\sigma_2\cos\theta(h/l+\sin\theta)}{K_s} \tag{3.27}$$

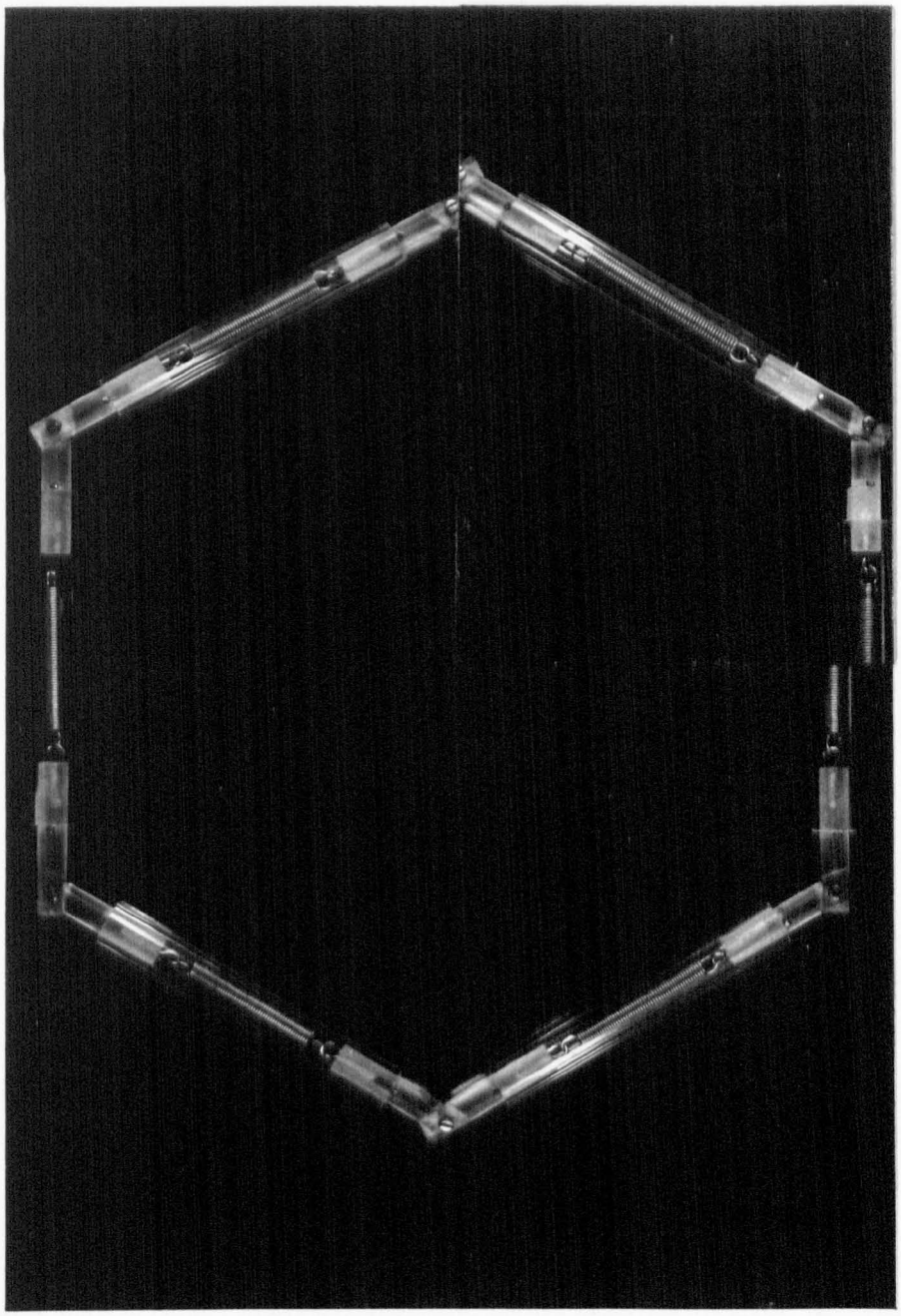

Fig.3.5 *Model constructed from perspex rods, tubes and springs to demonstrate deformation of a cell by stretching alone. The top right hand corner shows the effect of loading the frame in direction 1.*

Therefore the modulus in direction 2 is

$$E_2=\frac{K_s}{b\cos\theta\left(h/l+\sin\theta\right)} \tag{3.28}$$

The strain in the 1 direction due to the extension δ_1 is

$$\varepsilon_1=\frac{b\,\sigma_2\cos\theta\sin\theta}{K_s} \tag{3.29}$$

The Poisson's ratio is therefore

$$\nu_{21}=-\left(\frac{\sin\theta}{\sin\theta+h/l}\right) \tag{3.30}$$

By considering the forces acting on the cell edge when loaded in direction 1 (Fig.3.7) similar equations can be derived.

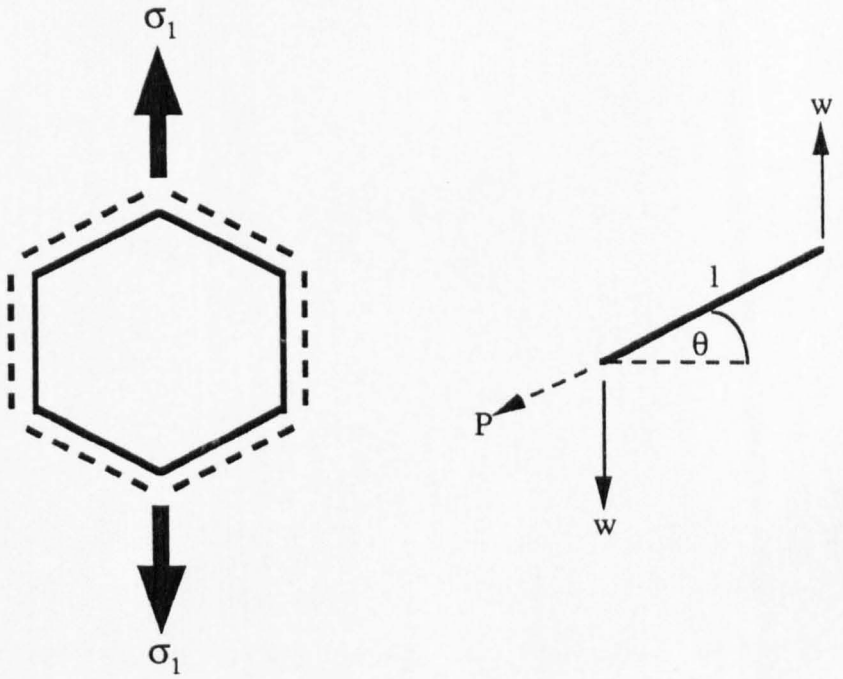

Fig.3.7 *Hexagonal cell deforming by stretching of the cell walls due to a tensile load applied in direction 1.*

However, in this orientation it should be noted that the cell walls of length h also extend. The force constant (K_s^h) for these walls is

$$K_s^h = \frac{E_s b t}{h}$$

Comparison with equation 3.6 enables us to write K_s^h in terms of K_s i.e.

$$K_s^h = \left(\frac{l}{h}\right) K_s$$

and thus the strain in direction 1 is given by

$$\varepsilon_1 = \frac{2b\,\sigma_1 h\cos\theta}{l\,K_s(h/l + \sin\theta)} + \frac{(b\,\sigma_1 l\cos\theta\sin\theta)\sin\theta}{l\,K_s(h/l + \sin\theta)}$$

$$\varepsilon_1 = \frac{b\,\sigma_1\cos\theta(2h/l + \sin^2\theta)}{K_s(h/l + \sin\theta)} \qquad (3.31)$$

The strain in the 2 direction is

$$\varepsilon_2 = \frac{b\,\sigma_1\cos\theta\sin\theta}{K_s} \qquad (3.32)$$

The modulus in the 1 direction is therefore

$$E_1 = \frac{K_s(h/l + \sin\theta)}{b\cos\theta(2h/l + \sin^2\theta)} \qquad (3.33)$$

and the Poisson's ratio is

$$\nu_{12} = \frac{-\sin\theta(h/l + \sin\theta)}{2h/l + \sin^2\theta} \qquad (3.34)$$

Note that when θ is positive, i.e. the cell is hexagonal in shape, both ν_{12} and ν_{21} are negative in value. Substituting $(-\theta)$ into these equations produces the equivalent expressions for the re-entrant cell. It should also be noted that in the re-entrant case the direction of the forces in the walls of length l is reversed whilst the forces in the other walls remain unchanged. Unlike the other models the relationship

$$\nu_{12} = \frac{1}{\nu_{21}}$$

does not apply except for specific conditions e.g. $h/l = 1$, $\theta = 30^{o}$ and $h/l = 2$, $\theta = 0^{o}$. The reciprocal relation $\nu_{12}E_2 = \nu_{21}E_1$ however, holds true for all cell geometries.

Gibson *et al.* (1988b) derived Young's moduli and Poisson's ratio expressions for a hexagonal cell honeycomb subjected to a biaxial stress deforming by both flexure and stretching of the cell walls. It can be shown (Appendix 1) that for the conditions of a uniaxial applied stress and deformation only occurring by stretching that these equations reduce to 3.28, 3.33, 3.30 and 3.34.

The in-plane shear modulus can be obtained by considering the shear stresses acting on the cell node shown in Fig.3.8.

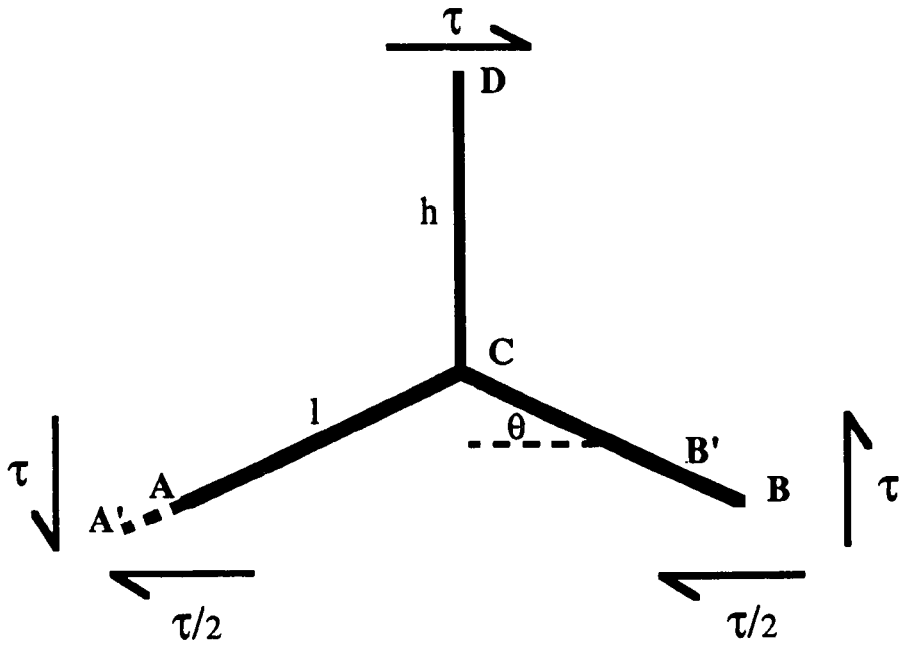

Fig.3.8 *In-plane shear deformation of the unit cell due to stretching of the cell walls.*

The horizontal shear stress τ acting on the unit cell is given by the expression

$$\tau = \frac{F_2}{2lb\cos\theta} = \frac{F_1}{(h + l\sin\theta)b} \tag{3.35}$$

where F_1 and F_2 are the forces acting in the 1 and 2 directions respectively. Re-arranging this equation enables F_1 to be written in terms of F_2 i.e.

$$F_1 = \frac{F_2(h + l\sin\theta)}{2l\cos\theta} \tag{3.36}$$

If F_2=F then

$$\tau_2 = \frac{F}{2lb\cos\theta} \tag{3.37}$$

and

$$\tau_1 = \frac{F(h + l\sin\theta)}{2l\cos\theta} \times \frac{1}{(h + l\sin\theta)b} = \frac{F}{2lb\cos\theta} \tag{3.38}$$

The component P^* of F_2 acting along member AC is given by

$$P^* = \frac{F\cos\theta}{2} \tag{3.39}$$

and the component P^{**} of F_1 acting along AC is

$$P^{**} = F_1\sin\theta = \frac{F(h + l\sin\theta)\sin\theta}{2l\cos\theta} \tag{3.40}$$

The total force P acting along AC is therefore

$$P = P^{**} + P^*$$

$$P = \frac{F\cos\theta}{2} + \frac{F(h + l\sin\theta)\sin\theta}{2l\cos\theta} \tag{3.41}$$

The point A moves an amount δ_{AC} to A' due to the force P. This extension is obtained from the expression for the stretching constant K_s (Eqn.3.6)

$$\delta_{AC} = \frac{P}{K_s} \tag{3.42}$$

Substituting for P gives

$$\delta_{AC} = \frac{F}{2K_s}\left[\cos\theta + \frac{(h + l\sin\theta)\sin\theta}{l\cos\theta}\right] \tag{3.43}$$

The horizontal deflection δ_2 due to the extension δ_{AC} is given by

$$\delta_2 = \delta_{AC}\cos\theta$$

$$\delta_2 = \frac{F}{2K_s}\left[\cos^2\theta + \frac{(h + l\sin\theta)\sin\theta}{l}\right] \tag{3.44}$$

The vertical deflection δ_1 across the unit cell is

$$\delta_1 = 2\delta_{AC}\sin\theta \tag{3.45}$$

The factor of 2 arises because the member CB shortens as much as AC extends.

Therefore

$$\delta_1 = \frac{F\sin\theta}{K_s}\left[\cos\theta + \frac{(h + l\sin\theta)\sin\theta}{l\cos\theta}\right] \tag{3.46}$$

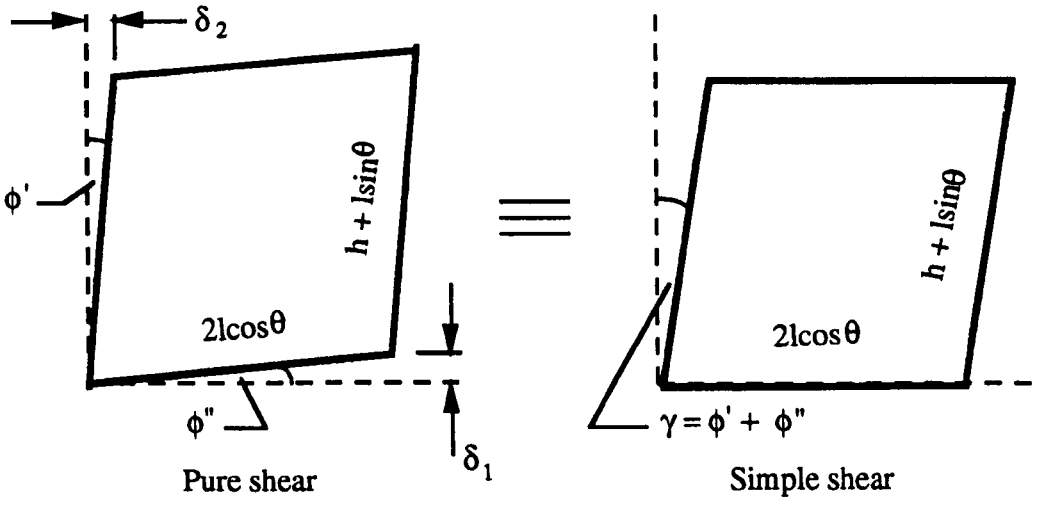

Fig.3.9 *The relationship between pure shear and simple shear.*

If the unit cell is considered to deform by simple shear then, as can be seen from Fig 3.9, the shear strain γ is given by

$$\gamma = \frac{\delta_1}{2l\cos\theta} + \frac{\delta_2}{h + l\sin\theta} \tag{3.47}$$

$$\gamma = \frac{F}{2K_s}\left[\cos\theta + \frac{(h + l\sin\theta)\sin\theta}{l\cos\theta}\right]\left[\frac{(\cos\theta)}{h + l\sin\theta} + \frac{(\sin\theta)}{l\cos\theta}\right] \tag{3.48}$$

The shear modulus G is the ratio of the shear stress and the shear strain i.e.

$$G = \tau/\gamma \tag{3.49}$$

Therefore

$$G_{12} = \frac{K_s}{b}\left[\frac{l\cos\theta(h + l\sin\theta)}{(l\cos^2\theta + (h + l\sin\theta)\sin\theta)^2}\right] \tag{3.50}$$

Graphs for the stretching model are shown in Fig.3.10.

For a regular hexagon equation 3.5 reduces to

$$G_{12} = \frac{K_s}{b\sqrt{3}}$$

which is the same result as obtained from Gillis' graphite model (Eqn.2.38) when $K_h = \infty$, i.e. when only stretching occurs.

(a)

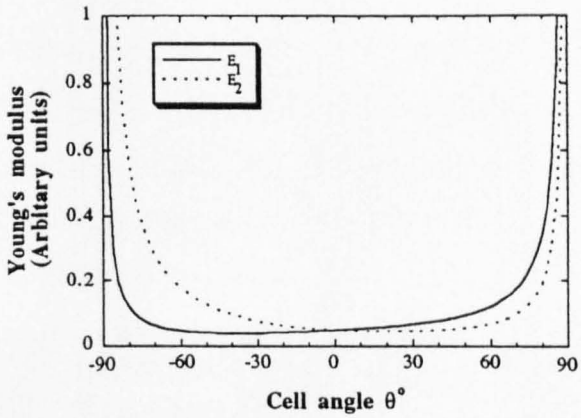

(b)

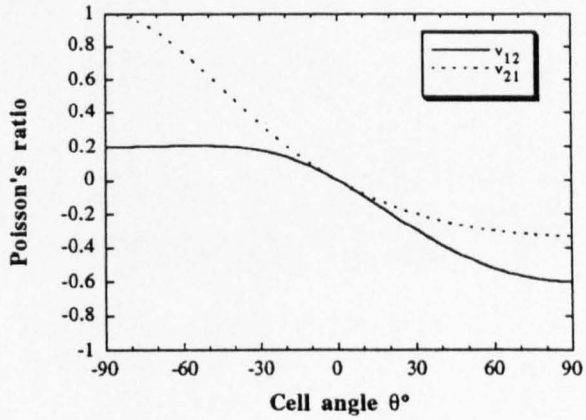

(c)

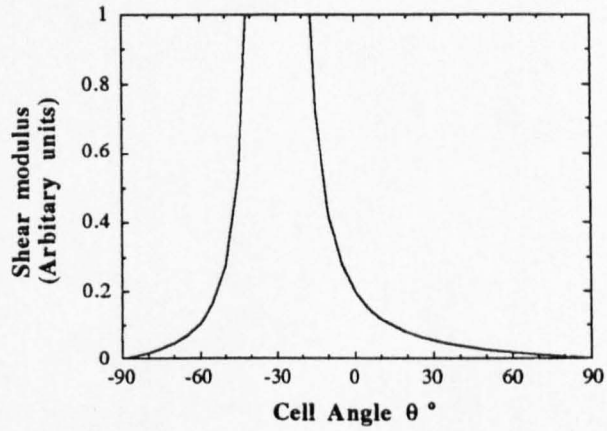

Fig.3.10 *Theoretical plots for the stretching model*
(a) *Modulus vs. cell angle derived from equations (3.28) and (3.33)*
(b) *Poisson's ratio vs. cell angle derived from equations (3.30) and (3.34)*
(c) *Shear modulus vs. cell angle derived from equation (3.50)*

3.5 Hinging

The hinging model relies on the cell walls being stiff in both the axial and transverse directions. Elastic hinges at the joints enable the cell to deform when a load is applied and restore the cell to its original shape when the load is removed. The cell deforms by changes in the cell angle alone. Fig.3.11 shows the cell of a cardboard honeycomb deforming by hinging.

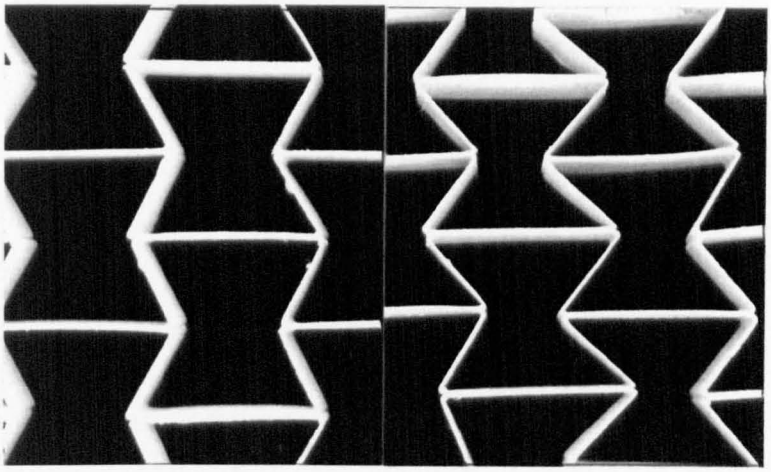

Fig.3.11 *Re-entrant cardboard cells unloaded (left) and deforming by hinging due to load applied in direction 2 (right).*

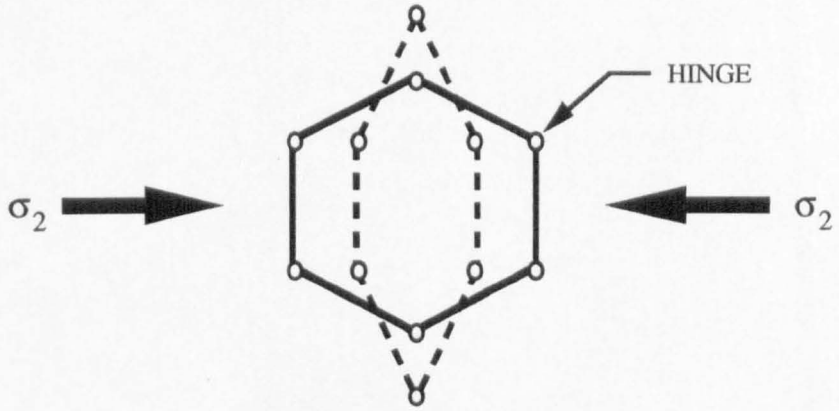

Fig.3.12 *Hexagonal cell deforming by hinging due to load applied in direction 2.*

Consider a hexagonal cell as shown in Fig.3.12. If we assume that the material from which the cell is manufactured has a 'Force Constant' K_h which determines the deflection δ, caused when a load is applied to the cell wall (Fig 3.13),

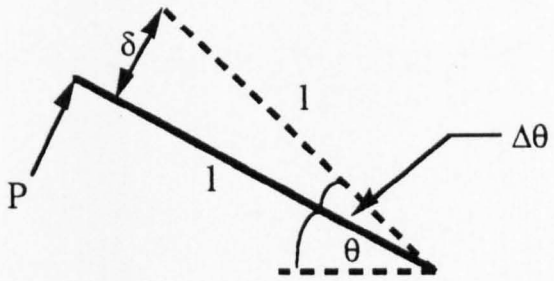

Fig.3.13 *The hinging mechanism.*

we can say that

$$P=K_h\delta \tag{3.51}$$

where P=Applied Load

δ=Deflection

If the cell is subjected to a compressive load in direction 2 then the forces acting on the cell edge of length l are given by

$$P=W\sin\theta \tag{3.52}$$

where $W=\sigma_2(h + l\sin\theta)b$

b= Honeycomb thickness

Substituting for P and W gives

$$\delta=\frac{\sigma_2 bl\sin\theta(h/l + \sin\theta)}{K_h} \tag{3.53}$$

The strain in direction 2 is therefore given by

$$\varepsilon_2=\frac{-\sigma_2 b\sin^2\theta(h/l + \sin\theta)}{K_h\cos\theta} \tag{3.54}$$

and the modulus in direction 2 by

$$E_2=\frac{K_h\cos\theta}{b\sin^2\theta(h/l + \sin\theta)} \tag{3.55}$$

The strain in direction 1 is

$$\varepsilon_1=\frac{\sigma_2 b\ \sin\theta\cos\theta}{K_h} \tag{3.56}$$

and hence the Poisson's Ratio in the 2 direction is

$$\nu_{21}=\frac{-\varepsilon_1}{\varepsilon_2}$$

$$=\frac{\cos^2\theta}{(h/l\ +\sin\theta)\sin\theta} \tag{3.57}$$

If the honeycomb is compressed in direction 1 then by a similar method we can determine that

$$\varepsilon_2=\frac{\sigma_1 b\ \cos\theta\sin\theta}{K_h} \tag{3.58}$$

$$\varepsilon_1=\frac{-\sigma_1 b\ \cos^3\theta}{K_h(h/l\ +\sin\theta)} \tag{3.59}$$

$$E_1=\frac{K_h(h/l\ +\sin\theta)}{b\ \cos^3\theta} \tag{3.60}$$

$$\nu_{12}=\frac{\sin\theta(h/l\ +\sin\theta)}{\cos^2\theta} \tag{3.61}$$

Comparing this result with the expression for ν_{21} we can see that

$$\nu_{12}=\frac{1}{\nu_{21}}$$

Again by substituting $(-\theta)$ into these equations we obtain expressions to describe the behaviour of a re-entrant cell.

As in the stretching model the in-plane shear modulus is obtained by considering the effects of the shear stresses τ acting along the sides of the unit cell in both the 1 and 2 directions (Fig.3.14). The cell walls are rigid so that no flexing or stretching occurs. All the movement occurs due to the hingeing at point C.

The point A is subjected to a force F_1 acting in direction 1 and a force F_2 acting in direction 2. As previously shown if

$$F_2 = F$$

then

$$F_1 = \frac{F(h + l\sin\theta)}{2l\cos\theta} \tag{3.62}$$

The component P^* of F_2 acting perpendicular to the member AC is given by

$$P^* = \frac{F\sin\theta}{2} \tag{3.63}$$

The component P^{**} of F_1 acting perpendicular to AC is given by

$$P^{**} = -F_1\cos\theta = -\frac{F(h + l\sin\theta)}{2l} \tag{3.64}$$

N.B. This expression is negative because P^{**} causes counter clockwise rotation of the member AC.

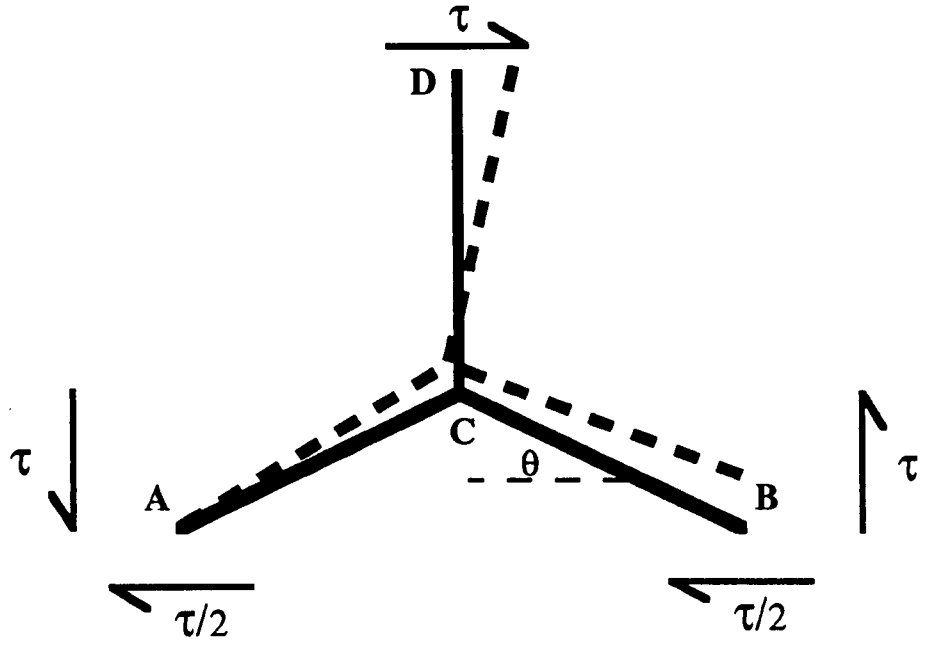

Fig.3.14 *In-plane shear due to hinging.*

The total force P acting perpendicular to the member AC is therefore

$$P = P^* + P^{**}$$

$$P = \frac{F}{2}\left[\sin\theta - \frac{(h + l\sin\theta)}{l} \right]$$

$$P = -\frac{Fh}{2l} \tag{3.65}$$

The force P rotates AC through an angle $\Delta\theta$ such that the point A is deflected an amount δ_{AC}. From Eqn.3.1 we know that

$$\delta_{AC} = \frac{P}{K_h} \tag{3.66}$$

The displacement in direction 2 due to δ_{AC} is

$$\delta_2^* = \delta_{AC}\sin\theta = \frac{P\sin\theta}{K_h} \tag{3.67}$$

and the horizontal displacement of point D due to the force F_2 is

$$\delta_2^{**} = \frac{F}{K_h^h} = \frac{F}{K_h C} \tag{3.68}$$

where C is a constant, enabling $K^h{}_h$, for a cell wall of length h, to be written in terms of K_h , the force constant for a wall length l. For the bending mechanism (eqn. 3.16) $C=(l/h)^2$ and for shear (eqn. 3.10) $C=l/h$. The total deflection in direction 2 is therefore

$$\delta_2 = \frac{P\sin\theta}{K_h} + \frac{F}{K_h^h} = \frac{F}{K_h}\left[\frac{-Ch\sin\theta + 2l}{2Cl}\right] \tag{3.69}$$

and the total displacement in direction 1 is

$$\delta_1 = \frac{2P\cos\theta}{K_h} = -\frac{Fh\cos\theta}{K_h l} \tag{3.70}$$

If we assume that the unit cell shown in Fig.3.14 deforms by simple shear then the shear strain γ is given by

$$\gamma = \frac{\delta_1}{2l\cos\theta} + \frac{\delta_2}{h + l\sin\theta}$$

$$\gamma = \frac{F}{2lK_h}\left[\frac{2l - Ch\sin\theta}{(h + l\sin\theta)} - \frac{h}{l}\right] \tag{3.71}$$

The remote shear stress τ is given by

$$\tau = \frac{F}{2lb\cos\theta} \tag{3.72}$$

Hence the shear modulus is

$$G_{12} = \frac{F}{2lb\cos\theta} \times \frac{2lK_h}{F}\left[\frac{Cl(h + l\sin\theta)}{Ch(h + l\sin\theta) + l(2l - Ch\sin\theta)}\right]$$

$$G_{12} = \frac{K_h}{b\cos\theta}\left[\frac{Cl(h + l\sin\theta)}{Ch(h + l\sin\theta) + l(2l - Ch\sin\theta)}\right] \tag{3.73}$$

Evaluating equation 3.73 for a regular hexagon give

$$G_{12} = \frac{K_h}{h\sqrt{3}}$$

which is the same result obtained from the Gillis graphite model when only hinging occurs. i.e. $K_s = \infty$

Graphs for the Young's moduli, Poisson's ratio and in-plane shear modulus obtained from the hinging model when $h/l = 2$ and $K_h = 1$ are shown in Fig.3.15. Compare these graphs with those for the flexure model shown in Fig.3.4. The Young's modulus plots are the same since we put $K_h = K_s = 1$ but in reality we would expect $K_s << K_h$ and hence the modulus would be proportionately lower. The Poisson's ratios are always identical and the shear modulus for hinging is significantly lower than that for flexure.

(a)

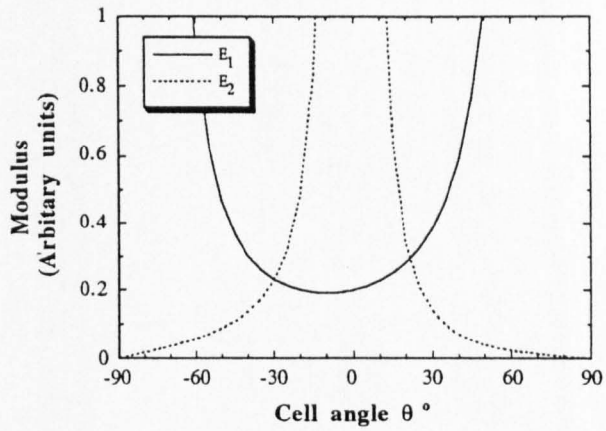

(b)

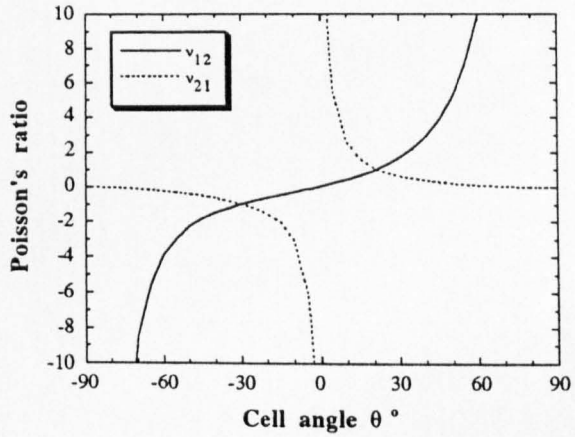

(c)

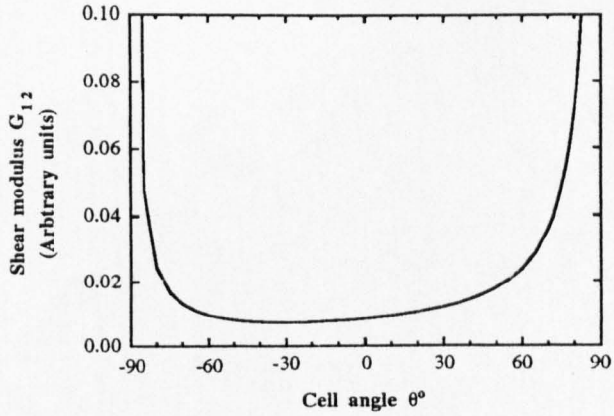

Fig.3.15 *Theoretical plots for the hinging model when h/l=2*
(a) Modulus vs. cell angle derived from equations (3.55) and (3.60)
(b) Poisson's ratio vs. cell angle derived from equations (3.57) and (3.61)
(c) Shear modulus vs. cell angle derived from equations (3.73)

	E_1	E_2	ν_{12}	ν_{21}	G
Flexure	$\frac{K_f(h/l + \sin\theta)}{b\cos^3\theta}$	$\frac{K_f\cos\theta}{b\sin^2\theta(h/l + \sin\theta)}$	$\frac{\sin\theta(h/l + \sin\theta)}{\cos^2\theta}$	$\frac{\cos^2\theta}{(h/l + \sin\theta)\sin\theta}$	$\frac{K_f l^2(h/l + \sin\theta)}{bh^2(2h/l + 1)\cos\theta}$
Stretching	$\frac{K_s(h/l + \sin\theta)}{b\cos\theta(2h/l + \sin^2\theta)}$	$\frac{K_s}{b\cos\theta(h/l + \sin\theta)}$	$\frac{-\sin\theta(h/l + \sin\theta)}{2h/l + \sin^2\theta}$	$\frac{-\sin\theta}{h/l + \sin\theta}$	$\frac{K_s}{b}\left[\frac{l^2\cos\theta(h/l + \sin\theta)}{(l\cos^2\theta + l(h/l + \sin\theta)\sin\theta)^2}\right]$
Hinging	$\frac{K_h(h/l + \sin\theta)}{b\cos^3\theta}$	$\frac{K_h\cos\theta}{b\sin^2\theta(h/l + \sin\theta)}$	$\frac{\sin\theta(h/l + \sin\theta)}{\cos^2\theta}$	$\frac{\cos^2\theta}{(h/l + \sin\theta)\sin\theta}$	$\frac{K_h}{b\cos\theta}\left[\frac{C(h/l + \sin\theta)}{2 + C(h/l)^2}\right]$

Table 3.1 *Summary of expressions for elastic constants obtained from the flexure, stretching and hinging models.*

3.6 A General Model

A summary of the equations derived for the elastic constants of each model is given in Table 3.1. By summing the deflections in directions 1 and 2, we can combine the three models to obtain a general model. For example, if we consider a honeycomb loaded in direction 1 then the strains in direction 1 arising from deformation by stretching and hingeing are given by equations 3.31 and 3.59. The strain in direction 1 caused by flexure of the cell walls has been shown by Gibson *et al.* (1982, 1988a) to be

$$\varepsilon_1=\frac{\sigma_1 b l^4 \cos^3\theta}{12E_s I(h+l\sin\theta)} \tag{3.74}$$

where I=Second moment of area of the cell wall. Rewriting this in terms of the force constant for flexure K_f (Eqn.3.4) gives

$$\varepsilon_1=\frac{\sigma_1 b\cos^3\theta}{K_f(h/l+\sin\theta)} \tag{3.75}$$

The total strain in direction 1, obtained by summing equations 3.31, 3.59 and 3.75, is thus

$$\varepsilon_1^{Total}=\left[\frac{\sigma_1 b\cos\theta}{h/l+\sin\theta}\right]\left[\frac{\cos^2\theta}{K_f}+\frac{\cos^2\theta}{K_h}+\frac{2h/l+\sin^2\theta}{K_s}\right] \tag{3.76}$$

The modulus in direction 1 is then given by

$$E_1=\frac{\sigma_1}{\varepsilon_1^{Total}}$$

hence

$$E_1=\frac{1}{\frac{b\cos\theta}{(h/l+\sin\theta)}\left[\frac{\cos^2\theta}{K_f}+\frac{\cos^2\theta}{K_h}+\frac{(2h/l+\sin^2\theta)}{K_s}\right]} \tag{3.77}$$

The strain in direction 2, due to flexing, arising from the applied stress σ_1 is given by the expression

$$\varepsilon_2=\frac{\sigma_1 b l^3 \cos\theta \sin\theta}{12 E_s I} \tag{3.78}$$

Writing in terms of the force constant this becomes

$$\varepsilon_2=\frac{\sigma_1 b \cos\theta \sin\theta}{K_f} \tag{3.79}$$

Summing this expression with 3.32 and 3.58 gives the total strain in direction 2

$$\varepsilon_2^{Total} = \sigma_1 b \cos\theta \sin\theta\left[-\frac{1}{K_f}-\frac{1}{K_h}+\frac{1}{K_s}\right] \tag{3.80}$$

Dividing this expression by 3.76 gives the Poisson's ratio

$$\nu_{12} = \frac{-\sin\theta}{(h/l + \sin\theta)}\left[\frac{-\frac{1}{K_f}-\frac{1}{K_h}+\frac{1}{K_s}}{\frac{\cos^2\theta}{K_f}+\frac{\cos^2\theta}{K_h}+\frac{2h/l+\sin^2\theta}{K_s}}\right] \tag{3.81}$$

Using a similar method the following general expressions can be obtained for E_2 and ν_{21}.

$$E_2 = \frac{1}{b\,(h/l + \sin\theta)\left[\frac{\sin^2\theta}{K_f\cos\theta}+\frac{\sin^2\theta}{K_h\cos\theta}+\frac{\cos\theta}{K_s}\right]} \tag{3.82}$$

$$\nu_{21} = \frac{\sin\theta.\cos\theta\left[\frac{1}{K_f}+\frac{1}{K_h}+\frac{1}{K_s}\right]}{(h/l + \sin\theta)\left[-\frac{\sin^2\theta}{K_f\cos\theta}-\frac{\sin^2\theta}{K_h\cos\theta}+\frac{\cos\theta}{K_s}\right]} \tag{3.83}$$

Gibson's expression for the shear strain written in terms of the flexure force constant is

$$\gamma=\frac{F h^2(l+2h)}{2K_f l^3(h + l\sin\theta)} \tag{3.84}$$

Summing this with expressions 3.47 and 3.71 the general shear modulus expression is obtained

$$G_{12} = \frac{1}{\left(\left[\frac{bh^2(l + 2h)\cos\theta}{K_f l^2 (h + l\sin\theta)} \right] + \frac{1}{K_h} \left[\frac{Ch^2 + 2l^2}{Cl(h + l\sin\theta)} \right] b\cos\theta \right) \left(+ \frac{b(l\cos^2\theta + (h + l\sin\theta)\sin\theta)}{K_s} \left[\frac{\cos\theta}{(h + l\sin\theta)} + \frac{\sin\theta}{\cos\theta} \right] \right)} \quad (3.85)$$

If, for example, we put $K_h=K_s=\infty$ the above equations reduce to those for the flexure model. Similarly putting $K_h=\infty$ we obtain a flexing and stretching model with identical solutions to those obtained when evaluating the Gibson's biaxial loading model (Appendix 1) for a uniaxial applied stress. It must be emphasised however that these expressions are only valid for small elastic displacements in which geometric nonlinearities can be ignored.

References

EVANS,K.E. and NKANSAH,S.C.,
Nature,
Vol. 353, Page 124, 1991.

GIBSON,L.J., and ASHBY,M.F.,
"Cellular Solids : Structure & Properties",
a) Chapter 4, Pages 76-82
b) Chapter 4, Pages 97-98
Pergamon Press Ltd., Oxford. (1988).

GIBSON,L.J., ASHBY,M.F., SCHAJER,G.S., and ROBERTSON,C.I.,
Proceedings of the Royal Society, London.
Vol.A382, Page 25. 1982.

GILLIS,P.P.,
Carbon,
Vol. 22, Pages 387-391. 1984.

JONES,J.L., BALL,R.C.,
Macromolecules,
Vol.24, Pages 6369-6377. 1991.

ROARK,R.J. and YOUNG,W.C.,
"Formulas for stress and strain", 5th Edn.
(McGraw-Hill, London, 1976)

ROTHENBERG,L., BERLIN,A.A. and BATHURST,R.J.,
Nature,
Vol.354, Pages 470-472, 1991.

4) THEORY DISCUSSION

4.1 Introduction

In the first part of this chapter the effects of variations in the cell geometry are investigated for each of the three models. The moduli E_1 and E_2, and the Poisson's ratios ν_{12} and ν_{21} are plotted against the cell angle θ for various values of h/l and t/l. To simplify the calculations the plots have been obtained by putting $E_s=h=l=b=1$ for various values t and putting $E_s=l=b=1$, $t=0.1$ for various values of h and using the shear model for hinging.

4.2 The force constants

The properties of the force constants K_f, K_s and K_h are compared in Fig.4.1 having evaluated the equations 3.4, 3.6 and 3.16 for the conditions:

$$E_s=l=b=1, \qquad G_s \approx E_s/3=1/3, \qquad q=l/10$$

The shear modulus of the bulk cell wall material $G_s \approx E_s/3$ is a general assumption for an elastic material and using this value we can evaluate the global shear model for K_h (Eqn.3.10). In reality to evaluate this shear model for K_h we need to know G_H, the shear modulus of the material in the "hinge", which is not necessarily the same as G_s and is likely to be considerably lower (see on). The local shear model for K_h (Eqn.3.16) is obtained directly from E_s. $l/10$ may at first appear to be rather large as an estimate for the effective length (q) of the hinge, but for the card honeycombs used in the experiments the folds were typically 1mm in width and l was a constant length of 10mm.

It is apparent from the three models discussed here that if the force constant K_i is high in value then the contribution of that particular mechanism to the overall deformation will be small. For the honeycombs used in these tests the value of t/l is in the range 0.01 to 0.02 so that K_s (Eqn.3.6) is large compared to K_f (Eqn.3.4) and K_h (Eqns.3.10 & 3.16) and stretching can be ignored (Fig.4.1).

Stretching only becomes a significant mechanism when $t/l > 1$.

K_f (Eqn.3.4) has the lowest value and thus explains why the flexure model has been so successful. However, as already stated the properties of the material operating as the hinge can be significantly different from those of the bulk cell wall material. If they are lower, as might be expected, due to local damage from the folding of the card then $K_h < K_f$ and hinging for example, will dominate as shown with the card honeycombs. Of the two proposed hinging mechanisms local hinging (Eqn.3.16) predominates over global shear deformation (Eqn.3.10) when $t/l < 0.2$.

4.3 Effects of cell geometry on the flexure model

Fig.4.2 shows the modulus E_1 plotted against the cell angle. Very high moduli are achieved when the cell angle is numerically large (i.e. $40^o \leq |\theta| \leq 90^o$) and the cell walls of length l become oriented parallel to the load direction. It is obvious that for hexagonal cells, as the h/l ratio is increased there is a significant increase in the value of E_1 particularly when the cell angle is large. The curves are all skewed to the left so that the minimum value of E_1 is achieved at $\theta = -5^o$ when $h/l = 3$ and $\theta = -10^o$ when $h/l = 2$. The modulus E_1 of a honeycomb of given h/l is thus reduced as the angle becomes negative.

For a given h/l ratio, to obtain the same value of E_1 in a re-entrant cell as in an hexagonal cell it is necessary to increase the size of the re-entrant angle i.e. making it more negative. For example, a hexagonal cell of the geometry $h/l = 2$ and $\theta = 30^o$, has a modulus, from Fig.4.2, of $E_1 = 4$. To achieve an equivalent modulus in a re-entrant cell of the same h/l ratio requires a cell angle of -50^o which almost doubles the relative density of the core (Fig.4.3).

The maximum values of E_2 occur when the cell angles are small and the walls of length l lie along the direction of loading. Interestingly, increasing the h/l ratio reduces the value E_2 for a given cell angle (Fig.4.4). The graph of E_2 vs. θ is not quite symmetrical, with a minimum at $\theta = 0^o$, so that a re-entrant cell of geometry

h/l =2, θ=-30° has a higher modulus E_2 than the corresponding hexagonal cell of geometry h/l =2, θ=30°.

Figs.4.5 & 4.6 show the effect of t/l ratio on the moduli E_1 and E_2 respectively. For these particular plots E_s=h =l =b =1. Again the plot of E_1 is skewed to the left and greatly increases when $t/l \geq 0.1$. For most honeycomb structures however $t << l$ so small variations in t/l have little effect on the value of E_1. As before E_2 decreases as E_1 increases but by a smaller amount.

The Poisson's ratio is only affected by the value of h/l since equations 3.19 and 3.20 are independent of t. Figs.4.7 and 4.8 show the effects of h/l on the Poisson's ratios ν_{12} and ν_{21} respectively. A significant feature of both these graphs is that ratios much less than -1 and much greater than +1 are achieved. As can be seen from Fig.4.6 increasing the value of h/l increases the numerical value of the effective Poisson's ratio of both hexagonal and re-entrant cells. ν_{21} is correspondingly reduced Fig.4.8. It should also be noted that the graphs are not symmetrical. For example a hexagonal cell of geometry h/l =2, θ=30° has a Poisson's ratio ν_{12}=2 whereas the re-entrant cell h/l =2, θ=-30° has ν_{12}=-1. A limitation of the model is that at large angles approaching +90° and -90° infinite Poisson's ratios are predicted. This is clearly unrealistic as at θ=±90° the cell has completely collapsed and all the cell walls are aligned in the direction of the applied force, in which case ν_{12} must be the same as the Poisson's ratio of the cell wall material. i.e. $\nu_{12}=\nu_s$.

The maximum shear modulus (Fig.4.9) is achieved at θ=±90° since when cos θ=0° in equation 3.33, $G_{12}=\infty$. Increasing the value of h/l reduces the value of G_{12} over the majority of the cell angle range.

When $t << l$ there is a small scaling effect on the shear modulus. When $t/l > 0.1$ large increases in shear modulus occur (Fig.4.10) since $K_f = f(t/l)^3$.

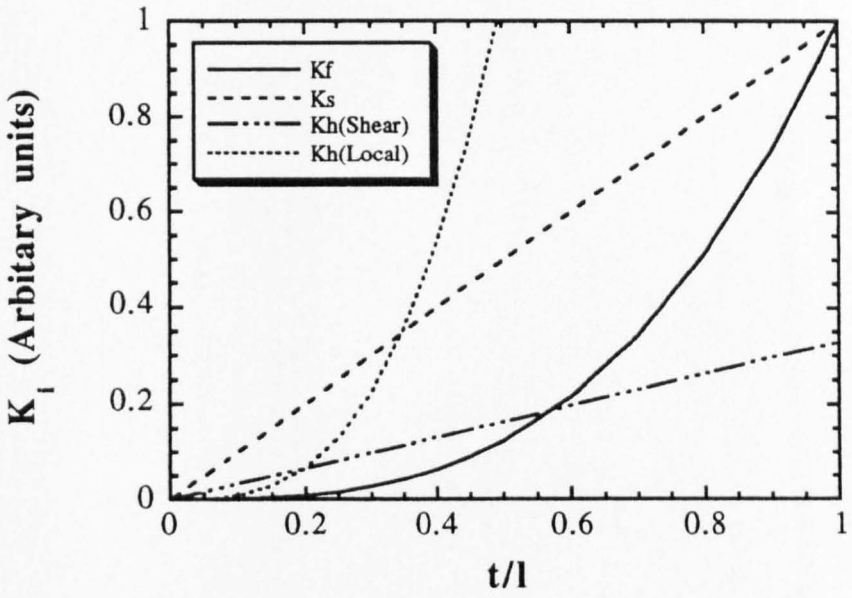

Fig.4.1. *Plot of K_i vs. t/l showing the relative behaviour of the force constants. The K_i with the lowest value for a given t/l determines the dominant deformation mechanism.*

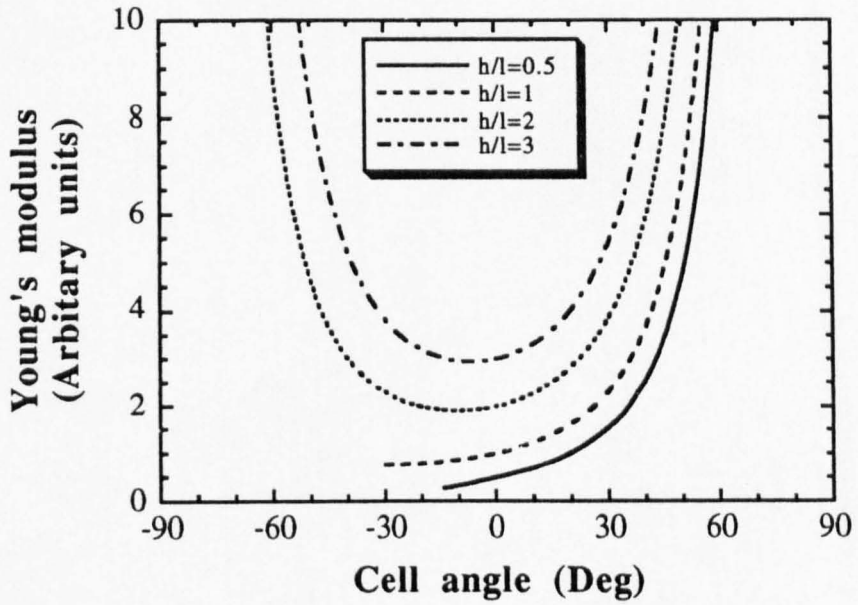

Fig.4.2. *Plot of E_1 vs. θ (Eqn.3.22) for the flexure model showing the effect of varying the h/l ratio.*

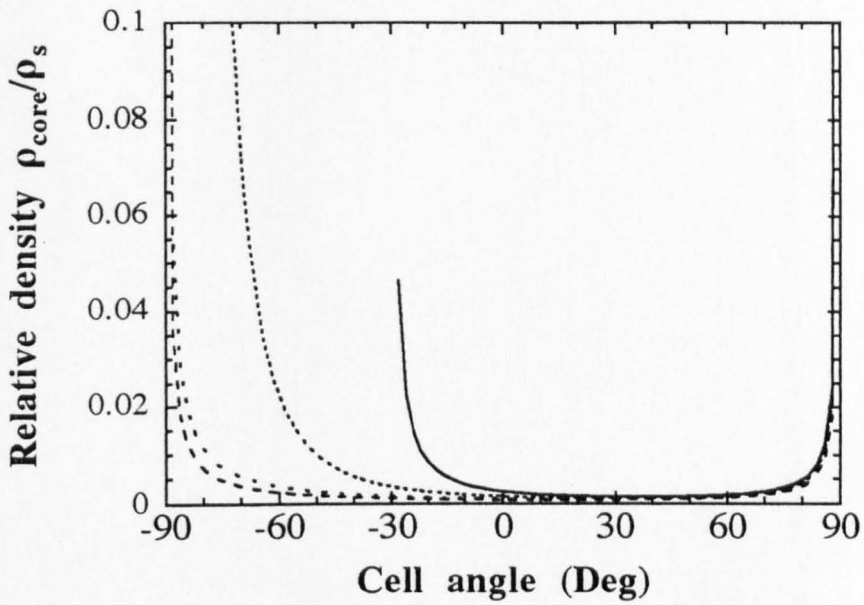

Fig.4.3. *Plot of relative density vs. θ (Eqn.2.10) showing the effect of varying the h/l ratio.*

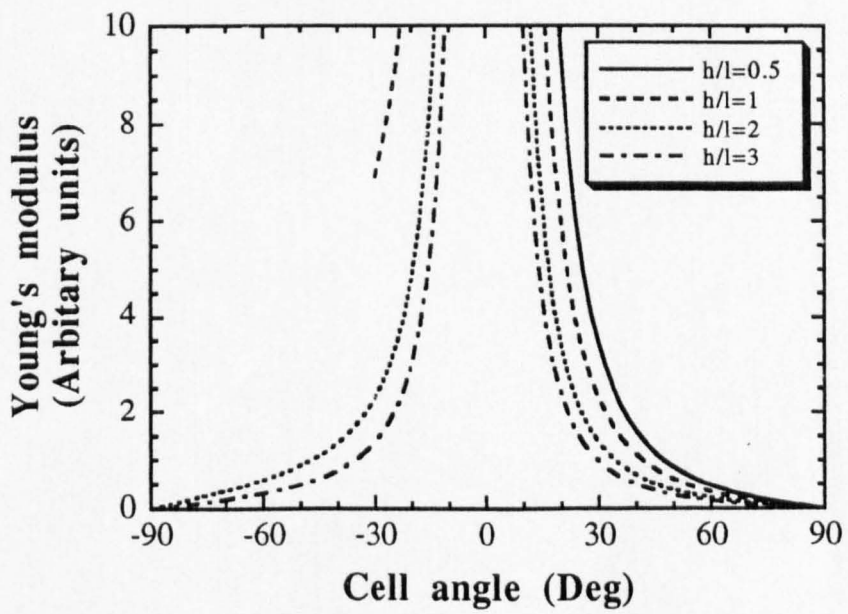

Fig.4.4. *Plot of E_2 vs. θ (Eqn.3.23) for the flexure model showing the effect of varying the h/l ratio.*

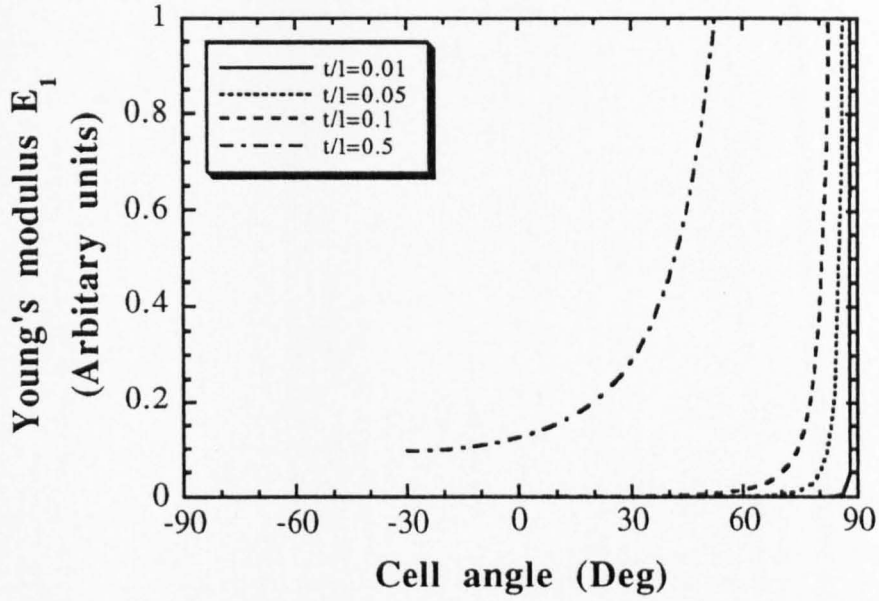

Fig.4.5. *Plot of E_1 vs. θ (Eqn.3.22) for the flexure model showing the effect of varying the t/l ratio.*

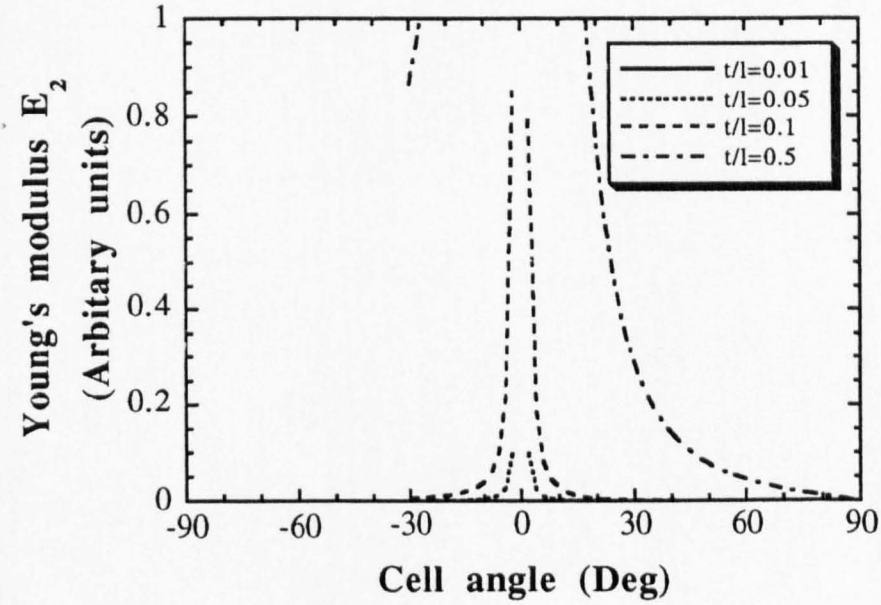

Fig.4.6 *Plot of E_2 vs. θ (Eqn.3.23) for the flexure model showing the effect of varying the t/l ratio.*

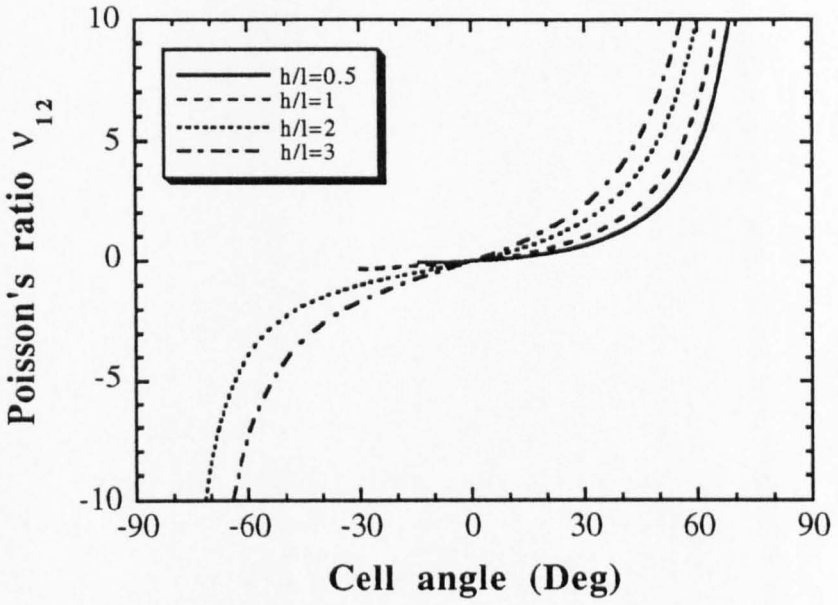

Fig.4.7 *Plot of ν_{12} vs. θ (Eqn.3.19) for the flexure and hinging models showing the effect of varying the h/l ratio.*

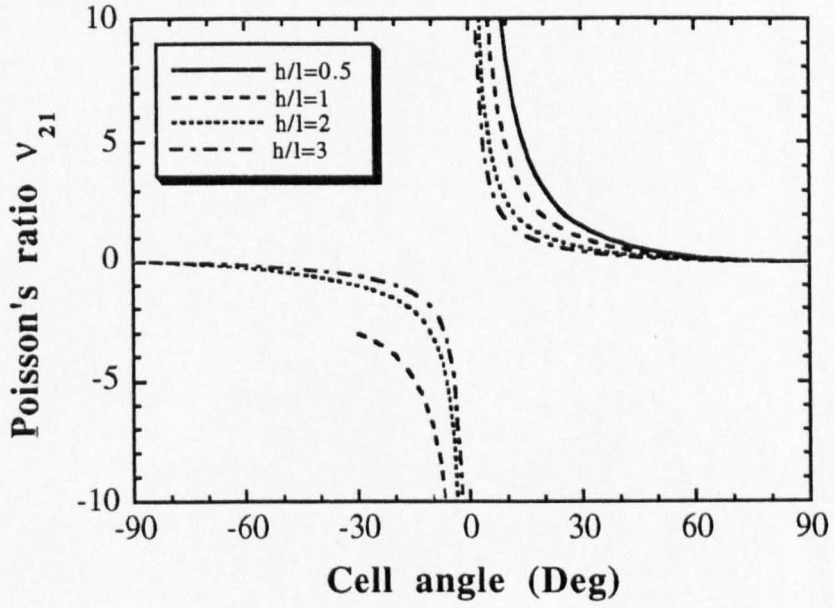

Fig.4.8 *Plot of ν_{21} v θ (Eqn.3.20) for the flexure and hinging models showing the effects of varying the h/l ratio.*

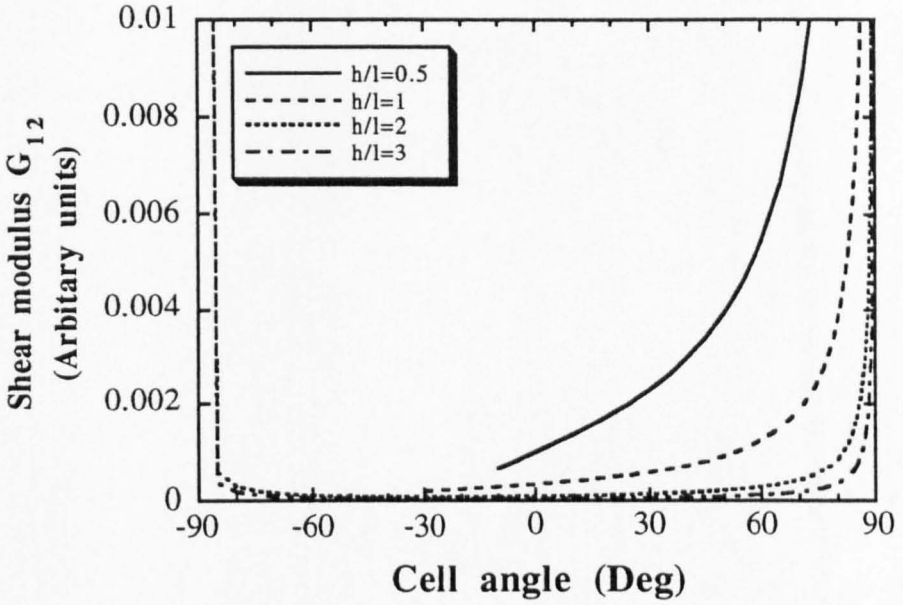

Fig.4.9. *Plot of G_{12} vs. θ (Eqn.3.24) for the flexure model showing the effect of varying the h/l ratio.*

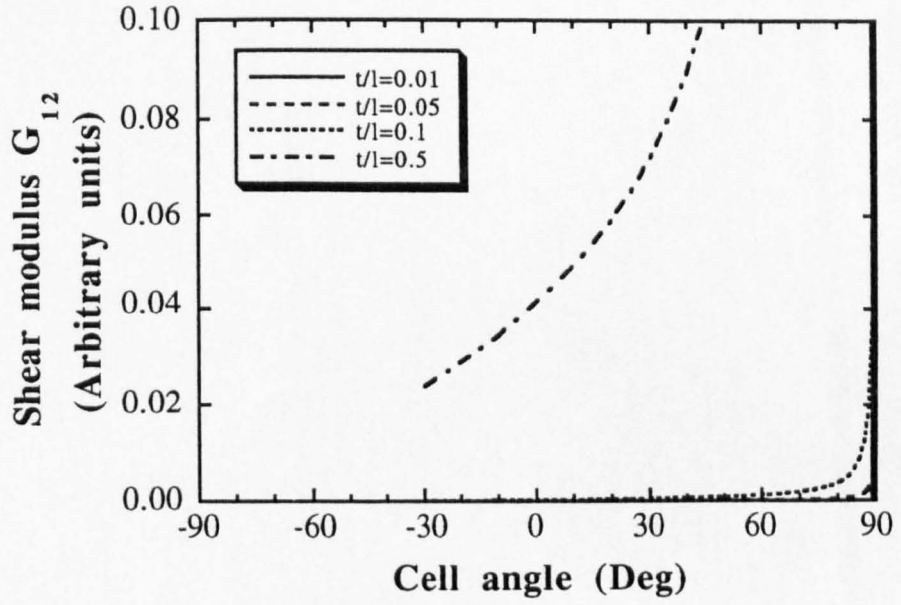

Fig.4.10. *Plot of G_{12} vs. θ (Eqn.3.24) for the flexure model showing the effect of varying the t/l ratio.*

4.4 Effects of cell geometry on the hingeing model

The graph of E_1 vs. θ (Fig.4.11) and E_2 vs. θ (Fig.4.12) are identical in shape to those for the flexure model, only differing in the value of the force constant K_i. This is obvious when the equations (3.22) and (3.60), (3.23) and (3.55) are compared. The hingeing mechanism is operative at much lower forces than those required for flexure. The effects of *h/l* on the modulus E_1 and E_2 are significantly reduced as a result. Similarly the effects of *t/l* on the moduli E_1 (Fig.4.13) and E_2 (Fig.4.14) are identical to those on the flexure model only differing in the value of the force constant K_h

Comparison of equation (3.19) with (3.61), and (3.20) with (3.57) shows that the effects of *h/l* on the Poisson's ratios ν_{12} and ν_{21} are identical to those for flexure model and are shown in Figs.4.7 and 4.8.

Fig.4.15 shows the reduction in the in-plane shear modulus caused by increasing the *h/l* ratio for a conventional hexagonal cell.

Changing the *t/l* ratio has the same scaling effect on the in-plane shear modulus for the hingeing model as it does in the flexure model. The values of shear modulus for hinging are however much smaller (Fig.4.16).

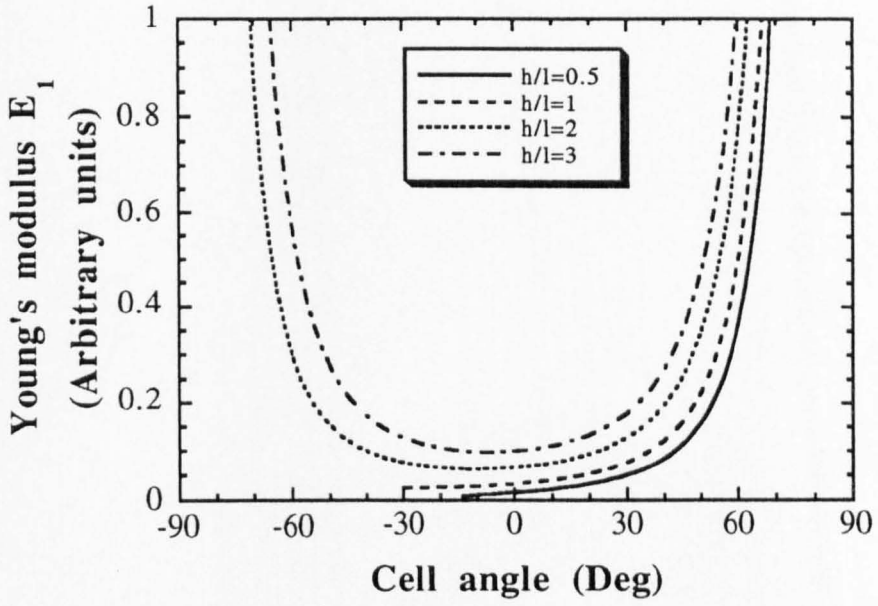

Fig.4.11 *Plot of E_1 vs. θ (Eqn.3.60) for the hinging model showing the effect of varying the h/l ratio.*

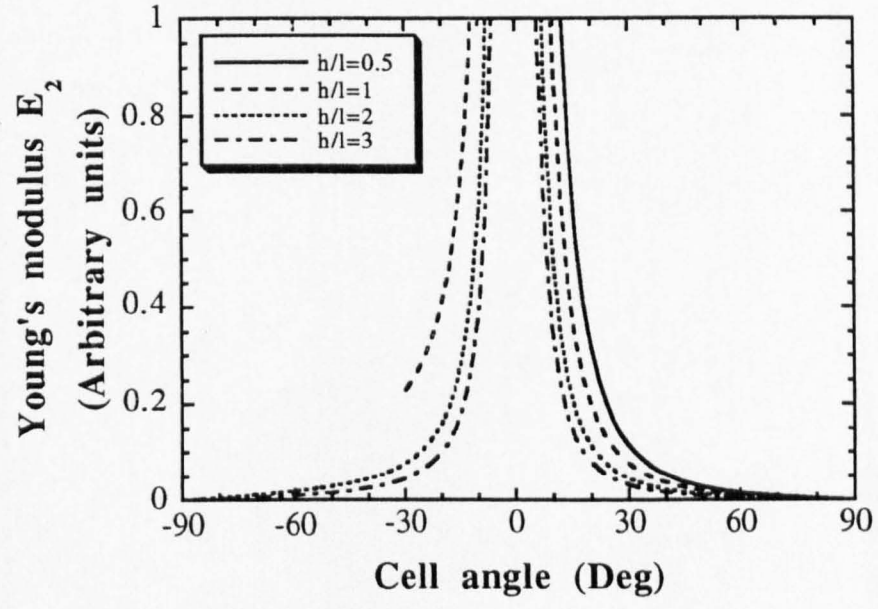

Fig.4.12 *Plot of E_2 vs. θ (Eqn.3.55) for the hinging model showing the effect of varying the h/l ratio.*

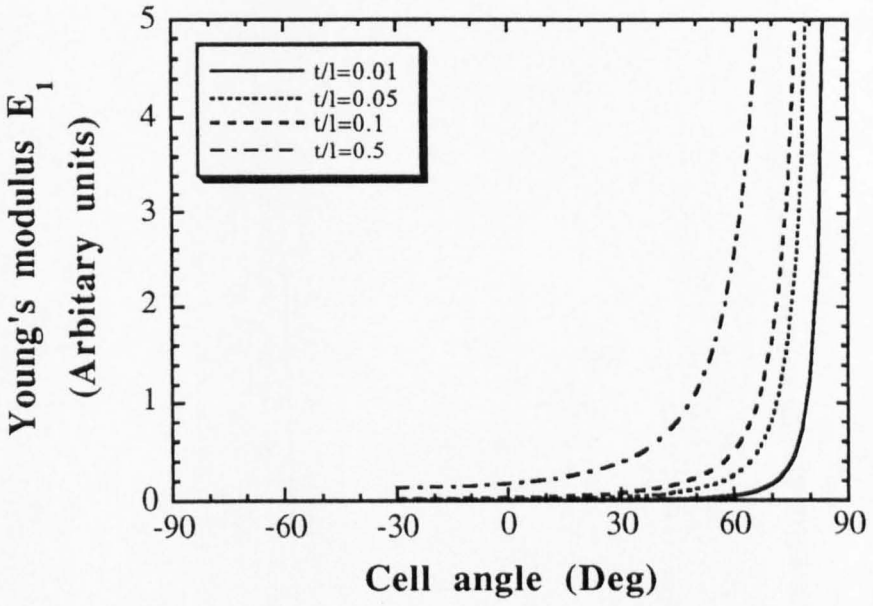

Fig.4.13 *Plot of E_1 vs. θ (Eqn.3.60) for the hinging model showing the effect of varying the t/l ratio.*

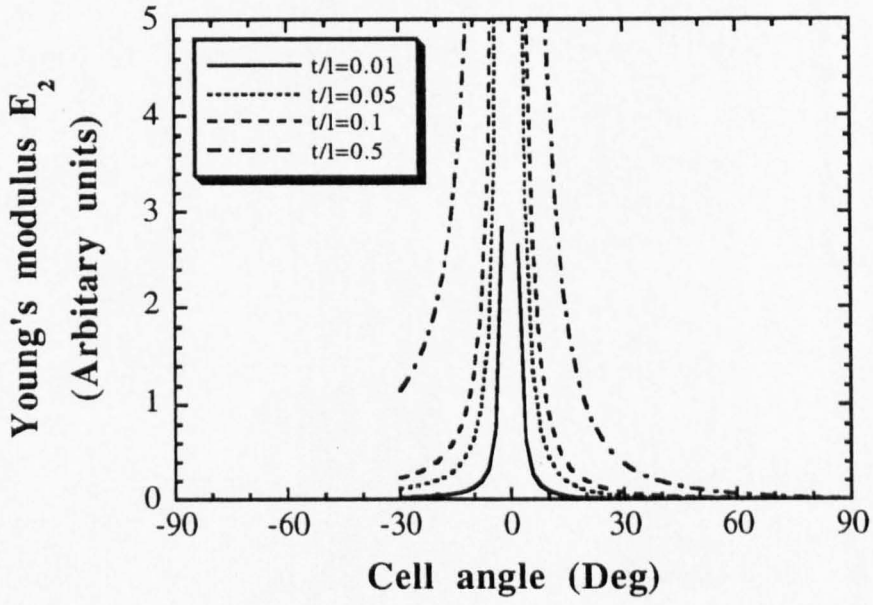

Fig.4.14 *Plot of E_2 vs. θ (Eqn.3.55) for the hinging model showing the effect of varying the t/l ratio.*

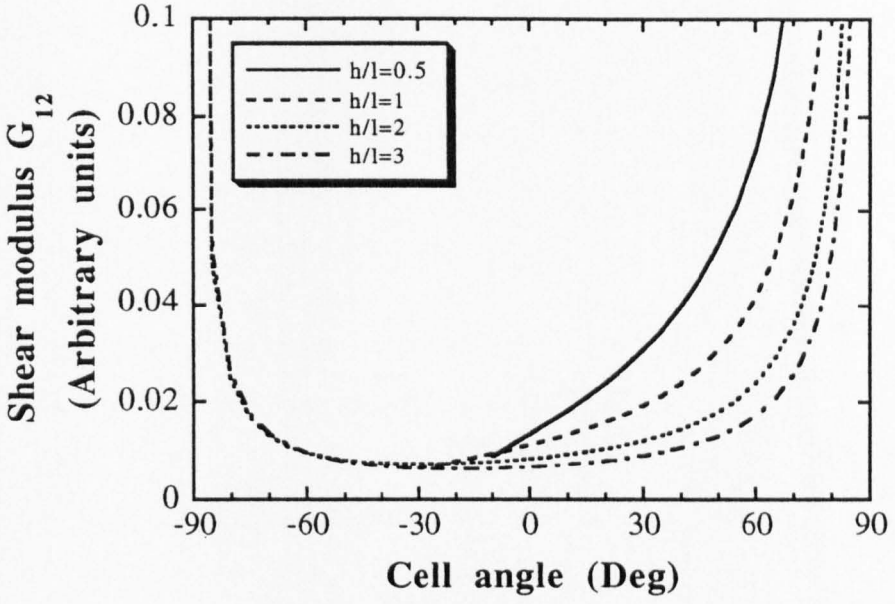

Fig.4.15 *Plot of G_{12} vs. θ (Eqn.3.73) for the hinging model showing the effect of varying the h/l ratio.*

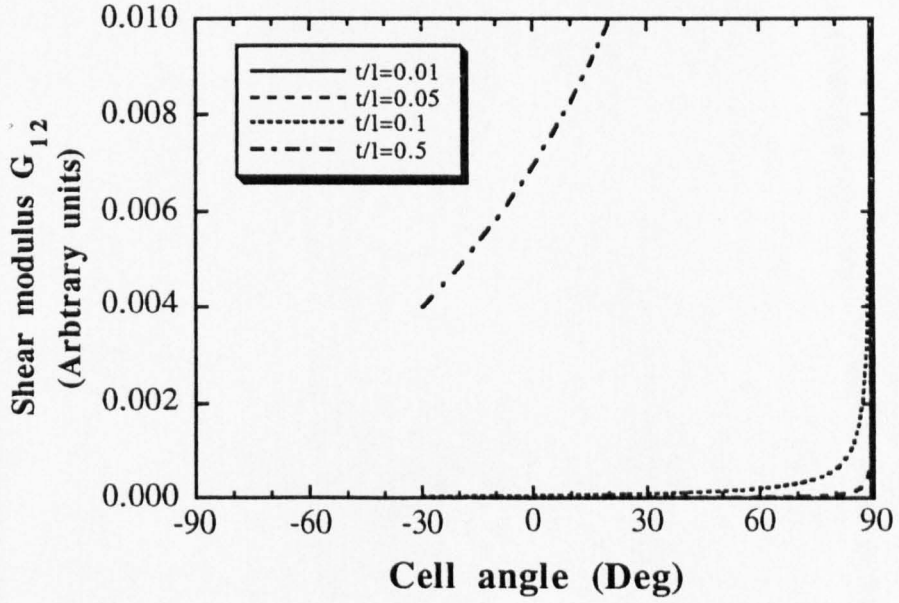

Fig.4.16 *Plot of G_{12} vs. θ (Eqn.3.73) for the hinging model showing the effect of varying the t/l ratio.*

4.5 Effects of cell geometry on the stretching model

Unlike the modulus graphs for flexure and hingeing the moduli E_1 and E_2 both reach their maxima at $\pm 90^o$ i.e. the cell walls lie parallel or perpendicular to the applied force. Fig.4.17 shows that the plot of E_1 is skewed to the left with the minimum value of E_1 moving further to the right as h/l is increased. The value of E_1 rapidly rises when the cell angle lies in the ranges $\theta > 60^o$ and $\theta < -70^o$. Increasing the value of h/l causes an increase in E_1 for a given angle for re-entrant cells and a decrease in E_1 for hexagonal cells.

The effects of h/l on E_2 for stretching are less marked than on E_1 (Fig.4.18).E_2 decreases as h/l increases and the graph is skewed to the right. This latter effect is caused by the $(h/l + \sin\theta)$ term in equation 3.27 the minimum value of which increases as h/l increases. When the cell becomes re-entrant the effect of h/l is much more dramatic. For a cell angle of -30^o, changing h/l from 3 to 1 causes an almost five fold increase in E_2.

As expected the t/l ratio is important to the moduli in stretching since the latter is directly related to the cross-sectional area of the cell walls and the amount of material available to stretch. As t/l increases so does E_1(Fig.4.19). As already mentioned in most applications $t << l$ so significant changes in E_1 only occur when θ approaches 90^o.

The graph of E_2 vs. θ (Fig.4.20) is skewed to the right with a minimum at $\theta = 30^o$. Again this modulus increases rapidly as t/l increases but in the majority of cases $t << l$. For a hexagonal cell a high value of E_2 is achieved as θ approaches 90^o.

The plots for Poisson's ratio are shown in Figs.4.21 and 4.22. The most important feature is that both ν_{12} and ν_{21} are positive for re-entrant cells and negative for hexagonal cells. The plots are not symmetrical. Increasing h/l increases the numerical value of ν_{12} (Fig.4.21) and decreases the value of ν_{21} (Fig.4.22). For the plots shown square symmetry (i.e. $\nu_{12}=\nu_{21}$) can only be

acheived for the conditions of $h/l=2$ when θ is negative and for values of h/l when θ is positive.

The plot for the in-plane shear modulus is shown in Fig.4.23. Unlike the models for flexure and hingeing, changing the value of the h/l ratio does not have a simple effect. When $h/l \geq 1$ increasing the value of h/l moves the maximum value of G_{12} further to the right. However for the particular case of $\theta = 30^{o}$ changing the value of h/l seemingly has no effect.

In the region $30^{o}<\theta<90^{o}$ reducing h/l causes a small increase in the value of G_{12} and when $\theta<30^{o}$ increasing the value of h/l gives rise to a dramatic increase in G_{12}. It is worth noting that the maximum values of shear modulus can only be achieved when $h/l \leq 2$.

Increasing the t/l ratio causes a small increase in the shear modulus when $t<<l$, the effect being most pronounced when $\theta=30^{o}$ (Fig.4.24). Again when $t/l>0.1$ there is a dramatic increase in shear modulus.

Using the geometries for the experimental honeycombs the elastic constants, written in terms of the force constants, are listed in Table 4.1.

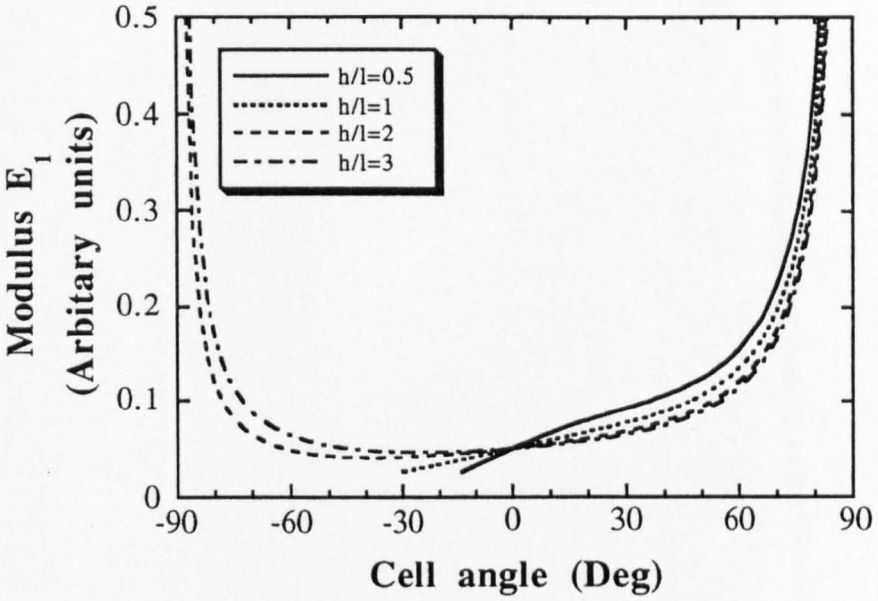

Fig.4.17 *Plot of E_1 vs. θ (Eqn.3.33) for the stretching model showing the the effect of varying the h/l ratio.*

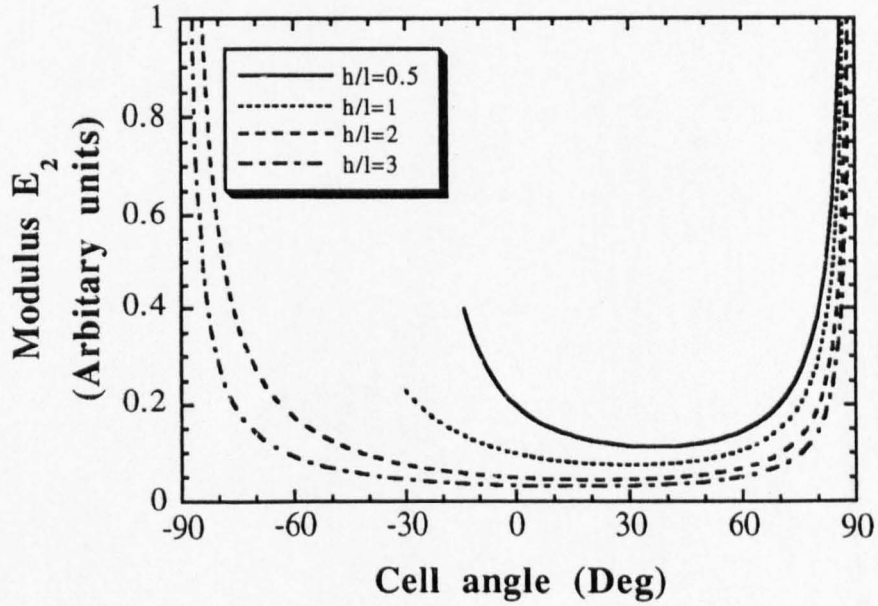

Fig.4.18 *Plot of E_2 vs. θ (Eqn.3.28) for the stretching model showing the the effect of varying the h/l ratio.*

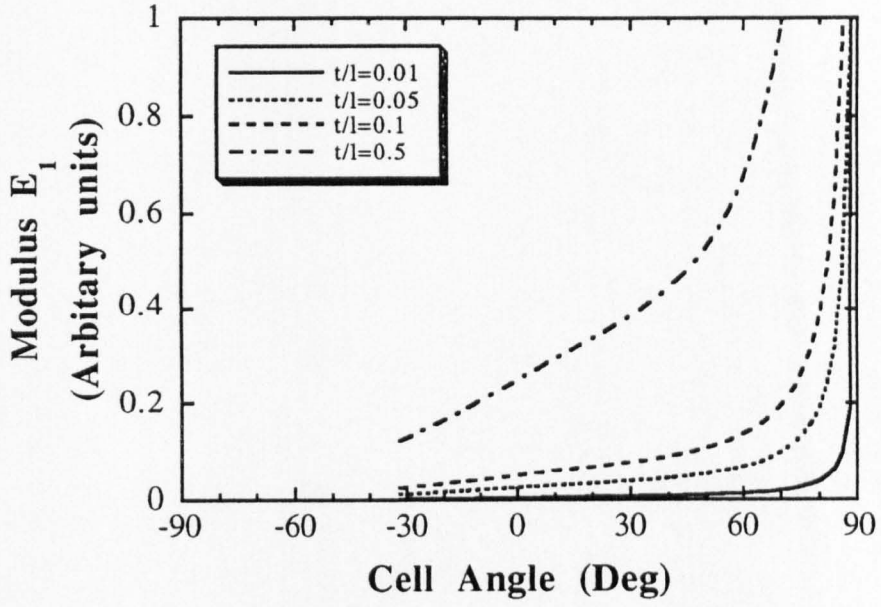

Fig.4.19 *Plot of E_1 vs. θ (Eqn.3.33) for the stretching model showing the effect of varying the t/l ratio.*

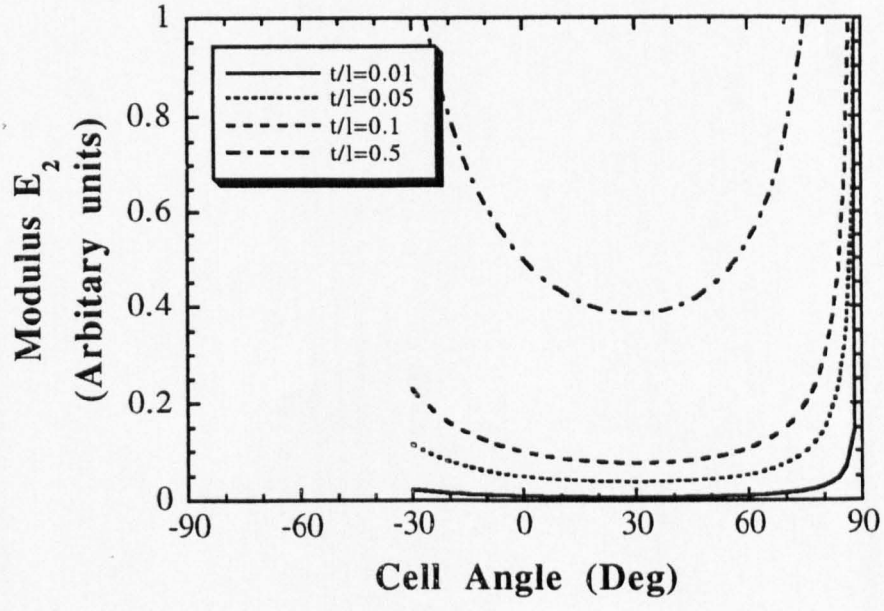

Fig.4.20 *Plot of E_2 vs. θ (Eqn.3.28) for the stretching model showing the effect of varying the t/l ratio.*

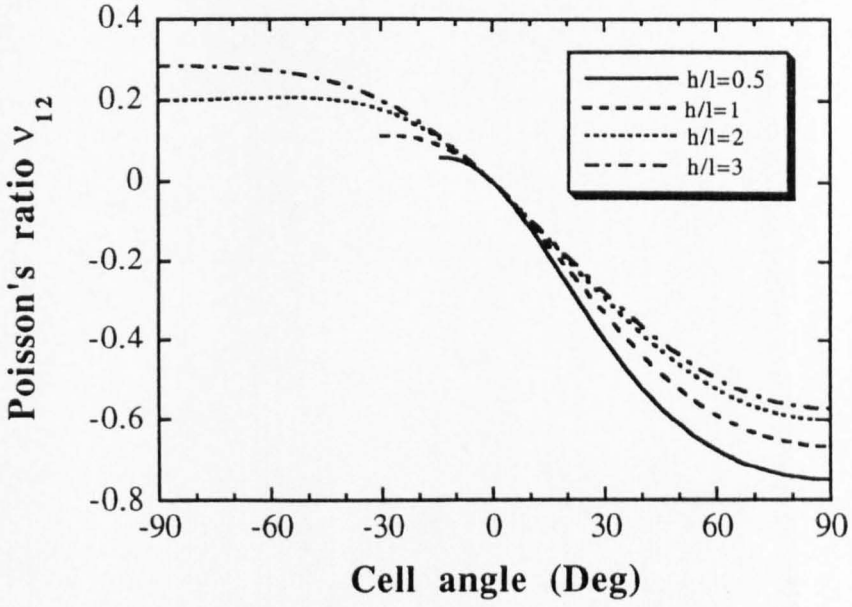

Fig.4.21 *Plot of ν_{12} vs. θ (Eqn.3.34) for the stretching model showing the effect of varying the h/l ratio.*

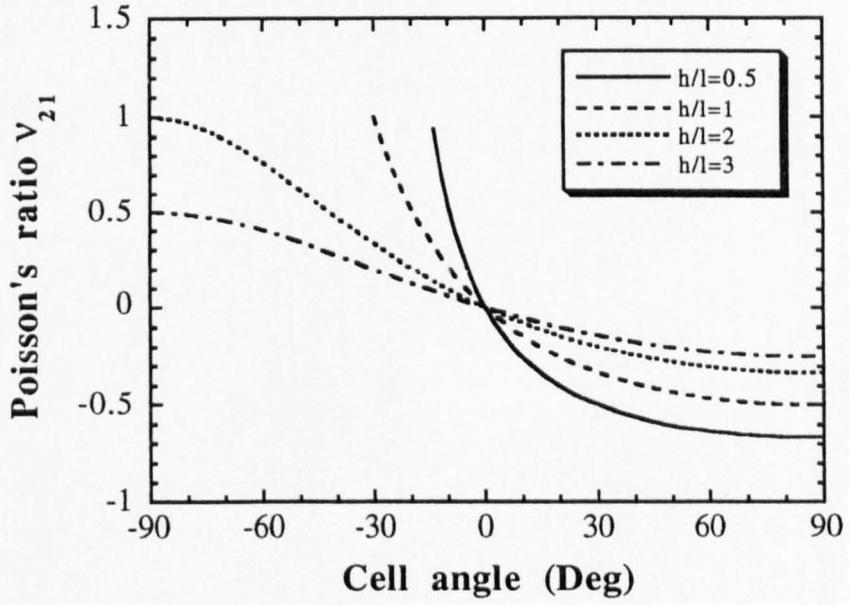

Fig.4.22 *Plot of ν_{21} vs. θ (Eqn.3.30) for the stretching model showing the effect of varying the h/l ratio.*

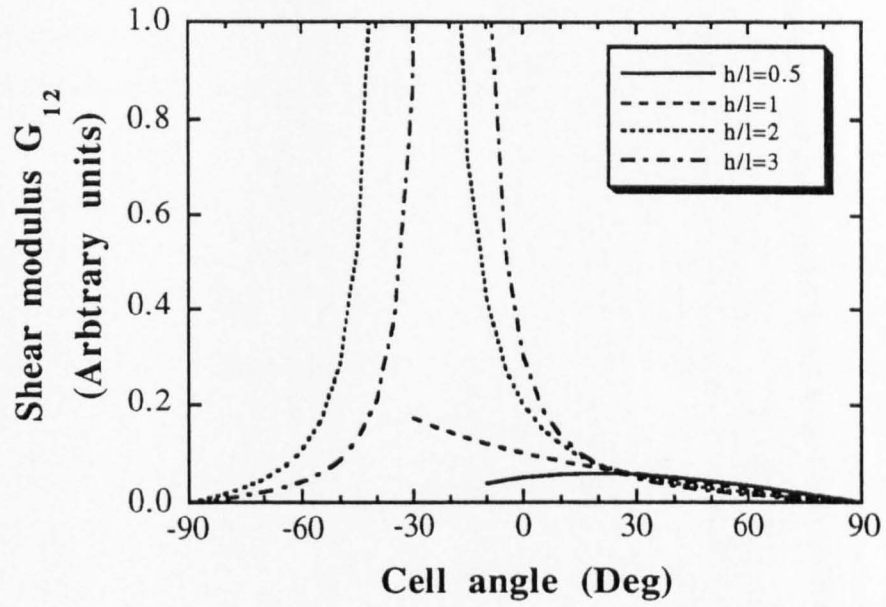

Fig.4.23 *Plot of G_{12} vs. θ (Eqn.3.50) for the stretching model showing the effect of varying the h/l ratio.*

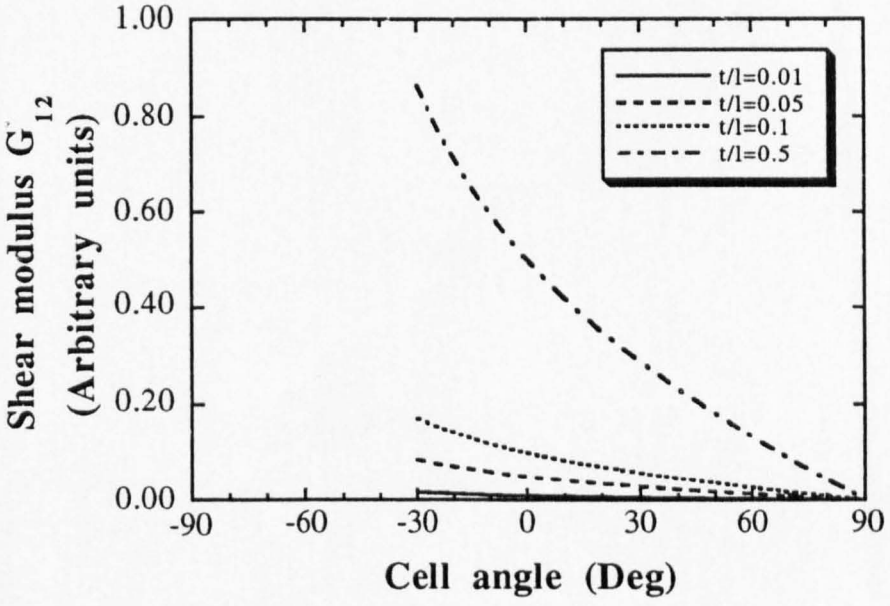

Fig.4.24*Plot of G_{12} vs. θ (Eqn.3.50) for the stretching model showing the effect of varying the t/l ratio.*

4.6 The effects of double wall thickness in direction 1

The honeycombs used in the tests (cf. Sections 5.6 & 5.7), and most commercial honeycombs, have a double wall thickness in the ribbon direction (1 in Fig.2.1) because of the way in which they are manufactured. As already seen in Chapter 2 this can affect the mechanical properties of the core.

The equations for the three models, summarised in Table 3.2, assume a uniform cell wall thickness t, and as $t<<h$ or l the width of an individual cell has been approximated to $2l\cos\theta$. To more accurately model commercial honeycombs the double wall thickness in direction 1 can be allowed for by adding $2t$ to the width of the cell Fig.4.25 and calculating the deflections of the walls length h using a width $2t$. The modified equations incorporating the double wall thickness in direction 1 are listed in Table 4.2.

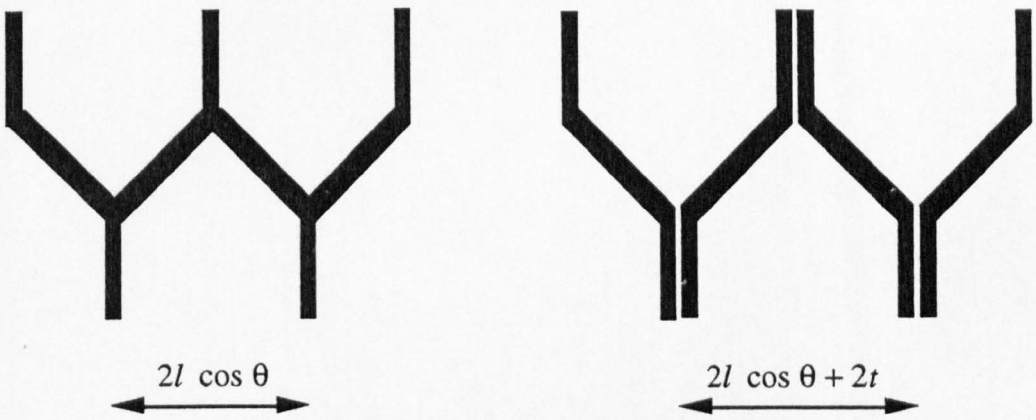

Fig.4.25 *Approximation of cell width for uniform cell wall thickness t (left) and for double wall thickness in direction 1 (right).*

Fig.4.26 compares the uniform wall thickness and double wall thickness equations for the flexure model. As can be seen from the graphs there is minimal effect on the Young's moduli and Poisson's ratio so equations 3.19, 3.20, 3.22 and 3.23 are quite adequate to describe both cases (Gibson, 1988).

The shear modulus G_{12} is however increased as might be expected (Klintworth *et al.*, 1988) due to the increased stiffness of the walls of length *h*. (N.B. Klintworth *et al.* modified Gibson's expression to obtain the equation 2.27 simply by assuming that the double thickness walls were infinitely stiff and do not flex at all). In this thesis the small amount of flexibility of the double thickness wall is allowed for.

Figs.4.27a show an obvious increase in the modulus E_1 for the stretching model due to the increase in the cross-sectional area of the cell walls of length *h*. There is no effect in direction 2 as all the deformation occurs due to stretching of the single thickness walls of length *l* alone, as in the case of uniform cell wall thickness.

The Poisson's ratio in direction 1 is increased (Fig.4.27b) because the extension, and hence the strain, of the honeycomb in direction 1, for a given load, is reduced due to the increased cross sectional area of the walls length *h* . The strain in direction 2 remains unaffected. As

$$\nu_{12} = \frac{-\varepsilon_2}{\varepsilon_1}$$

the value of ν_{12} increases due to the reduction in ε_1.

The shear modulus G_{12} (Fig.4.27c) is unaffected by the double wall thickness in direction 1 since all movement occurs due to the stretching or compression of the members length *l*.

As with the flexure model there is little or no effect on the Young's moduli or Poisson's ratios for hingeing (Fig.4.28a & b). This is because the increased thickness of the cell walls length *h* does not affect the dimensions of the cell walls length *l*, hence the moments causing the walls to rotate remain the same. It is surprising therefore, that there is a significant reduction in the in-plane shear modulus G_{12} (Fig.4.28c).

It is obvious then, that for the honeycombs used in the tests described here that the following expressions may give a better fit to the experimental data than equations 3.24, 3.33 and 3.34.

$$\text{Flexure model } G_{12} = \frac{K_f l^3 (h + l \sin\theta)}{b h^2 (l + h/4)(t + l\cos\theta)} \tag{4.1}$$

$$\text{Stretching model } E_1 = \frac{K_s (h + l \sin\theta)}{b (l\cos\theta + t)(h/l + \sin^2\theta)} \tag{4.2}$$

$$\text{Stretching model } \nu_{12} = \frac{-(h + l\sin\theta)(\sin\theta\cos\theta)}{(l\cos\theta + t)(\sin^2\theta + h/l)} \tag{4.3}$$

$$\text{Hinging } G_{12} = \frac{K_h (l\cos\theta + t)(h + l\sin\theta)}{Cb(h\cos\theta - \sin\theta[\cos\theta(h + l\sin\theta) + \sin\theta(l\cos\theta + t)] + 2b(l\cos\theta + t)^2} \tag{4.4}$$

Aluminium models deforming by flexure

	E_1 (Eqn.3.22)	E_2 (Eqn.3.23)	ν_{12} (Eqn.3.19)	ν_{21} (Eqn.3.20)	G_{12} (Eqn.3.24)	ρ_H/ρ_s (Eqn.2.11)
Hexagonal cell h=l=10mm, b=20mm, θ=+30°	$0.1155K_f$	$0.1155K_f$	1.0	1.0	$0.0287K_f$	$0.115t$
Re-entrant cell h=b=20mm, l=10mm, θ=-30°	$0.1155K_f$	$0.1155K_f$	-1.0	-1.0	$0.0043K_f$	$0.154t$

Card models deforming by hinging

	E_1 (Eqn.3.60)	E_2 (Eqn.3.55)	ν_{12} (Eqn.3.61)	ν_{21} (Eqn.3.57)	G_{12} (Eqn.3.73)	ρ_H/ρ_s (Eqn.2.11)
Hexagonal cell h=b=20mm, l=10mm, θ=+30°	$0.193K_h$	$0.069K_h$	1.667	0.6	$0.0241K_h$	$0.092t$
Re-entrant cell h=b=20mm, l=10mm, θ=-30°	$0.1155K_h$	$0.1155K_h$	-1.0	-1.0	$0.0144K_h$	$0.154t$

Table 4.1 *Comparison of the theoretical elastic properties and relative densities for the honeycombs used in the experimental tests in terms of the force constants K_f and K_h, and the cell wall thickness t.*

	E_1	E_2	ν_{12}	ν_{21}	G_{12}
Flexure	$\frac{K_f(h/l + \sin\theta)}{b\cos^2\theta(\cos\theta + t/l)}$	$\frac{K_f(\cos\theta + t/l)}{b\sin^2\theta(h/l + \sin\theta)}$	$\frac{\sin\theta(h/l + \sin\theta)}{\cos\theta(\cos\theta + t/l)}$	$\frac{\cos\theta(\cos\theta + t/l)}{(h/l + \sin\theta)\sin\theta}$	$\frac{K_f l^2(h/l + \sin\theta)}{bh^2(\cos\theta + t/l)(1 + h/4l)}$
Stretching	$\frac{K_s(h/l + \sin\theta)}{b(\cos\theta + t/l)(h/l + \sin^2\theta)}$	$\frac{K_s(\cos\theta + t/l)}{b\cos^2\theta(h/l + \sin\theta)}$	$\frac{-\sin\theta\cos\theta(h/l + \sin\theta)}{(\cos\theta + t/l)(h/l + \sin^2\theta)}$	$\frac{-(\cos\theta + t/l)\sin\theta}{(h/l + \sin\theta)\cos\theta}$	$\frac{K_s}{b}\left[\frac{l^2(\cos\theta + t/l)(h/l + \sin\theta)}{(2l^2(\cos\theta + t/l)(h/l + \sin\theta)\sin\theta\cos\theta) + \sin^2(h + l\sin\theta)^2 + \cos^2\theta(l\cos\theta + t)^2}\right]$
Hinging	$\frac{K_h(h/l + \sin\theta)}{b\cos^2\theta(\cos\theta + t/l)}$	$\frac{K_h(\cos\theta + t/l)}{b\sin^2\theta(h/l + \sin\theta)}$	$\frac{\sin\theta(h/l + \sin\theta)}{\cos\theta(\cos\theta + t/l)}$	$\frac{\cos\theta(\cos\theta + t/l)}{(h/l + \sin\theta)\sin\theta}$	$\frac{K_h}{b}\left[\frac{C(\cos\theta + t/l)(h/l + \sin\theta)}{C(h\cos\theta - t\sin\theta)[\cos\theta(h/l + \sin\theta) + \sin\theta(\cos\theta + t/l)] + 2(\cos\theta + t/l)^2}\right]$

Table 4.2 *Summary of expressions for elastic constants obtained from the flexure, stretching and hinging models, allowing for double wall thickness in direction 1.*

a)

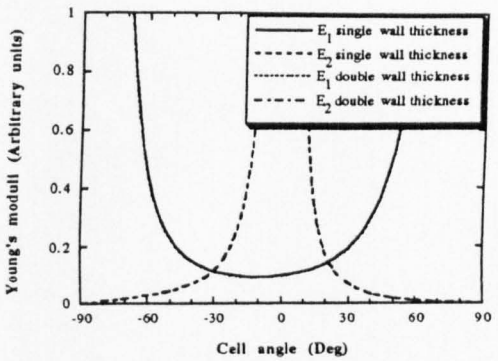

b)

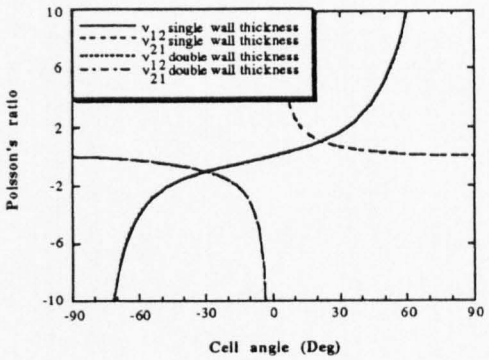

c)

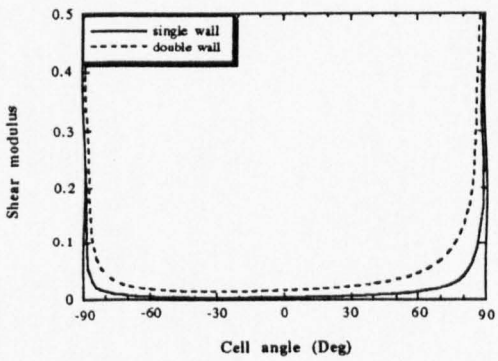

Fig.4.26 *The effects of double wall thickness in direction 1 on E, ν and G from the flexure model are shown above by plotting against the results for specimens with all cell walls of uniform thickness.(h/l =2)*

a) Young's moduli E_1 and E_2 - no effect.

b) Poisson's ratio ν_{12} and ν_{21} - no effect.

c) Shear modulus G_{12} - small increase especially in the the region $60^o<\theta<90^o$.

a)

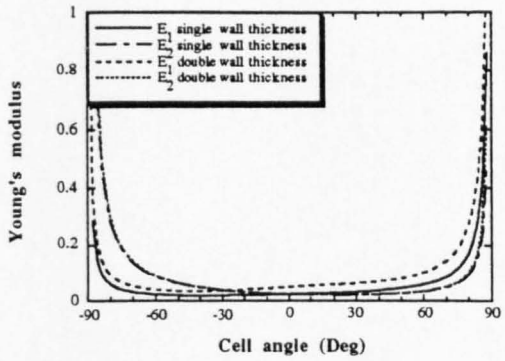

b)

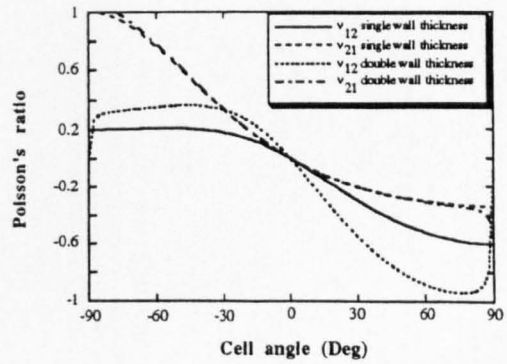

c)

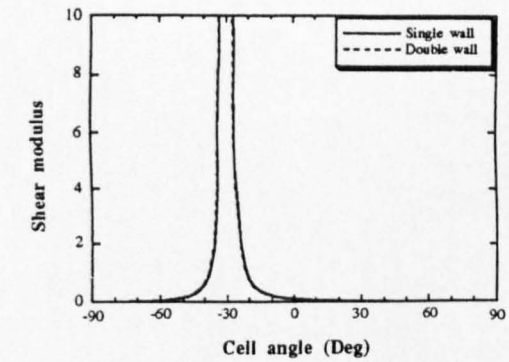

Fig.4.27 *The effects of double wall thickness in direction 1 on E, ν and G from the stretching model are shown above by plotting against the results for specimens with all cell walls of uniform thickness.(h/l =2)*
a) Young's moduli E_1 and E_2 - E_1 is increased slightly over the full range of angles. There is no effect on E_2.
b) Poisson's ratio ν_{12} and ν_{21} - Magnitude of ν_{12} is increased over the full range of angles. No effect on ν_{21} except when θ approaches $\pm 90^o$.
c) Shear modulus G_{12} - no effect.

a)

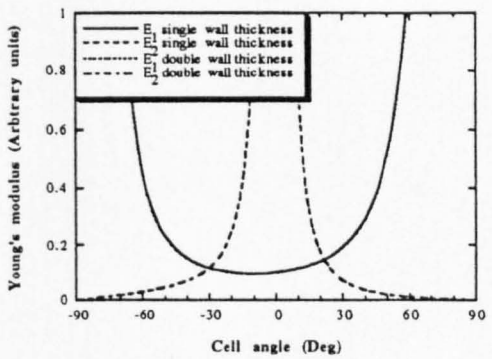

b)

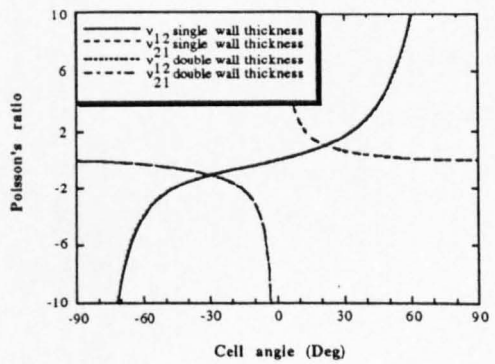

c)

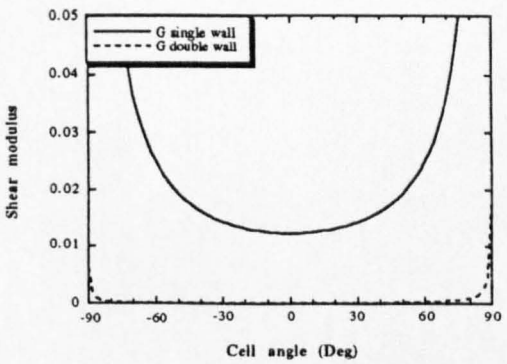

Fig.4.28 *The effects of double wall thickness in direction 1 on E, ν and G from the hinging model are shown above by plotting against the results for specimens with all cell walls of uniform thickness.(h/l =2)*

a) Young's moduli E_1 and E_2 - no effect.

b) Poisson's ratio ν_{12} and ν_{21} - no effect.

c) Shear modulus G_{12} - decreases over the full range of angles.

References

GIBSON,L.J., & ASHBY,M.F.,
"Cellular Solids : Structure & Properties",
Chapter 4, Page 76,
Pergamon Press, London (1988).

KLINTWORTH ,J.W. & STRONGE,W.J.,
International Journal of Mechanical Science,
Vol.30 No.3/4, Pages 273-292, 1988

5) EXPERIMENTAL METHODS

5.1 Introduction

Gibson's flexure model (1982, 1988) was successfully developed to describe the elastic properties of conventional hexagonal cell honeycombs when loaded in the plane of the material, and also showed good agreement with experimental results derived for the specific case of a rubber re-entrant cell of geometry h/l =2 and θ=-30^{o}. More recent work on the re-entrant cell structure, using cardboard honeycombs (Caddock 1991, Masters, 1993), has demonstrated the existence of the hinging mechanism for which an elastic deformation model has been derived; q.v. Chapter 3. The main area of interest for the experimental tests was therefore the measurement of the in-plane elastic properties of both re-entrant and hexagonal celled honeycombs, made from various materials, and comparison of these results with predictions from the models.

Tensile and compressive tests enabled the effective moduli and Poisson's ratios of the honeycomb materials to be determined and a 'picture frame' rig was used for measuring the in-plane shear moduli.

When examining the re-entrant structure it is apparent that as it is compressed there is a significant increase in the density due to the negative Poisson's ratio. An interesting extension of this phenomenon is to consider what happens when a section of auxetic honeycomb is subjected to local indentation. We might expect the densification of the material under the indenter to resist further deformation and to investigate this, tests were performed, in-plane, on both card and aluminium specimens with differently shaped indenters. If the indentation behaviour of the core can be related to the models described in Chapter 3 then these same models may be of use as a simple method of predicting the indentation behaviour of 3-D foams.

The main use of honeycomb materials is as a core in sandwich panels, where its ability to withstand an out-of-plane crushing load is important e.g. aircraft internal floors and cargo liners. The increased density of the re-entrant honeycombs is naturally expected to increase the maximum crushing load due to the greater area of cell wall material available to support the load. Of more interest however, was to determine whether or not any potential benefit was obtained from the acute angle in the re-entrant cell inhibiting the onset of cell wall buckling and ultimate failure, thus raising the strength of the panel. To investigate this compression tests were performed on small areas of honeycomb containing multiple cells. Another critical factor for the failure load is the thickness b of the core (Reichard, 1972), so tests were performed on single cells of varying heights.

The radii of curvature have already been shown (Section 2.11) to be related to the Poisson's ratio of the material. A slight modification to the method described by Caddock *et al.* (1991) for measuring the radii of curvature, enables the typical curvatures achievable with the re-entrant structure to be demonstrated.

Finally the plate deflection test was devised as a method of comparing the out-of-plane flexural stiffnesses of the hexagonal and re-entrant celled honeycombs.

The experiments undertaken can be divided into three categories

1) Determination of moduli of the cell wall materials
2) Measurement of the effective, in-plane, elastic properties of both hexagonal and re-entrant honeycombs
3) Examination of specific properties of the core materials e.g. out of plane crush strength, radii of curvature, drapeability.

with the following primary objectives:-

a) to examine the validity of the hinging model which was developed to describe the particular deformation mechanism demonstrated by card honeycombs,

b) to demonstrate that both the hinging and flexing models could be applied equally well to either re-entrant or conventional cell cores.

c) to compare the behaviour of hexagonal and re-entrant cell core materials in a number of useful applications.

5.2 Material selection

Aluminium foil used in commercial honeycomb manufacture was provided by Ciba Geigy. The foil could be simply cut on a guillotine and easily folded by hand in a jig to produce preforms of specific cell angles. Cartridge paper was selected for making out-of-plane compression specimens because of its absorbency. Polyester resin was selected for use on these compression specimens as its low viscosity enabled the paper honeycombs to be easily dipped.

Clay coated card, used extensively in the packaging industry, was chosen for making the cardboard honeycombs as it could easily be folded by hand without a great reduction in strength and was readily bonded with polyvinyl acetate (PVA) paper adhesive.

5.3 Basic material properties

5.3.1 Elastic properties of paper, paper/resin and card materials

The moduli of the card used in these experiments were determined by performing tensile tests on parallel sided specimens of material cut to the dimensions specified in BS 4415 Part II (Fig.5.1).

The specimens were tested using flat jaws, card end tabs being used to prevent tearing of the specimen at the jaw edges. The end tabs were bonded to the specimens using PVA paper adhesive. Specimens were cut both parallel and perpendicular to the the fibre direction of the paper.

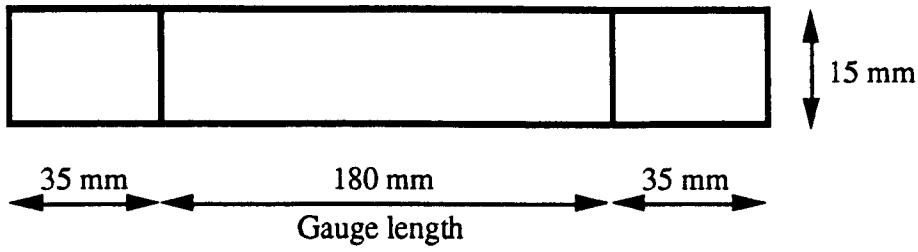

Fig.5.1 *Dimensions for card tensile specimens according to BS 4415 Part II*

Folding the card must obviously alter its properties in the vicinity of the crease line. Tensile tests were therefore carried out on short specimens with a single fold at the centre, perpendicular to the tensile axis. The gauge length was taken as the width of the crease line (1mm approx.).

5.3.2 Elastic properties of Aluminium

The modulus of the aluminium was measured using a 12.5mm wide specimen of foil to the dimensions shown in Fig.5.2

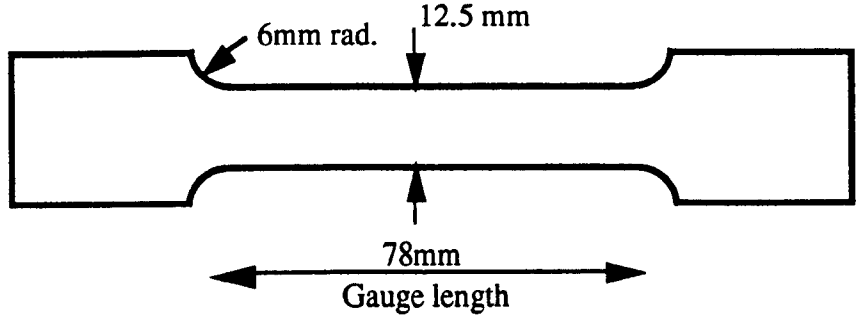

Fig.5.2 *Dimensions of aluminium foil tensile specimens.*

Specimens were cut both parallel to and perpendicular to the rolling direction. Several specimens were prepared at once by clamping sheets of foil between hardened steel formers. The excess was removed with a file and then the specimens were finished to size with a fine grade abrasive paper to ensure there were no stress raisers at the edges of the specimens. As the material was in the annealed state no difference in properties was found between the specimens produced in different directions. The tests were performed on an Instron 1185 servo-mechanical testing machine.

5.3.3 Determination of K_f and K_h

E_f was obtained by measuring the initial gradient of the load/extension curves from the tensile tests on strips of aluminium foil (q.v. section 5.4). Substituting into equation (3.4) gives the value K_f.

To directly measure K_h a piece of card 100mm wide was folded in half after scoring along the centre line with a blunted scalpel blade. The material on one side of the fold was bonded to a flat rigid surface, and that on the other side was stiffened by folding up about 5mm of material along each edge. Known loads were applied to the uppermost edge and photographs taken, from which the change in angle could be measured. The arrangement is shown schematically in Fig.5.3.

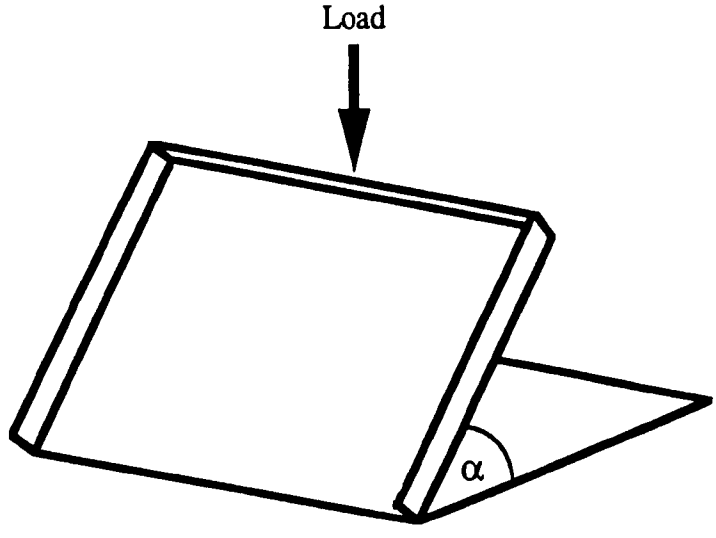

Fig.5.3 *Schematic diagram showing the arrangement for measuring K_h.*

From the original definition of the force constant (Eqn 3.1) we can write

$$K_h = \frac{F}{\delta} = \frac{W\cos\alpha}{l\sin\alpha} \qquad 5.1$$

where W is the applied load and F is the component of W acting perpendicular to the member length *l*. Plotting $W\cos\alpha$ against $l\sin\alpha$, K_h can be obtained.

It proved difficult to measure the spring constant K_h of the card directly but by plotting the experimental results against the theoretical curves for E_1 and E_2 obtained for various values of K_h a best fit value was obtained. This value was used for all subsequent evaluation of the models.

5.4 Cell geometries

In general three cell types were selected for investigation and these are shown in Fig.5.4.

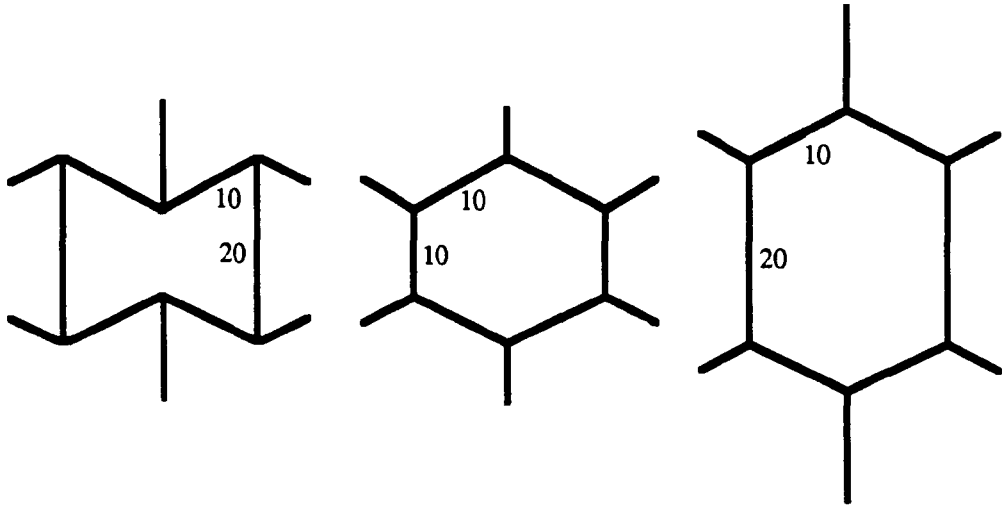

Fig.5.4 *Primary cell configurations used for specimens (All dimensions in mm)*

The re-entrant cell geometry of h =20mm, l =10mm was chosen to allow all cell angles between 0^o and -90^o to be achieved. The hexagonal geometries were then selected to give an equal cell area by selecting the equivalent positive cell angle when h =10mm and l =10mm, and identical cell wall lengths for the equivalent positive cell angle when h =20mm and l =10mm.

5.5 Fabrication of honeycombs in the laboratory

To verify the mathematical models, examples of both hexagonal and re-entrant cell honeycombs were fabricated by hand in the laboratory to the dimensions listed in Table 5.1.

Honeycomb	h (mm)	l (mm)	b (mm)
Hexagonal cell cardboard	20	10	20
Re-entrant cell cardboard	20	10	20
Hexagonal cell aluminium	10	10	10
Re-entrant cell aluminium	20	10	10

Table 5.1 *Cell dimensions of honeycombs used for tensile tests.*

Card honeycombs were made by folding narrow strips of 0.21mm card along crease lines, pre-marked by scoring with a blunt edge, to form box pleats which were then glued together using a PVA paper adhesive.

Aluminium honeycombs were made from 0.1 mm foil cut into 10mm wide strips and folded around appropriately shaped formers (Fig.5.5) to produce either hexagonal or re-entrant cell shapes. The folded strips were degreased in acetone prior to glueing together to form a honeycomb. Attempts to bond these folded preforms together using an epoxy resin were unsuccessful as its high viscosity prevented easy application without seriously deforming the thin preforms.

Aluminium soldering was not considered practicable and the most successful method of bonding was found to be cyanoacrylate ("superglue") adhesive. The instantaneous bonding of this type of adhesive also facilitated fabrication of the honeycomb specimens. These specimens performed well under the low strains used for in-plane testing but it was found that the "superglue" bonds failed easily at the on-set of buckling in the out of plane compression tests. This was inconsistent with the usual modes of failure observed in out-of-plane compression of metal honeycombs (Wierzibicki, 1983). It was therefore decided to produce compression test specimens, which deform by elastic flexing, by soaking paper honeycombs, produced from 0.16mm cartridge paper, in polyester resin.

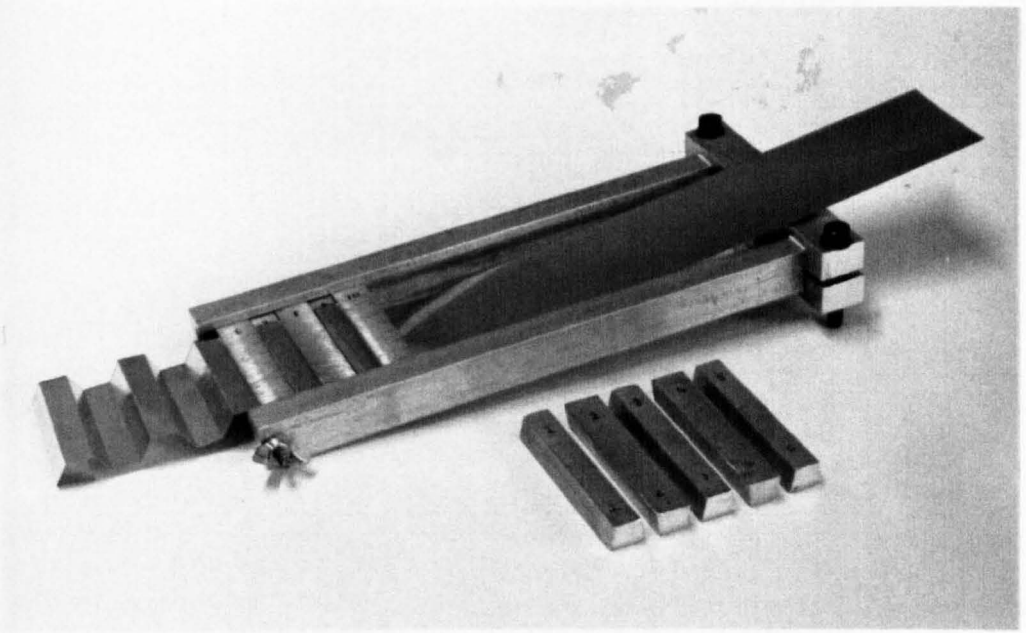

Fig. 5.5 *Jig for producing hexagonal and re-entrant cell preforms from aluminium strip. A hexagonal preform is shown during manufacture - the blocks around which the strip is folded are in the foreground.*

5.6 Effective properties of core materials

5.6.1 Measurement of Elastic properties of honeycombs

The elastic properties of the honeycombs were determined by performing tensile tests on specimens of honeycomb with their long axes oriented parallel to both the 1 and 2 directions of the honeycomb. Due to the relatively large cell sizes (Fig.5.4) used the specimens required for the tensile tests were of the order of 1m in length by 0.15m wide to enable dimension changes to be measured with reasonable accuracy and also to avoid end effects. To establish the gauge length required to eliminate end effects in the mechanical tests, two gauge lengths were marked on each specimen. The great flexibility of the honeycombs (particularly the card structures) meant that specimens of this length deformed under their own weight and it was therefore necessary to support the specimens horizontally on rollers during the tests (Fig.5.6).

(N.B.Friction loses in the pulley arrangement were investigated by wrapping the wire once around the pulley and hanging known masses on the end. The

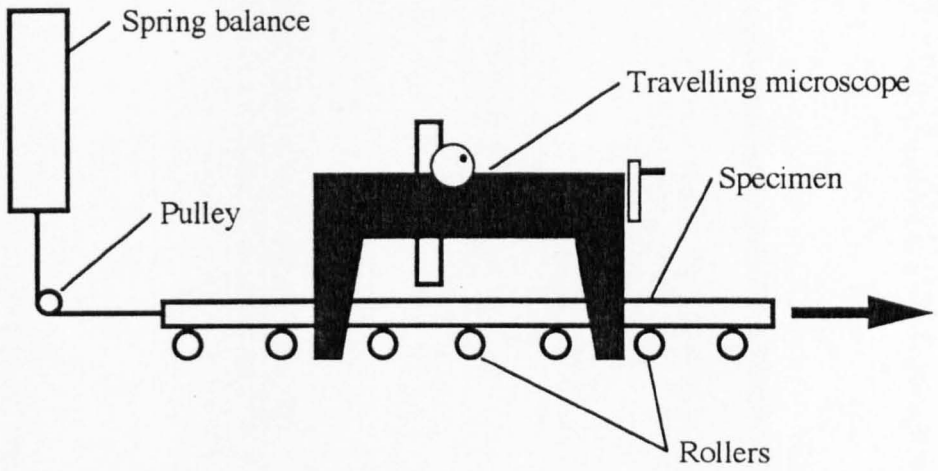

Fig.5.6 *Experimental setup for measuring elastic properties of honeycombs.*

differences between the actual masses and those recorded by the spring balance were negligible). The load was measured directly with a spring balance and the extension of the two gauge lengths measured with a travelling microscope. Stress/strain plots were generated for both gauge lengths. The procedure was repeated for different specimen lengths until the stress/strain plots coincided. Tests were performed in both 1 and 2 directions. It was established that to avoid end effects the gauge length needed to be ≤1/6 of the specimen length.

Having established the optimum gauge length the tensile tests were repeated, but in addition to measuring the longitudinal extension the lateral expansion/contraction was also measured. Gibson's work (1988) shows aluminium honeycombs behave elastically up to 10% strain whilst Fig.5.7 shows that card honeycombs can be assumed to behave elastically below 5% strain.

The moduli were determined from the initial gradients of the load/extension curves and were plotted against cell angle for each honeycomb. Poisson's ratio for each increment in load was calculated from the true longitudinal and lateral strains and again plotted against the cell angle. In order to compare these with the theoretical values of E_1 and E_2 for the flexure and hingeing models it was necessary to obtain values for K_f and K_h as described in section 5.3.3.

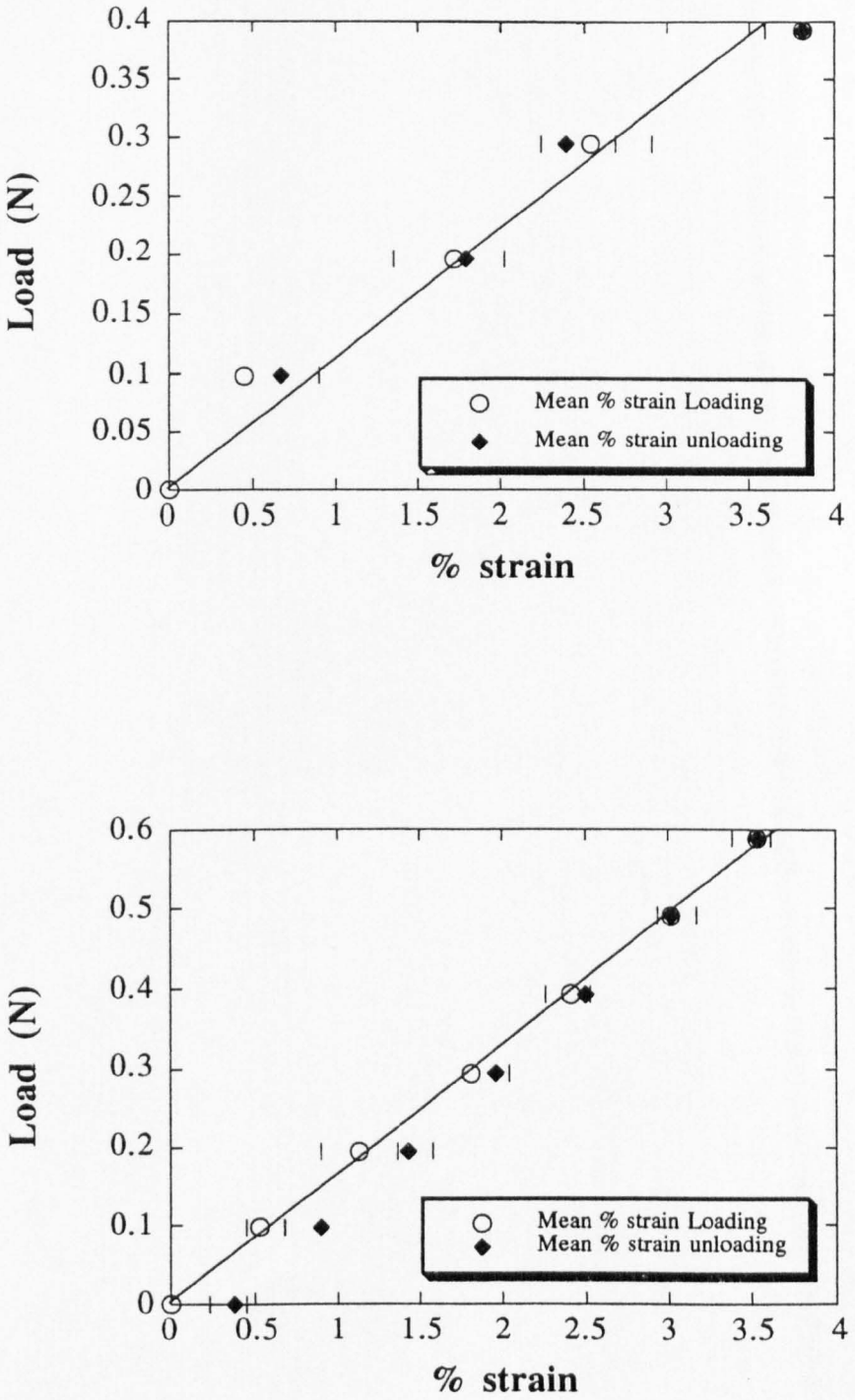

Fig.5.7 *Load vs. strain plots for hexagonal (top) and re-entrant (bottom) card honeycombs loaded and unloaded in direction 2 and not exceeding 5% strain.*

To avoid buckling effects compression tests were performed on 20mm thick, square (approx. 100mm x 100mm) specimens of honeycomb. Known loads were applied to a lightweight plate laid across the top of each specimen by means of a rod which was free to slide in a vertical guide tube (Fig.5.8). The deflections were recorded photographically using a camera of fixed focal length.

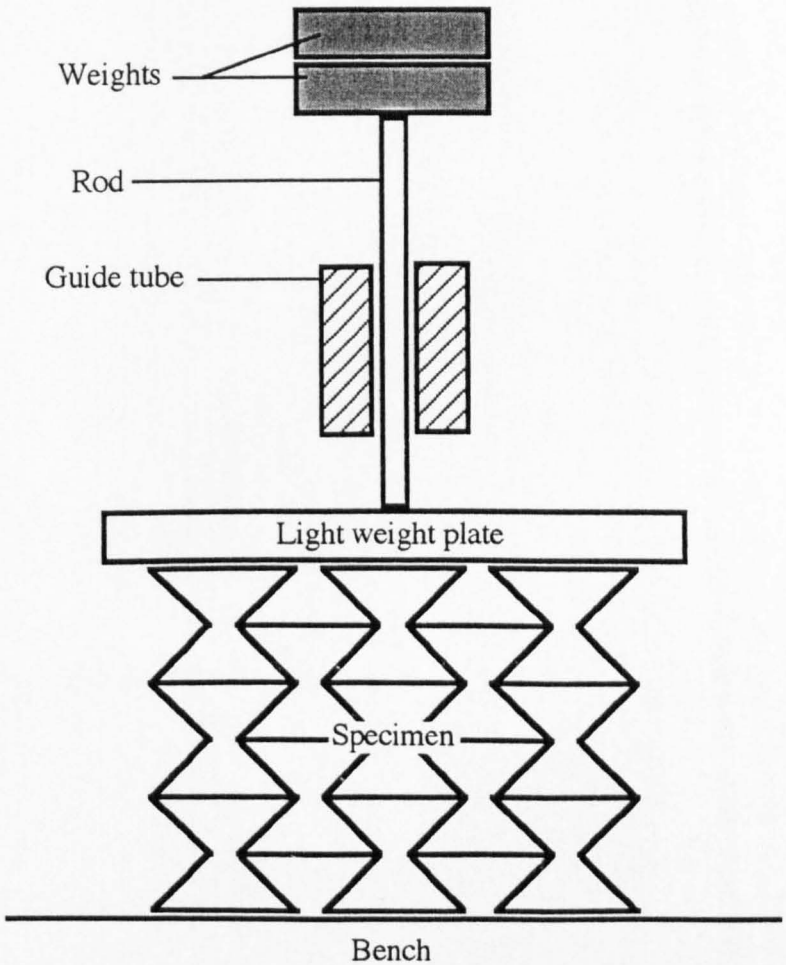

Fig.5.8 *Arrangement for in-plane compression tests*

5.6.2 In-plane shear test

These tests were performed on specimens of honeycomb contained in a "picture frame" rig as shown in the diagram Fig.5.9.

The pins at the corners are a sliding fit in the holes allowing the frame to hinge at the corners with a minimum of friction. The cut edges of the specimen were

bonded to strips of thin card the same size as the inside faces of the rig using a PVA paper adhesive. The outside of the strips were in turn bonded to the inside faces of the jig using an impact adhesive. To prevent the specimens shearing due to the frame deforming under its own weight the frame was held in the horizontal position and a force applied across diagonally opposite corners. The force P was measured directly using a spring balance and the deflection Δ from the dial test indicator.

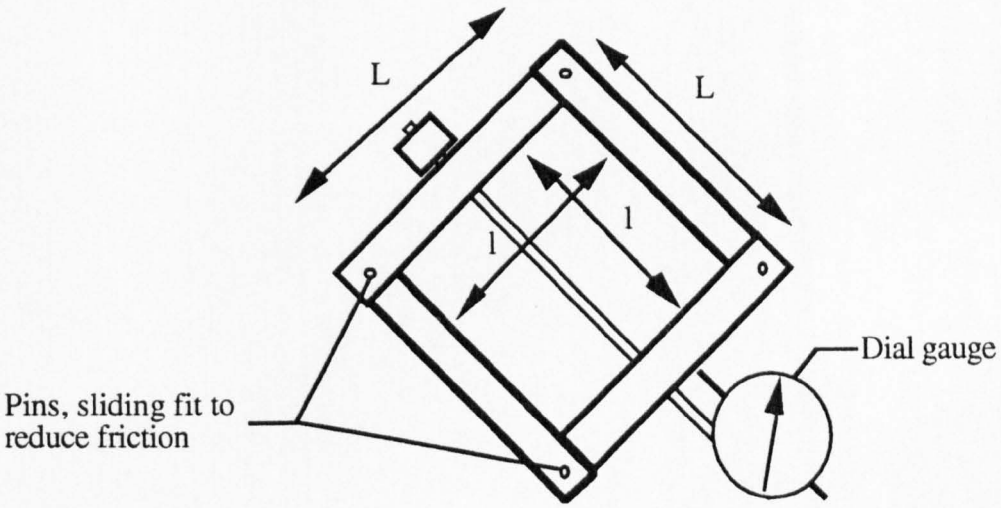

Fig.5.9 *Sketch of "picture frame" rig showing major dimensions.*

A detailed analysis of the forces acting in a "picture frame" rig has been provided by Penzien *et al.* 1964 but a much simpler approach, similar to that of Gibson *et al.* (1982), is used here since the forces required to deform the specimen are so small that increased friction in the pins due to lateral loads can be ignored.

From Fig.5.10 it is apparent that the shear strain can be calculated directly from the deflection of the frame i.e.

$$\gamma = \cos^{-1}\left(\frac{l - \Delta}{l}\right) \qquad (5.2)$$

From Fig.5.11 we obtain the relation between the applied force and the shear stress

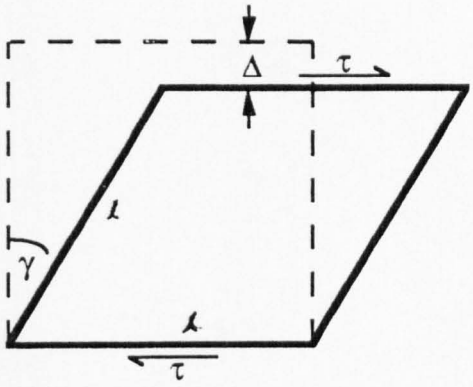

Fig.5.10 *Schematic diagram of simple shear showing how the shear strain γ and the deflection Δ can be obtained from the "picture frame" rig.*

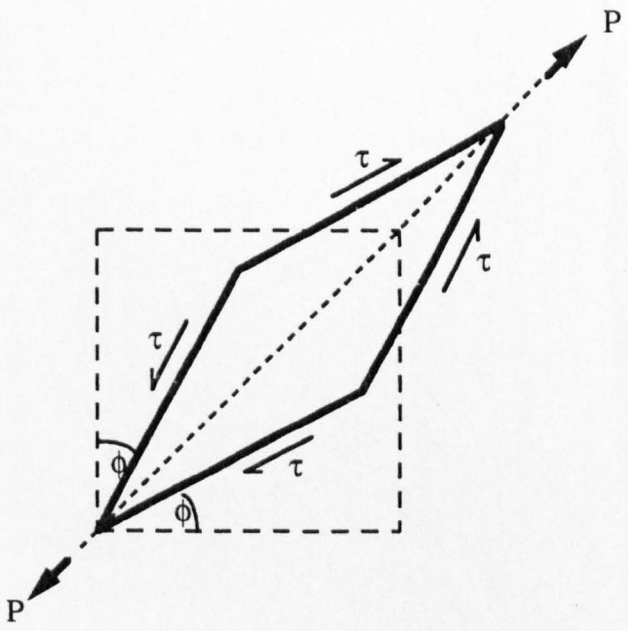

Fig.5.11 *Schematic diagram showing the relationship between the applied force P and the resultant shear force τ.*

$$\tau = P.\cos(45 - \phi) \tag{5.3}$$

which can be rewritten as

$$\tau = P.\cos\left(45 - \frac{\gamma}{2}\right) \tag{5.4}$$

for the particular condition of using a square frame.

The in-plane shear modulus G_{12} is simply obtained by measuring the gradient of the τ vs. γ plot.

5.7 Specific core material tests

5.7.1 In-plane indentation tests

These tests were conducted using the long specimens made for the tensile tests standing on their edge and a load applied to an indenter placed along the side of the specimen. Two indenters were used, one with a flat face 100mm wide and the other with a semi-circular face of 200mm diameter. The specimen was taped to the bench at the bottom corners to simulate the constraint of a large bulk of material. Vertical supports were not required as the specimens were sufficiently thick to prevent buckling out of the plane. The indenters were then pressed into the surface of the specimens using the same method as for the in-plane compression tests (Fig.5.8), and the depth of penetration below the surface was recorded photographically. Enlarging the photographic image, which also provides a useful deformation map for the material beneath the indenter (e.g.Fig.7.22), the penetration could be measured and related to both the applied load and the area of the indenter in contact with the specimen.

5.7.2 Out of plane compression tests - Multiple cells

To examine the effects of the re-entrant cell on the crush strength of honeycombs, samples of paper and resin coated paper specimens were manufactured in accordance to the dimensions specified in ASTM Specification C365-57. The samples made used the minimum number of cells required in this specification due to the time necessary to manufacture honeycombs by hand. The top and

bottom surfaces were bonded to skins of glass fibre, chopped strand mat (CSM) and polyester resin. This was done by laying a suitably sized piece of CSM on waxed glass plate and thoroughly wetting it through with resin. The honeycomb was then pressed into the wet skin and a weight applied to the top surface whilst the skin cured. The specimen was then turned over and the second skin was bonded to the core by the same method.

By making several specimens at once between two glass plates ensured that the top and bottom skins of each specimen were parallel. Specimens were then post cured in an oven at 80°C for 3 hours. For the resin coated cores the card honeycomb specimens were dipped in a bath of resin and the excess allowed to drain off prior to the application of the second skin.

To investigate the effects of the h/l ratio on the properties of the honeycomb compression specimens were made with the cell geometries listed in Table 6.2.

The compression tests were performed between platens, at a rate of 1mm per minute, on an Instron 4204 machine using a computer controlled data acquisition package. Plots of load vs. deflection were obtained for both hexagonal and re-entrant cell honeycombs.

5.7.3 Out of plane compression tests - Single cells

The effect of the core thickness was investigated using single paper cells of various lengths from b =5mm to 200mm sandwiched between thin card skins.Compression tests were performed on single cells of both re-entrant and hexagonal cells with cell angles of -30^{o} and $+30^{o}$ respectively. The cells were made to different heights (b) and included all the contacting walls cut to half their length (Fig.5.4). Card "skins" were bonded to each end of the cells to maintain the cell angles during the tests. By marking the cell shape on the "skins" prior to glueing them into place the cell angles could be controlled quite accurately.

5.7.4 Poisson's ratio by curvature measurements

The curvature measurements were made by using a modified version of the method described by Caddock *et al.* (1991). An approximately square sheet of honeycomb was bent over a former of known radius R_1, aligned with direction 1 in the honeycomb, to generate an orthogonal secondary curvature R_2 in direction 2. The latter was measured photographically, using a camera with a fixed focal length to maintain a constant magnification. Focusing was achieved by moving the camera back and forth on a focusing rail. With anticlastically curved panels a fine thread was strung across the centre of the curved specimen to enable the focus to be sharp at the plane of the primary or secondary curvature. With synclastically curved specimens the thread was draped along these planes to follow the convex contours of the deformed core.

The photographic negatives were mounted in transparency frames and a conventional projector was used to form an enlarged image of each curvature on a sheet of paper. The enlarged curvature profile was traced onto the paper for measurement. Care was taken to ensure that all these tracings were made at the same degree of enlargement. From the profiles, measurements were made of the arc heights BD at various chord lengths AC (Fig.5.12).

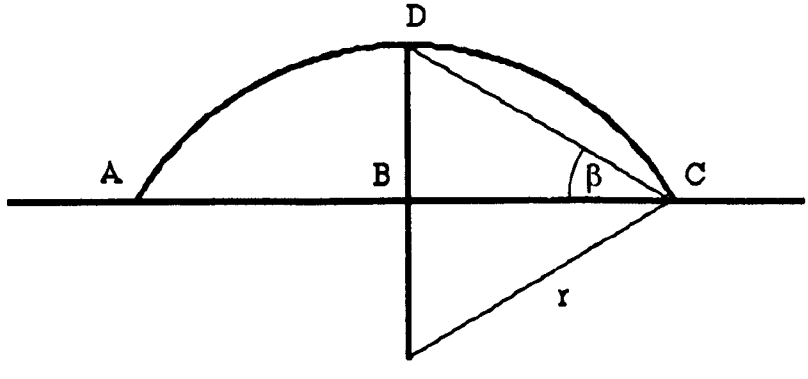

Fig.5.12 *Determination of radius of curvature.*

From Fig.5.12 we can see that

$$BC^2=r^2-(r-BD)^2 \tag{5.5}$$

and

$$\sin^2\beta=\frac{BD^2}{BD^2+BC^2} \tag{5.6}$$

where the angle β is given by

$$\beta=\frac{2\tan^{-1}BD}{AC} \tag{5.7}$$

Substituting for BC^2 in equation 5.6 we obtain an expression for the radius r

$$r=\frac{BD}{2\sin^2\beta} \tag{5.8}$$

Hence using the measured values of BD and AC in equations 5.7 and 5.8 we can obtain the radius of curvature R_2. For each specimen measurements were made over three primary curvatures of radius 0.5m, 0.7m and 1.0m. The curvature ratio method gives the best estimate of ν when the curvature approaches zero (Caddock *et al.* 1991). The ratio of the two radii is equal to the Poisson's ratio as shown in section 2.11.

5.7.5 Plate deflection tests

To examine the flexibility of the core when constrained, a square section of material was clamped along two opposite edges and left unsupported on the others. The specimen was also clamped between plates at it's centre so the specimen could really be described as two flat plates side by side each with one clamped and fixed edge and the other clamped but with a movable support Fig.5.13.

The elastic deflections of the central region of the specimen due to a load applied at the centre were recorded using a dial test indicator. By gradually increasing D and thus reducing the effective length of each plate Y we eventually reach a point

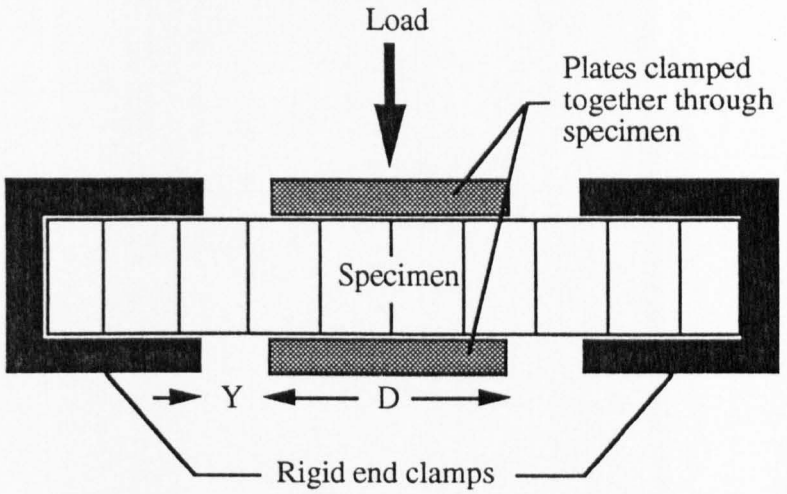

Fig.5.13 *Schematic diagram of set up for plate deflection test*

where we are measuring the through thickness shear of the honeycomb. Plots of deflection vs. load were made for various beam lengths.

Tests were carried out on cardboard, resin coated cardboard and aluminium honeycombs.

References

Specification C365-57 (Re-approved 1988)
ASTM,Philadelphia.

BS 4415 Part II (1986)
British Standards Institution, Milton Keynes.

CADDOCK,B.D.,EVANS,K.E. & MASTERS,I.G.
"Proceedings of the 8th International Conference on Composite Materials",
SAMPE Publications, Covina (1991).

GIBSON,L.J. & ASHBY,M.F.
"Cellular solids : Structure and Properties",
Chapter 4, Pages 76-81
Pergamon Press, London, (1988).

GIBSON,L.J.,ASHBY,M.F., SCHAJER,G.S. & ROBERTSON,C.I.
Proceedings of the Royal Society, London,
Vol.A382, Page 25. 1982.

MASTERS,I.G. & EVANS,K.E.
"Proceedings of the 2nd Canadian Conference on Composite Materials",
CACSMA, Montreal, 1993.

PENZIEN,J. & DIDRIKSSON,T.
AIAA Journal,
Vol.2, No.3, Pages 531-535. 1964.

REICHARD,T.W.
National Bureau of Standards, Washington D.C.
Building Science Series No.43, April 1972.

WIERZIBICKI,T.
International Journal of Impact Engineering,
Vol.1, No.2, Pages 157 174. 1983.

6) EXPERIMENTAL RESULTS

6.1 Introduction

In this chapter the results obtained from experiments with aluminium , card and paper honeycombs are presented. Analysis and interpretation of these results is carried out in chapter 7.

6.2 Elastic properties of raw materials

The load versus extension plots for the tensile tests on the paper, paper/resin and hinged card materials are shown in Figs.6.1 - 6.3. The initial moduli obtained from these plots are listed in table 6.1

Material	Modulus (GPa)
Paper	2.79
Paper + resin	3.58
Aluminium	25.00
Card, hinged	0.24

Table 6.1 *Mean moduli for materials used to fabricate the honeycombs*

Examination of the surface of the card and paper showed a preferred orientation of the fibres resulting from the manufacturing technique. For the card and paper specimens it was therefore necessary to cut specimens both parallel and perpendicular to the fibre direction. It is obvious from the initial gradients of the two plots that the properties are affected by the fibre orientation. As the honeycombs had been made from strips cut both parallel and perpendicular to the fibre orientation the mean value of the two moduli was used in any calculations.

The aluminium strip was supplied in the annealed condition and as can be seen from Fig.6.4 there is no particular variation in the modulus of specimens cut parallel to or perpendicular to the rolling direction. Again the mean value of the modulus was used for all calculations.

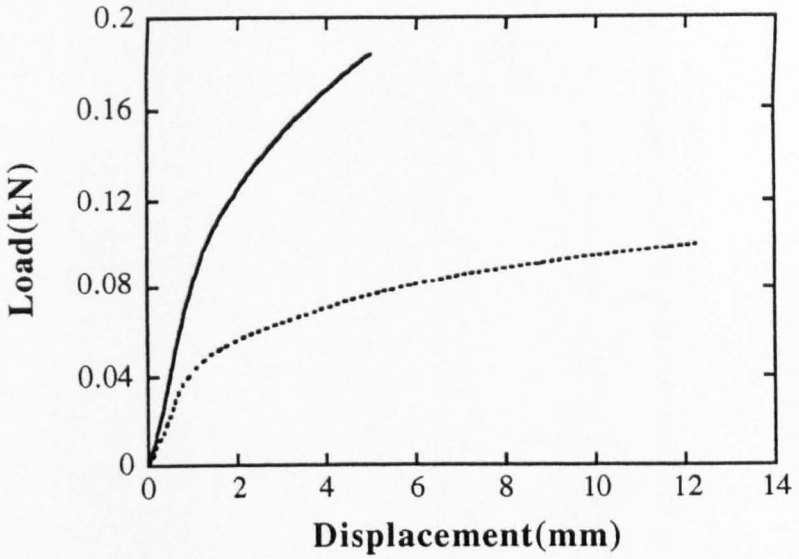

Fig.6.1 *Load vs. extension curves for 150μm cartridge paper specimens cut parallel (—) and perpendicular (•••) to the fibre direction.*

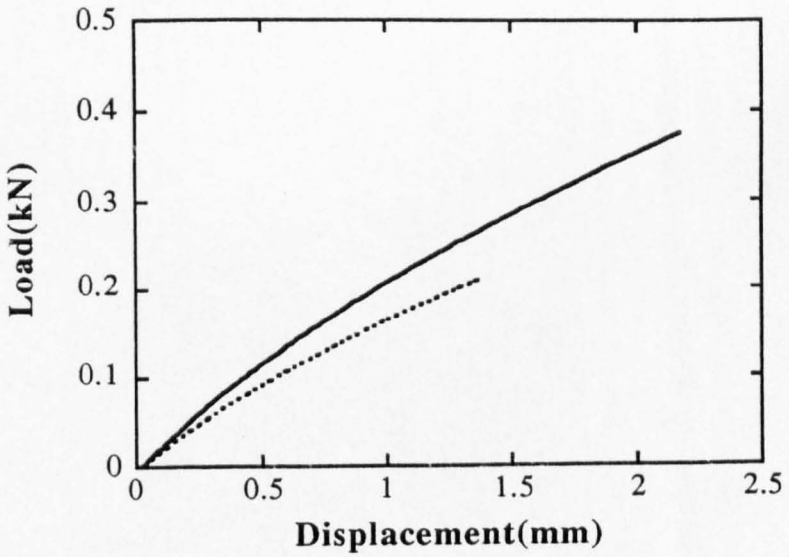

Fig.6.2 *Load vs. extension curves for resin impregnated, 150μm cartridge paper specimens cut parallel (—) and perpendicular (•••) to the fibre direction.*

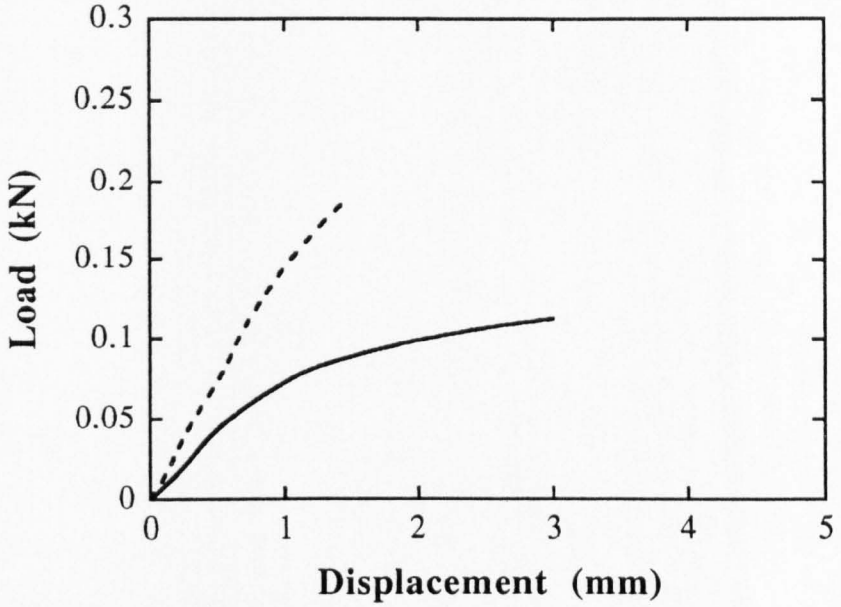

Fig.6.3 *Load vs. extension curves for hinged, 210μm clay coated cardboard specimens cut parallel (—) and perpendicular (•••) to the fibre direction.*

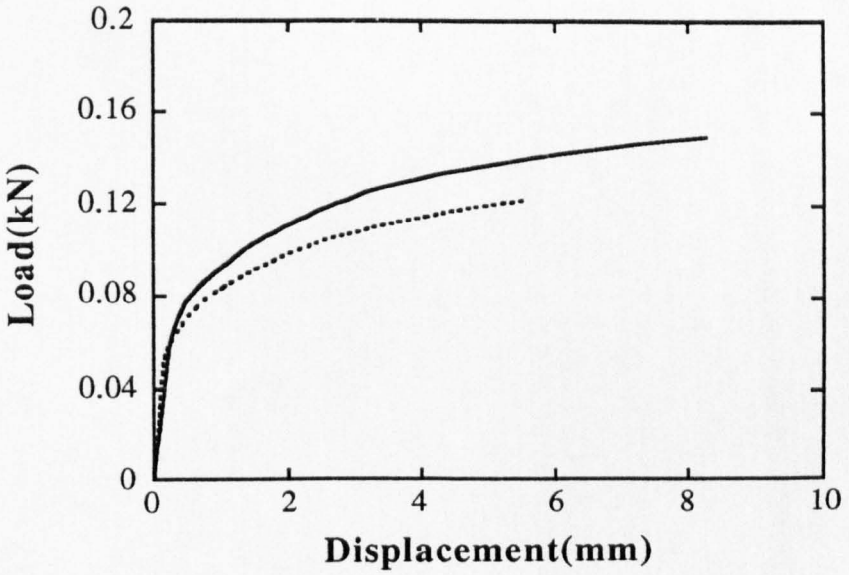

Fig.6.4 *Load vs. extension curve for 0.1mm annealed aluminium foil, for specimens cut both parallel (—) and perpendicular (• • •) to the rolling direction.*

6.3 Determination of K_f and K_h

As already mentioned in chapter 2 the flexure model of Gibson *et al.* (1981, 1982, 1988) has been successfully used to describe the behaviour of commercial honeycombs (e.g. Nomex™) which deform by flexing of the cell walls. The Gibson equations can be rewritten in terms of a force constant K_f (q.v. Section 3.2) which is simply evaluated by substituting the modulus E_s for the aluminium (Table 6.1) into equation 3.4 giving the result K_f=0.5Nmm^{-1}.

For the cardboard honeycombs the flexure model is no longer applicable since all the deformation occurs by the operation of hinges at the cell wall junctions. A model to describe this behaviour was developed in chapter 3 and again the equations can be written in terms of a force constant K_h (a function of the cell wall modulus and the cell dimensions *b*,*l* and *t*). Fig.6.5 is a plot of Load vs. angle (α) for a hinge in 210μm clay coated cardboard obtained by measuring the change in angle of a single hinge due to the application of known loads. K_h was determined from the gradient of the plot by evaluating equation 5.1.

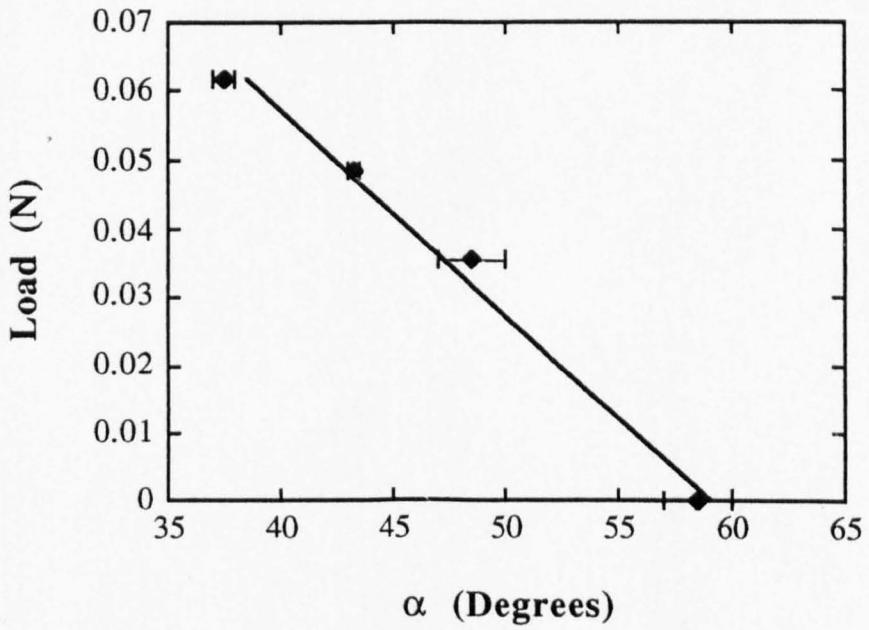

Fig.6.5 *Applied load vs. angle for a single hinge in 210μm clay coated card.*

Fig.6.6 shows that greater the number of times the hinge is operated the less resistant to deformation it becomes.

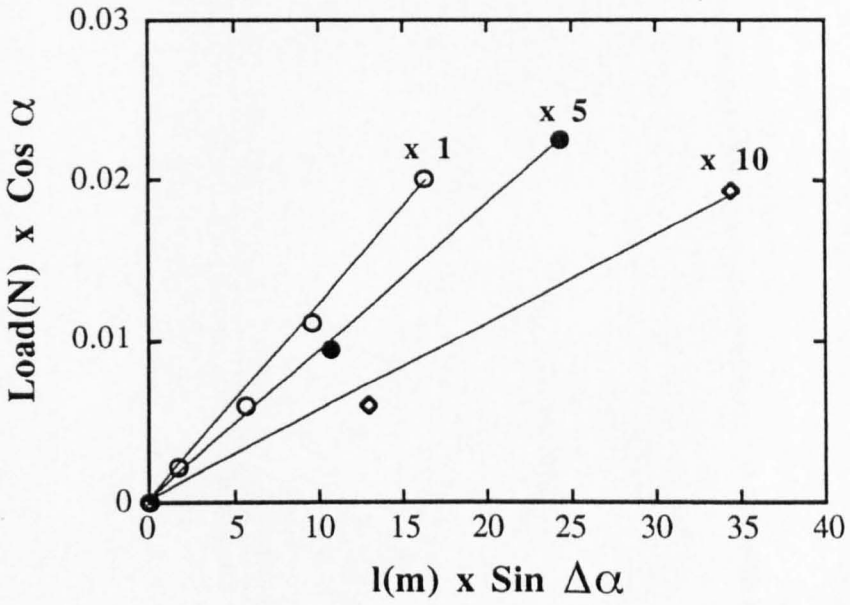

Fig.6.6 *Plots of Load x cos α vs. l x sin Δα for 210μm clay coated card specimens folded x1, x5 and x10 along the hinge line. The gradient of the plot equals the hinge constant* K_h.

6.4 Load/Extension curves for cardboard and aluminium honeycombs.

Specimens of card and aluminium honeycombs were loaded in tension and compression until complete debonding or collapse of the cells had occurred, to establish the overall shape of of the load/deflection curve. The data is presented here as load rather than stress vs. strain enabling a direct comparison between specimens which are an equal number of cells wide. The load can thus be related to the number of columns of cell walls deforming rather than the cross-sectional area of the specimen which alters significantly during the test.

Fig.6.7 shows the typical plot obtained for specimens of a hexagonal cell (h =20mm, l =10mm, θ=30^{o}), cardboard honeycomb loaded in the 1 and 2 directions. The maximum elongation is seen in direction 1 as when loaded in this direction the cell walls of length l =10mm rotate through an angle of 60^{o} until they become aligned in the direction of the applied load which then rapidly rises to the maximum strength of the cardboard.

Large extensions are achieved in direction 1 (Fig.2.1) for very small loads as the walls of length l lie almost perpendicular to the applied force thus providing the maximum moments around the points of hingeing.

When loaded in direction 2 the cell walls can only rotate through a relatively small angle of 30^{o} which causes very little extension of the specimen before all the walls are aligned in the direction of load.

Fig.6.8 shows the equivalent plots for a re-entrant celled card honeycomb of the same cell wall dimensions and a cell angle of -30^{o}. The degree of extension in direction 1 (Fig.2.1) is greatly increased as the moving walls must now rotate through an angle of 120^{o} before becoming aligned in the direction of the force. The point of inflection at an extension of approximately 20% corresponds to the the point at which θ=0^{o}. Beyond this point the cell shape becomes hexagonal.

Again when loaded in direction 2 only a small amount of extension is achieved due to the small angle change (-30^{o} to 0^{o}) and the force rises rapidly to its maximum.

It is apparent from Figs.6.7 & 6.8 that the initial parts of all four curves are approximately linear. Thus by keeping the strains to a maximum of 5% we can investigate the linear elastic behaviour of the cardboard honeycomb structures.

Figs.6.9 and 6.10 show the load/extension curves for the equivalent aluminium honeycombs. The plots for loading in direction 1 are of a similar shape to those for the card specimens (Figs.6.7 & 6.8) although there is a pronounced 'knee' at the beginning of the curve which can be attributed to the onset of plastic hingeing (Gibson *et al.* ,1988., Klintworth *et al.*, 1988).

The plots for loading in direction 2 initially rise steeply, showing linear behaviour as expected, but soon reach a plateau during which progressive failure of the adhesive bonds occurs. Very little permanent plastic deformation was observed for specimens orientated in this direction, suggesting that the honeycomb was still predominantly elastic when the adhesive bonds failed.

Figs.6.11 - 6.14 show the equivalent plots for aluminium and card honeycombs loaded in compression. The significant features to note are that again the initial deformation is approximately linear and that for both card and aluminium honeycombs loaded in direction 2 the re-entrant core is more resistant to deformation than the hexagonal. The latter effect was not observed for loading in direction 1 but this was probably due to masking of the effect by local collapse of the cells when the walls of length h move out of alignment with the direction of the applied force.

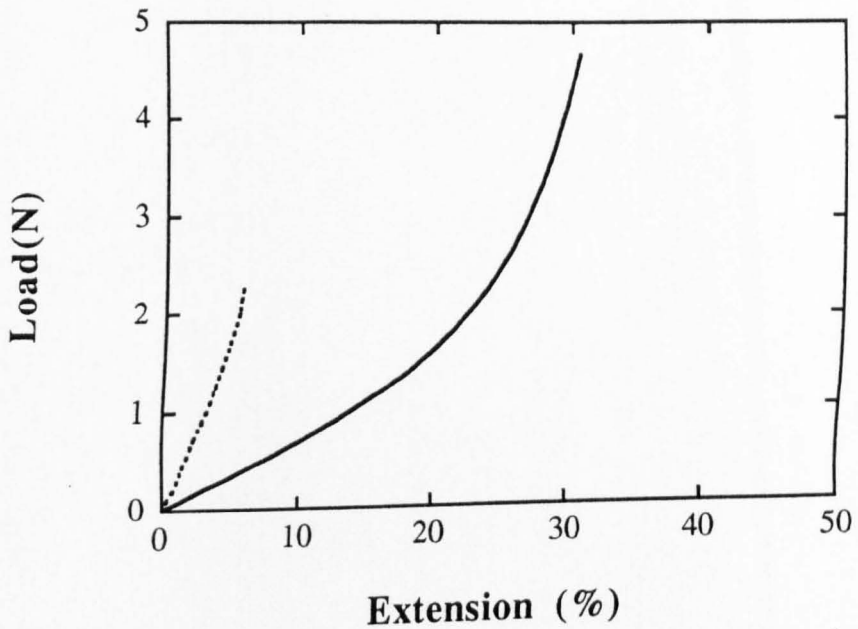

Fig.6.7 *Typical load/extension curves for hexagonal cell (h=20mm, l=10mm, θ≈40°), card honeycombs loaded in direction 1 (—) and direction 2 (···).*

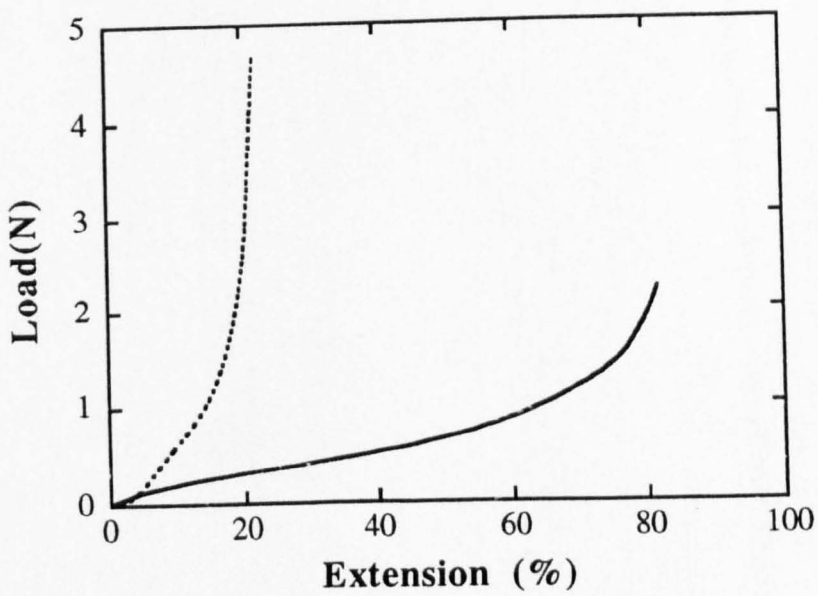

Fig.6.8 *Typical load/extension curves for re-entrant cell (h=20mm, l=10mm θ≈-32°), card honeycombs loaded in direction 1 (—) and direction 2 (···).*

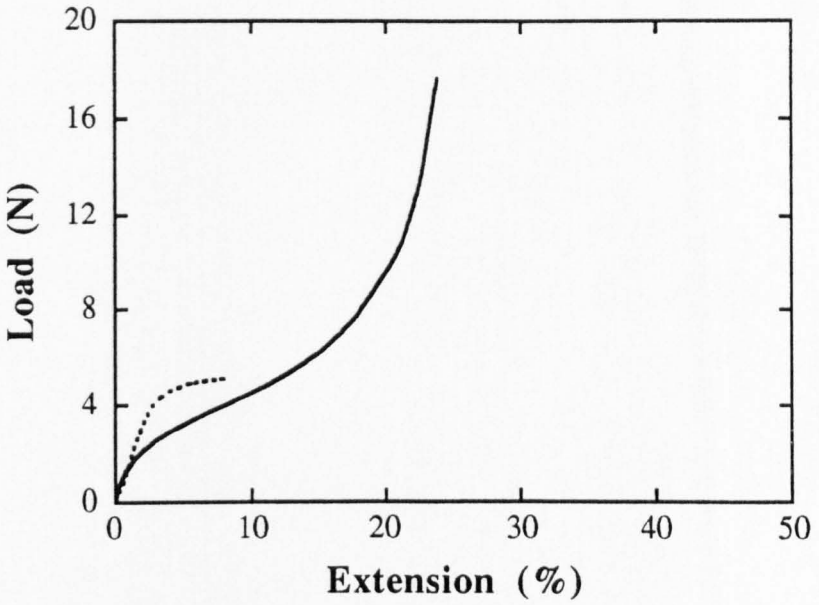

Fig.6.9 *Typical load/extension curve for a hexagonal cell ($h=l=10mm, \theta \approx 28^{o}$) aluminium honeycombs loaded in direction 1 (—) and direction 2 (⋯).*

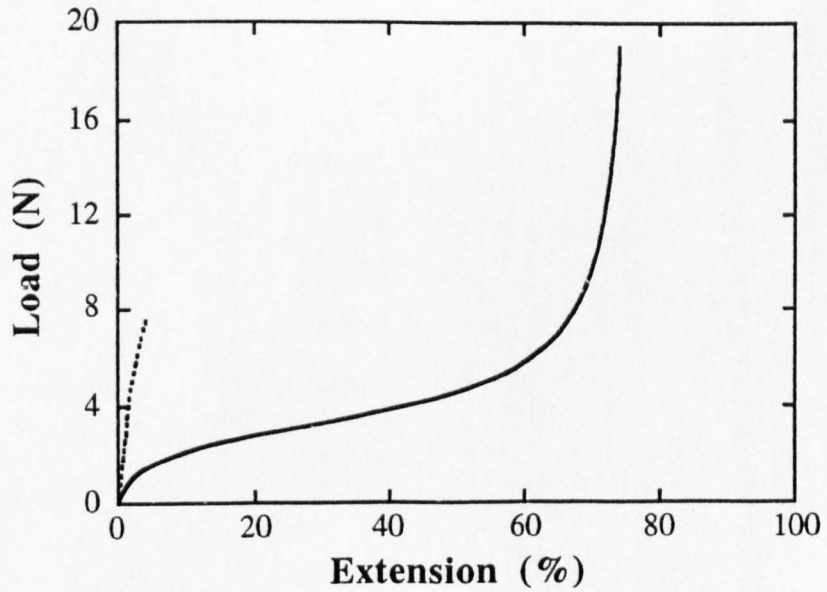

Fig.6.10 *Load/extension curve for a re-entrant cell ($h=l=10mm, \theta \approx -23^{o}$) aluminium honeycombs loaded in direction 1 (—) and direction 2 (⋯).*

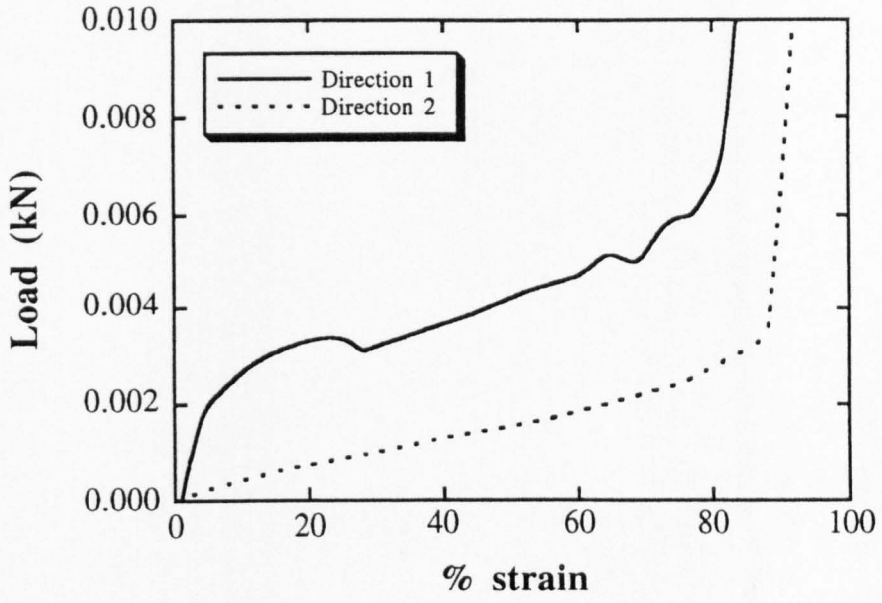

Fig.6.11 *Load/compression curves for hexagonal cell (h=20mm, l=10mm, θ≈48°) card honeycomb.*

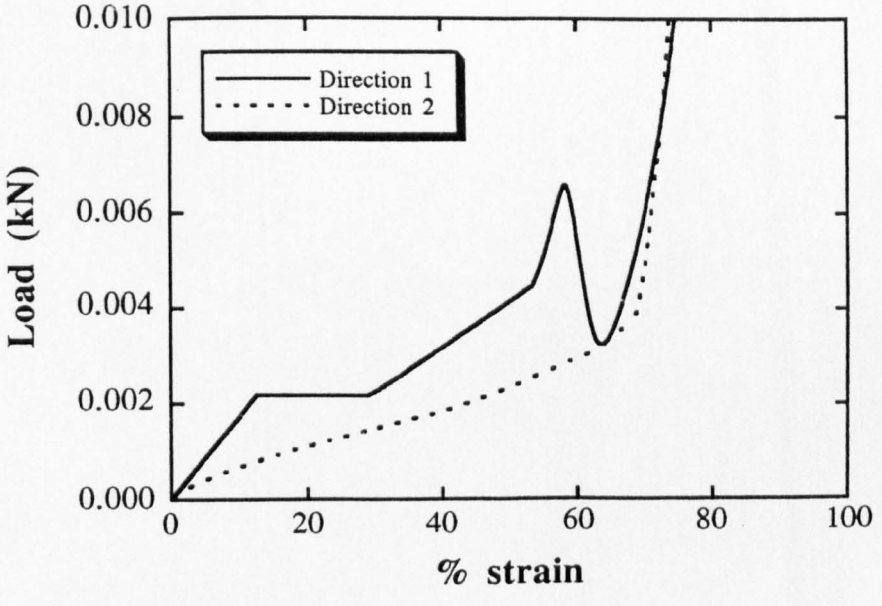

Fig.6.12 *Load/compression curves for re-entrant cell (h=20mm, l=10mm, θ≈-31°) card honeycomb.*

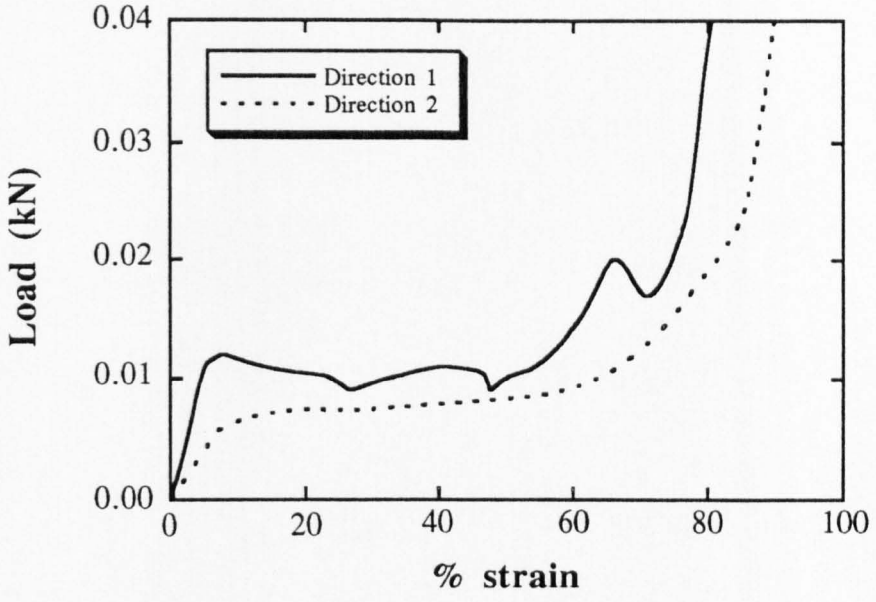

Fig.6.13 *Load/compression curves for hexagonal cell (h=10mm, l=10mm, θ≈37^{o}) aluminium honeycomb.*

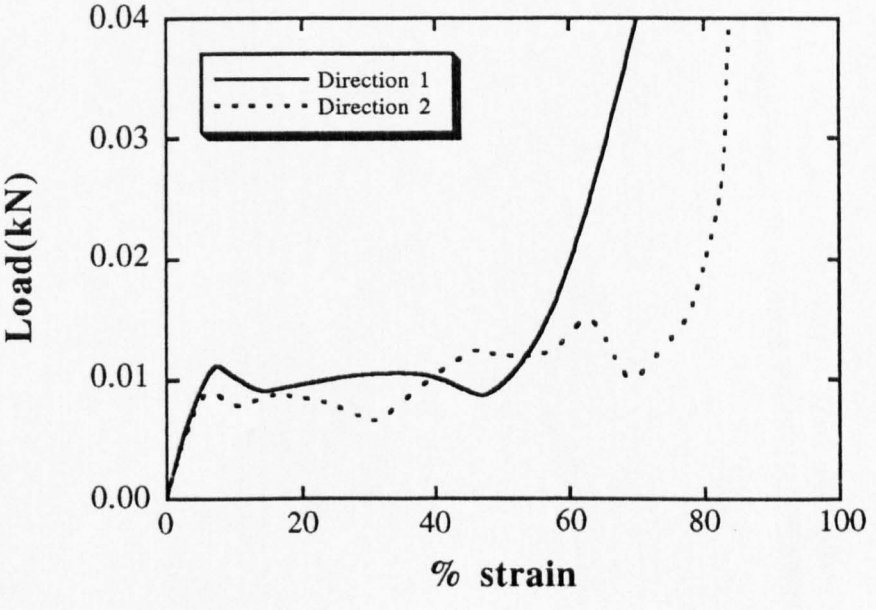

Fig.6.14 *Load/compression curves for re-entrant cell (h=20mm, l=10mm, θ≈-18^{o}) aluminium honeycomb*

6.5 Elastic modulus of honeycombs under small strains.

A typical load/extension curve for a card honeycomb, obtained using the method described in section 5.4 is shown in Fig.6.15 and shows that for the low strains (<5%) used in these experiments that linear behaviour is a reasonable assumption. The equivalent plot for aluminium honeycombs is shown in Fig.6.16 Results for both card and aluminium honeycombs compressed in direction 2 are shown in Figs.6.17 and 6.18. Note that in compression, unlike tension, the re-entrant structure is stiffer than the hexagonal.

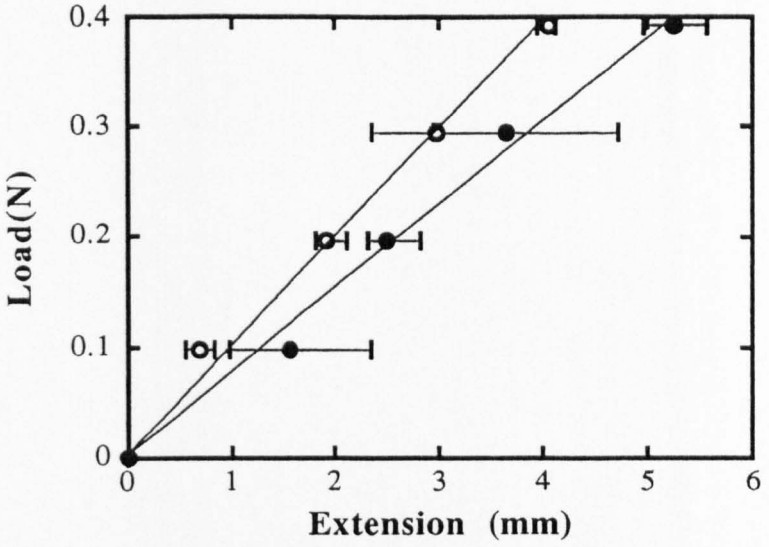

Fig.6.15 *Tensile load vs. extension plot for a* (o)*hexagonal (h=20mm, l=10mm, θ≈27°) and* (•)*re-entrant cell (h=20mm, l=10mm, θ=-39°) cardboard honeycombs loaded in direction 2.*

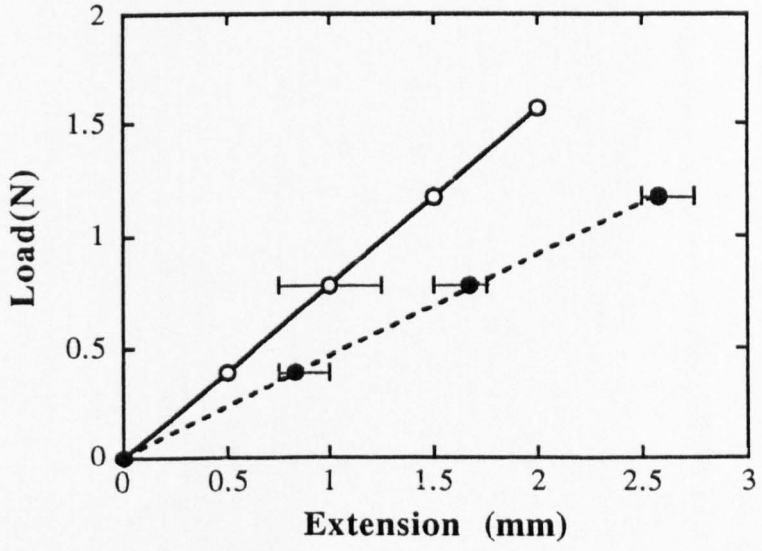

Fig.6.16 *Tensile load vs. extension plot for a* (o)*hexagonal (h=l=10mm, θ≈38°) and* (•)*re-entrant cell (h=20mm, l=10mm, θ≈-36°) aluminium honeycombs loaded in direction 1.*

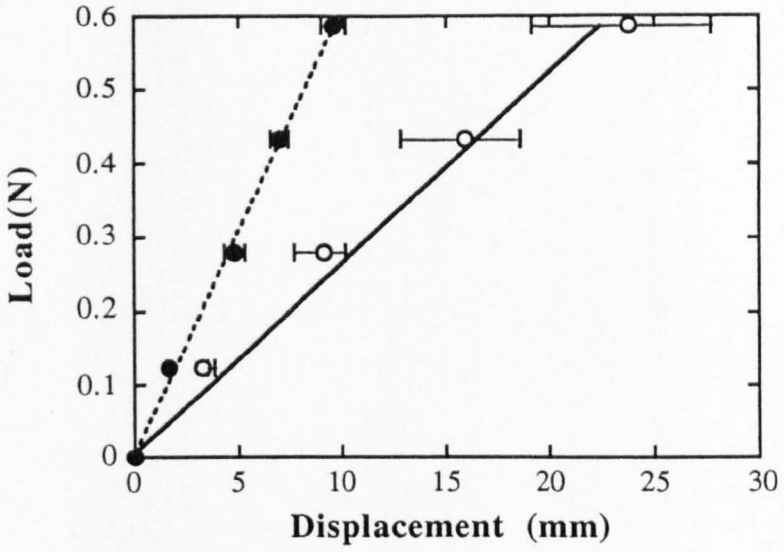

Fig.6.17 *Compressive load vs. displacement plot for a* (o)*hexagonal (h=20mm, l=10mm, θ≈49°) and* (•)*re-entrant cell (h=20mm, l=10mm, θ≈-33°) 210μm cardboard honeycombs loaded in direction 2.*

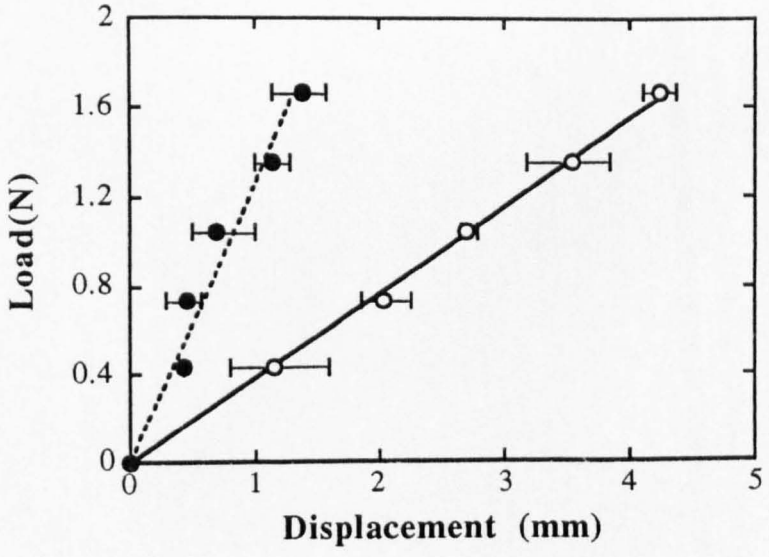

Fig.6.18 *Compressive load vs. Extension plot for a* (o)*hexagonal (h=l=10mm, θ=45°) and* (•)*re-entrant cell (h=20mm, l=10mm, θ=-24°) 100μm aluminium honeycombs loaded in direction 2.*

6.6 In-plane shear modulus

The tests performed give a direct comparison between the shear properties for equal areas of hexagonal and re-entrant cores. The load displacement curves are shown in Figs.6.19 - 6.22. It is apparent that the re-entrant cores despite having a higher density than the hexagonal equivalents have a much lower resistance to shear.

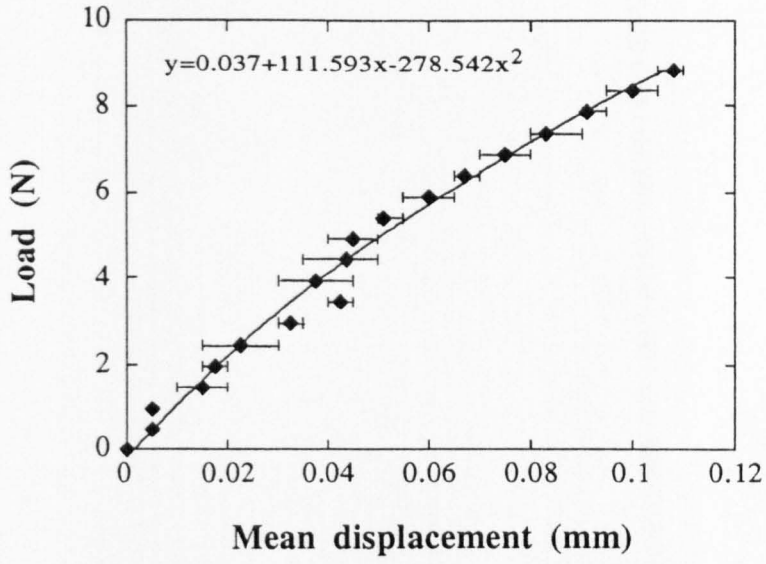

Fig.6.19 *Load vs. displacement curve for a regular hexagonal cell (h=l=10mm, $\theta \approx 31^{o)}$, aluminium honeycomb under in-plane shear.*

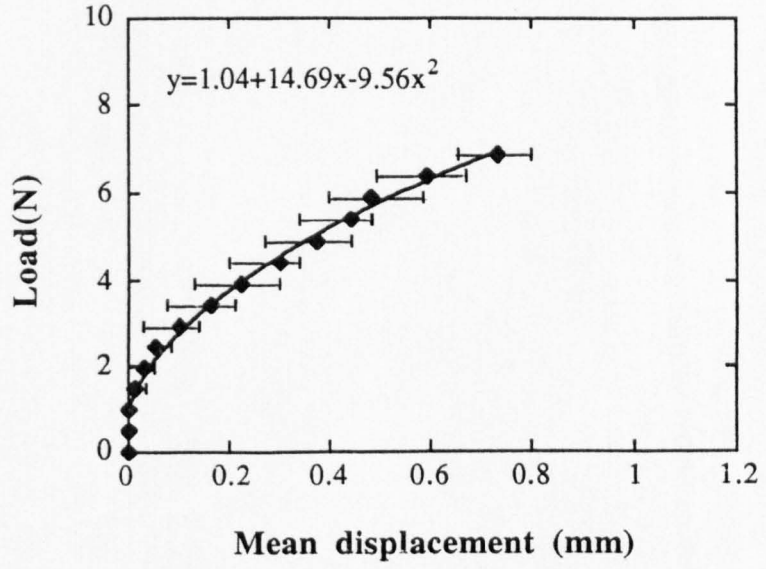

Fig.6.20 *Load vs. displacement curve for a re-entrant cell (h=20mm, l=10mm, $\theta \approx -23^{o)}$ aluminium honeycomb under in-plane shear.*

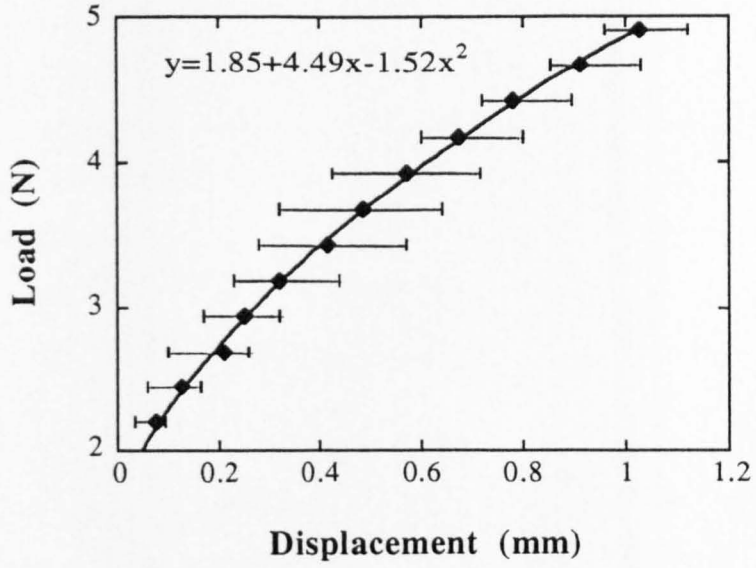

Fig.6.21 *Load vs. displacement curve for a hexagonal cell (h=20mm, l=10mm, $\theta \approx 40^{o}$) cardboard honeycomb under in-plane shear.*

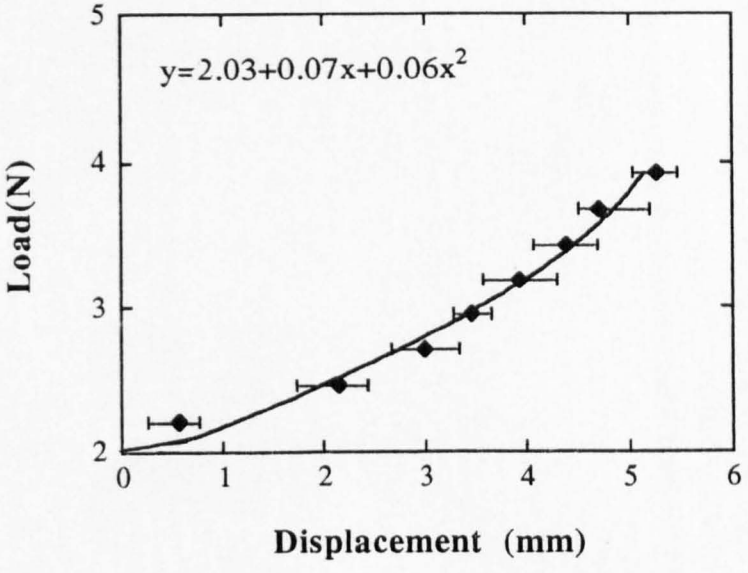

Fig.6.22 *Load vs. displacement curve for a re-entrant cell (h=20mm, l=10mm, $\theta \approx -30^{o}$) cardboard honeycomb under in-plane shear.*

6.7 In-plane indentation resistance

Tests were carried out on specimens orientated in both the 1 and 2 directions but it was difficult to obtain consistent results for elastic deflections in direction 1. This was because the double thickness walls are initially lying in the direction of the force and contacted on their ends by the surface of the indenter, quickly become misaligned (particularly with a circular indenter) and this, combined with irregularities in the construction of the honeycombs, results in local deformation of the cells directly under the indenter. Since we are primarily interested in the elastic deformation only, the results for loading in direction 2 will be considered here for analysis.

Figs 6.23 and 6.24 show the load deflection curves for hexagonal and re-entrant cell cardboard honeycombs loaded with a 100mm wide flat indenter and a 200mm diameter circular indenter respectively. In both cases the re-entrant core offers a greater resistance to indentation as can be seen by the steeper gradient of the plots. Similar behaviour was observed with the aluminium honeycombs as can be seen from Figs.6.25 and 6.26.

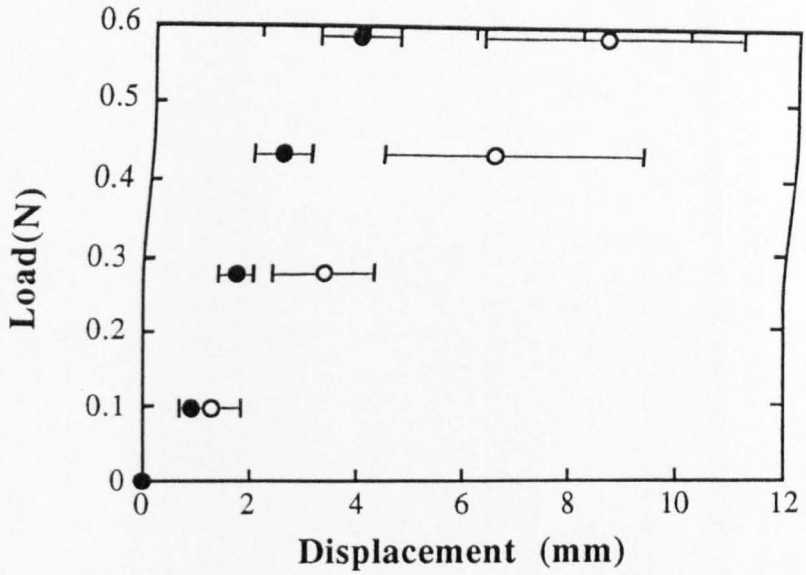

Fig.6.23 *Load vs. deflection plots for* (o)*hexagonal (h=20mm, l=10mm, θ≈48°) and* (•)*re-entrant cell (h=20mm, l=10mm, θ=-27°) card honeycombs indented in direction 2 by a 100mm wide flat indenter.*

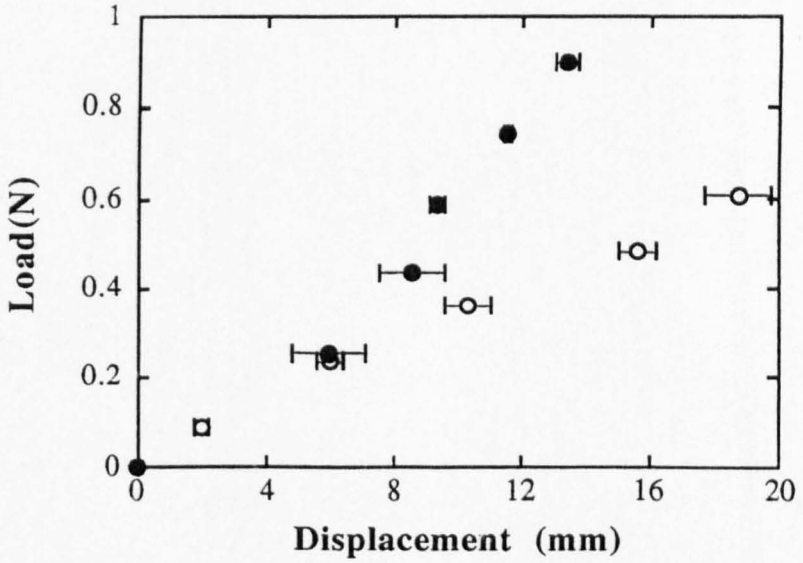

Fig.6.24 *Load vs. deflection plots for* (o)*hexagonal (h=20mm, l=10mm, θ≈48°) and* (•)*re-entrant cell (h=20mm, l=10mm, θ=-31°) card honeycombs indented in direction 2 by a 200mm diameter indenter.*

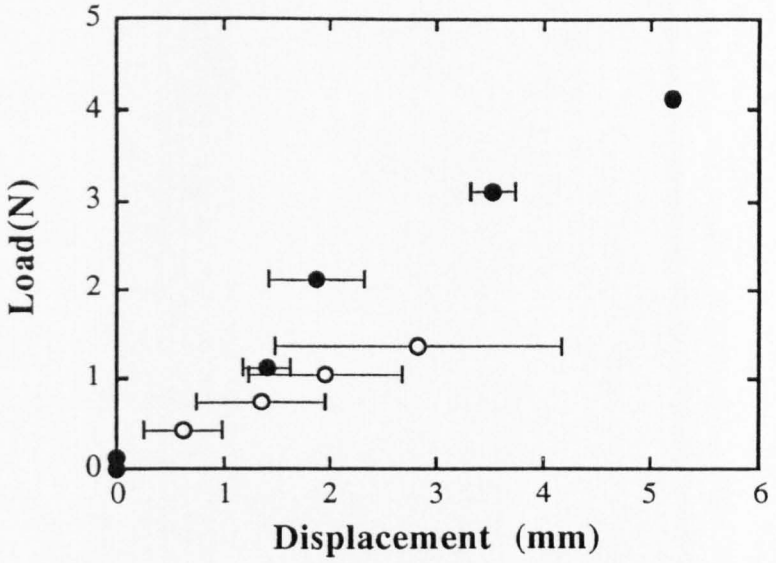

Fig.6.25 *Load vs. deflection plots for* (o)*hexagonal (h=l=10mm, θ=34°) and* (•)*re-entrant cell (h=20mm, l=10mm, θ=-17°) aluminium honeycombs indented in direction 2 by a 100mm wide flat indenter.*

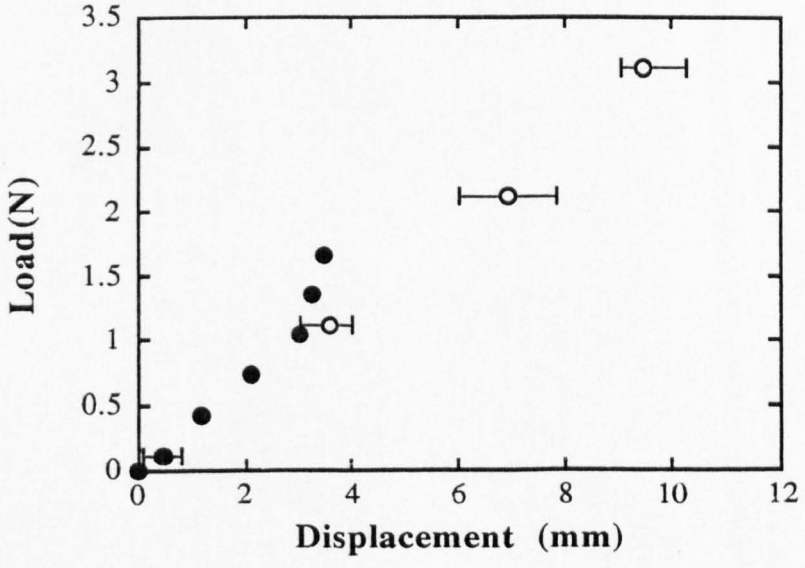

Fig.6.26 *Load vs. deflection plots for* (o)*hexagonal (h=l=10mm, θ≈45°) and* (•)*re-entrant cell (h=20mm, l=10mm, θ≈-23°) aluminium honeycombs indented in direction 2 by a 200mm diameter indenter.*

6.8 Out-of-plane compression tests

For the paper and paper/resin models used in these tests it was difficult to preset the cell angles to a specified value although as can be seen from table 6.2 the variation was normally kept within 5^{o} for each set of specimens.

The purpose of these tests was to evaluate the effect of varying the *h/l* ratio, and typical load vs. deflection curves for compression tests on small areas of paper/resin honeycombs, sandwiched between GRP skins, are shown in Figs. 6.27 and 6.28. Similar plots (Figs.6.29 and 6.30) were obtained for the paper cores. The mean failure stresses, obtained by dividing the failure load by the core area, are listed in Table 6.3 for both the paper and paper/resin honeycombs. The strains to failure are listed in Table 6.4.

	Compression strength (kPa)		
	***h/l* =1**	***h/l* =2**	***h/l* =3**
Hexagonal paper	167.62	103.37	--
Re-entrant paper	--	163.27	124.46
Hexagonal paper+resin	826.51	506.43	--
Re-entrant paper+resin	--	965.15	475.86

Table 6.3 *Mean failure stresses for paper and paper+resin honeycombs compressed in a direction parallel to the cell axes (Max error ±12.5%).*

	Strain to failure		
	***h/l* =1**	***h/l* =2**	***h/l* =3**
Hexagonal paper	0.0051	0.0057	--
Re-entrant paper	--	0.0051	0.0065
Hexagonal paper+resin	0.0159	0.0146	--
Re-entrant paper+resin	--	0.0138	0.0118

Table 6.4 *Mean strain to failure for paper and paper+resin honeycombs compressed in a direction parallel to the cell axes. (Max. error =±20%)*

Specimen	Specimen No.	Cell angle (Degrees) h/l=10/10	h/l=20/10	h/l=30/10
Hexagonal paper	HP1.1	36.7	--	--
	HP1.2	35.1	--	--
	HP1.3	36.2	--	--
	HP2.1	--	34.2	--
	HP2.2	--	34.2	--
	HP2.3	--	37.1	--
Hexagonal paper+resin	HR1.1	42.3	--	--
	HR1.2	38.4	--	--
	HR1.3	41.9	--	--
	HR2.1	--	34.1	--
	HR2.2	--	35.8	--
	HR2.3	--	36.6	--
Re-entrant paper	RP1.1	--	44.1	--
	RP1.2	--	39.8	--
	RP1.3	--	39.1	--
	RP2.1	--	--	50.0
	RP2.2	--	--	46.8
	RP2.3	--	--	47.7
Re-entrant paper+resin	RR1.1	--	41.4	--
	RR1.2	--	43.7	--
	RR1.3	--	40.9	--
	RR2.1	--	--	45.3
	RR2.1	--	--	50.0
	RR2.3	--	--	41.9

Table 6.2 *Cell angles for specimens used in out-of-plane compression tests.*

Paper and paper/resin honeycombs showed the same relative behaviour between the re-entrant and hexagonal cell shapes. It is apparent from the Tables 6.3 and 6.4 that in both the hexagonal and re-entrant cases the failure stress, and the strain to failure, are reduced as the *h/l* ratio increases. This is not unexpected as the density of the core is reduced as *h/l* increases thus reducing the amount of cell wall material available to support the load over a given area of honeycomb. The re-entrant cell honeycombs have higher densities than their hexagonal counterparts and thus have significantly higher failure loads.

All the specimens were compressed by 10mm from their original gauge length of approximately 50mm. On removal of the load a degree of recovery was noticed (Fig 6.31) with all the specimens but was particularly noticeable with the re-entrant paper/resin samples (Table 6.5).

Each specimen was retested again by compressing down to 40mm length. The load was found to gradually increase up to the point at which the first test was terminated, showing that there was no recovery in strength (Figs.6.27 and 6.28).

	Mean recovery (%)		
	***h/l*=10/10**	***h/l*=20/10**	***h/l*=30/10**
Hexagonal paper	30.2	46.0	--
Hexagonal paper+resin	49.0	49.8	--
Re-entrant paper	--	53.8	72.5
Re-entrant paper+resin	--	61.8	73.5

Table 6.5 *Mean recovery, expressed as a percentage of the original thickness (50mm), of paper and paper+resin honeycombs on removal of the load after being compressed by 10mm along their cell axes.*

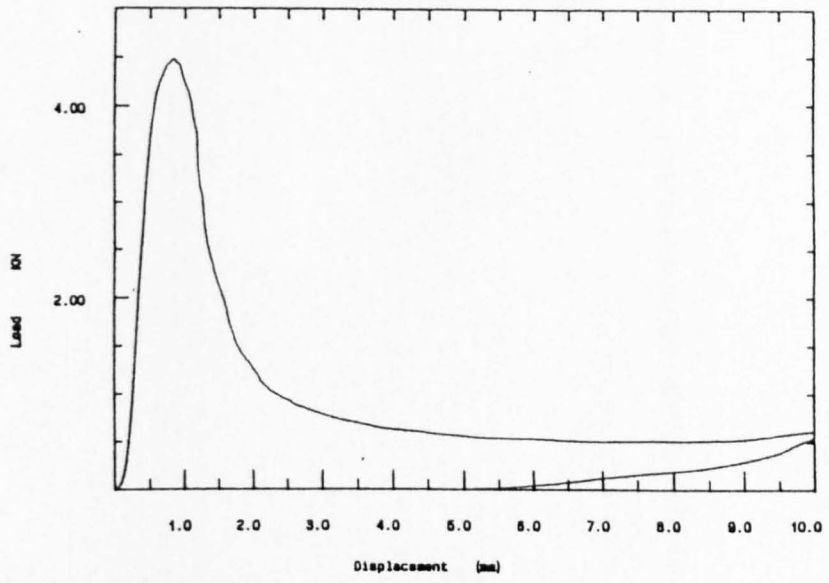

Fig.6.27 *Typical load/deflection plot (a) for a 50mm thick hexagonal cell paper/resin honeycomb compressed 10mm in the direction of the cell axes. (h=l=10mm). Curve (b) shows that there is no recovery of strength when the same honeycomb is reloaded up to 10mm deflection.*

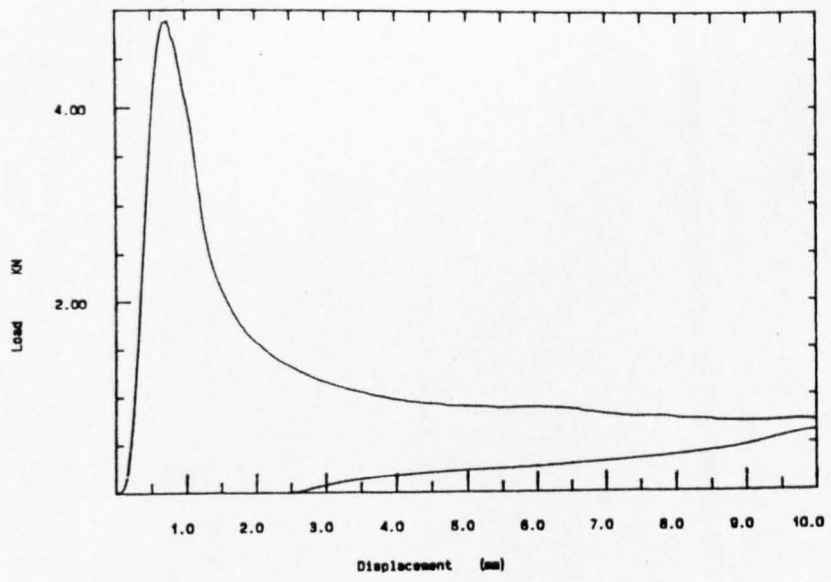

Fig.6.28 *Typical load/deflection plot (a) for a 50mm thick re-entrant cell paper/resin honeycomb compressed 10mm in the direction of the cell axes. (h=20mm, l=10mm). Curve (b) shows that there is no recovery of strength when the same honeycomb is reloaded up to 10mm deflection.*

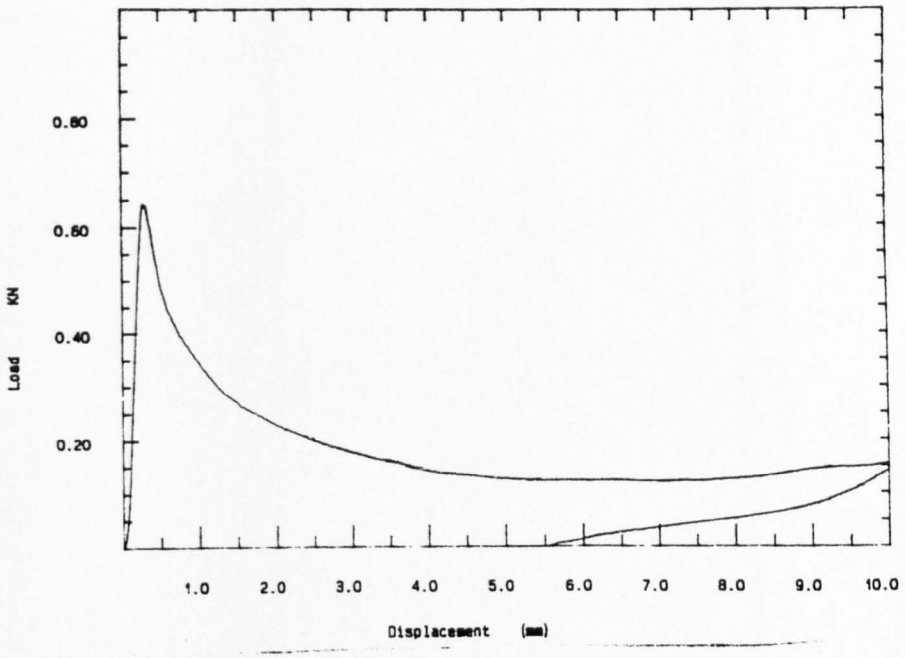

Fig.6.29 *Typical load/deflection plot (a) for a 50mm thick hexagonal cell paper honeycomb compressed 10mm in the direction of the cell axes. (h=l=10mm). Curve (b) shows that there is no recovery of strength when the same honeycomb is reloaded up to 10mm deflection.*

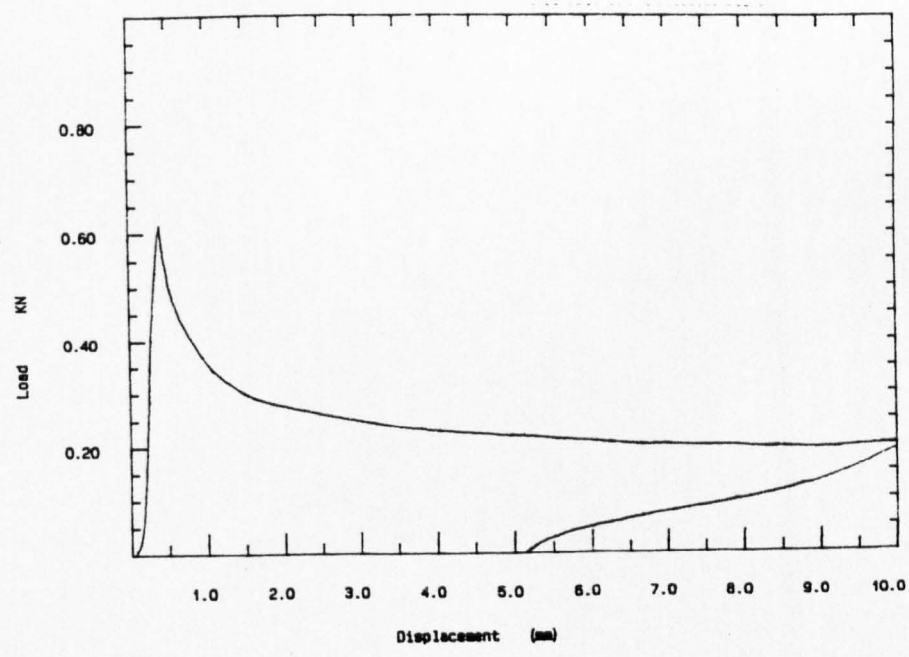

Fig.6.30 *Typical load/deflection plot (a) for a 50mm thick re-entrant cell paper honeycomb compressed 10mm in the direction of the cell axes. (h=20mm, l=10mm). Curve (b) shows that there is no recovery of strength when the same honeycomb is reloaded up to 10mm deflection.*

a)

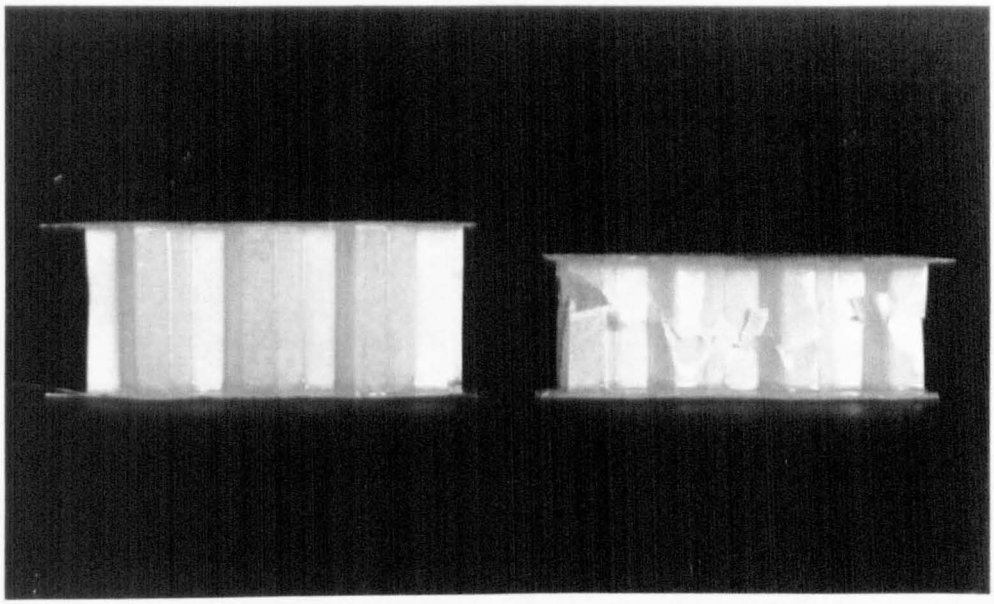

b)

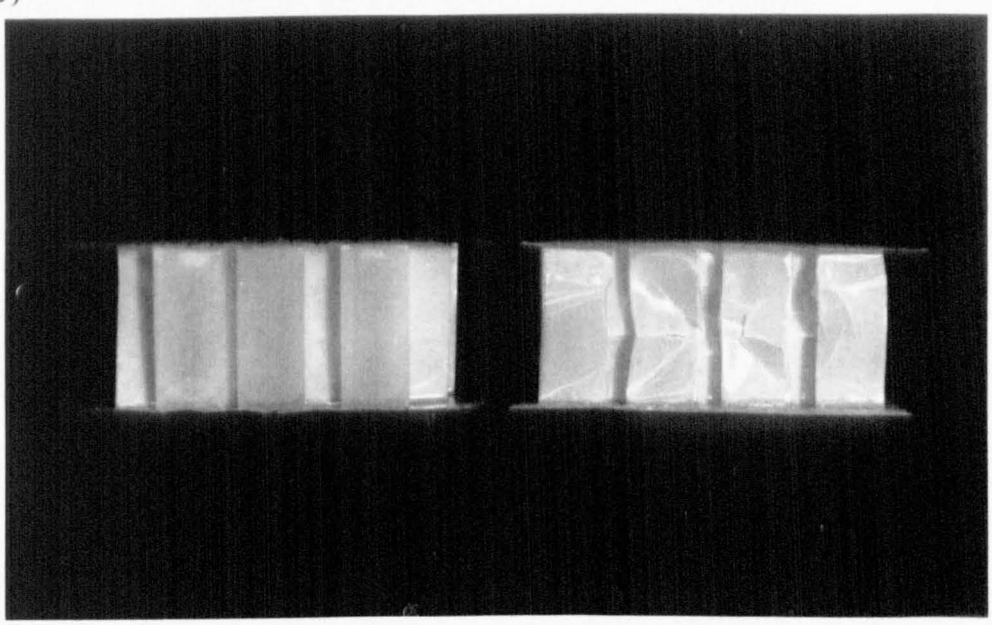

Fig.6.31 a) *50mm high section of hexagonal cell paper/resin honeycomb before (left) and after being compressed by 10mm (right).*
b) *50mm high section of re-entrant cell paper/resin honeycomb before (left) and after being compressed by 10mm (right). Note the large amount of recovery compared to the hexagonal honeycomb.*

6.9 Out-of-plane single cell compression tests

To evaluate the effects of the core thickness b on the out-of-plane strength, compression tests were performed on single cells of different axial lengths. To simulate the constraining effects of adjacent cells adjoining cell walls of lengths $h/2$ and $l/2$ (Fig.5.4) where included in the tests. A plot of failure load vs. b is given in Fig.6.32.

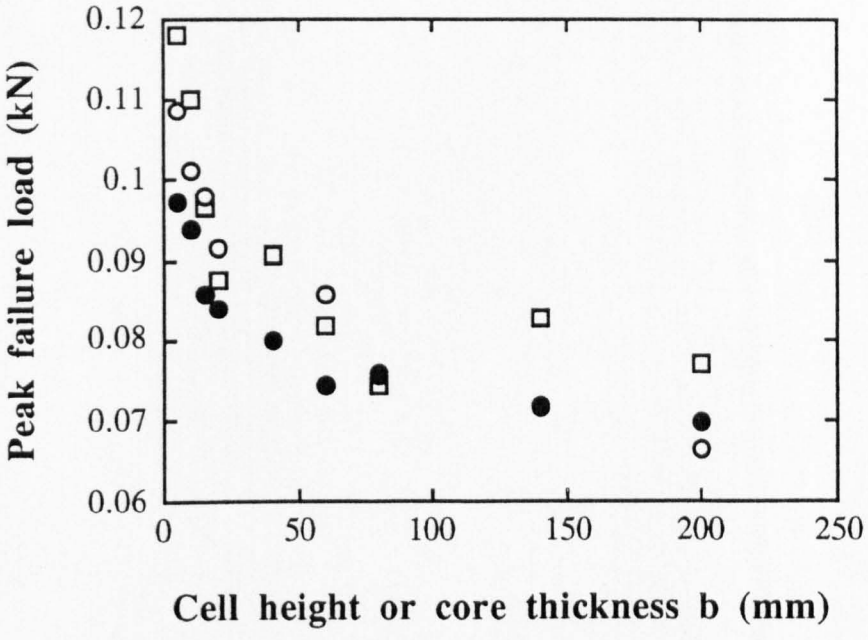

Fig.6.32 *Peak failure load vs. core thickness for single paper cells compressed along the cell axis. Hexagonal cells (□) h=20mm, l=10mm, θ=30°, (o) h=l=10mm, θ=30°. Re-entrant cell (•) h=20mm, l=10mm, θ=-30°.*

All three geometries used in these tests show significant increases in the load to failure when the axial length of the cell is less than 50mm in length. The regular hexagonal cell ($h=l$ =10mm) and the re-entrant cell (h =20mm, l =10mm) have very similar cell wall cross-sectional areas and as can be seen from Fig.6.30 have similar behaviour. The change in cell angle from +30° to -30° seems to have little effect. The irregular hexagonal cell (h =20mm, l =10mm) has a much larger cell wall cross sectional area and this can account for the higher failure loads observed.

The strain to failure is plotted against the core thickness (b) for single paper cells in Fig.6.33. The hexagonal and re-entrant cells show very similar behaviour over the range of cell lengths tested. Little variation in the strain is observed when $50<b<200$ but it rises rapidly when $b<20$mm

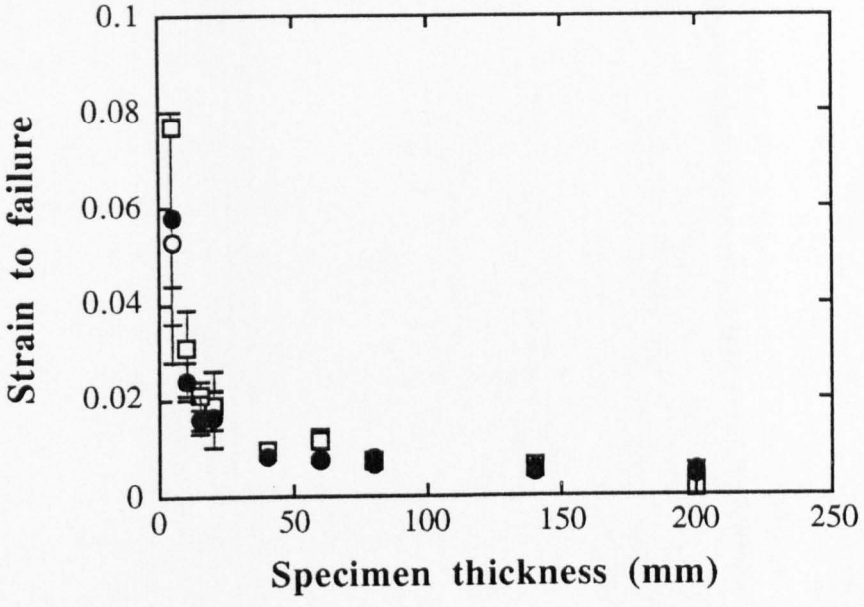

Fig.6.33 *Strain to failure vs. core thickness for single paper cells compressed along the cell axis. Hexagonal cells (□) h=20mm, l=10mm, θ=30°, (o) h=l=10mm, θ=30°. Re-entrant cell (•) h=20mm, l=10mm, θ=-30°.*

6.10 Poisson's ratio by curvature measurement

Figs.6.34 - 6.37 show the plots of radius R_2 in direction 2 vs. radius R_1 in direction 1 when a comparatively thin (20mm) sheet of honeycomb is bent out-of-plane. We know from Section 2.11 that the ratio of the two radii of curvature is equal to the Poisson's ratio. Hence evaluating equation 3.19 or 3.20 for the particular cell geometry under test we can predict the theoretical variation of R_2 with R_1. This is shown by the solid lines on the graphs. (N.B.The ratio $R_1/R_2=\nu_{12}$.and $R_2/R_1=\nu_{21}$).

Both the hexagonal (Fig.6.34) and re-entrant (Fig.6.35) card models achieve similar gradients to those predicted by the theory although the radii (R_2) are larger than expected. The increased flexibility of the cardboard structures, particularly the re-entrant cell structure, we would expect to improve drapeability and hence provide smaller radii than those predicted by the theory.

For aluminium, the hexagonal honeycomb deviates from linearity when $R_2>0.5$m i.e.R_2 is much larger than expected and is possibly explained by smaller value of *h/l* (1.0) which makes the honeycomb much stiffer reducing the range of curvatures over which R_1/R_2= Poisson's ratio applies. The aluminium re-entrant honeycomb is much more flexible and behaves as predicted by the theory.

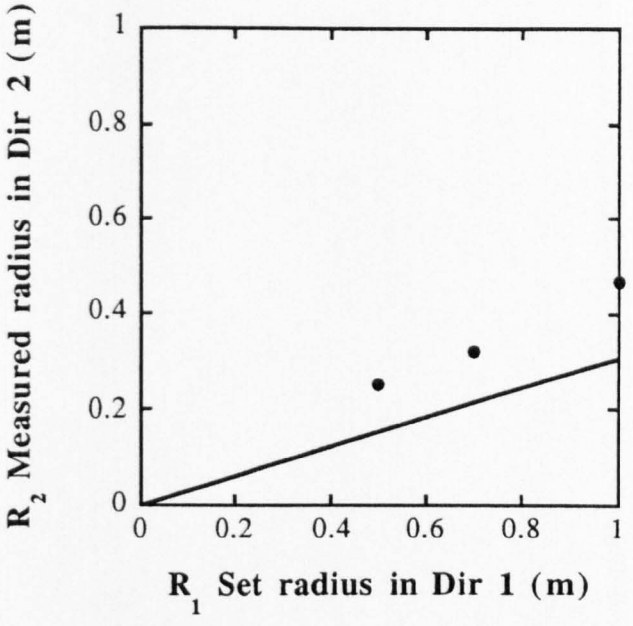

Fig.6.34 *Ratio of curvatures for a hexagonal cell (h=20mm, l=10mm, θ=42°) cardboard honeycomb determined by setting to known curvatures in direction 1 and measuring that in direction 2. (—) shows the theoretical variation of R_2 with R_1.*

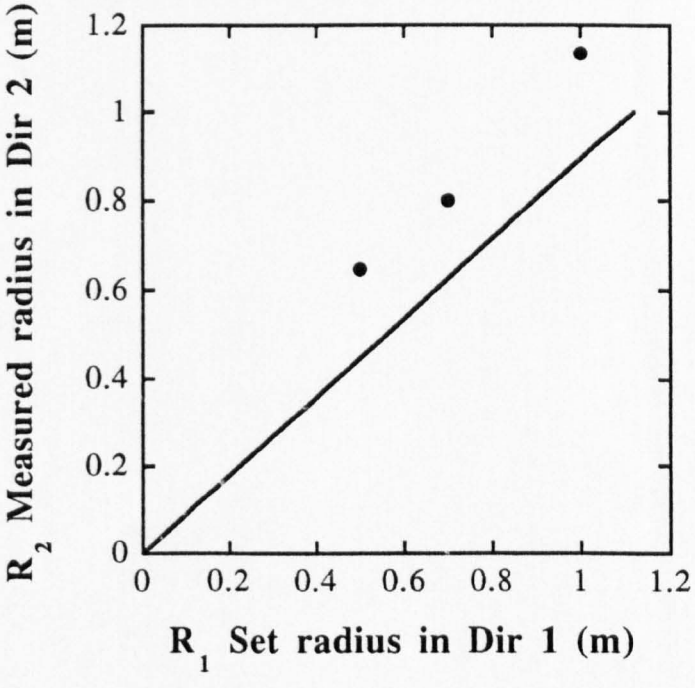

Fig.6.35 *Ratio of curvatures for a re-entrant cell (h=20mm, l=10mm, θ=-33°) cardboard honeycomb. Determined by setting to known curvatures in direction 1 and measuring that in direction 2. (—) shows the theoretical variation of R_2 with R_1.*

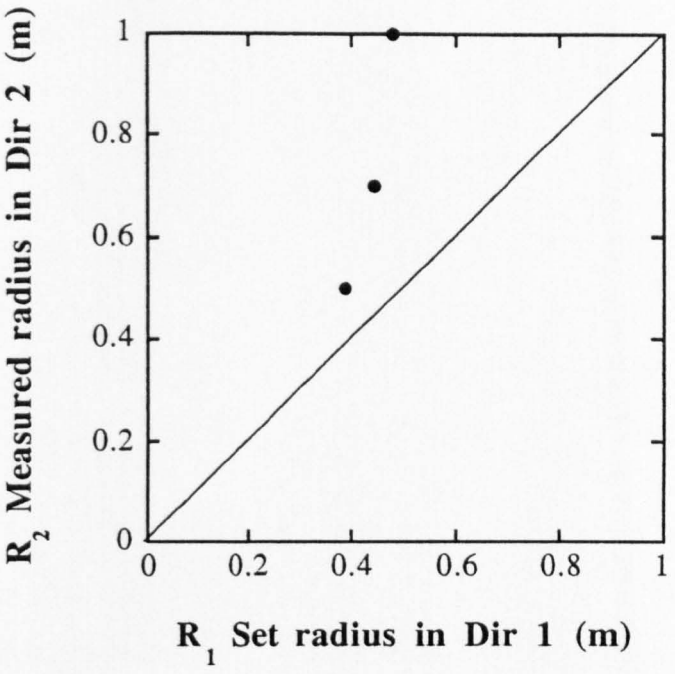

Fig.6.36 *Ratio of curvatures for a hexagonal cell (h/l=10mm, θ=30°) aluminium honeycomb determined by setting to known curvatures in direction 1 and measuring that in direction 2. (—) shows the theoretical variation of R_2 with R_1.*

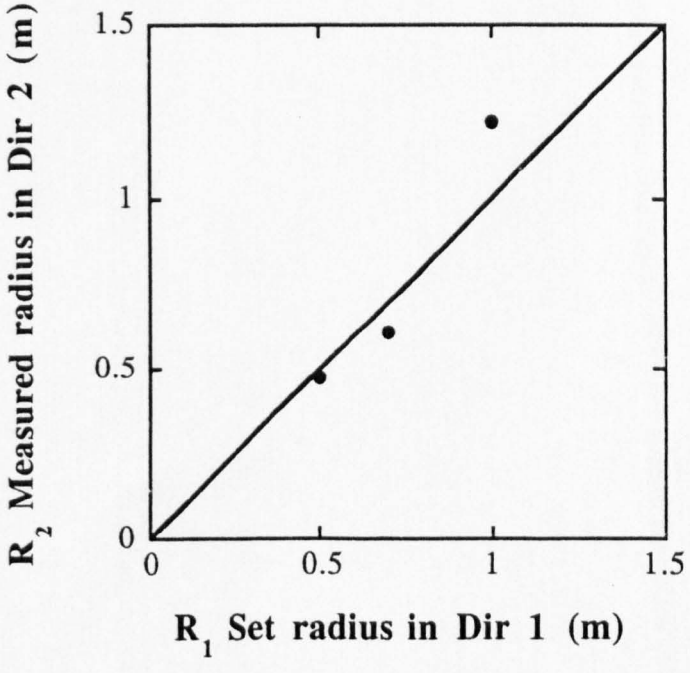

Fig.6.37 *Ratio of curvatures for a re-entrant cell (h=20mm, l=10mm, θ=-30°) cardboard honeycomb determined by setting to known curvatures in direction 1 and measuring that in direction 2. (—) shows the theoretical variation of R_2 with R_1.*

6.11 Plate deflection tests

Experiments with the cardboard honeycombs were inconclusive as it was difficult to obtain repeatable results. This was because of the high flexibility of the card honeycombs and the difficulty in producing a central clamping plate which was sufficiently stiff not to deform itself under the applied load and yet light weight enough not to deform the honeycomb under its own weight since the high flexibility of the core meant only very small loads were required. The resistance of the dial gauge also affected the results. However the stiffness of the honeycomb plate was observed to increase as the length was reduced.

The tests with the aluminium honeycombs were more consistent and the results for a honeycomb bent in a plane parallel to direction 1 are shown in Fig.6.38 and 6.39. Unfortunately insufficient material remained to fabricate honeycombs oriented in direction 2. It can be seen from Figs.6.38 and 6.39 that the hexagonal core is stiffer than the re-entrant and that in both cases the stiffness increases as the beam length is shortened.

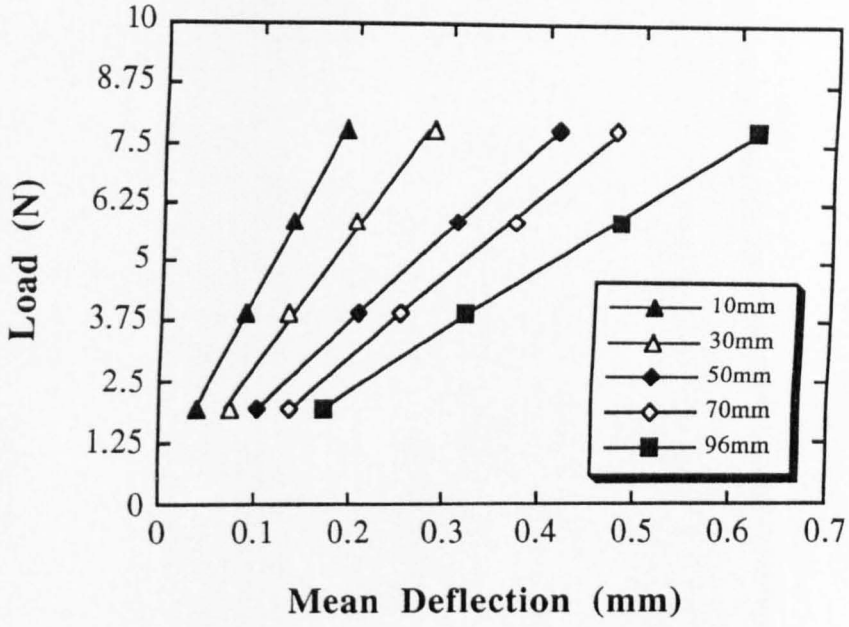

Fig.6.38 *Load vs. deflection plots for hexagonal cell, aluminium honeycomb beams, of varying length, bent in the plane of direction 1.*

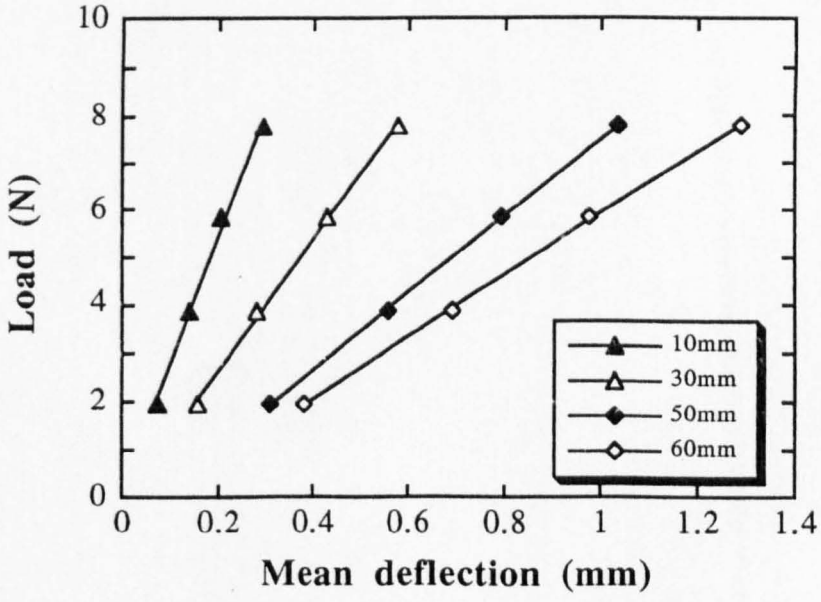

Fig.6.39 *Load vs. deflection plots for re-entrant cell, aluminium honeycomb beams ,of varying length ,bent in the plane of direction 1.*

References

GIBSON,L.J.
"Elastic and plastic behaviour of cellular materials"
Ph.D Thesis (Cambridge) 1981.

GIBSON,L.J., ASHBY,M.F.,SCHAJER,G.S. & ROBERTSON,C.I.
Proceedings of the Royal Society, London
Vol.382, Page 25. 1982.

GIBSON.,L.J. & ASHBY,M.F.
"Cellular Solids : Structure & Properties",
Chapter 4, Pages 76-82
Pergamon Press, London, (1988).

KLINTWORTH,J.W. & STRONGE,W.J.
International Journal of Mechanical Science,
Vol.30 No.3/4, Pages 273-292, 1988.

7) DISCUSSION Part I

7.1 Introduction

The manufacture of all the specimens by hand was extremely time consuming and limited the number which could be made. To overcome this problem most of the tests were repeated on the same specimens.

For the aluminium this is acceptable provided the deformation remains within the elastic limit. For the cardboard specimens their is a problem in that the value of the hinging constant K_h reduces the more times the hinges are operated (q.v. Section 6.3). This probably accounts for the spread in the results as ideally new specimens should have been used for each test. (N.B. Making specimens by hand it is difficult to keep the cell angles consistent, particularly with the card honeycombs where considerable variation can occur from one area of honeycomb to another. Thus it is unlikely that had new specimens been used for each test that degree of error in the results would have been much reduced). The small number of specimens actually used means that the results are more qualitative than quantitative but provide an insight into the behaviour of re-entrant celled cores and honeycombs which deform by hinging.

7.2 Determination of K_h

As already shown in section 5.5 the hinging constant K_h is the gradient of the $W\cos\alpha$ vs. $l\sin\alpha$ plot where W is the applied load, l the length of the cell wall and α the angle of the hinge. This graph for the card material is shown in Fig.7.1 and has a gradient = K_h=2.05 Nm^{-1}.

Assuming that $G_s \approx (1/3)E_s$ and using the value of E_S for hinged card listed in Table 6.1, equations 3.10 (global shear model) and 3.16 (local bending model) can be evaluated for the dimensions of the specimen used in the experiment. These equations yield the results of 248kNm^{-1} and 8.8 Nm^{-1} respectively. The

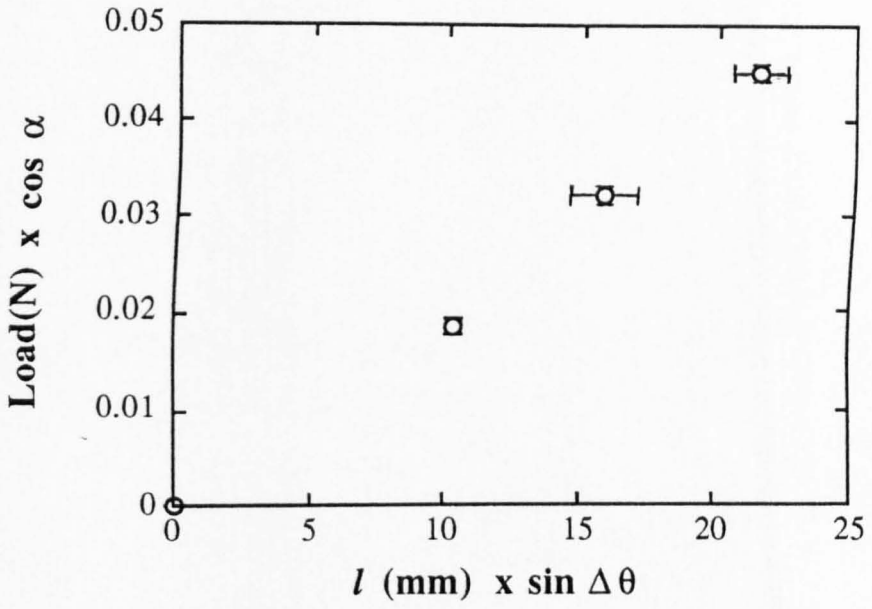

Fig.7.1 *Determination of K_h for 210μm cardboard. K_h=gradient=2.05 Nm^{-1}.*

global shear model grossly over-estimates the value of the hinge constant but the local hinge model provides a value which although slightly higher than that found directly by experiment , is of the same order of magnitude. This suggests that local hinging is a reasonable model for describing deformation by hinging and as has already be shown in section 6.3, K_h is affected by the number of times the hinge is operated. The value of K_h=67.2Nm^{-1} was found to achieve the best fit to the experimental data, obtained by applying uniaxial loads alternately in directions 1 and 2. It should be noted however that for each cell in a honeycomb eight hinges have to operate therefore for a fair comparison to the directly measured result we must divide 67.2 by 8. This implies that $K_h \approx 8$ which is of the same order of magnitude as that predicted by the local hinging model.

7.3 In-plane properties

7.3.1 Elastic modulus

The moduli E_1 and E_2 obtained from the load deflection curves are plotted against cell angle for a re-entrant card honeycomb in Figs. 7.2 and 7.3. For comparison

with the experimental results the theoretical equations (3.55) and (3.60) have been evaluated for different values of K_h. The experimental results follow the theoretical curves although the models appear to over estimate the values of E_1 and under estimate E_2. Comparing the equations (3.22 and 3.23) for the flexure model with those for the hinging model (3.55 and 3.60) we see that the expressions for the moduli differ only in the respective values of K_f and K_h. As the force constants are functions of the Young's modulus of the material, the moduli for the aluminium honeycomb are expected to be much higher than those for the cardboard and this can clearly be seen by comparing the values of E_2 in Figs.7.3 and 7.7. In both cases $h/l = 2$.

K_f and K_h are sensitive to small deviations in the values of l since they are both functions of $(h/l)^3$ (Eqns. 3.4 and 3.16) if local hinging is considered. The minor errors which exist in the geometry of the handmade honeycombs used in these experiments can account for the small discrepancies between the theory and the experimental results. Therefore within the limitations of the methods used here we can say that the flexure model applies equally well to re-entrant structures deforming by that mechanism. Similarly the hingeing model provides a simple method of predicting the elastic behaviour of card honeycombs.

For the specimens used in these experiments the re-entrant samples have a higher density than their hexagonal counterparts and have shown a small increase in E_2 combined with a reduction in E_1 as predicted by the theory. Examination of the equations for the models shows that the elastic properties are governed by the ratio of the cell wall lengths (ie. h/l) if the cell angle is kept constant. Thus specific values of E_i and ν_{ij} can be obtained for any required density of honeycomb. The limiting factor governing the density is the physical size of the cells, for a given wall thickness.

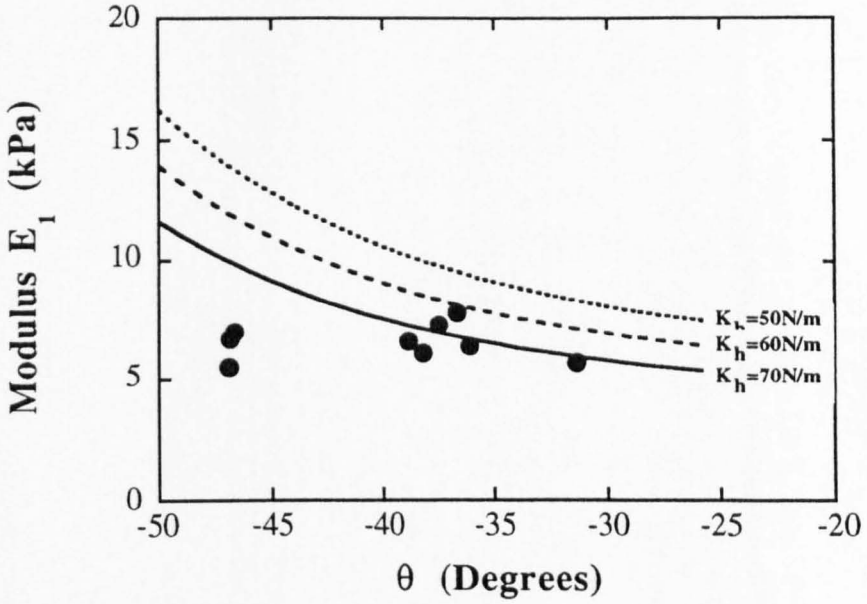

Fig.7.2 *Experimental(•) and theoretical(-) Young's modulus E_1 (for various K_h in Eqn.3.60) plotted against cell angle for a re-entrant cardboard honeycomb loaded in direction 1 (h=20mm, l=10mm).*

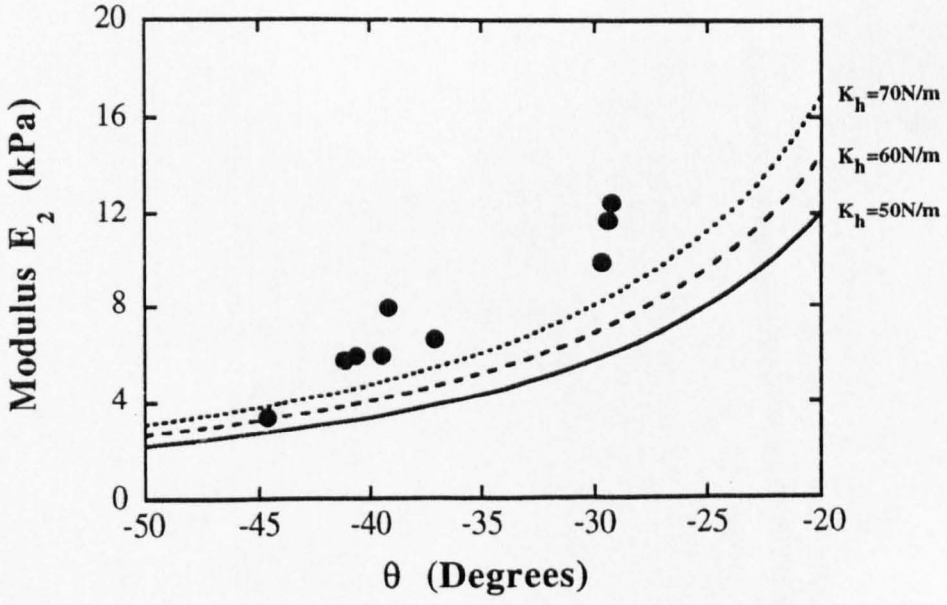

Fig.7.3 *Experimental(•) and theoretical(-) Young's modulus E_2 (for various K_h in Eqn.3.55) plotted against cell angle for a re-entrant cardboard honeycomb loaded in direction 2 (h=20mm, l=10mm).*

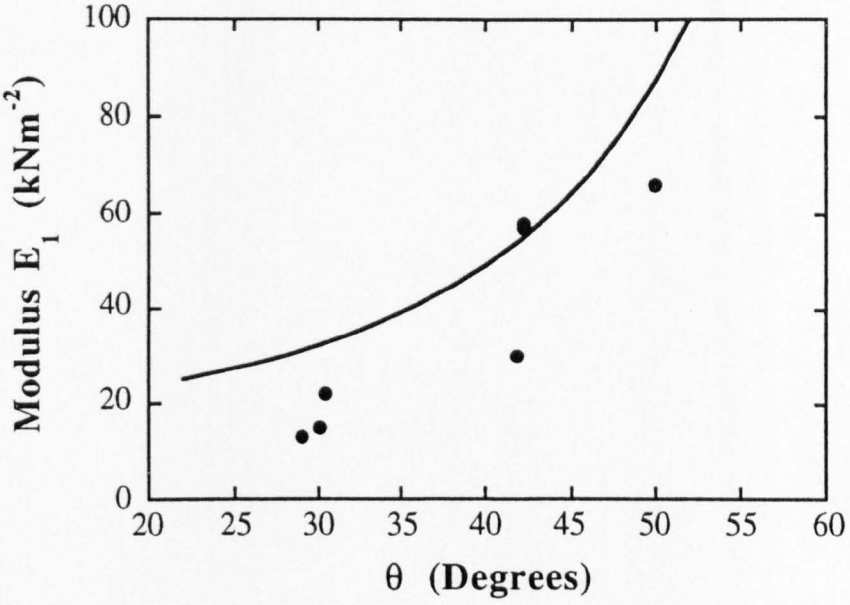

Fig.7.4 *Experimental(•) and theoretical(-) Young's moduli (for K_h=67.2Nm^{-1} in Eqn.3.60) plotted against cell angle for a hexagonal card honeycomb loaded in direction 1 (h=20mm, l=10mm).*

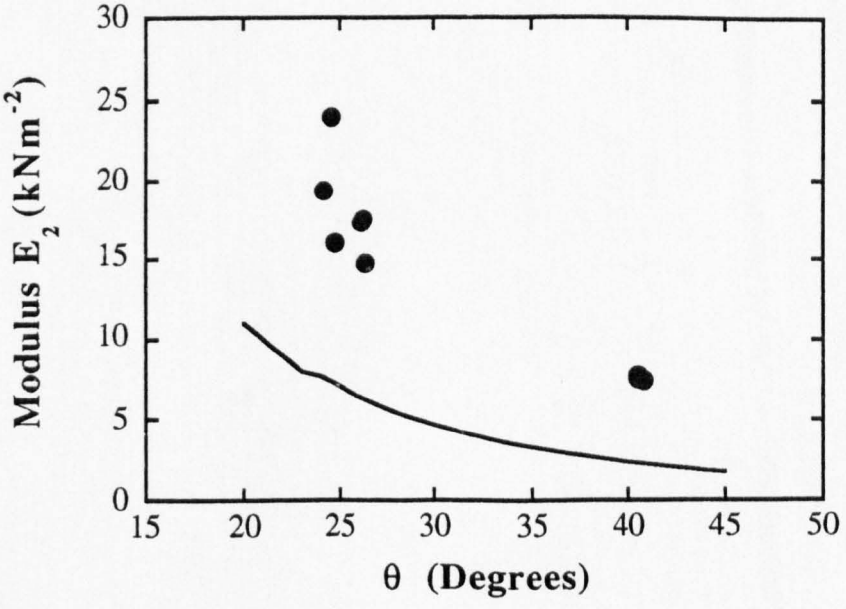

Fig.7.5 *Experimental(•) and theoretical(-) Young's moduli (for K_h=67.2Nm^{-1} in Eqn.3.55) plotted against cell angle for a hexagonal card honeycomb loaded in direction 2 (h=20mm, l=10mm).*

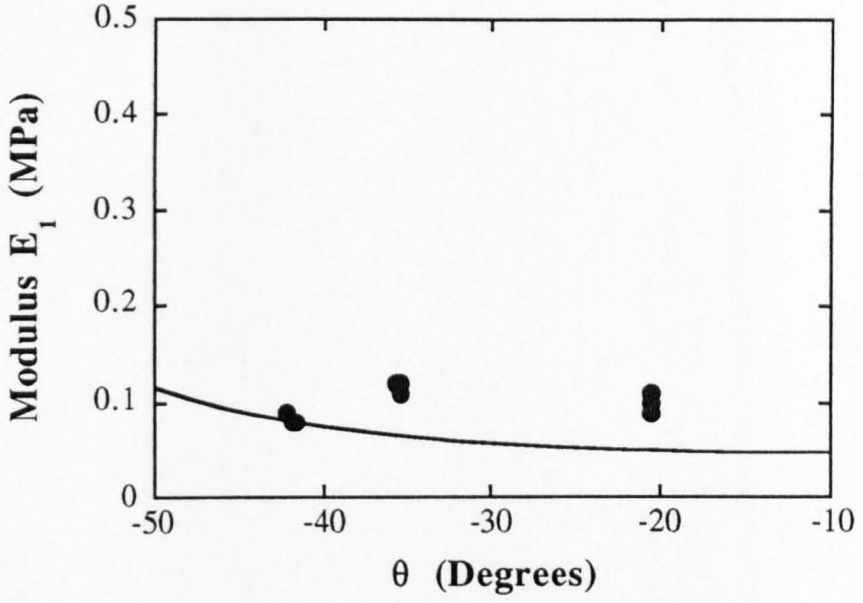

Fig.7.6 *Experimental(•) and theoretical(-) Young's moduli (for E_s=25GPa) plotted against cell angle for a re-entrant aluminium honeycomb loaded in direction 1 (h=20mm, l=10mm).*

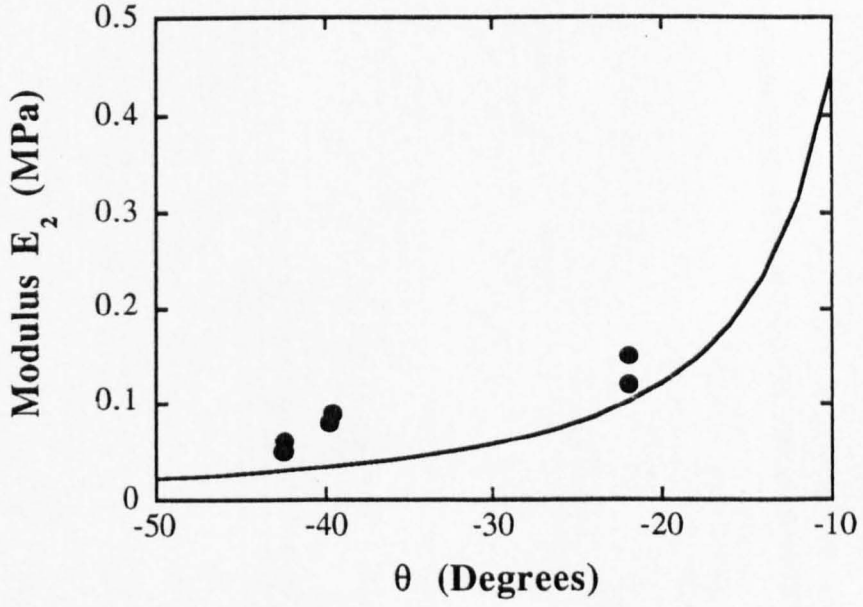

Fig.7.7 *Experimental(•) and theoretical(-) Young's moduli (for E_s=25GPa) plotted against cell angle for a re-entrant aluminium honeycomb loaded in direction 2 (h=20mm, l=10mm).*

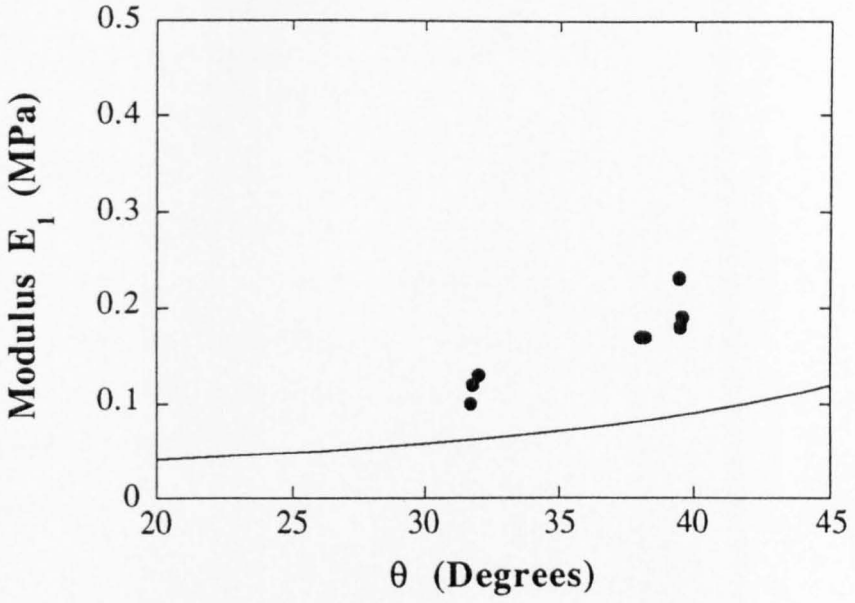

Fig.7.8 *Experimental(•) and theoretical(-) Young's moduli (for E_s=25GPa in Eqn.3.22) plotted against cell angle for a hexagonal aluminium honeycomb loaded in direction 1 (h=l=10mm).*

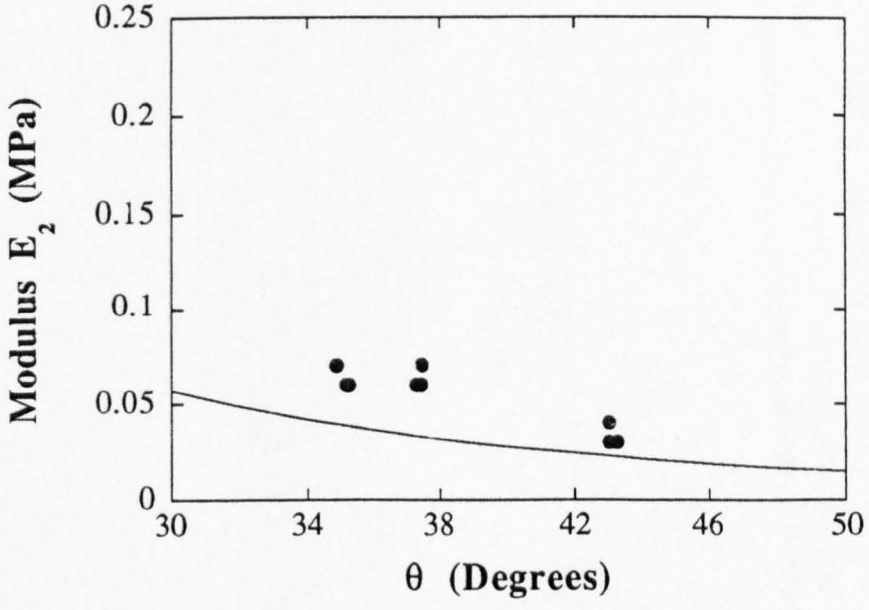

Fig.7.9 *Experimental(•) and theoretical(-) Young's moduli (for E_s=25GPa in Eqn.3.23) plotted against cell angle for a hexagonal aluminium honeycomb loaded in direction 2 (h=l=10mm).*

7.3.2 Poisson's ratio for honeycombs under small strains

The Poisson's ratios are independent of the load and are determined by the cell geometry alone (Table 3.1). Figs.7.10 - 7.13 show the Poisson's ratios for hexagonal and re-entrant cardboard honeycombs in the 1 and 2 directions.

Direct measurement of the cell walls with a ruler established that they typically deviated from their nominal lengths by ±1mm. The maximum (2.33) and minimum (1.73) values of h/l resulting from this deviation were used to evaluate the Poisson's ratio equations over the appropriate range of cell angles and these results are also shown on the plots. The experimental results predominantly lie between the upper and lower theoretical values showing good agreement with the model.

Figs.7.14 and 7.17 show the equivalent plots for aluminium honeycombs. There is considerably more scatter in the experimental data and the values measured are smaller than those predicted by the theory in both 1 and 2 directions. The degree of scatter can be accounted for by the increased error in reading the much smaller displacements which occur in the stiffer aluminium honeycombs.

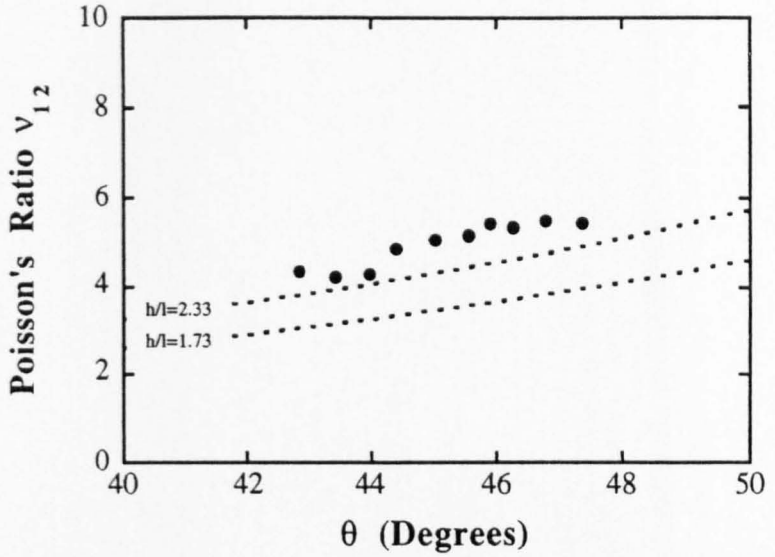

Fig.7.10 *Experimental(•) and theoretical(-) Poisson ratios plotted against cell angle for a hexagonal card honeycomb loaded in direction 1.*

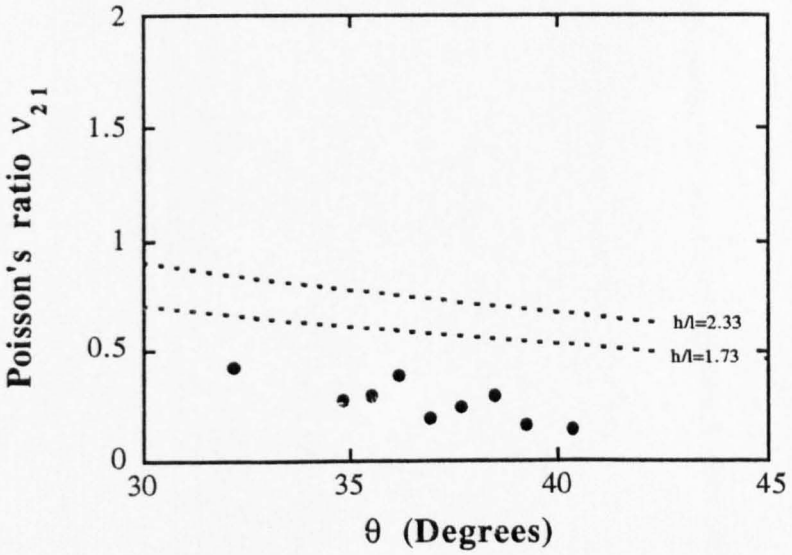

Fig.7.11 *Experimental(•) and theoretical(-) Poisson ratios plotted against cell angle for a hexagonal card honeycomb loaded in direction 2.*

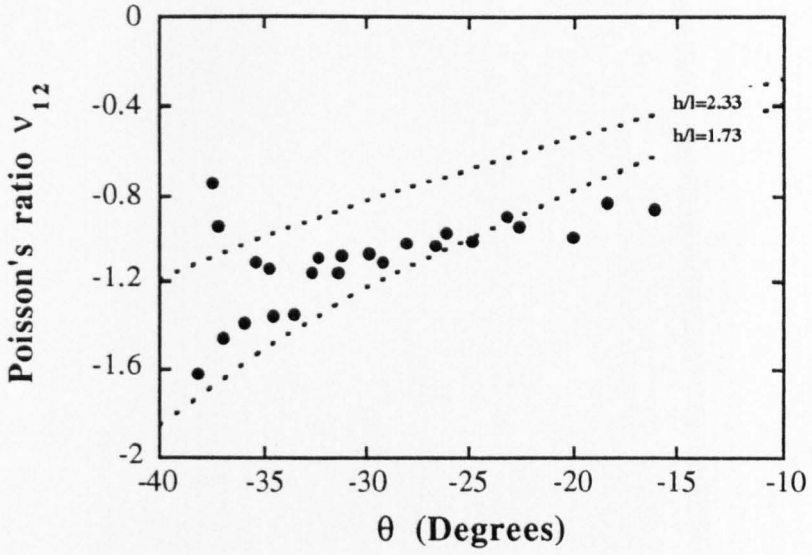

Fig.7.12 *Experimental(•) and theoretical(-) Poisson ratios plotted against cell angle for a re-entrant cardboard honeycomb loaded in direction 1.*

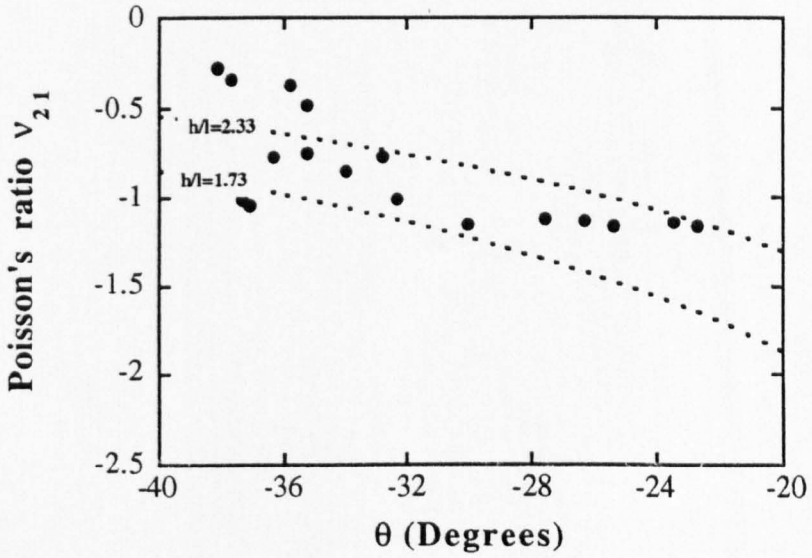

Fig.7.13 *Experimental(•) and theoretical(- -) Poisson ratios plotted against cell angle for a re-entrant cardboard honeycomb loaded in direction 2 (h=20mm, l=10mm).*

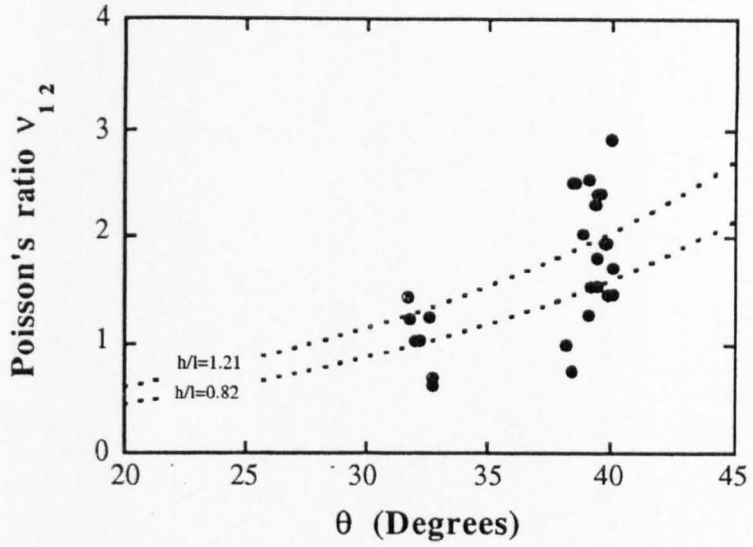

Fig.7.14 *Experimental(•) and theoretical(- -) Poisson ratios plotted against cell angle for a hexagonal aluminium honeycomb loaded in direction 1 (h=10mm, l=10mm).*

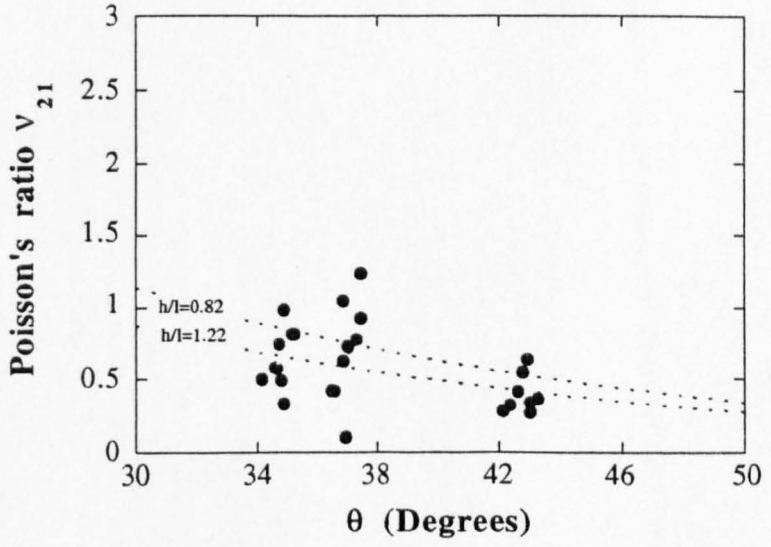

Fig.7.15 *Experimental(•) and theoretical(- -) Poisson ratios plotted against cell angle for a hexagonal aluminium honeycomb loaded in direction 2 (h=10mm, l=10mm).*

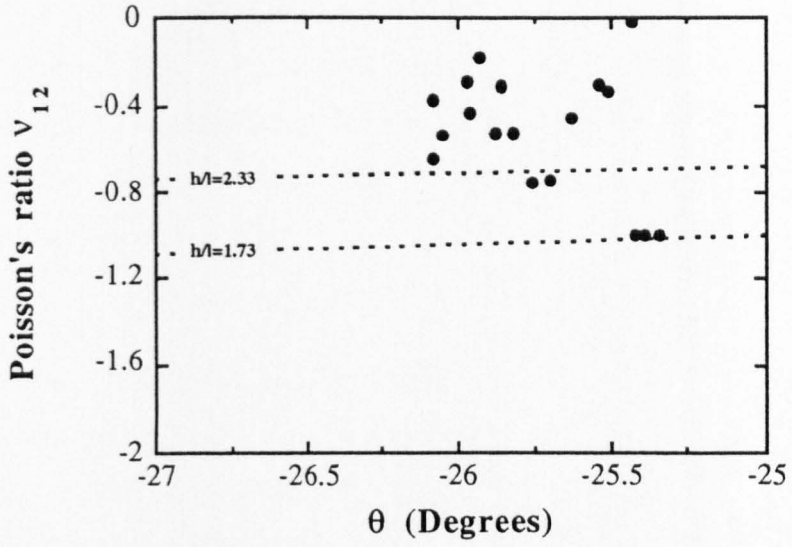

Fig.7.16 *Experimental(•) and theoretical(- -) Poisson ratios plotted against cell angle for a re-entrant aluminium honeycomb loaded in direction 1 (h=20mm, l=10mm).*

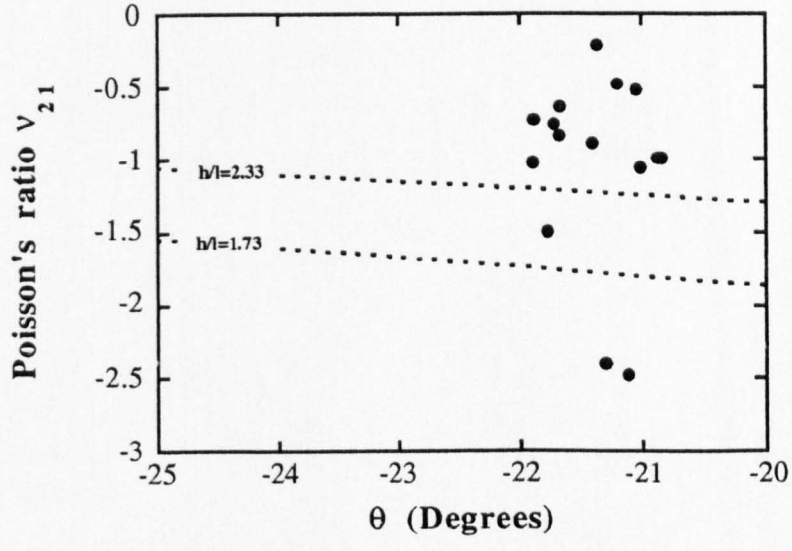

Fig.7.17 *Experimental(•) and theoretical(- -) Poisson ratios plotted against cell angle for a re-entrant aluminium honeycomb loaded in direction 2 (h=20mm, l=10mm).*

7.3.3 Shear modulus

The in-plane shear modulus required the use of a special "picture frame' rig similar to that used by Kelsey *et al.* (1958). The analysis of the forces produced in this experiment is quite complex and there has been some debate in the literature as to the suitability of this test for the measurement of shear modulus (Bowles *et al.* 1986, Lee *et al.* 1986). However, for the experiments reported here the same frame was used for all the specimens allowing a direct comparison of results.

The Abelbeck Software 'Kaleidagraph' programme was used to fit second order polynomial curves (by the least squares method) to the shear modulus data in Figs.6.14 - 6.19. Using the equations of these curves, expressions 5.2 and 5.4 can be evaluated allowing shear stress to be plotted against shear strain (Figs.7.18 & 7.19). The shear modulus is the gradient of the τ vs. γ plot.

All specimens were tested under identical conditions and the experimental shear modulus values are listed with the theoretical values obtained for the geometries used in Table 7.1. There is some error in the results but in both cases (ie. card and aluminium) the shear modulus is significantly less for the re-entrant core than the hexagonal equivalent, as expected from the theory. N.B. this is true for both cell configurations of h =20mm, l =10mm and h =l =10mm.

Sample	Cell angle (Deg)	G_{12} Theory (kPa)	G_{12} Experimental (kPa)
Al. hexagonal	+31	34.7	79.7
Al. re-entrant	-22	7.2	17.8
Card hexagonal	+40	0.9	9.4
Card re-entrant	-29	0.6	0.8

Table 7.1 *Experimental and theoretical in-plane shear moduli (obtained from equations 4.1 and 4.4) for aluminium and cardboard honeycombs.*

The results for the aluminium honeycombs are approximately double those predicted by the models. For the card models the discrepancies between the

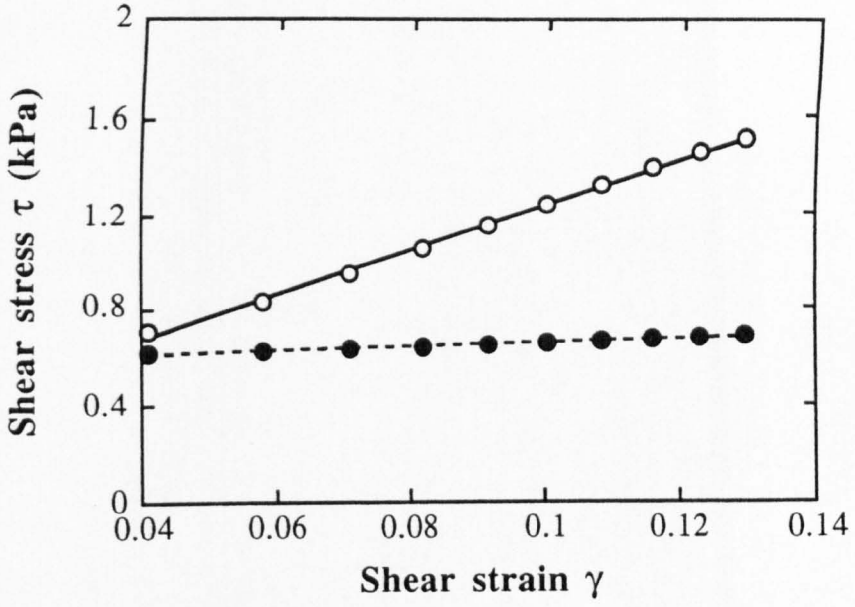

Fig.7.18 *Shear stress vs Shear strain for hexagonal (h=20mm, l=10mm, θ≈40°) and re-entrant (h=20mm, l=10mm, θ≈-29.5°) card honeycombs loaded in-plane.*

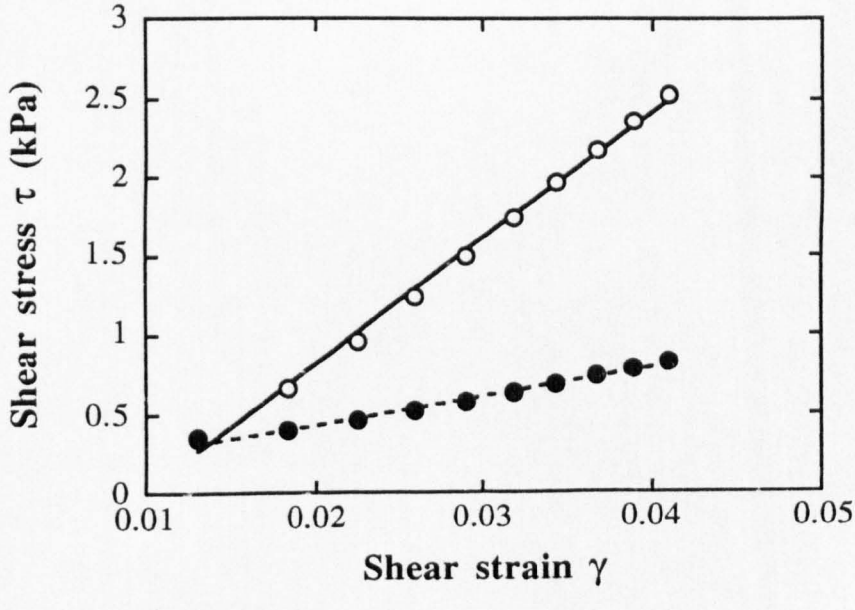

Fig.7.19 *Shear stress vs Shear strain for hexagonal (o) h=l=10mm, θ=31°, and re-entrant (•) h=20mm, l=10mm, θ≈-22°, aluminium honeycombs loaded in-plane.*

theory and experimental results are not as consistent. This suggests that the errors are at least partly due to the friction of the 'picture frame' rig arising from lateral forces exerted on the pins during the test. Using a larger specimen would then produce more reliable results.

7.3.4 Indentation

7.3.4.1 100mm flat indenter

Classical elasticity has been used to predict the behaviour of an elastic solid beneath an indenter (Johnson, 1983). Using this theory the stress fields beneath different indenters can be described by various mathematical expressions provided that the material is infinitely large in comparison to the size of the indenter. The large cell size used in these experiments enables strains at the edge of the indenter to be relieved and in addition the comparatively thin layer of material in relation to the size of the indenter so that the stress fields can pass right through the specimen. Thus by assuming that a block of material the full width of the indenter deforms through the complete thickness of the specimen we can use the expressions derived in chapter 3 to predict the indentation behaviour.

We know that the general definition of the force constant (Eqn.3.1) relates the displacement δ of the cell wall length l to the applied force. For the hinging mechanism the displacement δ is achieved by a small change in the cell angle $\Delta\theta$ (Fig.3.13). Thus if a cell is compressed in direction 2 (Fig.3.12) the change in the width of the cell δx is given by

$$\delta x = -2l\cos\theta + 2l\cos(\theta+\Delta\theta) \qquad (7.1)$$

When a piece of honeycomb is indented in-plane we can envisage three ways in which the indenter can be accommodated.

a) All deformation occurs in the single, uppermost row of cells directly in contact with the indenter (Fig.7.20).

b) All cells directly under the indenter deform by an equal amount through the

thickness of the specimen (Fig.7.21) i.e.$\delta x^{total} = \delta x N$ where N is the number of rows of cells.

c) The degree of deformation decays through the specimen from a maximum in the top row of cells in contact with the indenter to approximately zero at the bottom of the specimen.

For comparison with the experimental data $\Delta\theta$ was calculated, for each increment in load used in the experiment, from equation 3.8 using $K_h = 67.2 Nm^{-1}$ (q.v. section 7.2) for the particular cell geometry under test. δx was then obtained from equation 7.1 δx was then obtained from equation 7.1. A simple decay law which assumes the amount deflection occurring in any particular row of cells is half that occurring in the row above is easily obtained using the expression for the sum of a geometric series

$$\delta_x^{total} = \frac{\delta_x[1 - (1/2)^N]}{1 - 1/2} \qquad (7.2)$$

where N =No. rows of cells.

For these experiments N>5 so that deformation in the Nth row, according to equation 7.2 is approximately zero.

Fig.7.22 shows the load deflection curve of a hexagonal card honeycomb together with the theoretical plots from eqns 7.1 and 7.2 for the cases listed above. The experimental data points lie between the predictions for the decay law and all cells deforming equally.

Fig.7.24a clearly shows that the assumption that all the cells beneath the indenter deform equally is valid for a hexagonal cell, but the model overestimates the degree of indentation. This effect can be explained by the fact that the model does not allow for the lateral constraint imposed by the surrounding material away from the indenter.

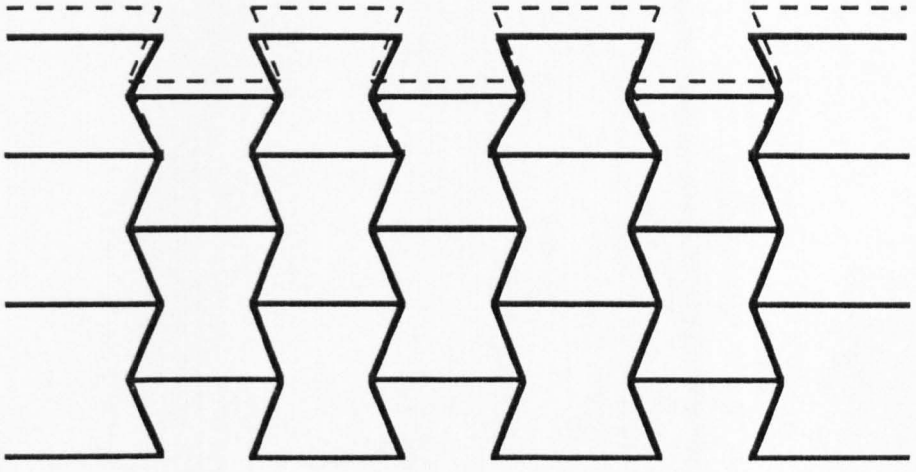

Fig.7.20 *Schematic diagram showing the effect if only the top row of cells under the indenter deform.*

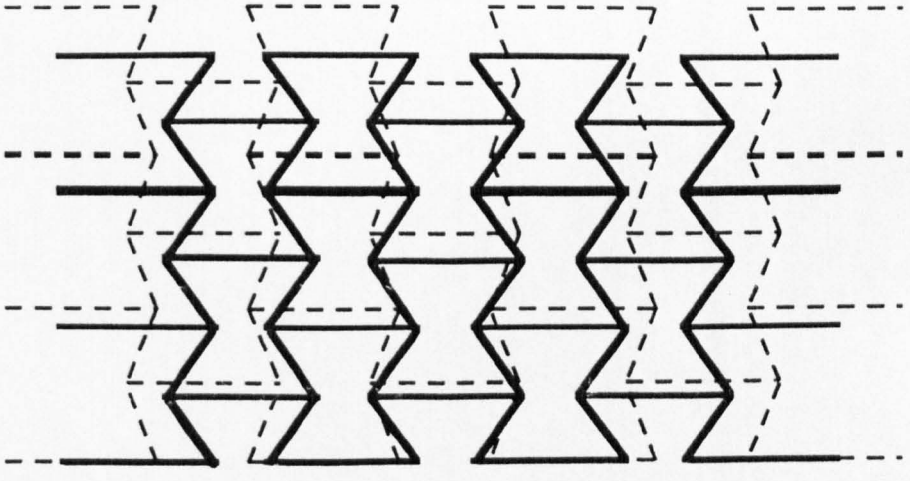

Fig.7.21 *Schematic diagram showing the effect if all cells under the indenter deform.*

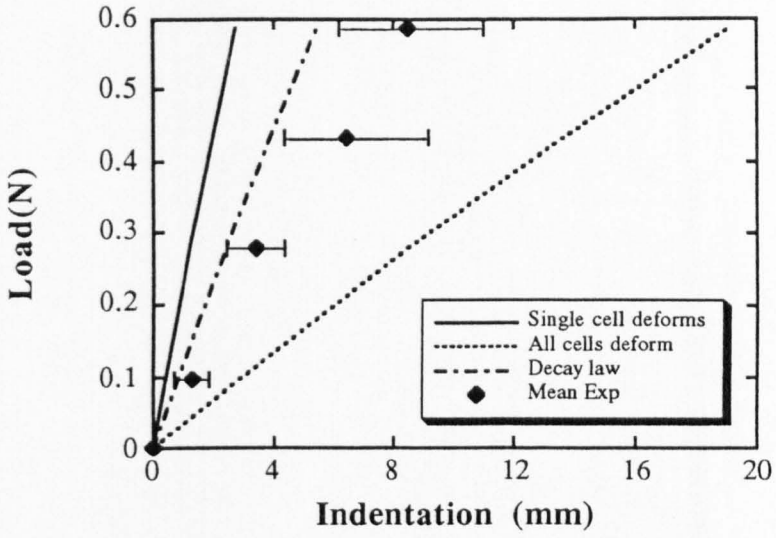

Fig.7.22 *Load/Displacement plot for a card hexagonal cell honeycomb ($\theta=50^{o}$), h=20mm, l=10mm) indented in direction 2 with a 100mm wide flat indenter. The lines show the displacements predicted by the theory if only the top row of cells deforms (-) and when all cells under the indenter deform (····)*

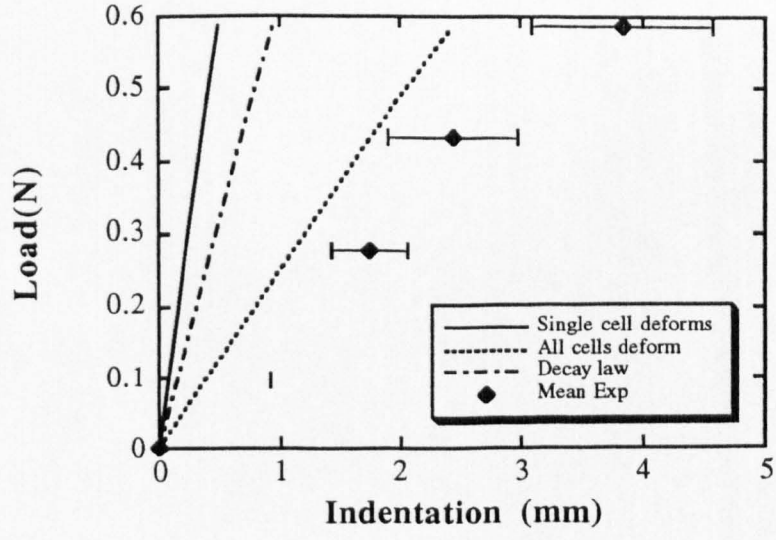

Fig.7.23 *Load/Displacement plot for a card re-entrant cell honeycomb ($\theta=-35^{o}$, h=20mm, l=10mm)indented in direction 2 with a 100mm wide flat indenter. The lines show the displacements predicted by the theory if only the top row of cells deforms (-) and when all cells under the indenter deform (····)*

a)

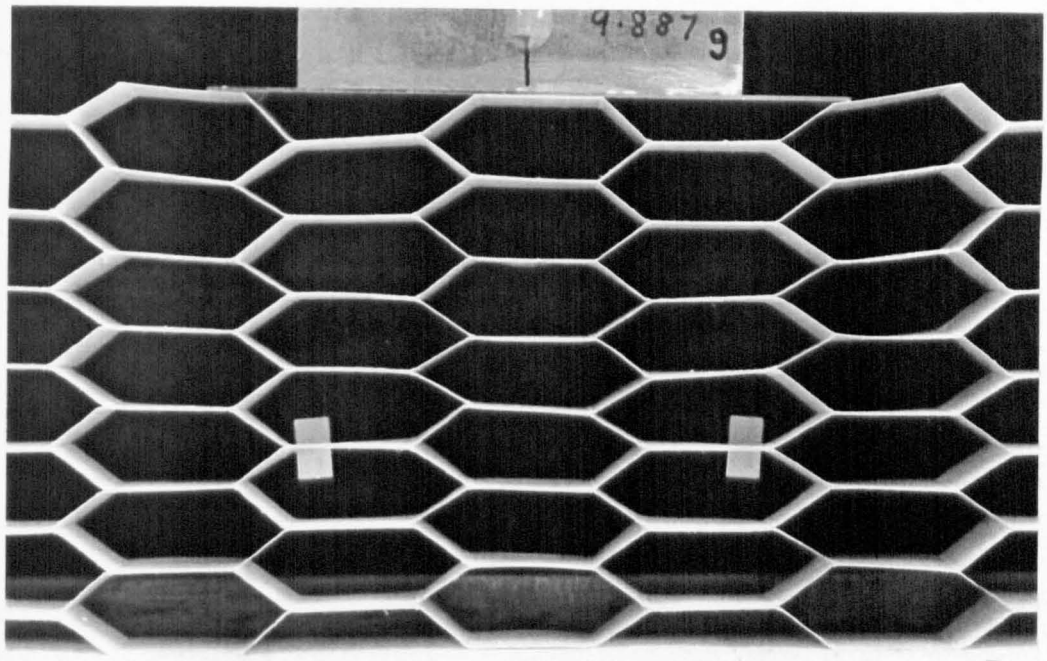

b)

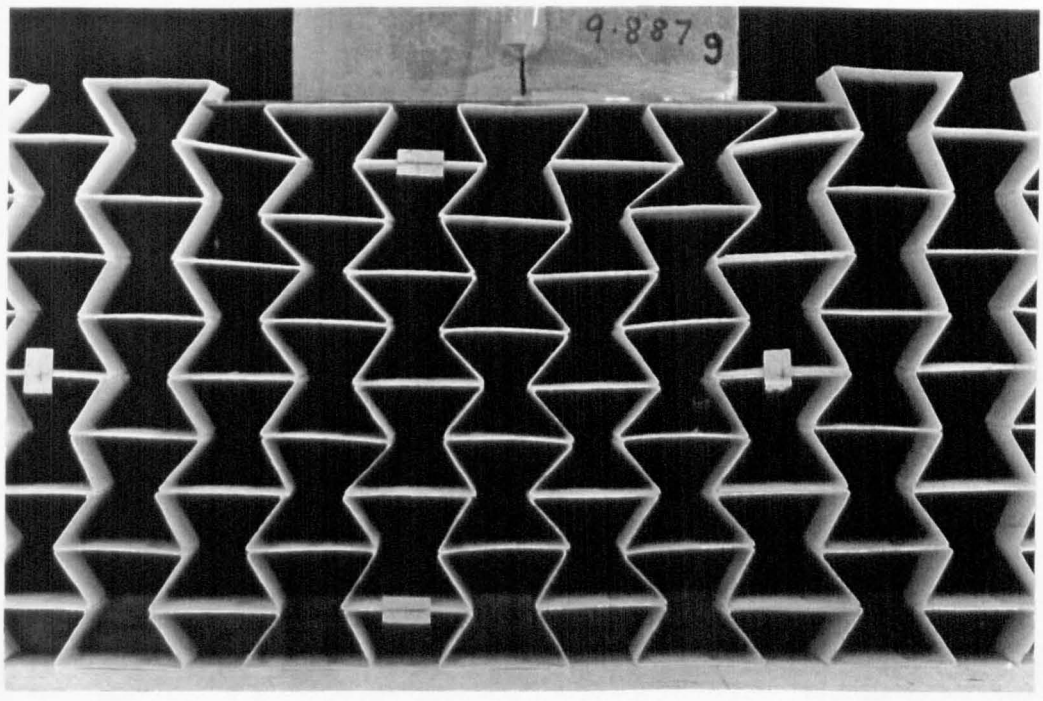

Fig.7.24 a) *Hexagonal cell card honeycomb(θ=50^{o}, h=20mm, l=10mm) indented in direction 2 by 100mm wide flat indenter.*
b) *Re-entrant cell card honeycomb (θ=-35^{o}, h=20mm, l=10mm) indented in direction 2 by a 100mm wide flat indenter.*
Note that in both cases all cells beneath the indenter appear to deform equally.

For the re-entrant cell honeycomb the assumption that all cells deform equally is valid (Fig.7.24b) although in this case the model underestimates the degree of indentation. This is possibly be explained by the increased flexibility of this type of core.

In the case of aluminium honeycombs under a flat indenter the displacements are much smaller than for the card but again all the cells beneath the indenter appear to deform equally. The deflection δx due to flexing of the cell walls is again derived from the general force constant equation (Eqn.3.1). In the flexure model however, the cell angle does not change, all the deformation arises from the flexing of the cell wall. If the end of the cell wall is deflected by a force P in direction 2 then the component F of P acting perpendicular to the wall is given by

$$F=P\sin\theta \tag{7.3}$$

The deflection δ_2 in direction 2 is simply

$$\delta_2=\delta\sin\theta \tag{7.4}$$

Substituting these expressions into equation 3.1 we obtain a linear relationship between the displacement δ_2 in direction 2 and the applied force i.e.,

$$\delta_2=\frac{P\sin^2\theta}{K_f} \tag{7.5}$$

N.B. this relationship is only valid for small deflections in the elastic region. The change in the width δx of a single cell (Fig.3.3) is thus

$$\delta x=2\delta_2=\frac{2P\sin^2\theta}{K_f} \tag{7.6}$$

Figs.7.25 and 7.26 show the load vs. displacement plots for hexagonal and re-

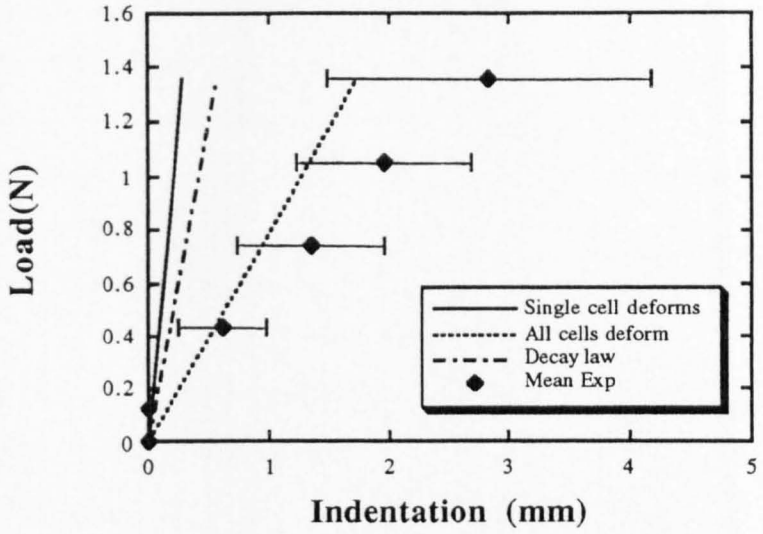

Fig.7.25 *Load/Displacement plot for an aluminium hexagonal cell honeycomb indented in direction 2 with a 100mm wide flat indenter. The lines show the displacements predicted by the theory if only the top row of cells deforms (-) and when all cells under the indenter deform (····)*

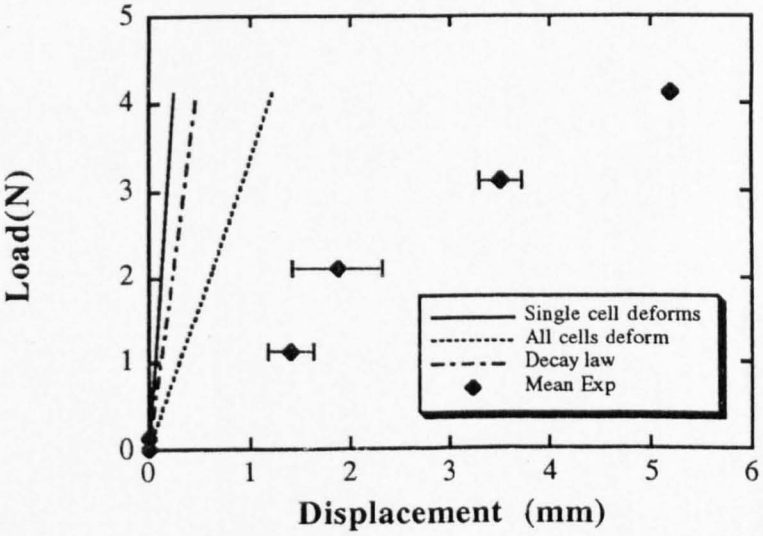

Fig.7.26 *Load/Displacement plot for an aluminium re-entrant cell honeycomb indented in direction 2 with a 100mm wide flat indenter. The lines show the displacements predicted by the theory if only the top row of cells deforms (-) and when all cells under the indenter deform (····)*

entrant aluminium honeycombs loaded in direction 2 with a 100mm wide flat indenter. Also included on the plots for comparison are the predicted load deflection curves obtained from equation 7.6 assuming *a)* only the top row of cells in contact with the indenter deform *b)* that all cells below the indenter deform equally through the thickness of the specimen and *c)* the degree of deflection decays through the specimen (using result of eqn.7.6 in eqn.7.2). The equal deformation assumption agrees most closely with the experimental data in the case of the hexagonal honeycomb (Fig.7.25).

For the re-entrant honeycomb (Fig.7.26) all three models over estimate the observed resistance to indentation.

7.3.4.2 **200mm diameter indenter**.

When we try to interpret the results obtained with a curved indenter we must consider the changing contact area of the indenter. If we assume that there is no "sinking" or "piling up" of the honeycomb in the vicinity of the indenter i.e. the specimen surface remains flat and the indenter remains in contact with the surface across the full width of the indentation, then we can more accurately describe the load as an applied stress obtained by dividing the applied load by the projected contact area of the indenter (Fig.7.27).

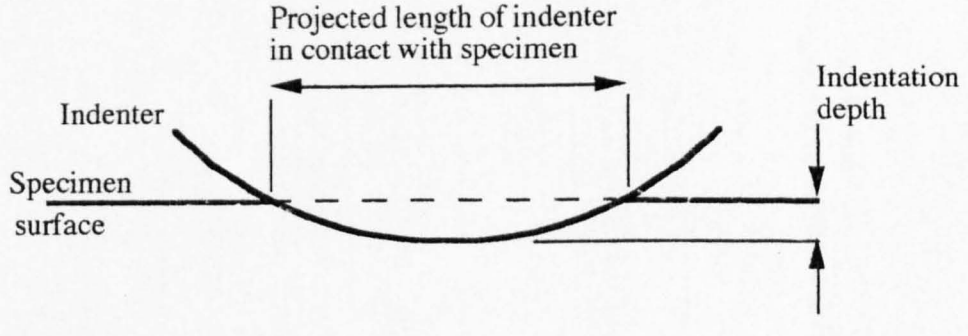

Fig.7.27 *Schematic diagram showing the indentation of the surface by a semi-circular indenter.*

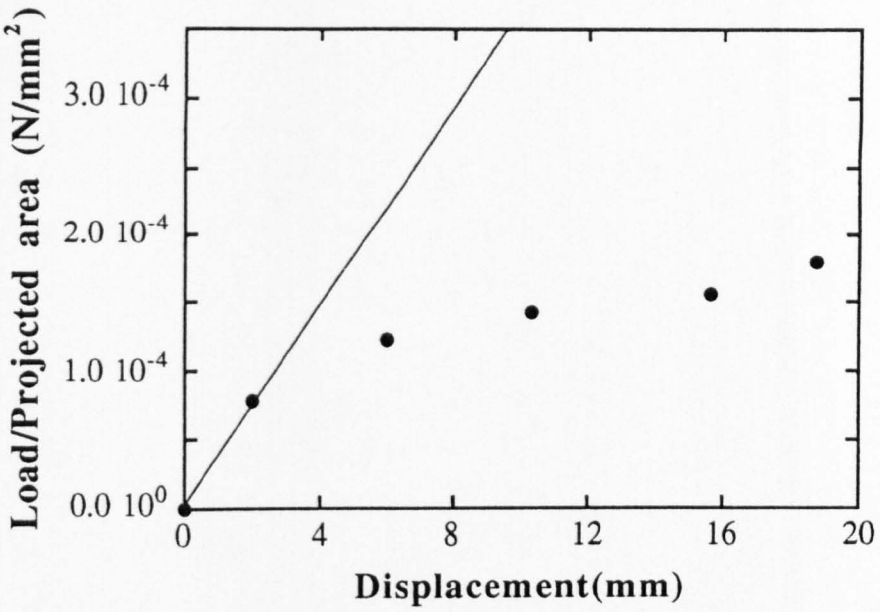

Fig.7.28 *Load/Projected area vs displacement plot a card hexagonal cell honeycomb indented in direction 2 with a 200mm diameter indenter. Downward deviation of data points from linearity is due to material being pushed aside by the indenter.*

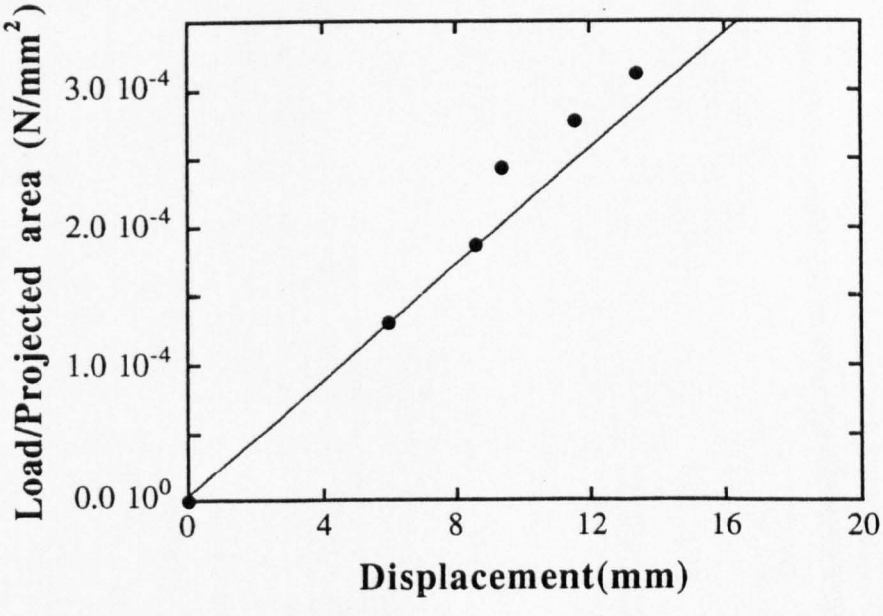

Fig.7.29 *Load/Projected area vs displacement plot a card re-entrant cell honeycomb indented in direction 2 with a 200mm diameter indenter. Upward deviation of data points from linearity is due to densification of the material as a result of the -ve Poisson's ratio.*

The projected area is determined by measuring the depth of indentation from the photographic image obtained during the experiment. Using equation 5.5 the chord length can be calculated and multiplying this by the thickness of the core gives the projected area. Plots of load/projected area vs displacement are shown in Figs.7.28 and 7.29 for card honeycombs. The solid line on the plots represents the theoretical deformation obtained from equation 7.1 in which $\Delta\theta$ was calculated from the applied stress which changes with the contact area. For the hexagonal honeycomb there is a downward deviation from the theoretical line as the cells collapse locally and material is 'pushed' aside by the indenter. For the re-entrant honeycomb there is a slight upward deviation from the theory as the resistance increases due to densification of the material below the indenter.

Taking the mean displacements from the load deflection plots and assuming that all the cells deform equally we can plot load/projected area vs strain. Fig.7.30 shows the plot for a hexagonal cell aluminium honeycomb. The theory underestimates the indentation resistance as expected (constraint of surrounding material) but the gradients are the same.

For the re-entrant aluminium case the initial gradient is similar to that predicted by the model (Fig.7.31) but the experimental data deviates as the single column of cells under the tip of the indenter deform. Only when the indenter contacts the adjacent columns of cells (Figs.7.32) does the resistance increase and the gradient returns to that predicted by the theory. The same behaviour is seen with the card honeycombs(Figs.7.33 and 7.34).

Application of the Hertz equation to the in-plane indentation analysis of honeycombs is not really a fair comparison since h and l should be much smaller than r the radius of the indenter. Also we have to assume that the properties of the material do not change during the test, which we have already shown to be incorrect since the elastic properties of the honeycombs are functions of the cell geometry. However using values of E and ν, calculated from the initial cell geometry, in the Hertz equation (2.31) produces the plots shown in Figs.7.35

and 7.36 for hexagonal and re-entrant celled, card honeycombs respectively. In both cases there is an initial linear region which can explain the apparently good fit between the experimental indentation results and the models for honeycombs under compression. It is also significant to note that the Hertz equation also shows that despite having reduced in-plane shear and Young's moduli the re-entrant honeycombs offer greater resistance to indentation.

This increased indentation resistance of a re-entrant structure despite reduced modulus compared to the equivalent hexagonal cell honeycomb was also observed by Lakes (1993) during his examination of the indentation of copper foams.

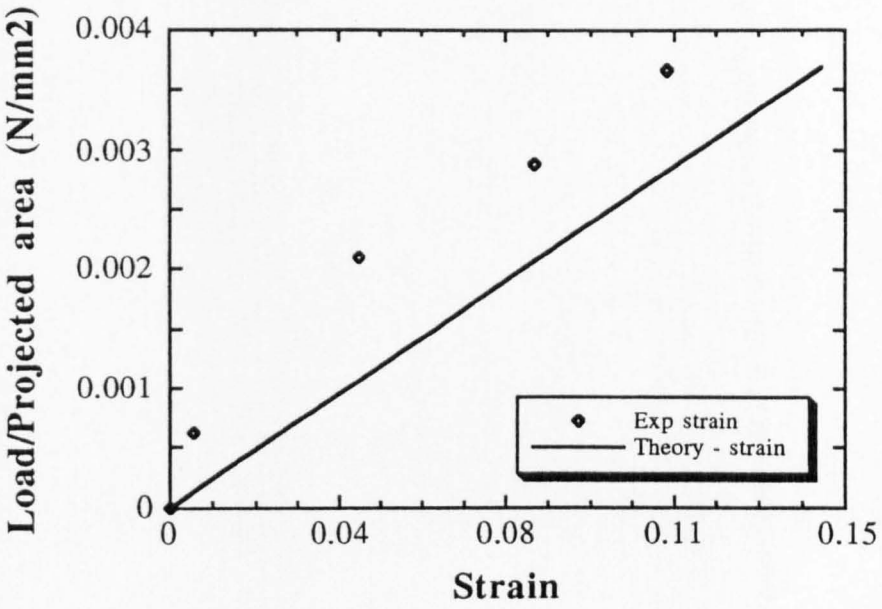

Fig.7.30 *Load/Projected area vs strain for a hexagonal cell, aluminium honeycomb. The solid line is the theoretical curve derived from the flexure model. (Loaded in direction 2)*

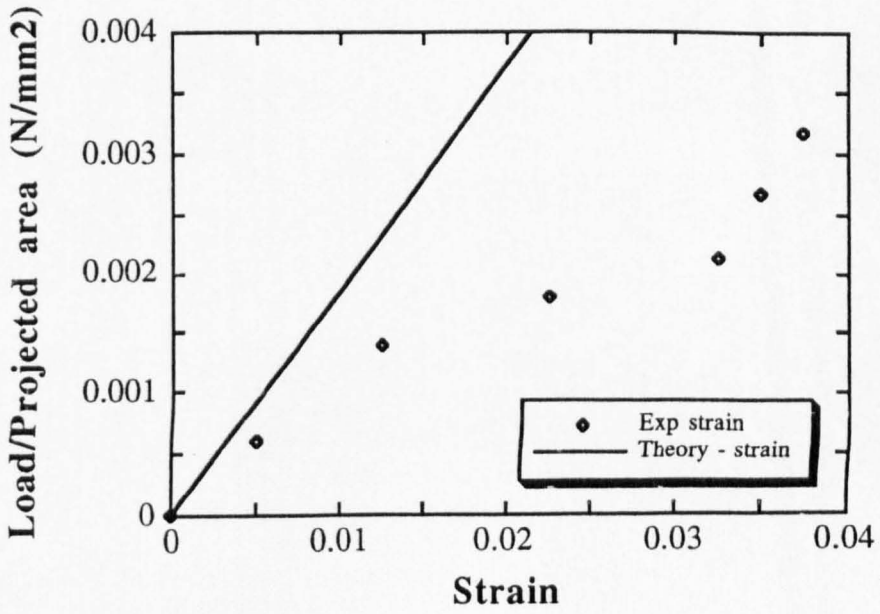

Fig.7.31 *Load/Projected area vs strain for a re-entrant cell, aluminium honeycomb. The solid line is the theoretical curve derived from the flexure model. (Loaded in direction 2)*

a)

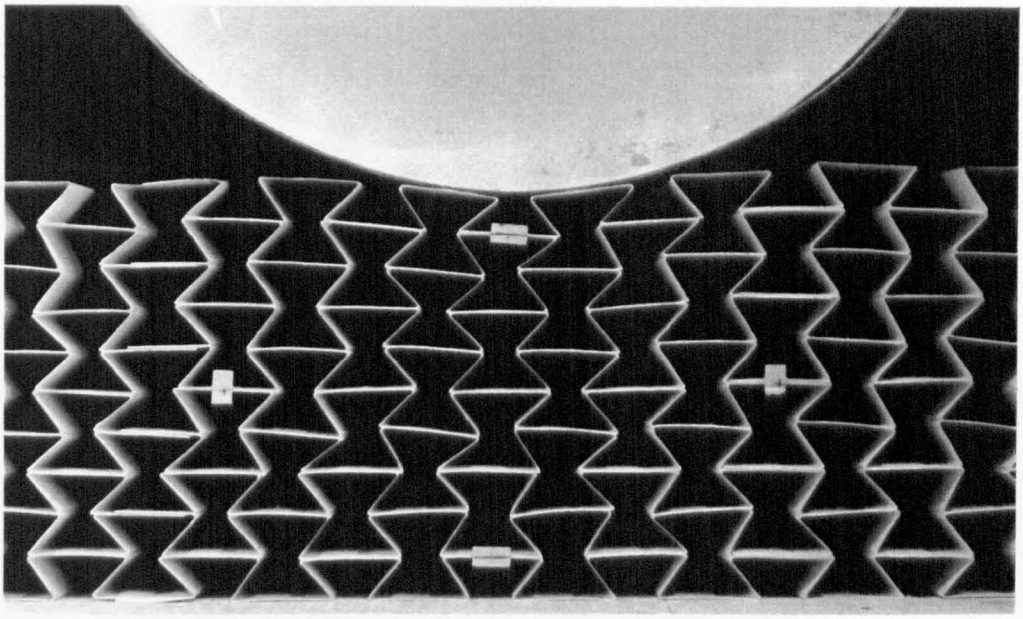

b)

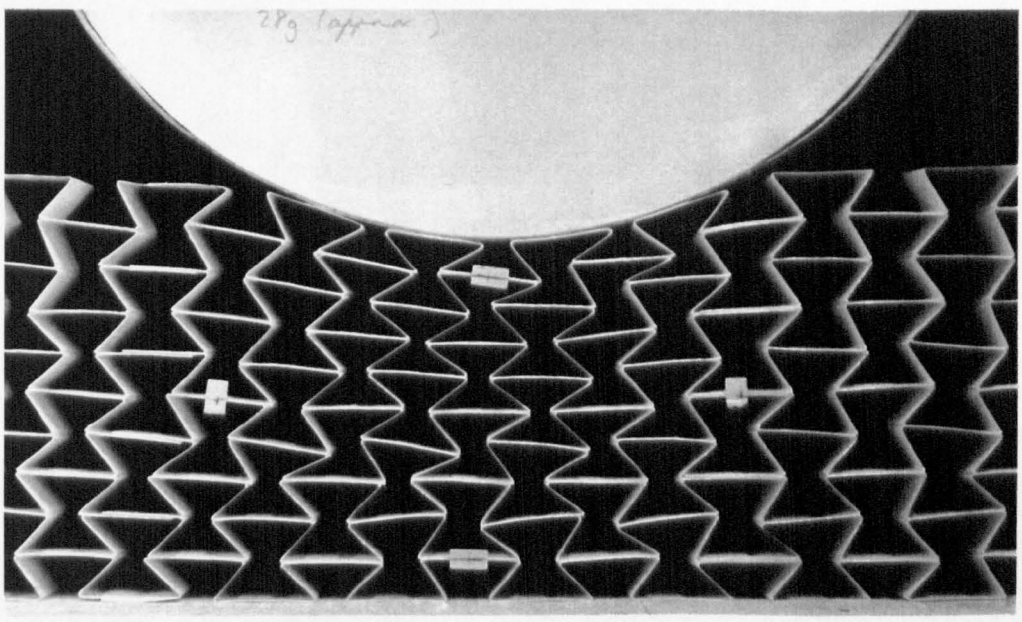

Fig.7.32 *Photograph of re-entrant honeycomb being indented by a 200mm diameter indenter.*
a) single column under tip of indenter deforming
b) adjacent columns of cells deforming

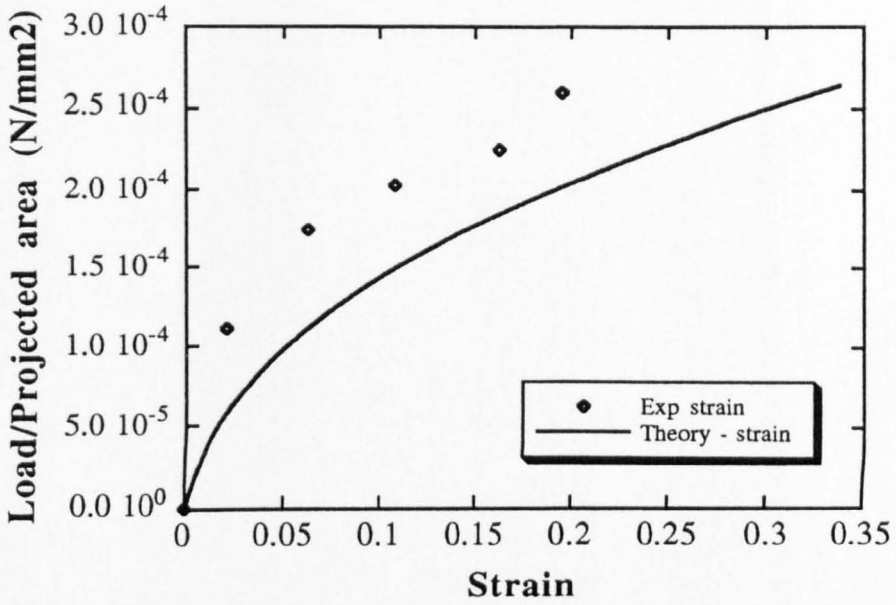

Fig.7.33 *Load/Projected area vs strain for a hexagonal cell, card honeycomb. The solid line is the theoretical curve derived from the hingeing model. (Loaded in direction 2)*

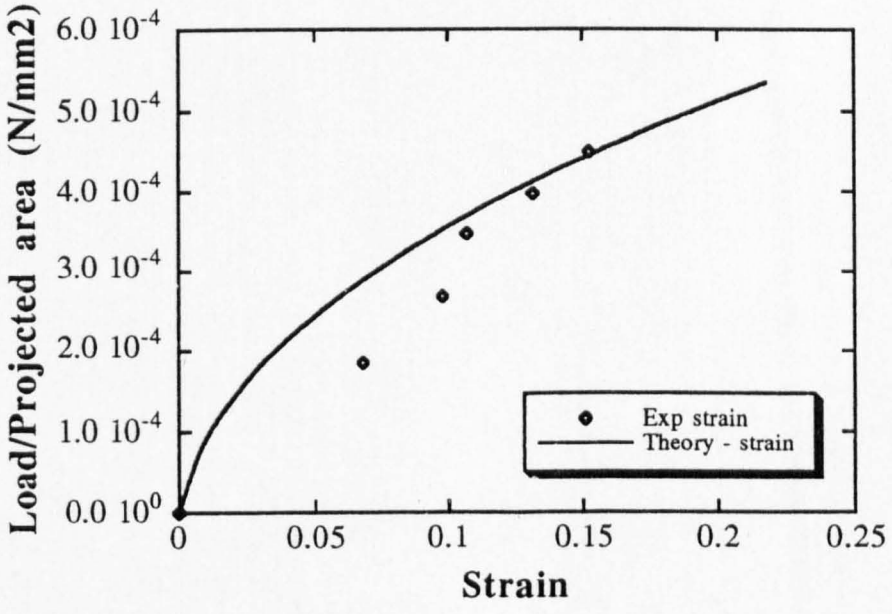

Fig.7.34 *Load/Projected area vs strain for a re-entrant cell, card honeycomb. The solid line is the theoretical curve derived from the hingeing model. (Loaded in direction 2)*

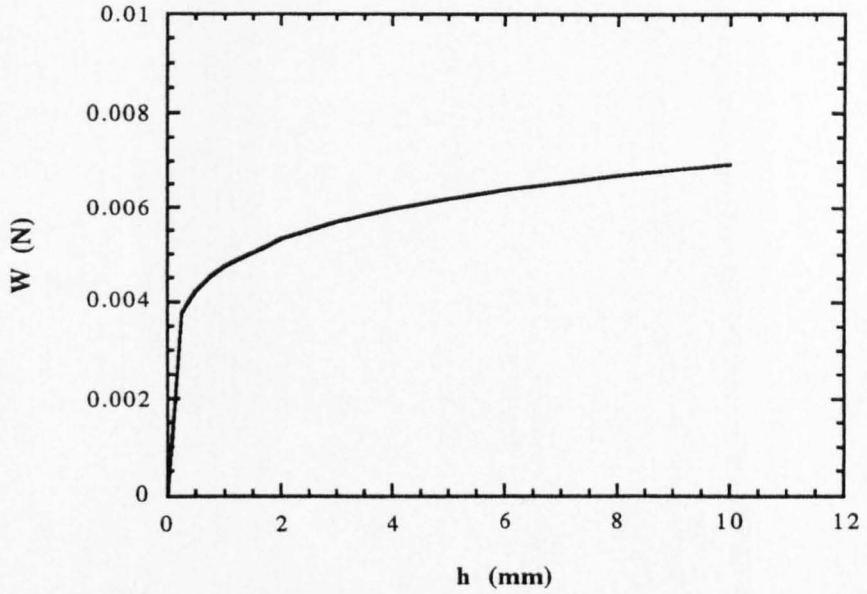

Fig.7.35 *Plot of the Hertz equation for a semi-circular indenter indenting a hexagonal cell card honeycomb in direction 2 (θ=51.70^{o}, K_h=67.2Nm^{-1})*

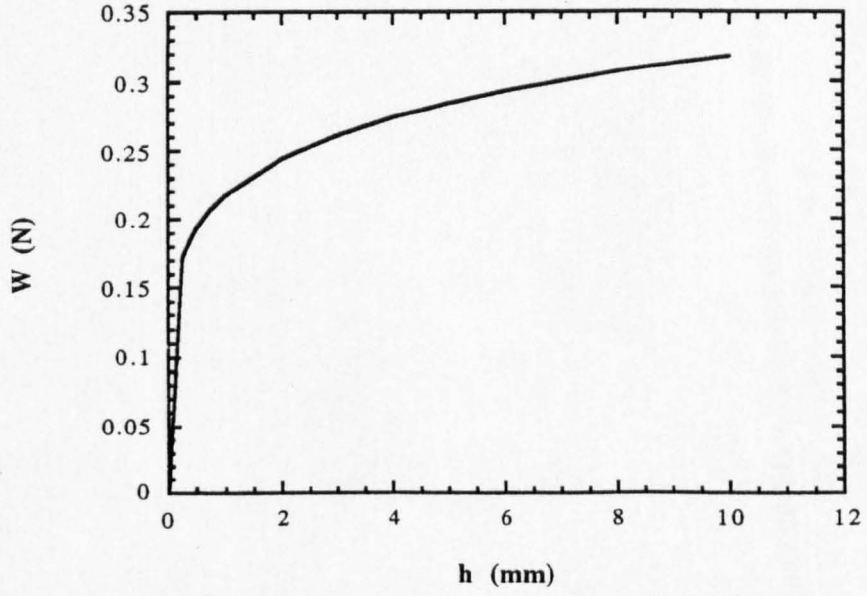

Fig.7.36 *Plot of the Hertz equation for a semi-circular indenter indenting a re-entrant cell card honeycomb in direction 2 (θ=-30.91^{o}, K_h=67.2Nm^{-1})*

7.4 Out of plane properties

7.4.1 Single cell compression

As already shown in section 6.8 the failure strengths for the hexagonal cells appear to be higher than those for the re-entrant cells. There are however, two important factors which affect these values of strength; the area of the core and the cross-sectional area of the cell walls supporting the load. Obviously these two areas are related and are functions of the core density. If we define the area fraction as

$$\text{Area fraction} = \frac{\text{Cross-sectional area of cell wall}}{\text{Area of a single cell}} \qquad (7.7)$$

then we can normalize the results, to give a measure of the failure stress per unit weight of core, by calculating the failure stress as

$$\text{Failure stress} = \frac{\text{Failure load}}{\text{Core area}} \times \frac{1}{\text{Area fraction}} \qquad (7.8)$$

The results listed in Table 6.3 are recalculated using equation 7.8 and shown in table 7.2

	(GPa)		
	h/l= 1	*h/l*= 2	*h/l*= 3
Hexagonal paper	7384	5018	--
Hexagonal paper+resin	25122	17403	--
Re-entrant paper	--	4219	3576
Re-entrant paper+resin	--	16498	10528

Table 7.2 *Failure stress/Area fraction for paper and paper+resin honeycombs loaded parallel to the cell axis.*

Again the hexagonal cells are stronger than the re-entrant cells and it is apparent that the *h/l* ratio is fundamental to the strength since as *h/l* increases the failure strength of both the hexagonal and re-entrant honeycombs is reduced. More

significant however is the *b/h* ratio were *b* is the thickness of the core.

Again calculating the failure stress as defined in equation 7.8 the results for the single cell tests shown in Fig.6.26 can be replotted against the *h/b* ratio as shown in Fig.7.37.

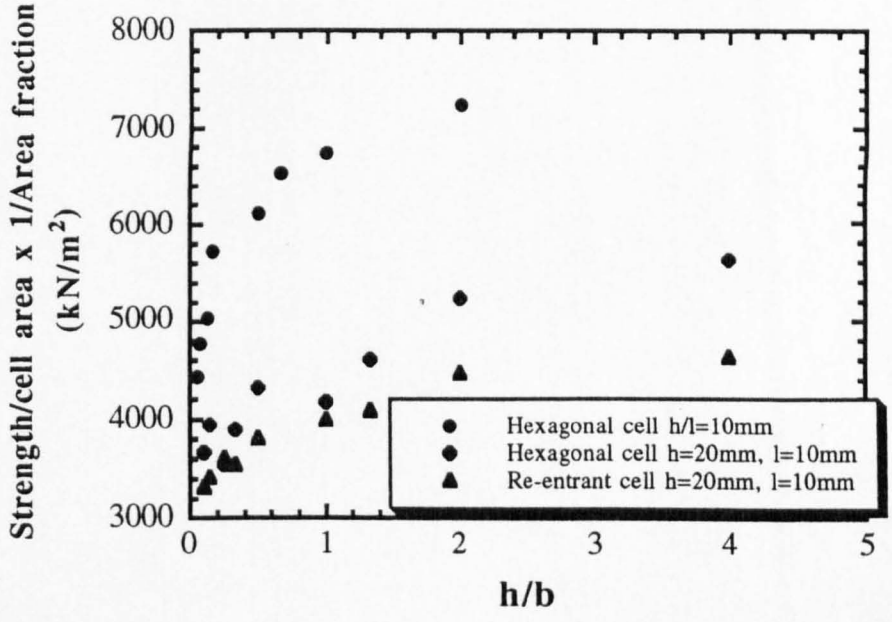

Fig.7.37 *Mean compressive strength vs h/b for single cartridge paper cells.*

As expected (Reichard, 1972) the strength rises rapidly when *h/b* <1. Also as can be seen from the plots for the hexagonal cells the strength is reduced as the *h/l* ratio is increased, confirming the results shown in table 7.2. The significant feature is the reduction in out-of-plane strength of the re-entrant cell compared with the conventional hexagonal cell which must be related to the *h/b* ratio.

The latter behaviour can be explained when the structure of the cell is considered (Fig.7.38).When *h/l* is small (i.e. of the order of 1) the cell walls **A** are constrained from buckling by their adjacent neighbours. As *h/l* increases **A** can buckle more easily and the twisting of the cell wall increases the local stresses at

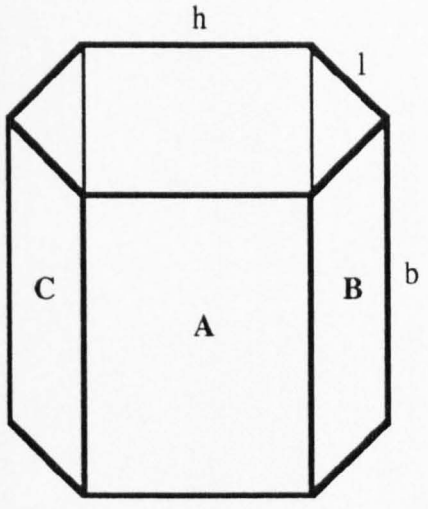

Fig.7.38 *Single hexagonal cell.*

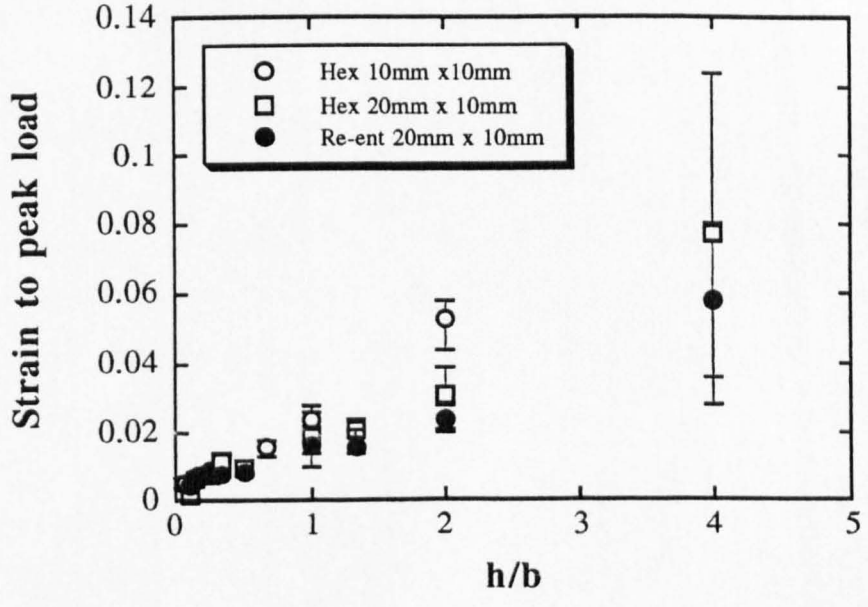

Fig.7.39 *Strain to peak load vs h/b for paper and paper resin honeycombs loaded along the axis of the cells.*

the cell wall junctions. The maximum load at which the junctions rupture, and failure can be considered to have occurred, thus decreases as h increases. When h is large there is a greater degree of elastic buckling which allows the honeycomb to recover when the load is removed. It can be seen from tables 6.3 and 6.4 that as h/l increases the failure load decreases and the amount of recovery increases.

The dimensions of the cell walls A are thus the important factor as the failure load decreases with increasing b for a fixed cell geometry (i.e. $h = l$ =Constant, θ=Constant) especially when $b > h$..

Plotting strain to maximum load against the h/b ratio (Fig.7.39) shows that strain increases with b as expected and also appears to show that the re-entrant core fails at lower strains than the equivalent hexagonal cell core. This is probably due to the acute angles between the cell walls in the re-entrant cell being less able to accommodate the stresses building up from elastic buckling.

7.4.2 Plate deflection tests

To gain a better insight into the effect of beam length on the stiffness of the honeycomb we can plot P/d vs beam length, where P=load and d=deflection, as shown in Fig.7.40. To enable a direct comparison of the hexagonal and re-entrant cell tests P/d has been multiplied by N^{-1} where N is the number of cells in the width of the beam.

The hexagonal cell produces a much stiffer honeycomb which can be attributed to the longer cell length (Fig.7.41). If the beam length is less than the cell length then the stiffness of the hexagonal and re-entrant cell honeycombs is approximately the same and corresponds to the through thickness shear modulus of the cell walls in direction 3. When the beam length is greater than the cell length the stiffness is reduced but the re-entrant cell becomes much less stiff than the hexagonal cell as the beam length increases. This can be explained by the

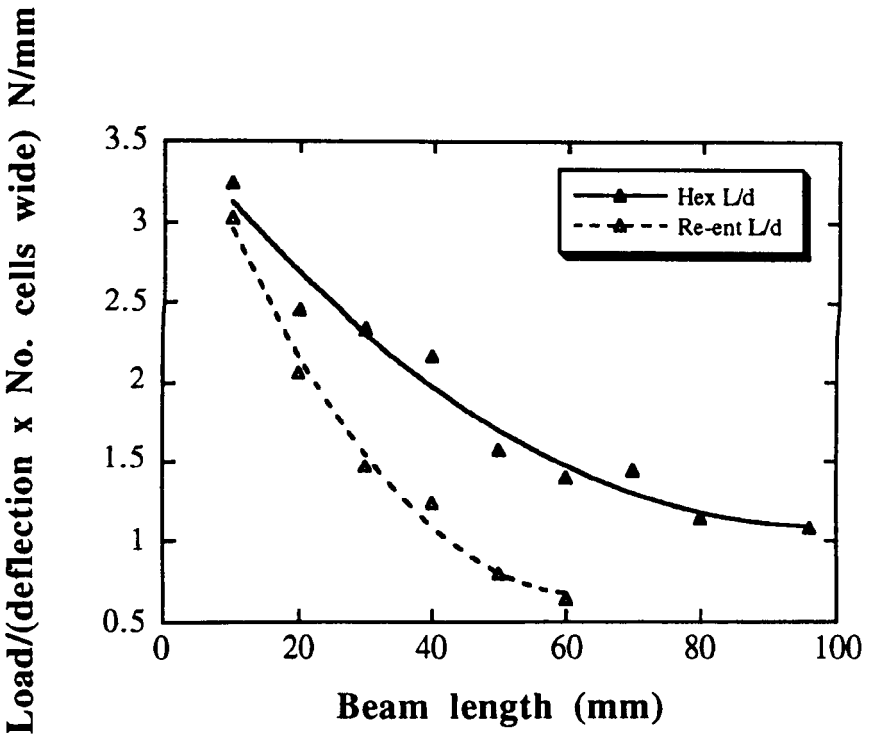

Fig.7.40 *Load/deflection vs beam length plots for hexagonal and re-entrant cell aluminium honeycombs bent in the plane of direction 1.*

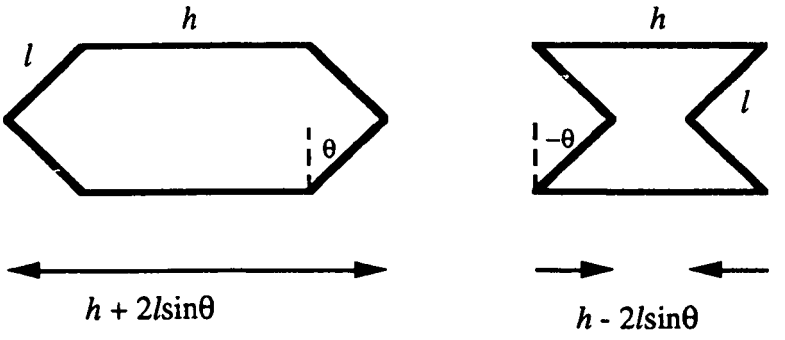

Fig.7.41 *Schematic diagram highlighting the difference in the effective cell lengths of the hexagonal and re-entrant cells.*

shorter effective cell length of the re-entrant cell which provides the greater flexibility. Insufficient material was available to make ' sheets of honeycomb oriented in direction 2. However it is anticipated that as there is no difference in the lateral dimensions of the re-entrant and hexagonal cells, their behaviour when bent in the plane of direction 2 will be identical.

References

BOWLES,K.J. & VANNUCCI,R.D.
ASTM test methods and design allowables for fibrous composites
Vol.2 Conference proceedings, 3-4 November 1986.

JOHNSON,K.L.
"Contact mechanics",
Chapter 4, Pages 84-105,
Cambridge University Press, Cambridge. (1987).

KELSEY,S., GELATELY,R.A. & CLARK,B.W.
Aircraft Engineering,
Pages 294-302, 1958.

LAKES,R.S & ELMS,K.
Journal of Composite Materials,
Vol.27 No.12, Pages 1193-1202, 1993.

LEE,S. & MUNRO,M.
Composites
Vol.17, No.1, 1986.

TABOR,D.
"Hardness of metals",
Chapter IV, Page 44,
Clarendon Press. (1951).

REICHARD,T.W.
National Bureau of Standards, Washington D.C.
Building Science Series No.43, April 1983.

8) DISCUSSION Part II

8.1 Benefits of the re-entrant cell shape

As already shown in the previous section the re-entrant structure has a lower shear modulus than the hexagonal cell and the Young's modulus is lower in tension for the re-entrant structure and higher in compression. The latter effect is also observed in in-plane indentation and is attributed to the densification of the honeycomb under the indenter.

The hinging mechanism requires such low loads to operate that comparatively small areas of honeycomb can deform under their own weight. When the honeycomb is bent out-of-plane twisting of the cell walls length l occurs (Abd El-Sayed,1976). Increasing the core thickness b increases the core stiffness making it more resistant to bending out of plane.

The radii of curvature generated by elastic deformation, when bending a core out of plane, are controlled by the cell angle and the h/l ratio. This is predicted by the plate deflection theory (section 2.11) which relates the radii to the effective Poisson's ratios of the core, which are of course functions of h/l The effect of varying the h/l ratio for a hexagonal honeycomb is shown in Fig.8.1. When bending a hexagonal cell honeycomb out of plane the positive Poisson's ratio requires the curvature to be anticlastic (Fig.1.3). The contrary curvatures, which must be achieved in the plane of the honeycomb to generate this, have a stiffening effect.

In the re-entrant case where the curvature is synclastic this stiffening effect is lost, resulting in a core which can readily deform under it's own weight. This produces a highly drapeable core (Fig. 8.2). In a re-entrant card honeycomb the presence of hinges at the cell wall junctions, which operate at extremely low loads, results in a further reduction in stiffness.

Section AA : h=20mm, l=5mm
BB : h=20mm, l=10mm
CC : h=20mm, l=15mm
DD : h=20mm, l=20mm

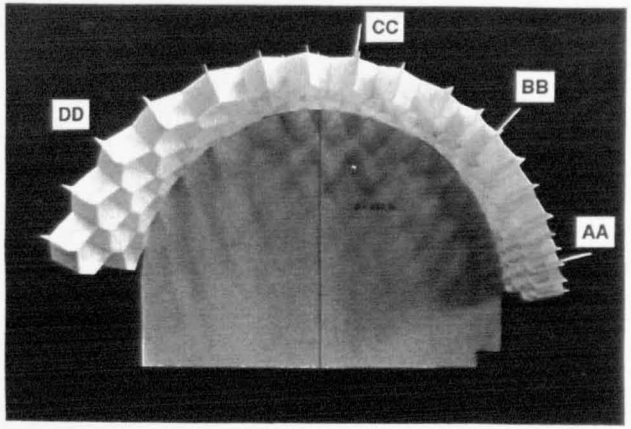

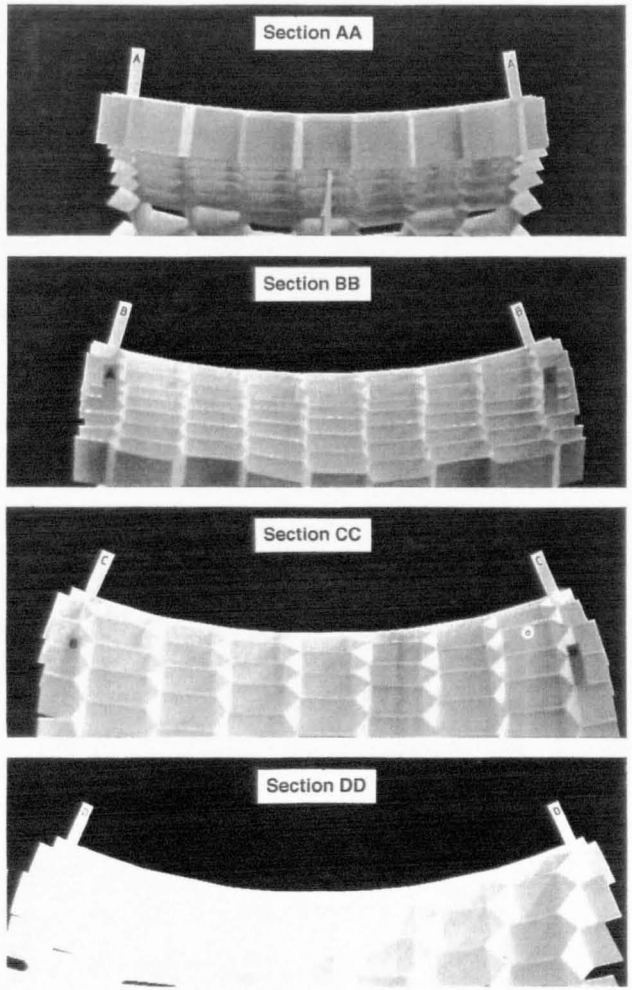

Fig.8.1 Effect of varying cell shape on the secondary curvature of a hexagonal cell honeycomb.

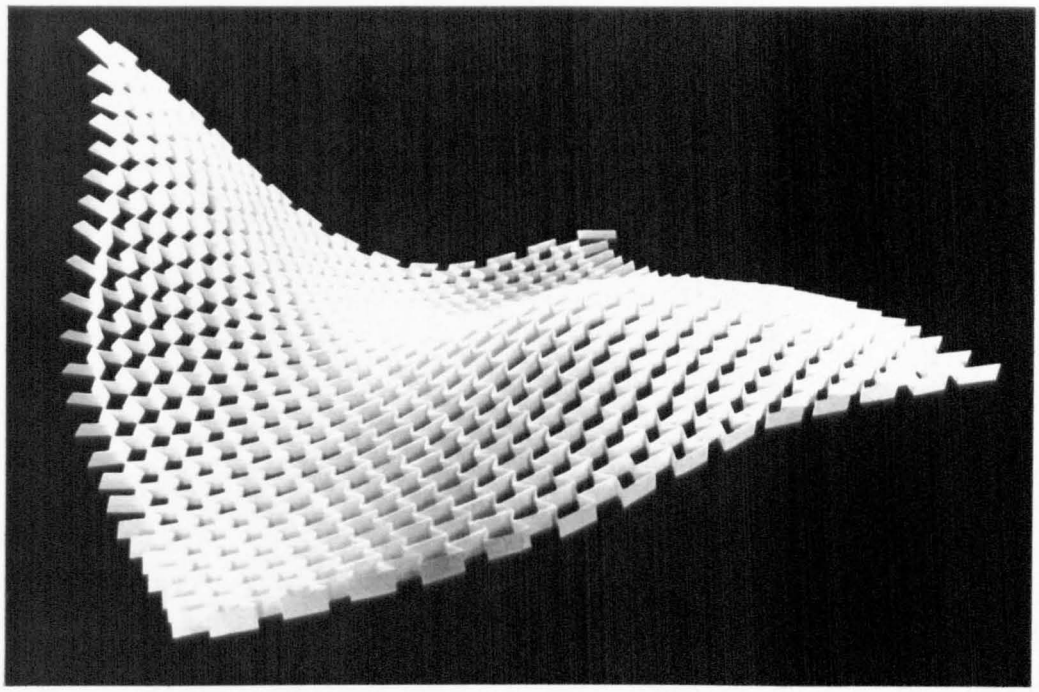

Fig.8.2 *A 210μm card honeycomb demonstrating the drapeability of the re-entrant cell structure. (h=20mm, l=10mm)*

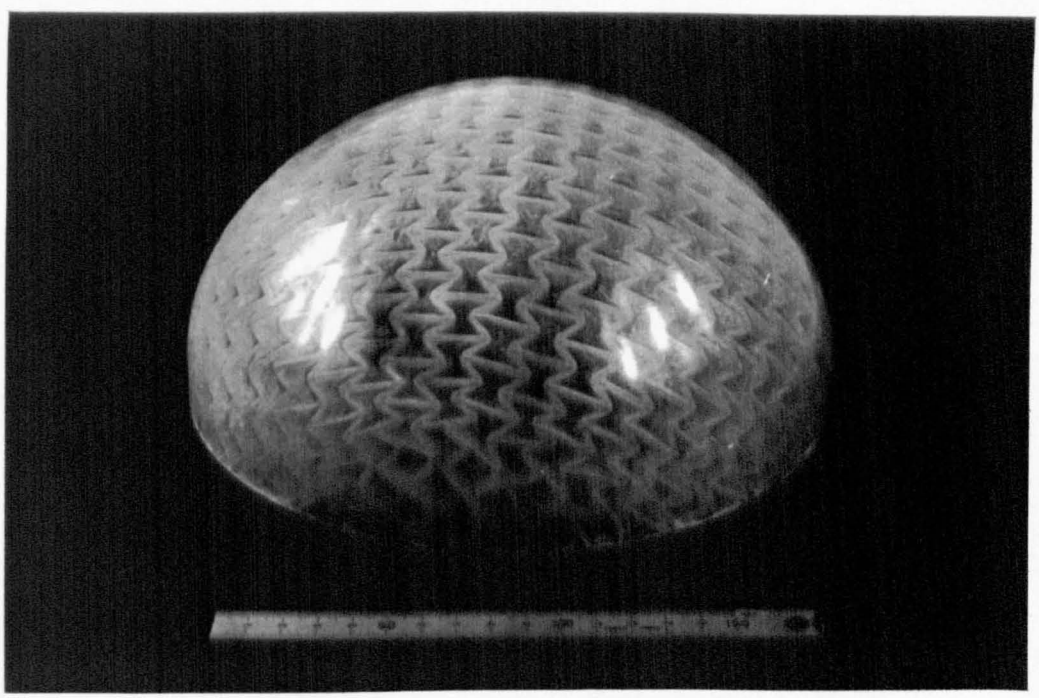

Fig.8.3 *240mm diameter GRP dome backed by a re-entrant cell, resin coated card honeycomb. (h=20mm, l=10mm)*

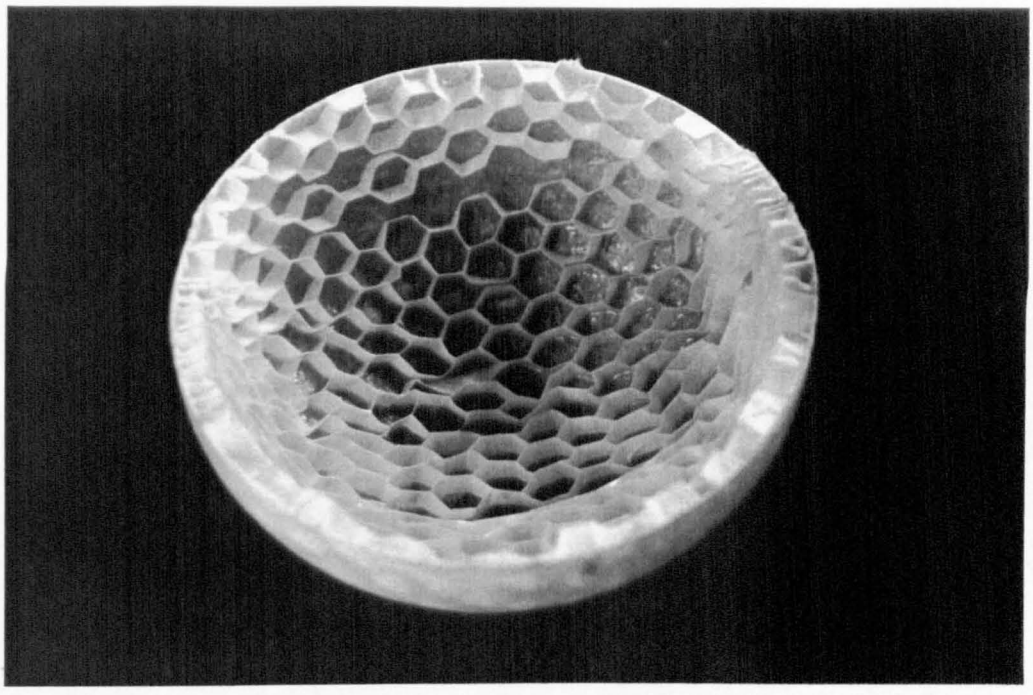

Fig.8.4 *240mm diameter GRP dome backed by a hexagonal cell, resin coated card honeycomb. (h=l=10mm) . Note the damage to the core compared with Fig.8.3.*

Unlike the hexagonal celled core the re-entrant core can be forced into very tight curvatures without damage to the cellular structure. To illustrate this a 240mm diameter dome, comprising a GRP skin backed with a resin coated, re-entrant celled (h =20mm, l =10mm), 210μm card honeycomb was constructed and this is shown in Fig.8.3. The honeycomb conforms well to the shape of the dome without damage to the cellular structure. Fig 8.4 shows a similar dome produced using a hexagonal celled core (h =l =10mm), note how the core has become overstretched in direction 2 leading to rupture of the glued joints.

The disadvantage of the re-entrant celled structure is however, its much increased density over the hexagonal cell (typically 66% for cells of an equivalent area) particularly as the smaller the radii required the smaller the cell size which must be used.

8.2 Optimum core geometry.

The selection of a particular cell geometry is a careful balance between the required elastic properties and the density of the honeycomb.

The Young's moduli for all three models are functions of the *h/l* ratio and the cell angle θ (Table 3.2) but are also governed by the physical size of the cells since $K_i=f(t/l,b)$. The Poisson's ratio is only controlled by the *h/l* ratio and θ and is thus independent of the cell size.

The most common application of honeycombs is in sandwich panels where their low density is important. The effect of density on the moduli can be examined by dividing the modulus equations 3.22 and 3.23 for the flexure model and 3.55 and 3.60 for the hinging model by the relative density (Eqn. 2.10). The resulting graph (Fig.8.5) is of similar shape to the E_i vs θ plots shown in Fig.4.2. The plot for E_1 is skewed to the left and increasing the *h/l* ratio gives an increase in the modulus per unit density. It is apparent that for any specific modulus there is a choice between a conventional or auxetic cell shape.

Fig.8.6 shows the corresponding plot for E_2/relative density. The plot is symmetrical about $\theta=0^o$ where E_2 tends to ∞ and 0 at $\theta=\pm 90^o$. Unlike E_1 the best values of E_2 per unit density are achieved when *h/l* is small.

The effect of relative density on the in-plane shear modulus is shown in Figs.8.7 and 8.8 for the flexure and hinging models. Again the highest and therefore best values are obtained by the hexagonal cell shape for both models although the actual maxima are only achieved when $75^o<\theta<90^o$.

The most important properties in sandwich panel applications are the through thickness shear moduli G_{13} and G_{23} since these prevent the skins from sliding over one another (Allen. 1969). If we assume that for most applications we require $G_{13}=G_{23}$ then by combining equations 2.2 and 2.3 we obtain the

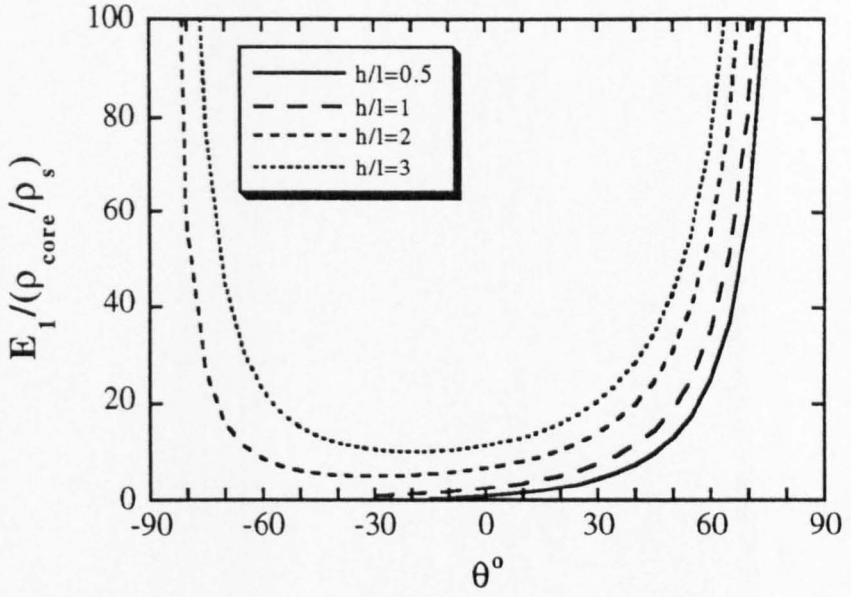

Fig.8.5 *Modulus E_1/Relative density vs cell angle for the flexure and hinging models. Note the similarity in shape to Fig.4.2.*

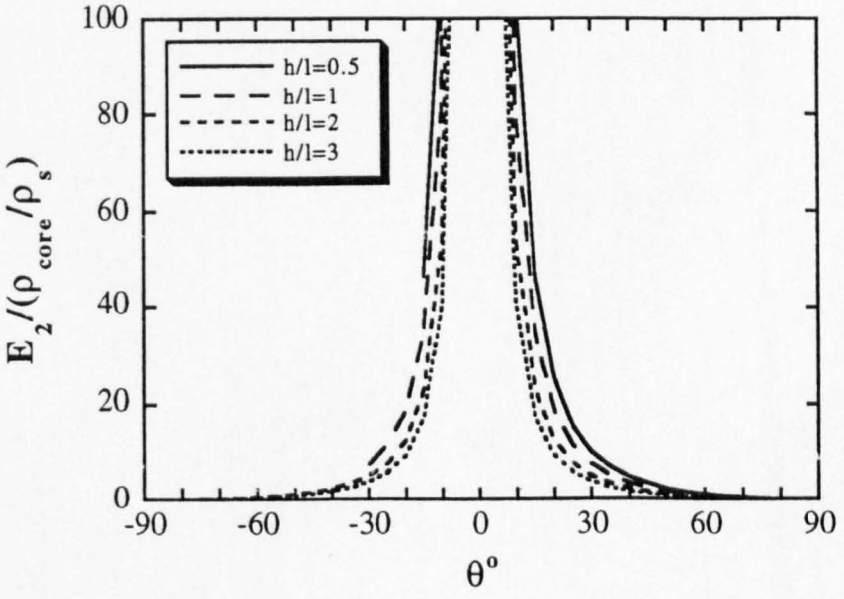

Fig.8.6 *Modulus E_2/Relative density vs cell angle for the flexure and hinging models. The plot is symmetrical around $\theta=0^o$.*

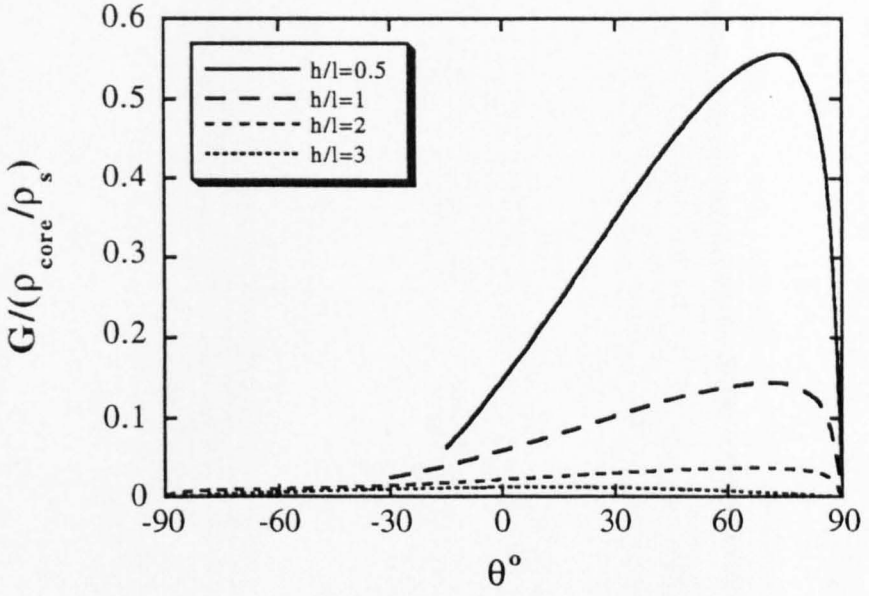

Fig.8.7 *In-plane shear modulus/Relative density vs cell angle for the flexure model. Hexagonal cells provide much higher moduli per unit density.*

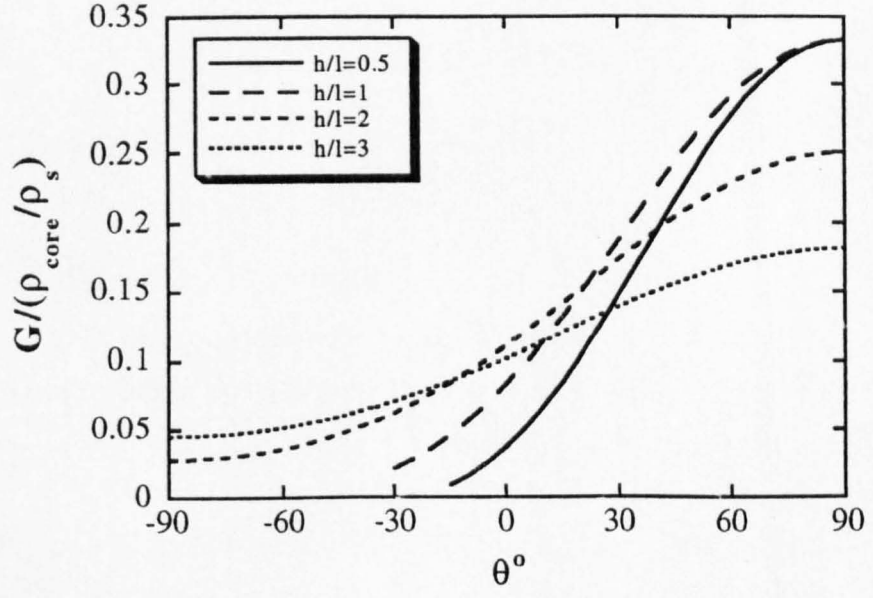

Fig.8.8 *In-plane shear modulus/Relative density vs cell angle for the hinging model. Again the hexagonal cells provide higher moduli per unit density over the whole range of cell angles.*

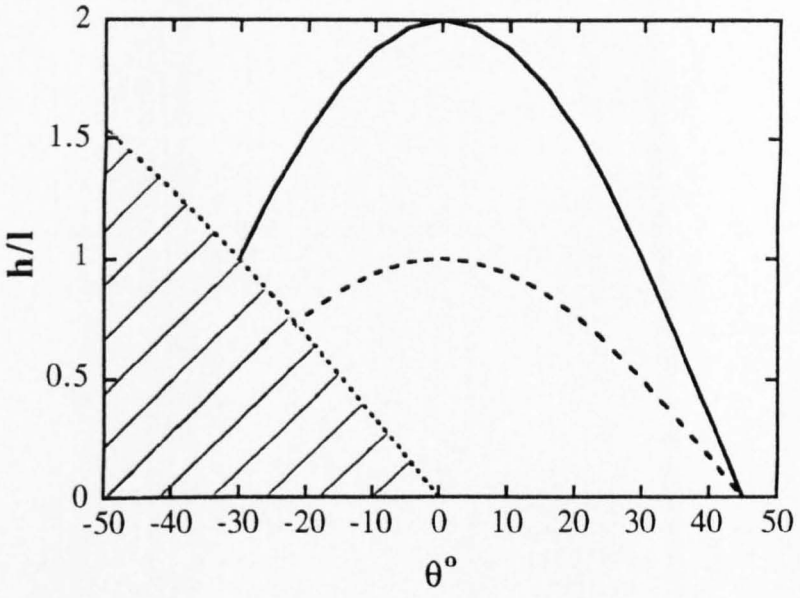

Fig.8.9 *Plot showing the values of h/l and θ required to achieve equal through thickness shear moduli in directions 1 and 2 when all cell walls are of uniform thickness (—) and when* $t_h = 2t_l$ *(- - -).*

relationship

$$h/l = 2-4\sin^2\theta \qquad (8.1)$$

if all the cell walls are of equal thickness and

$$h/l = 1-2\sin^2\theta \qquad (8.2)$$

if we allow for the double thickness (Eqns.2.3 and 2.5) of the walls length h i.e. $t_h = 2t_l$. These equations are plotted in Fig.8.9. It is apparent that for the hexagonal cells all geometries in the ranges $0<h/l<2$ and $0^o<\theta<45^o$ are permissible when $t_l = t_h$. When $2t_l = t_h$, h/l must lie in the range $0<h/l<1$.

The range of angles available for the equivalent re-entrant cells is controlled by the h/l ratio. The limits of the permissible values are shown by the shaded area in Fig.8.9.

The minimum density for the core is achieved when h/l is maximum i.e. $h/l = 2$

when $t_l = t_h$. and $h/l = 1$ when $2t_l = t_h$.. For both these conditions $\theta = 0^o$ thus producing a perfectly square cell for the first case and a rectangular cell for the latter.

8.3 Molecular Modelling

Nkansah *et al.* (1994) used the flexure model of Gibson to determine the Young's moduli and Poisson's ratios for theoretical structures of the type shown in Fig.8.9. They compared their results to those obtained from a proprietary molecular modelling programme ('Polygraf™') and finite element analysis.

To evaluate the model they used the constants listed in Table 8.1. The moduli E_s was determined from the average of the radii and experimental force constant data of a C-C single bond and a C≡C triple bond. Their results for moduli E_1 and E_2 are reproduced in Table 8.2 together with the results obtained from the general model (Eqns. 3.72 - 3.75). The Poisson's ratios are shown in Table 8.3.

As already shown by Nkansah *et al.* the flexure model consistently over estimates the values of E and ν predicted by molecular modelling. This implies that although flexure is the dominant mechanism, as might be expected from examining Fig. 4.1 in the range $0.13 < t/l < 0.18$, there must be contributions from the other mechanisms. As E_s is known K_f and K_s can be determined from equations 3.4 and 3.6 to evaluate the general model. The value of K_h is obtained by assuming either local bending (eqn. 3.16) or global shear (eqn. 3.10). In the latter case it is assumed that $G_s \approx (1/3)E_s$ which results in a value of K_h very close to that of $70 Nm^{-1}$ used by Gillis (1984) for a C=C bond in graphite. As can be seen from Table 8.2 the general model, in which global shear is assumed, agrees well with the results from molecular modelling.

The Poisson's ratios ν_{12} (Table 8.3) from the general model, again assuming global shear, lie between those values obtained from the molecular model and the finite

element model and agree more closely than the flexure model alone. The values of ν_{21} for the general model are higher than those obtained from the other models particularly for the auxetic molecules.

These results suggest that this approach may be a rapid first order technique for predicting the properties of more complex 2 and 3D molecular networks constructed from molecular repeat units, for which the force constants K_f, K_h and K_s have been established by experiment or from molecular modelling.

Fig.8.10 *Two of the theoretical molecular structures investigated by Nkansah et al. (1994). The structures are termed 1,4 flexyne (top), 1,4 reflexyne (bottom) where the numerals refer to the number of C≡C bonds.*

	1-4 flexyne	2-6 flexyne	2-2 flexyne	1-4 re-flexyne	2-6 re-flexyne	2-8 re-flexyne
h(m)=	1.38E-09	1.56E-09	9.02E-10	1.38E-09	1.86E-09	2.34E-09
l(m)=	6.63E-10	9.02E-10	9.02E-10	6.64E-10	9.04E-10	9.04E-10
b(m)=t(m)=	1.21E-10	1.21E-10	1.21E-10	1.21E-10	1.21E-10	1.21E-10
Theta(Deg)=	3.00E+01	2.99E+01	2.99E+01	-2.82E+01	-2.82E+01	-2.83E+01
Theta(Rad)=	5.24E-01	5.22E-01	5.22E-01	-4.93E-01	-4.91E-01	-4.94E-01
Es(Pa)=	6.82E+12	6.82E+12	6.82E+12	6.82E+12	6.82E+12	6.82E+12
Kf(N/m)=	5	2	2	5	2	2
Kh(N/m) local bending=	8	3	3	8	3	3
Kh(N/m) global shear=	101	74	74	101	74	74
Ks(N/m)=	152	111	111	151	111	111

Table 8.1 *Constants used for the calculation of young's moduli and Poisson's ratios from molecular, finite element and analytical models (Nkansah et al. 1994)*

			1-4 flexyne	2-6 flexyne	2-2 flexyne	1-4 reflexyne	2-6 reflexyne	2-8 reflexyne
Molecular model	**Tension**	**E1**	143.75	56.82	23.97	117.39	25.74	33.90
		E2	55.87	19.74	34.78	85.00	38.64	22.50
	Compression	**E1**	135.87	72.22	35.00	120.00	34.00	45.45
		E2	51.78	14.86	27.86	78.33	28.38	30.21
Finite element model		**E1**	197.32	81.15	56.31	116.53	47.82	59.39
		E2	66.64	28.32	55.31	119.58	51.09	35.75
Flexure model		**E1**	166.85	65.34	38.34	98.35	65.34	51.19
		E2	56.24	22.75	38.71	102.20	22.75	30.71
General model	**(local bending)**	**E1**	92.81	33.65	23.17	54.97	22.52	29.66
		E2	33.07	15.80	23.39	59.54	24.82	18.48
General model	**(global shear)**	**E1**	133.69	50.14	35.45	79.34	33.96	44.4
		E2	48.86	24.17	35.78	87.61	37.86	28.19

Table 8.2 *Comparison of moduli (GPa) results from the molecular, finite element and analytical models.*

			1-4 flexyne	2-6 flexyne	2-2 flexyne	1-4 reflexyne	2-6 reflexyne	2-8 reflexyne
Molecular model	**Tension**	v12	0.769	1.379	0.897	-0.313	-0.647	-0.849
		v21	0.295	0.503	0.858	-0.378	-0.877	-0.664
	Compression	v12	0.965	1.205	0.781	-0.292	-0.741	-0.943
		v21	0.347	0.447	0.796	-0.253	-0.726	-0.541
Finite element model		v12	1.492	1.565	0.936	-0.853	-0.893	-1.188
		v21	0.504	0.547	0.920	-0.874	-0.952	-0.714
Flexure model		v12	1.722	1.695	0.995	-0.981	-0.963	-1.291
		v21	0.581	0.590	1.005	-1.019	-1.038	-0.774
General model	**(local bending)**	v12	1.501	1.380	0.952	-0.859	-0.896	-1.183
		v21	0.663	0.710	1.052	-1.122	-1.093	-0.815
General model	**(global shear)**	v12	1.403	1.332	0.929	-0.805	-0.862	-1.130
		v21	0.663	0.729	1.080	-1.183	-1.125	-0.839

Table 8.3 *Comparison of Poisson's ratio results from the molecular, finite element and analytical models.*

References

ALLEN.H.G.
"Analysis and design of structural sandwich panels",
Chapter 1, Page 1
Pergamon Press Ltd., London (1969).

GILLIS,P.P.
Carbon,
Vol.22, Pages 387-391. 1984

NKANSAH,M., EVANS,K.E. & HUTCHINSON,I.J.
Modelling Simulation in Materials Science and Engineering,
Vol.2, Pages 337-352, 1994

"POLYGRAF™"
Molecular simulations Inc.,
199 South Los Robles Avenue, Suite 540,
Pasadena, California 91101, U.S.A..

9) CONCLUSIONS & FUTURE WORK

9.1 Introduction

The main conclusions of this work fall into three categories:-

the applications of re-entrant, auxetic honeycombs,

general models for predicting the material properties of honeycombs,

the use of this modelling approach in molecular honeycombs

9.2 Conclusions

1) The re-entrant cell shape generates a negative in-plane Poisson's ratio which results in synclastic curvature when the honeycomb is bent out-of-plane. This combined with the low forces required for hinging produces a highly drapeable core.

2) The hinging mechanism requires much lower forces to operate than the flexure model and thus dominates and as a result is particularly advantageous in producing highly drapeable cores.

3) The re-entrant structure provides much greater resistance to in-plane indentation than the hexagonal cell due to densification of the structure.

4) In general however, the mechanical properties of the re-entrant celled structure are lower than the equivalent hexagonal celled cores and the density is increased.

5) Honeycombs will deform by one or a combination of three mechanisms: flexure, stretching or hinging depending on the cell geometry and the elastic properties of the cell wall material. The examples examined here were aluminium which deforms predominantly by flexing and card honeycombs which deform predominantly by hinging.

6) A general model based on force constants for all three mechanisms can be used as a simple method of estimating the properties of both hexagonal and re-entrant cell honeycombs.

7) The models can be used to predict the behaviour of both hexagonal and re-entrant molecular structures, with a view to providing a rapid first order calculation of their properties.

9.3 Future work

The use of drapeable, re-entrant celled honeycombs requires further development, particularly in the area of fabrication by an automated route. This would increase the availability of material enabling more thorough and rigorous evaluation of auxetic honeycombs to be undertaken. An important area to look at is their performance as a core in sandwich panels which would necessitate undertaking:-

1) Through thickness shear tests
2) Three and four point bend tests on sandwich panels containing re-entrant celled honeycombs.
3) Static and dynamic impact tests on curved sandwich panels containing re-entrant celled honeycombs.

More useful materials than card should be investigated, one possibility being thermoplastics in which hinges could easily be formed by local necking of the material (cf. lids on shampoo bottles etc.), and also the development of structural applications where the densification during compression or indentation could be exploited e.g. in energy absorption.

Finally comparison between the simple analytical approach developed in this thesis and full molecular modelling of 3D molecular structures requires further investigation.

APPENDIX 1 - Biaxial, in-plane loading.

Gibson *et al* (1988) developed a deformation model for a honeycomb subjected to biaxial loading, by considering both stretching and flexing of the cell walls. The following equations for strain were derived in which the first term is the flexing component and the second the stretching component.

$$\varepsilon_1 = \frac{1}{E_1}(\sigma_1 - \nu_{12}\sigma_2) + \frac{1}{E_s(t/l)}\left[\sigma_2 \sin\theta\cos\theta + \frac{\sigma_1 \cos\theta(h/l + \sin^2\theta)}{h/l + \sin\theta}\right] \quad \text{(A1.1)}$$

$$\varepsilon_2 = \frac{1}{E_2}(\sigma_2 - \nu_{21}\sigma_1) + \frac{1}{E_s(t/l)}\left[\sigma_2(h/l + \sin\theta)\cos\theta + \sigma_1 \sin\theta\cos\theta\right] \quad \text{(A1.2)}$$

If we assume that no flexing occurs (i.e.E_1 and E_2 are ∞) and set $\sigma_1=0$ then equations A1.1 and A1.2 reduce to

$$\varepsilon_1 = \frac{\sigma_2 \sin\theta\cos\theta}{E_s(t/l)}$$

$$\varepsilon_2 = \frac{\sigma_2(h/l + \sin\theta)\cos\theta}{E_s(t/l)}$$

The Poisson's ratio ν_{21} is given by

$$\nu_{21} = -\frac{\varepsilon_1}{\varepsilon_2} = -\frac{\sin\theta}{h/l + \sin\theta} \quad \text{(A1.3)}$$

and theYoung's modulus E_2 by

$$E_2 = \frac{\sigma_2}{\varepsilon_2} = \frac{E_s(t/l)}{\cos\theta(h/l + \sin\theta)}$$

Re-writing the latter in terms of the force constant K_s (eqn. 3.6) gives

$$E_2 = \frac{K_s}{b\cos\theta(h/l + \sin\theta)} \quad \text{(A1.4)}$$

Similarly putting $\sigma_2=0$ we obtain the following equations for ν_{12} and E_1 when the honeycomb is loaded in direction 1.

$$\nu_{12} = - \frac{\sin\theta\left(h/l + \sin\theta\right)}{\left(2h/l + \sin^2\theta\right)} \qquad \text{(A1.5)}$$

$$E_2 = - \frac{K_s\left(h/l + \sin\theta\right)}{b\cos\theta\left(2h/l + \sin^2\theta\right)} \qquad \text{(A1.6)}$$

These are the same equations derived for the stretching model in chapter 3, section 3.4.

Reference

GIBSON,L.J. & ASHBY,M.F.
"Cellular Solids: Structure and Properties",
Chapter 4, Page 98,
Pergamon Press, Oxford (1988).